Assessing the Viability of Tenera Oil Palm Shells as Fine and Coarse Aggregates in Structural Lightweight Concrete: Microstructure and Mechanical Properties

by

Mohammed Fadhil HAMA

Department of Civil Engineering

Faculty of Science and Engineering

Thesis submitted to The University of Nottingham for
the degree of Doctor of Philosophy

OCTOBER 2023

Abstract

Oil palm shells (OPS), a significant waste product of the oil palm industry, have raised environmental concerns due to their abundance and disposal challenges. Researchers have explored the potential use of OPS as coarse aggregates in structural lightweight concrete (SLWC) to address these issues. However, most studies lack specific OPS variety information, although indications by the thickness and accompanying figures point to the prevalent use of Dura OPS. The emergence of Tenera, a hybrid oil palm variety with thinner OPS, has significant implications, as it offers a 57% reduction in OPS thickness and a 30% increase in palm oil production compared to Dura OPS. Over 90% of oil palm farmers in Malaysia have already switched to the Tenera fruit, suggesting that the Dura variety may be phased out in the future.

Concrete science acknowledges that changes to aggregate properties, such as size or thickness, can impact a concrete's mechanical property. Therefore, the primary focus of this study was to assess the mechanical properties of Tenera OPS when used individually as coarse and fine aggregates in SLWC, comparing them to normal weight concrete (NWC) of similar grade. Distinct mix designs and superplasticizers were employed, with a comprehensive analysis of density, permeable voids, and water absorption over time. Mechanical properties, including compressive strength, flexural tensile strength, modulus of elasticity, and drying shrinkage, were evaluated throughout a 365-day period in both cured and air-cured conditions. Microstructural analysis and ultrasonic pulse velocity testing were also performed.

A key finding is that the use of Tenera OPS as coarse aggregates in OPS concrete (coarse OPSC) results in a notable reduction in compressive strength compared to Dura OPS under similar mix designs. However, Tenera OPS exhibits more promising outcomes when employed as fine-sized aggregates in concrete (fine OPSC). Microstructural analysis reveals fewer void spaces in fine OPSC, attributed to the swelling and shrinking characteristics of OPS when exposed to moisture and drying. The favourable shape of fine-sized OPS contributes to better performance and reduced cement consumption. By utilizing OPS in a saturated surface dry (SSD) state, both coarse and fine OPS in concrete facilitate internal curing. In terms of mix designs, fine OPSC demands 263% less cement content to achieve equivalent 28-day compressive strength compared to coarse OPSC, and only 14% more cement content than NWC, which showcases potential economic and environmental advantages. Despite its higher coarse aggregate content, the density of fine OPSC meets lightweight concrete (LWC) requirements and exhibits lower permeable voids and water absorption compared to coarse OPSC. This suggests enhanced durability. Fine OPSC also

demonstrates early strength development superior to both NWC and coarse OPSC and maintains superior strength at 365 days. In contrast, coarse OPSC displays the lowest flexural tensile strength in cured conditions but excels in air-cured conditions, indicating susceptibility to moist environments, which is beneficial for continued cement hydration. Unexpectedly, the deterioration of coarse OPS, likely due to white-rot fungi, affects specific mechanical properties when exposed to curing regimes, a phenomenon not observed in fine OPSC. Furthermore, fine OPSC exhibits comparable dynamic and static modulus of elasticity (MOE) values to NWC, while coarse OPSC exhibits significantly lower MOE values. Drying shrinkage values for fine OPSC are similar to or slightly lower than NWC, whereas coarse OPSC displays significantly higher drying shrinkage values, almost three times that of NWC and fine OPSC. While drying shrinkage almost ceases after 365 days for NWC and fine OPSC, it continues at a significantly higher rate for coarse OPSC.

This study offers critical insights and recommendations for future research, including strategies to mitigate OPS swelling and shrinking effects in concrete, refining mix designs, exploring additives to reduce cement content, examining performance under various environmental conditions, and conducting extended duration testing to further advance the utilization of OPS in sustainable construction practices.

Acknowledgement

To begin with, all praise is due to Almighty Allah (God) for granting me the health, wisdom, and ability to carry out this research successfully. It would not have been possible without his mercy upon me.

I would like to express my earnest thankfulness to my research supervisors Dr. Mohammed Parvez Anwar and Dr. Teck Leong Lau, for allowing me to work with them and for their enormous guidance, patience, and genuine support throughout the research. It's been a pleasure working with them. I would like to acknowledge the technical, financial, and academic support given by University of Nottingham, especially the Laboratory staff. Above all, I am most grateful to my entire family for their support and prayers. Not forgetting my close friends, unfortunately, I cannot list all their names. I am also thankful to my beloved wife for her support and patience throughout my study. Also, when my daughter and son are old enough to read this, both of you have been the best gift ever and have always kept a smile on me and encouraged me to finish my work.

At last, this piece of work is dedicated to my dearest parents. Words cannot express how happy I am for your sincere love and support throughout my life.

Table of Contents

List of Figures

XI

List of Tables

List of Equations

List of Abbreviations

OPS	Oil palm shell
OPSC	Oil palm shell concrete
NWC	Normal weight concrete
F-OPS	Fine-sized oil palm shell
C-OPS	Coarse-sized oil palm shell
Fine OPSC	Fine-sized oil palm shell concrete
Coarse OPSC	Coarse-sized oil palm shell concrete
LWA	Lightweight aggregate
NWA	Normal weight aggregate
LWC	Lightweight concrete
SLWC	Structural lightweight concrete
UPV	Ultrasonic pulse velocity
BS	British standard
ASTM	American Society for Testing and Materials
ACI	American Concrete Institute
SP	Superplasticizer
C.A.	Coarse aggregate
F.A.	Fine aggregate
HSLWC	High-strength lightweight aggregate concrete
SF	Silica fume
GGBFS	ground granulated blast furnace slag
PVA	Polyvinyl alcohol
SSD	Saturated surface dry

Chapter 1.   Introduction

In the late 1950s, the Malaysian government shifted from rubber to the oil palm industry, which has now become one of Malaysia's largest exports, having grown in recent decades among all its agricultural-based industries. The growth of oil palm industries is also evident in neighbouring countries such as Thailand, Indonesia, and the Philippines (Shahbandeh, 2022). Records show that Malaysia produced 18.5 million metric tons of palm oil in 2022, whereas Indonesia had the largest production of 48.2 million metric tons, respectively, 23.4% and 61.2% of the world's total 2022 production of 78.8 million metric tons. The total palm oil production in 2010 was 46.3 million metric tons, therefore having increased by 70% in a course of only 12 years (CPOPC, 2023).

While the farming industry is the primary beneficiary of the production and export of palm oil, the resulting expansion of the oil palm industry has several downsides. When the oil is extracted from the fruits by the mills, substantial amounts of waste are produced, namely empty fruit bunches, mesocarp fruit fibres, and oil palm shells (OPS), creating the problem of biomass waste overload. This results in disposal difficulties for operators and increases the operation cost. The OPS is directly obtained by breaking the fruit exterior (and drawing out the oil palm) and is dumped in large quantities in local landfills as it serves no other purpose for the industry (Vincent, 2011). In the oil palm mill process, a total of 5.5% of OPS waste is produced (Abdullah & Sulaiman, 2013). This indicates that, in 2022, more than one million metric tons of OPS waste were produced only in Malaysia, and a total of over 4.3 million metric tons of global OPS production in 2022 and expected to increase in the future. It is therefore necessary to tackle waste disposal issues caused by the oil palm industries in Malaysia and other oil palm-producing countries.

OPS waste has significant potential in various renewable and sustainable applications, such as solid fuels for steam boilers in palm oil mills (Awalludin, et al., 2015). However, such a process is deemed to be non-environmentally friendly by causing emission problems, which are discouraged by the Malaysian government (Abdullah & Sulaiman, 2013). Another application that has been utilized for the last four decades is by using the OSP as coarse aggregate replacement in concrete, initially formulated by Abdullah et al. in 1984. Many other investigations have followed later (Kareem, et al., 2022).

Concrete is a crucial construction material, composed of cement, water, and aggregates. Due to its high demand in industries and urban areas, large quantities of raw materials are required to produce concrete. One of the main reasons for its popularity is the ability to improve and develop the characteristics of each component (Swamy, 2007). However, the

1

current concrete industry generates unwanted environmental impacts that can be reduced by substituting conventional raw materials with agricultural waste. This approach can minimize sourcing and transport costs while also reducing the amount of waste sent to landfills (Tavakolu & Hashempour, 2018). Regulations imposed by Departments of Environment over the world have tried different efforts to improve the recycling of these by-products (Corinaldesi, 2011). Concentrating on developing countries that have the highest demand for concrete, environmentally sustainable concrete structures can be built by using these agricultural wastes and industrial by-products (Shafigh, et al., 2010). This has economical and several practical advantages. Also, to assure an appropriate living atmosphere and safety for the coming generations, good coherence must be attained by engineers and scientists in the development of the construction industry. For such reasons, many countries in the world concentrate on sustainable concrete with main objectives such as developing low energy resources, decreasing carbon dioxide (CO_2) gas emissions & amount of pollution, efficient use of waste materials, increasing the serviceable age of the structures, flexible construction of buildings, and developing the thermal mass of concrete in a structure to reduce energy demand (Meyer, 2009).

To achieve sustainable concrete structures, many countries are focusing on developing low-energy resources, decreasing CO_2 emissions and pollution, using waste materials efficiently, increasing the lifespan of structures, and reducing energy demand. With an estimated global population of eleven billion people by the 21st century, the demand for concrete and common goods is expected to increase significantly (Rosković & Bjegović, 2005). Ordinary concrete typically contains about 60 - 80% aggregate by mass (Mamlouk & Zaniewski, 2014). By the year 2050, it is estimated that around eighteen billion tonnes of concrete are demanded (Mehta & Monteiro, 2006). Currently, the demand for conventional construction aggregates is around 11 billion tons per year (Golewski, 2019), valued at US$553 billion (ReportLinker, 2023) as of 2022, whereas the total waste of OPS is around 4.3 million tons annually. Since the density of OPS is roughly only a third that of conventional coarse aggregate, therefore, in terms of volume up to US$664 million of the conventional aggregate could be potentially saved annually by utilising OPS as aggregate in concrete.

Numerous researchers have investigated the use of Dure OPS in concrete concerning its mechanical and structural properties (Hamada, et al., 2020). In order for engineers to confidently employ OPS concrete (OPSC) as a viable construction material, the properties of OPS as an aggregate and OPSC must be comprehensively understood. Hence, this study has collected published content on the mechanical properties of OPSC up to the current state of progress and identified key factors that influence such properties. However, recent developments in high-yield oil palm fruit have resulted in a change in the physical

2

characteristics of OPS, referred to as Tenera OPS. The most notable change in physical characteristics is the shell thickness, which is reduced by an average of 57% compared to Dura OPS. However, a significant gap in the existing literature pertains to the lack of specific information regarding the variety of oil palm shells (OPS) used in most studies. Observations drawn from the thickness measurements and associated data suggest a prevailing tendency to employ Dura OPS. Notably, a considerable portion of OPSC research has been conducted within a closely connected network of academic institutions in Malaysia. This network is likely to have sourced OPS from a singular origin and conducted experiments in the same research facilities, potentially accounting for the prevalence of Dura OPS in these studies. Nevertheless, given that Tenera OPS exhibits different physical characteristics than Dura OPS, it is expected to affect the mechanical properties of OPSC. Additionally, while some researchers have discovered superior mechanical properties with crushed OPS, studies have solely focused on using OPS as coarse aggregate, and no investigation has yet been conducted on utilizing OPS as fine-sized aggregates.

This study aims to re-investigate the fundamental mechanical properties of OPSC by utilizing Tenera OPS as a replacement for both coarse and fine aggregates separately. The properties of coarse- and fine-sized OPSC (coarse and fine OPSC) were compared to those of normal weight concrete (NWC) with similar strength grades. The mix design for OPSC made with coarse-sized OPS (C-OPS) was developed by adapting certain parameters from previous research, with further modifications made to achieve the desired strength and density. In contrast, mix design for fine OPSC required novel methods. Initially, mortar cubes with fine-sized OPS (F-OPS) were produced using different treatment methods, including several proposed in this study. Subsequently, different F-OPS to total aggregate ratios followed by different cement contents were investigated to determine the final mix design for fine OPSC. Both coarse and fine OPSC were aimed to achieve a strength and density within the limits required to produce structural lightweight concrete (SLWC), in accordance with British Standard (BS) (BS EN 206, 2021). The study also investigated the influence of superplasticizer (SP) on the workability and compressive strength of both coarse and fine OPSC and compared them to those of NWC. With the selected mix designs, the three concretes with similar strength grades were evaluated and compared with respect to their fundamental mechanical properties from early ages up to 1 year. The tests included compressive strength, flexural tensile strength, dynamic and static modulus of elasticity, drying shrinkage, permeable voids, and water absorption properties under cured and air cured regimes. Additionally, ultrasonic pulse velocity (UPV) and microscopic analysis tests were performed alongside the mechanical tests.

3

1.1. Aim

The main aim of this research is to address the viability of Tenera oil palm shell (OPS) as an aggregate in concrete in terms of its fundamental mechanical properties.

1.2. Objectives

The objectives of this study are organized into two complementary parts:

A. Assessment of Tenera OPS and comparison with Dura OPSC:

1. To examine the physical and mechanical properties the Tenera OPS as fine and coarse aggregate and compare them to Dura OPS as coarse-sized aggregate.

2. To assess fine and coursed sized Tenera OPSC as a structural lightweight concrete (SLWC) and compare its performance with Dura OPSC and NWC at a 20 MPa grade strength.

B. Assessment of hardened properties:

1. To investigate and analyze key factors for the influence of superplasticizers (SP) in Tenera OPSC.

2. To compare the mechanical properties of fine and course Tenera OPSC to NWC over a period of one year.

To achieve these objectives, fundamental mechanical tests will be conducted on all three concrete types, with comparisons made between the results obtained from each concrete type at various time intervals exposed to cured and air cured regimes. The ultimate goal of this investigation is to determine the viability of using Tenera OPS in concrete production, both as a coarse and fine-sized aggregate, and to assess the long-term durability and strength of Tenera OPSC in comparison to NWC.

1.3. Novelty of Research

While previous studies have investigated the use of Dura OPS as a coarse aggregate in concrete, to the best of the authors knowledge, there is limited research on the use of Tenera OPS as coarse and fine aggregate in concrete. Given that Tenera OPS is thinner and weaker than Dura OPS, it can be crushed into fine-sized particles and used as a fine aggregate alongside conventional coarse aggregate. This approach can help eliminate the undesirable weak half-hollow-spherical thin shape of OPS, resulting in better mechanical performance and a more viable SLWC.

This novel approach of using Tenera OPS as a fine aggregate in concrete has the potential to improve the sustainability of concrete production by reducing the reliance on traditional aggregates and utilizing a by-product of the palm oil industry.

1.4. Research Questions

This study aims to address the following research questions:

1. What is the current state of knowledge on OPSC in terms of its mechanical properties, and are there any particular investigations on the new Tenera variety type OPS?

2. Can Tenera OPS as coarse aggregate in OPSC perform comparably to Dura OPS, as observed in previous research?

3. What treatment method is suitable for Tenera OPS to be used as a fine aggregate in concrete?

4. Does the mechanical performance of OPSC improve when Tenera OPS is used as a fine aggregate instead of a coarse aggregate?

5. How does the mechanical behavior of Tenera fine and coarse OPSC perform compared to that of NWC with similar grade strengths over the short- to long-term?

6. Is the utilization of Tenera OPS still viable for producing SLWC?

7. Can the deficiency in bonding between OPS and the cement matrix in OPSC be investigated through microstructural analyses?

By addressing these research questions, this study will contribute to a better understanding of the potential and limitations of Tenera OPS as a sustainable alternative to traditional aggregates in concrete production. Furthermore, the study's findings may provide insights into the development of effective and efficient methods for incorporating Tenera OPS into concrete and improving its mechanical performance.

1.5. Scope and limitations

The scope of this study includes a thorough investigation into the use of Tenera OPS as a sustainable alternative in the production of SLWC. The study thoroughly investigates and compares the physical and mechanical properties of Tenera OPS in both fine and coarse sizes. It evaluates Tenera OPS as an aggregate replacement for traditional coarse aggregates in SLWC. Furthermore, the study investigates Tenera OPS's potential as a fine-sized aggregate and assesses the impact of superplasticizers (SP) in both coarse and fine Tenera OPSC. Over a 365-day period, the experimental phase includes in-depth analyses

of microstructural characteristics, compressive strengths, flexural tensile strengths, modulus of elasticity, and drying shrinkages in a cured and air cured regime.

While this study aims to provide valuable insights into the application of Tenera OPS in concrete, some limitations must be acknowledged. The research focuses primarily on the properties and performance of Tenera OPS in the context of SLWC with a specific grade strength of 20 MPa after 28 days moist curing. Variations in concrete mix designs, environmental conditions, and grade strength can all produce different results. Furthermore, while the study focuses on the mechanical properties of Tenera OPSC, other specific characteristics such as durability under harsh environmental conditions, long-term behaviour, and potential economic considerations may necessitate additional research. Furthermore, the research does not address the production or scalability aspects of using Tenera OPS in the construction industry, which are potential future research areas. Finally, because the study's findings are based on laboratory experiments, their real-world applicability should be considered alongside practical considerations and local construction practices.

1.6. Thesis Overview

This thesis consists of five chapters as follows:

Chapter 1. Introduction

Chapter 1 offers an in-depth introduction to the research's background and motivation. It explores the oil palm industry, its environmental challenges, and the extensive production of oil palm waste, particularly OPS. The chapter outlines the thesis's central focus, which is to investigate OPS utilization as fine and coarse aggregate replacements in structural lightweight concrete, addressing their fundamental mechanical properties by comparing them to NWC with similar grade strengths. It also introduces the research objectives and underscores the research gap that drives this study.

Chapter 2. Literature Review

In this chapter, information on oil palm production is delved upon, providing key statistics, and outlining the environmental challenges posed by the extensive generation of oil palm waste. It highlights the potential solution of utilizing oil palm shells (OPS) as aggregate replacements in concrete to mitigate waste disposal issues. A detailed literature review examines the mechanical performance of oil palm shell concrete (OPSC) while identifying research gaps that motivate the novel work undertaken in this study.

Chapter 3. Methodology

Chapter 3 outlines the methodology adopted to achieve the study's objectives. It details the experimental procedures, including material characterization to assess their physical

properties. The chapter also explores the formulation of mix designs for normal weight concrete (NWC) and OPSC, both in coarse and fine aggregate configurations. These mix designs serve as the basis for subsequent testing and comparison of the fundamental mechanical properties. Furthermore, details for each testing method are outlined with references to code of standards.

Chapter 4. Results and Discussions

Chapter 4 presents the results obtained from the experiments and delves into in-depth discussions. The discussions aim to address the core research questions, shedding light on the implications of the findings and their significance within the context of the study.

Chapter 5. Conclusions and Recommendations

The final chapter encapsulates the main findings of the study, offering a concise summary of the research outcomes. Additionally, it provides recommendations for future research endeavours, building on the insights gained from this investigation.

Chapter 2. Literature Review

The purpose of this chapter is to review the past and current research on mechanical properties of OPSC, firstly by expounding upon the oil palm extraction process from which OPS is obtained and identifying key characteristics of OPS that may be primarily influencing concrete mix and strength in OPSC. The review is consequently divided into different sections, isolating each mechanical property of both fresh and hardened OPSC. Moreover, contemporary trends in OPS farming are discussed, specifically the changes in OPS shell characteristics, and how they may affect the future viability of OPSC, which is commented on summary section of this review.

2.1. Oil Palm Shell Characteristics

2.1.1. Oil Palm Tree and its Production

The oil palm tree, scientifically known as "Elaeis guineensis," is believed to have been used during the time of the Pharaohs in Egypt approximately 5,000 years ago (Cottrell, 1991). The tree, which originated in the East African jungle forest, thrives in tropical climates and is primarily grown for its oil (Loh, et al., 2013). It is now grown as a plantation-based industry in Southeast Asia, South America, and Sub-Saharan countries, with crude palm kernel oil and crude palm oil being the main products (Mielke, 2000). The tree's fruit resembles a plum, as shown in Figure 2.1, and it has an average planting cycle of around 25 years for optimal productivity (Pantzaris & Ahmed, 2002).

Figure 2.1 Palm tree and its fruit (Gar, 2019)

2.1.2.   Oil Palm Milling Process

The oil palm milling process typically consists of six parts:

- Extraction of palm fruits from trees in bunches.

- Sterilization of fruit bunches in airtight vessels to limit wounding and preserve oil.

- Threshing to separate the palm fruit from the fruit bunches.

- Digesting to separate the pulp (flesh) from the nut (shells) and crush the palm pulp.

- Pressing of the pulp to release the oil.

The palm oil is extracted from the fresh fruit bunches by a machinal process. Within the mechanical process, the nuts (shells) are separated by means of "cracking" and are then separated. A schematic overview of this process is seen in Figure 2.2 (a). Some of the wastes (OPS and fibre) are used for burning to produce energy. However, not all wastes are burnt. This is because most of the waste has high water contents and thus serves as a poor fuel without cumbersome prior drying. Moreover, when burnt at high water content, it presents considerable emission problems which are discouraged by the Malaysian government. The wastes are therefore mostly left unused in open lands, as evident in Figure 2.2 (b). This open disposal would eventually cause storage problems (Abdullah & Sulaiman, 2013).
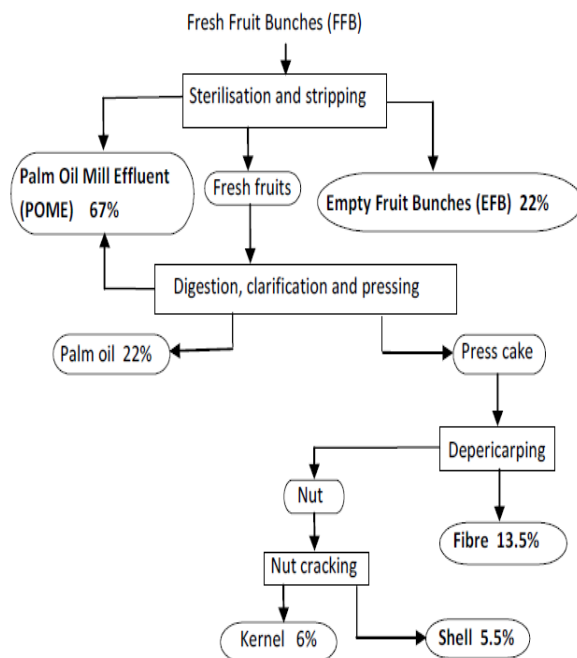
(a)

(b)

Figure 2.2 (a) Simplified process flow diagram of an oil palm mill (Abdullah & Sulaiman, 2013) (b) Dumping of OPS in open lands in Selangor, Malaysia.

2.1.3. Oil Palm Shell Varieties

One of the most principal factors worth mentioning is that the oil palm tree produces distinct types of fruit species that have varying shell thicknesses. There are two known species of the oil palm tree family (Arecaceae), *Elaeis guineensis* and *Elaeis oleifera* (less cultivated species) (Baudouin, et al., 1997). The *E. guineensis*, which is predominantly planted in Malaysia, is a monecious species, and mainly a hybrid between Dura and Pisifera, also known as the Tenera variety (Zulkifli, et al., 2010), see Figure 2.3. The Dura type is known to have a thick shell with thicknesses between 2 – 8 mm, while the Pisifera (sterile tree) is known to be shell-less. The hybrid type variety Tenera produces fruit with a very thin shell as seen in Figure 2.4. The thinner shell of Tenera with thicknesses between 0.5 – 4 mm, allows for 30% more extractable oil in the fruit part, called the Mesocarp/flesh/pulp compared to Dura (Lai, et al., 2012). The yielding and profit of the plantations of the Tenera and Dura types are presented in Table 2.1, clearly indicating that more oil may be extracted from the Tenera-type shells, leading to higher profits. In 2021 Singh et. al, mentioned that Malaysia started adapting the Tenera variety in the 1960s, and in 2017 the Tenera production has grown to 90.61% of the total oil palm tree harvest area compared to 8.09% for Dura and almost 2% for Pisifera (Singh, et al., 2021). It is therefore believed that the Dura type shells will be outsourced in the future.
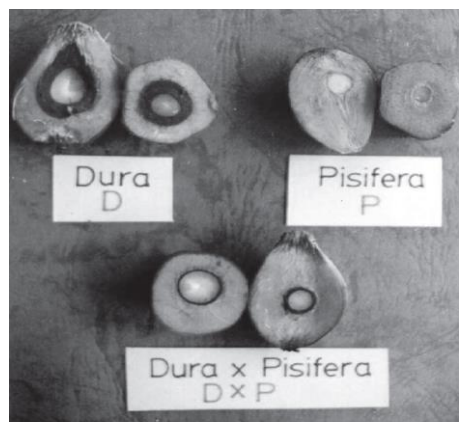
Figure 2.3 Commercial oil palm D x P hybrid seed production (Lai, et al., 2012)
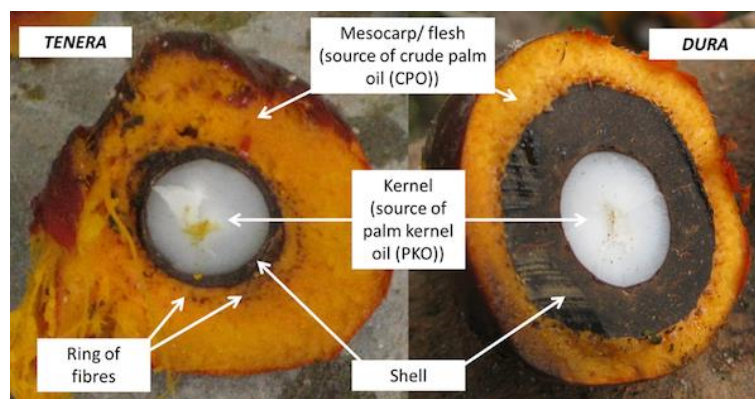
Figure 2.4 Tenera vs Dura (Lai, et al., 2012)

Nevertheless, based on the images and physical characteristics found in the literature, most of the research studied in this review fails to specify which OPS type was used. However, the images provided by research, one can identify that most researchers used the Dura type, for instance in Figure 2.5 (a). Thus, the Dura type shell has been primarily used in OPSC research. Since the Tenera shells are much thinner, the physical characteristics also alter, thus different mechanical behaviour is expected in concrete, see Figure 2.5 (b). For instance, a recent paper on OPS shows extremely subpar compressive strength, and it is likely Tenera OPS has been employed, although it cannot be confirmed (Azunna, 2019). Singularly, Yew et al. (Yew, et al., 2014a) found Dura OPSC to be considerably stronger in compression than Tenera OPSC. It is therefore crucial to re-examine the fundamental mechanical behaviour of Tenera OPSC.

Table 2.1 Oil production in plantations with two types of planting materials (Woittiez, 2019)

	Tenera	Dura
Total oil yield (t/ha)	5.5	3.8
Selling price for farmers	3600 US$/ha	3600 US$/ha
Selling price for mill	4290 US$/ha	2964 US$/ha
Profit for mill	690 US$/ha	-636 US$/ha

(a)　　　　　　　　　　　　　　　(b)
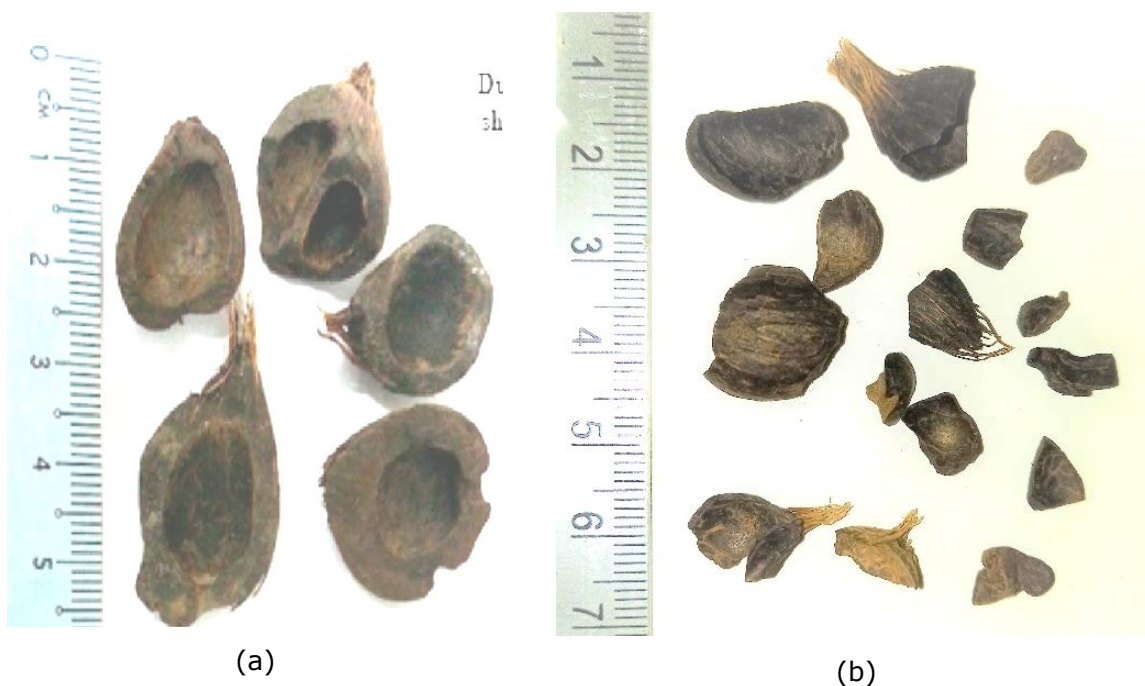
Figure 2.5 (a) Dura shells from (Yew, et al., 2021) and (b) Tenera shells (used in this study)

2.1.4.　Implementation of OPS in Concrete

In most early investigations on OPSC, researchers were eager to improve the mechanical properties of OPSC. This was mostly done by improving its mix proportions. Since OPS is classified as a lightweight aggregate (LWA), the procedure for mix design will be different from normal weight aggregates (NWA) (Kovler & Roussel, 2011). Mannan et al. confirmed

that the ACI method for the LWC is not applicable for OPSC. They therefore used trial and error tests with different mix proportions and concluded to have reached an acceptable mix design with a 28-day compressive strength of 24 MPa (Mannan & Ganapathy, 2001a). However, this was only achieved with a high cement content of 480 kg/m^3. With such high cement contents in NWC, strengths between 40 - 50 MPa could be achieved (Mehta & Monteiro, 2006). This is mainly because OPS is weaker than NWA (Okpala, 1990), it therefore requires higher cement content (Kosmatka, et al., 2002). Mix proportions of OPSC are further explained in Section 2.2.3 and outlined in Table 2.5. The characteristics of the OPS has the same density to other LWA, such as pumice and expanded clay, where the weight is around 60% less against conventional coarse aggregate, see Table 2.3. Subsequently, concrete made with OPS falls below 2000 kg/m^3. This indicates that OPSC is within the density requirements of lightweight concrete (LWC) according to both (ACI Committee 213R-14, 2014) (1120 – 1920 Kg/m^3) and by (BS EN 206, 2021) (800 – 2000 kg/m^3). Because of its low-density value compared to NWC, its use is appealing due to the reduction of the structural dead load. Further on this matter is explained in Section 2.2.4. Researchers today have further enhanced physical and mechanical properties such as the compressive strength of OPSC (Shafigh, et al., 2011b). High strength lightweight aggregate concrete (HSLWC) of OPSC has been produced with compressive strengths over 50 MPa, with a cement content of 550 kg/m^3, superplasticizers (SP), and 5% of silica fume (SF) (Yew, et al., 2015b).

2.1.5. Physical Properties of OPS

Arguably the most important factors that may alternate the mechanical properties of OPSC are the physical properties of the OPS itself (Alengaram, et al., 2013a). Since the OPS is extracted from milling machines, the shape of the OPS can alter depending on how it is extracted or broken. The most common shapes are reported to be irregular flaky, circular, angular, and/or polygonal, with shell thickness ranging from 0.25 – 8 mm and possessing spiky and rough broken edges (Prusty & Patro, 2015). The texture is reported to be 'fairly smooth' on both inner and outer side of the shell with colours varying from black to dark grey (Shafigh, et al., 2010). With such physical characteristics, a good workability is expected, albeit with low bonding propensity to the cement matrix, which is discussed in detail in Section 2.2.5. A key factor to mention is the size distribution of the OPS. Data has been collected from researchers having performed sieve analysis on OPS and is shown in Table 2.2 and plotted in Figure 2.6. Also, the average fineness modulus is reported to be 6.04 (Table 2.3), which is in the normal range of coarse aggregates (Neville, 1995).

Table 2.2 Grading of OPS aggregate

Reference	Passing through sieve size (mm)							
	20	12.5	9.5	8	4.75	3.35	2.36	1.18
(Mannan & Ganapathy, 2002b)	100	92.86	72.22	-	9.65	-	1.03	0.34
(Shafigh, et al., 2011d)	100	100	78.49	-	22.5	-	4.74	1.76
	100	100	100	-	24.17	-	5.64	2.04
(Shafigh, et al., 2011b)	100	96.37	83.26	59.17	13.68	-	1.02	0.49
	100	100	100	92.39	27.87	-	10	0.43
(Shafigh, et al., 2012)	100	100	100	-	27.9	10	0.4	-
(Shafigh, et al., 2014a)	100	-	99.8	-	2.2	-	0	0
(Jumaat, et al., 2015)	100	100	67.1	-	4	0	0	0
(Aslam, et al., 2015)	100	96.80	84.24	61.20	2.98	-	-	-
(Farahani, et al., 2017)	100	96.85	81.5	-	13.91	2.46	-	-
Average	100	98.1	86.7	70.9	14.9	4.2	2.9	0.7
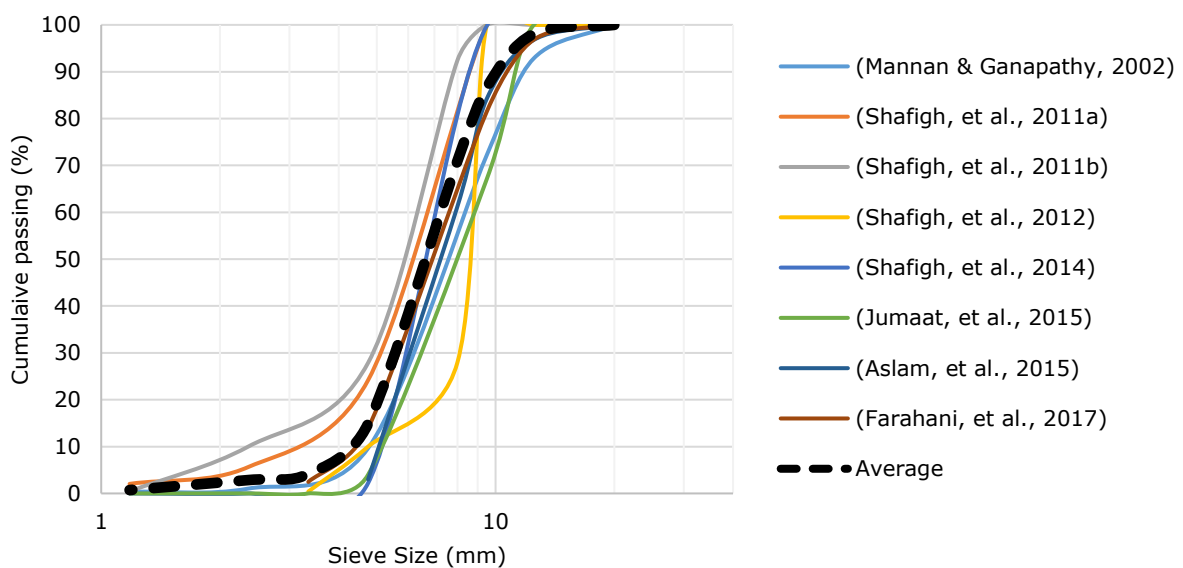
Figure 2.6 Grading of OPS from various researchers

Shafigh et al. (Shafigh, et al., 2012) investigated crushed OPS (not fine sized) with uncrushed OPS at 28 days and made the following highlights:

- Crushed OPS have 55% higher compressive strength than uncrushed OPS (34 MPa vs 53 MPa).

- Splitting tensile strength of crushed OPSC is much higher by 24% than uncrushed OPS (2.8 MPa vs 3.5 MPa).

- Flexural tensile strength of crushed OPS is significantly higher than uncrushed OPS by 66% (4.4 MPa vs 7.0 MPa).

- The sensitivity of crushed OPS in poor curing is much lower than uncrushed OPS.

Similarly, Yew et al. (Yew, et al., 2014b) also studied the effects of crushed OPS with uncrushed OPS. Yew found an increase of 19% in compressive strength for crushed OPS compared to uncrushed, which is significantly lower compared to Shafigh et al. This might be since Yew et al. studied the OPS at different age categories of 3 – 5, 6 – 9 and, 10 – 15 years old OPS, whereas Shafigh et al. did not mention the age of the OPS. However, as seen from Figure 2.7, a difference in distribution can be seen of the crushed OPS, where Yew, et al. has a gap graded size distributing of the crushed OPS.
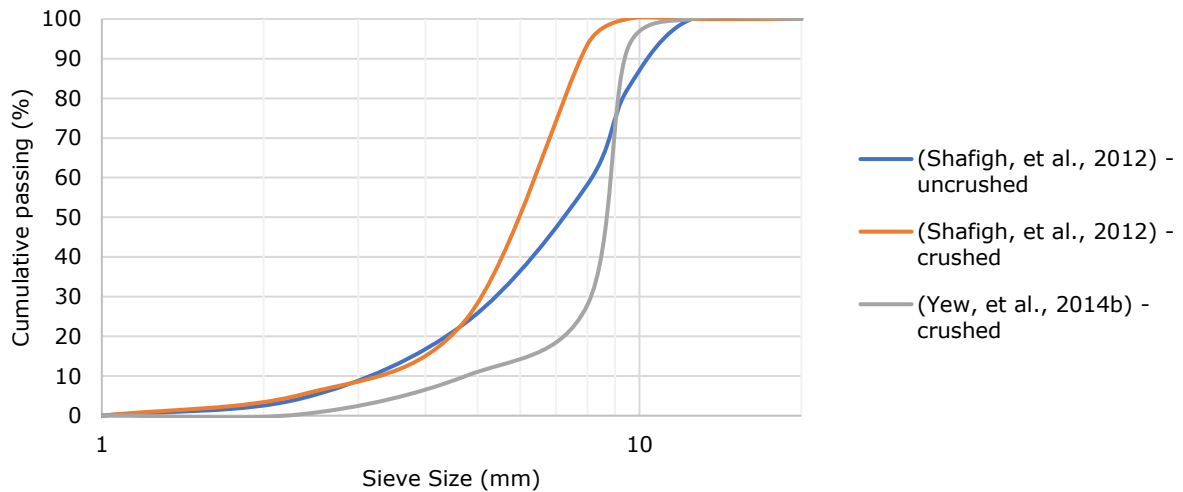
Figure 2.7 Sieve Analysis of crushed and uncrushed OPS (Shafigh, et al., 2012) & (Yew, et al., 2014b)

Both authors theorized the increase in compressive strength of crushed OPS is due to a reduction of the smooth surface from both the interior and exterior of the OPS. Furthermore, the crushed OPS will have a different shape, especially at the jagged, rough edges, potentially creating a better area for bonding with the cement matrix, see Figure 2.8 (a).

(a)   (b)
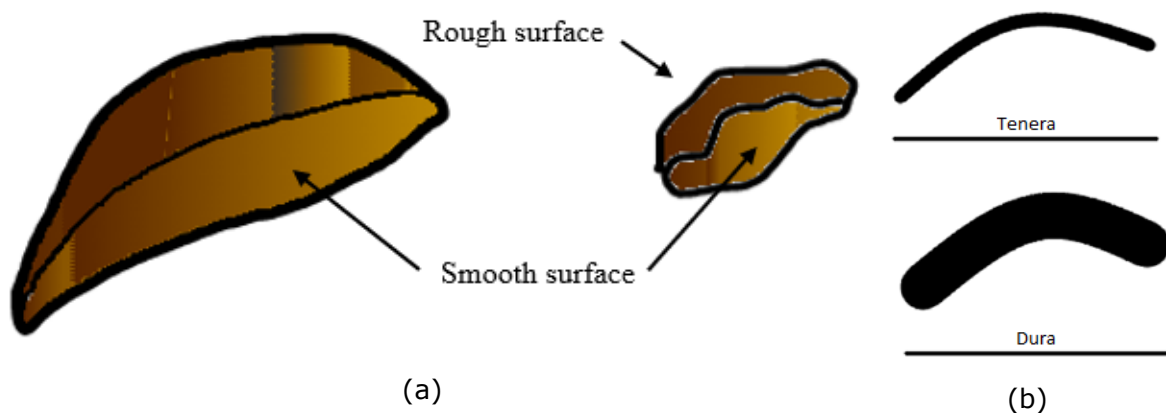
Figure 2.8 (a) Uncrushed (left) and crushed (right) OPS (b) Cross-sectional illustration of the thickness difference of Tenera (left) and Dura (right) OPS shells, despite similar height and width dimensions

14

Nevertheless, the sieve analysis only accounts for the general overall shape of the OPS and the thickness of the shells is not primarily distinguished. Different thicknesses of same shell size can pass through the same sieve size, as illustrated in a sketch seen in Figure 2.8 (b). Hence, sieve analysis may not be a good measurement of OPS characteristics as aggregates, and average (or range of) OPS shell thicknesses would need to be determined to ensure accurate, translatable mechanical effects in OPSC.

Keshvadi et al. (Keshvadi, et al., 2011) categorized the oil palm fruit into three different bunches, namely the 'top', 'middle', and 'bottom', to separate their approximate height locations on the fruit trees. They primarily found that the ripeness of the fruit makes a significant difference to the crushing strength it can withstand, and subsequently the location of the oil palm fruit on the tree will affect its stage of ripeness and thus its crushing strength. Furthermore, the authors noted that the mean loading force of the Tenera shell before failure was approximately 838 N but could reach as high as 1472 N for the top bunch. This was tested using a Universal Testing Machine (UTM) with a cylindrical probe having a soft tip (Keshvadi, et al., 2011). It is difficult to ascertain the stress the oil palm fruit can handle, as the curvature of the fruit and roughness of its surface area may not provide complete contact area for the soft tip. However, 838 N subjected a diameter of 6 mm would give a stress of approximately 30 MPa. According to Yang and Huang (Yang & Huang, 1998), theoretically most LWA fall in the range of 15-30 MPa, hence OPS is viable as a coarse aggregate, but this does not explain its subpar performance when implemented in concrete. Abbas et al. (Abbas, et al., 2006) subjected oil palm fruit to thermal softening via constant steam pressure of 40 MPa and temperatures of 140 °C for 1.5 hours. This is to simulate the sterilization process undergone by the fruit milling. They performed Textural Profile Analysis (TPA) using a 2 mm steel probe and found the hardness of the Tenera oil palm kernel was reduced by 97% post sterilization (154 N for fresh vs 67 N for sterilized), and cohesiveness of the shell was down to 0.66 from 0.94 (Abbas, et al., 2006). As most OPS used in concrete is a waste product, it has also been subjected to sterilization, which would similarly reduce its ability to withstand deformation, possibly to below the 15 MPa of most acceptable LWA (Yang & Huang, 1998). Yew et al. (Yew, et al., 2014b) managed to achieve exceptionally high compressive strengths on Dura OPS based concrete, where the palm fruits were extracted from 10 - 15-year-old oil palm trees, and were not sterilized but rather just air-dried, correlating with the aforementioned-physical characteristics.

As the primary concern of the oil palm industry is high yield effective extraction of oil, a reduction in the hardness of the shell would ease the milling process, albeit would result in weaker shells that are not conducive as an LWA. Noteworthy, to the authors knowledge, almost none of the researched literature on OPSC conducted detailed textural analysis,

hardness, or cohesion tests on OPS before their incorporation in concrete, similar to the absence of information on the type of OPS being used. Okpala (Okpala, 1990) attempted to determine the abrasion and crushing value of OPS (sourced in Nigeria, in 1990), and concluded that typical tests for aggregates are not appropriate for the shell, however their shells showed high resistance to abrasion. This appears to be a glaring omission and significantly holds back any meaningful implementation of OPS in concrete, as relative to typical mineral based LWA (such as expanded shale, clay, etc), organic OPS can vary considerably in its hardness and strength characteristics due to its natural, chemical molecular makeup. This results in unclear performance of OPSC, which is illustrated and discussed in detail in Section 2.2.3.

2.1.6. Water Absorption of OPS

Another crucial factor that can alternate the mechanical properties of OPSC is the water absorption of OPS. When water is captured by the aggregate in the voids, it is not available for the cement to hydrate, or to improve the workability of plastic concrete (Mamlouk & Zaniewski, 2014). LWA's normally have higher water absorption than the conventional aggregate, as LWA are porous and absorbs water into their interiors, whereas solid NWA adsorb water mostly on the surface (Chandra & Berntsson, 2002). For NWA, the water absorption is normally between 0.5 – 1% (Neville, 1995). However, in the case of LWA, since the porosity differs depending on the material, the difference in water absorption between different LWA could be high compared to NWA. Many pores are exhibited in OPS as seen in Figure 2.9, mainly due to its organic origin with sizes of around 23 µm.
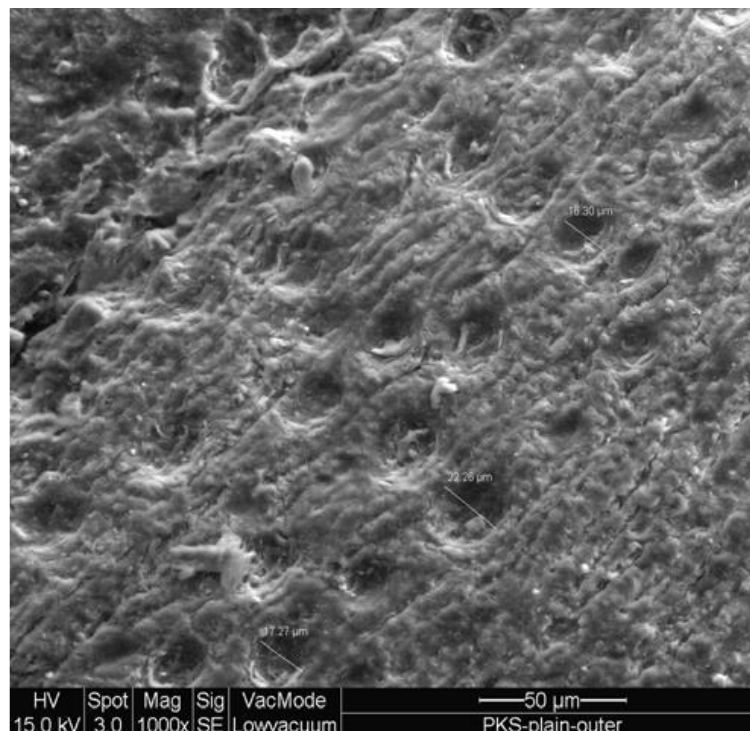
Figure 2.9 Micro-pores on outer surface of OPS (Alengaram, et al., 2013a).

16

The lowest water absorption is reported to be 18.7% and the highest 33% as seen in Table 2.3. While the main reason for high absorption rate is due to the porosity of OPS, the variance in water absorption between research may be owing to the distinct species type, age of samples, climate of area cultivated, dryness of samples, human error, etc. Additionally, the sterilization process from the milling of oil palm fruit may also affect the porosity and water absorption capacity of OPS. Many researchers have treated the OPS by cleaning it with a detergent to remove dirt and other unwanted materials (such as loose fruit fibres), and used the OPS aggregate in a saturated surface dry (SSD) state in the mix to avoid the shells taking away the water required for the cement (Hamada, et al., 2020). However, no specific research has directly evaluated if such treatment is necessary or effective with regards to OPSC's mechanical properties. Having said that, by bringing OPS at SSD state, authors have observed acceptable mechanical properties of OPSC. Furthermore, there have been no direct reported measurements to observe if water has been diverted from the cement hydration by the absorption of the OPS when used in dry state as well, which is not a simple endeavour. One issue important to mention regarding the range of water absorption values (18.7 – 33.3%) is that most researchers use the method by weight, which can lead to a false similarity of experiment. As OPS is regularly used in SSD conditions, the exact water absorbed by the shell may vary depending on the shell characteristics (e.g., amount of pores, dryness) leading to a different proportion of volume mix, as well as free water content in the OPSC mix.

Table 2.3 Physical properties of OPS from various researchers

Reference	Water absorption (%) 24 Hrs.	Fineness modulus.	Density range (Kg/m³)	
			Loose	Comp.
(Abdullah, et al., 1984) (Okafor, 1988) (Okpala, 1990) (Basri, et al., 1999) (Mannan & Ganapathy, 2001a) (Mannan & Ganapathy, 2002b) (Mannan & Ganapathy, 2004) (Mannan, et al., 2007) (Teo, et al., 2007) (Alengaram, et al., 2008a) (Jumaat, et al., 2009) (Teo, et al., 2010) (Gungat, et al., 2013) (Noor, et al., 2017) (Huda, et al., 2016) (Shafigh, et al., 2011d) (Ting, et al., 2020) (Shafigh, et al., 2012) (Yap, et al., 2013) (Shafigh, et al., 2014a) (Ahmmad, et al., 2014) (Islam, et al., 2016) (Alengaram, et al., 2011a) (Alengaram, et al., 2013b) (Yap, et al., 2014) (Mo, et al., 2014a) (Gibigaye , et al., 2017) (Anuar, et al., 2017) (Yap, et al., 2017) (Khankhaje, et al., 2016) (Foong, et al., 2015)	18.7 – 33.3	5.78 – 6.41	500 - 600	512 - 740

2.2. Hardened Properties of OPSC

The concrete's mechanical properties evaluate its performance by doing investigations such as compressive strength, flexural tensile strength, modulus of elasticity, and drying shrinkage. Improvement in compressive strength of concrete will in most cases improve its mechanical properties (Mamlouk & Zaniewski, 2014).

All three mix ingredients of concrete (cement, water, and aggregates) have an influence on the properties of concrete. In NWC, the compressive strength mostly depends on the specifics of the cement paste. However, in the case of LWC, it is mostly dependant on the characteristics of the LWA (Newman, 1993).

As mentioned earlier, in 1984 Abdullah et al. commenced research on utilizing OPS as coarse aggregate in concrete (Abdullah, et al., 1984). By replacing 100% of the conventional coarse aggregates with OPS, he conducted 28-day compressive strength tests where he obtained results for up to 20 MPa. The author referred to OPS as "the hard-stony endocarp but are lightweight and naturally sized." He further added, when used in concrete mix, the waste product does not infect or make toxic substances due to organic origin. Four years later, Okafor also investigated OPS as a coarse aggregate in concrete (Okafor, 1988). Okafor found comparable results to Abdullah, however by refining the cement, water, and fine aggregate content, 28-day compressive strengths up to 30 MPa was achieved whilst having a density of 1758 kg/m^3. Just two years later, (Okpala, 1990) did similar mix proportions as Okafor and confirmed similar results, further verified by (Abdullah, 1997). This encouraged other researchers in the coming years to investigate OPSC for its physical, concrete liquid state, concrete hardened state, mechanical, structural, and durability properties. Some have even made applications such as a footbridge and a small house from OPSC (Teo, et al., 2006b).

2.2.1. Water-cement Ratio of OPSC

A direct relation exists between the w/c ratio and the strength of the concrete (Kosmatka, 2006), where lower the w/c ratio, stronger the concrete, albeit less workable in fresh state. Typically, LWA are saturated prior to mixing so as not to absorb any amount of water that effects the w/c ratio content of the fresh concrete as well as the workability. OPS has been reported to not deteriorate the concrete (Abdullah, et al., 1984), however this author did not substantiate this claim with any evidence. Adding additional water above the required content, is not a solution since the OPS would not immediately absorb all the water it can as is shown by (Katte, et al., 2022) that it would take at least 7 – 8 hours to absorb 90 – 95% of that of 24 hours. However, a study showed that LWA, specifically sintered fly ash aggregate Polly-tag, if left to absorb water for a specific set of time and then used in the mix, could enhance the adhesion of cement paste resulting in higher strengths of concrete,

along with better durability (Domagala, 2015). Seemingly interesting, no studies have investigated such experiments on OPS.

Also, high w/c ratio, different specific gravity of materials, and/or incorrect proportion of concrete mix ingredients may cause bleeding (Tyler, 1956). However, in the case of LWC, bleeding is expected to be less than NWC. This is because in LWC, part of bleeding water will move in the pores of the LWA. Unlike the conventional aggregate where the bond is on the surface, LWA retains water internally, which may increase bleeding upon mix agitation (Chandra & Berntsson, 2002). It is also observed that the amplitude of bleeding can be reduced by using viscosity agents before setting time. The agents can thicken the water, thus slowing down the bleeding process (Khayat, 1998). One of such agents, ground granulated blast furnace slag (GGBFS), was found to increase the viscosity of a concrete mixture with OPS. The floating of the OPS aggregates is prevented which minimizes the occurrence of bleeding in the concrete (Shafigh, et al., 2013b). A report by (Muthusamy, et al., 2015) mentioned when high amount of water is added to the concrete mix with OPS, excessive bleeding occurred, due to the segregation of the lightweight OPS aggregates (which float to the top) and sand components from the mix, ultimately resulting in a top surface layer of cement-OPS. The author concluded that when low amount of sand is used in the mix, segregation and bleeding would occur. In addition, when excessive amount of SP is used, it could cause severe bleeding (Ting, et al., 2020).

Since OPS has high water absorption, Mannan et al. (Mannan, et al., 2006) pre-treated OPS aggregates with different solutions such as polyvinyl alcohol (PVA), and exposed OPS to severe environmental conditions incorporating alkaline (NaOH), acidic (H_2SO_4), and sulphatic ($MgSO_4$) compounds, where OPS aggregates were soaked for 7 days in the respective solutions, specifically 1 mol of sodium hydroxide (NaOH), 0.1 mol of sulphuric acid (H_2SO_4), and 5.2% of magnesium sulphate ($MgSO_4$). The authors observed the possibility to decrease the water absorption of the OPS aggregate by 82% by pre-treating OPS with 20% PVA solution, which may have resulted in stronger adhesion between the OPS and cement paste. However, the author did not further analyse the results via microscopic images to see the surface effect of the OPS after treatment. However, in a subsequent study by (Traore, et al., 2018), treatment experiments on OPS were done to find the effect on physical and mechanical properties of OPSC. The study focused on OPS treatment with lime (CH), sodium silicate (SS), polyvinyl alcohol (PVA), heat treatment (TH) and OPS as SSD state. Traora confirmed the same findings for PVA having the lowest water absorption on OPS as done by Mannan. The author mentioned that the PVA made a thick coating on the OPS, which explains the reduction in water absorption, evident in SEM images as seen in Figure 2.10. However, the author concluded that the CH treatment showed the highest improvements in mechanical properties compared to the control OPSC

and other treatments. They mentioned that the CH treatment improved the adherence between the treated OPS and cement paste, verified by having the highest flexural strength result. A study by (Nadh, et al., 2021) used nano silane as a coating for OPS to reduce the water absorption. The nano coating reduced the water content from 23% to 8%. The nano coating made the pore diameter of OPS to be 0.5 – 1.5 micrometres compared 2 – 5 micrometres of conventional aggregates.
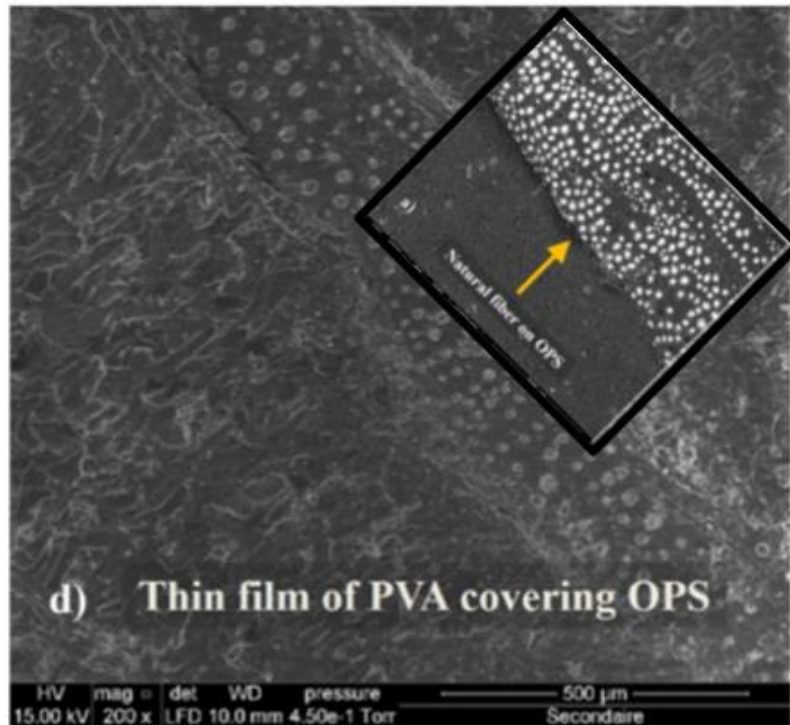
Figure 2.10 SEM images of OPS surface after PVA treatment compared to untreated (Traore, et al., 2018).

2.2.2.   Workability of OPSC

Several researchers have tried to increase OPSC strength by reducing the water content, which can lead to a practicality issue, namely low workability. To ensure a concrete mix can be handled with ease to properly fit the formwork, the workability of the mix must be controlled. Thus, the quantity of water present in the mix should be of proper ratio. However, the physical shape of the coarse aggregate also plays a vital role (Neville, 1995). A slump of 50 – 75 mm is deemed adequate for structural LWC compared to a slump of 100 – 125 mm for NWC (Mehta & Monteiro, 2006).

Employing OPS in an SSD-state prior to mixing allows for controlling mix workability, however an increase of OPS content decreases the mechanical strength of OPSC (Hamada, et al., 2020), while the low content of OPS in the mix does not significantly impact slump, as summarized in Table 2.4. Additionally, Alengaram, et al. mentioned that the size and proportion of OPS used in the mix did not cause any change in the workability (Alengaram,

et al., 2010a). A report by (Yew, et al., 2014a) mentioned when OPS is heat treated at 150 °C for 1 hour, the workability is improved by 20%. The author mentioned that the cause of this is because "heat treatment decreases the swelling–shrinkage of wood, which in turn increases its dimensional stability and durability, permeability, quality of surface treatment, as well as decrease equilibrium moisture content". However, the author didn't quantifiably confirm the shrinkage of OPS. Other authors increased the workability by pre-treating OPS with PVA solution (Chai, et al., 2014), (Mannan, et al., 2006) and (Traore, et al., 2018).

Table 2.4 Slump test results (cement: sand: OPS)

Reference	Mix proportion (C: S: OPS)	w/c	Slump (mm)
(Abdullah, et al., 1984)	1:2:0.6	0.40	0 – 260 mm
(Okafor, 1988)	1:1.70:2.08	0.48	8
	1:1.88:2.18	0.54	28
	1:2.1:1.12	0.65	50
(Okpala, 1990)	1:1:2	0.5 –	3 – 80 mm
	1:2:4	0.8	(Collapsed at w/c: 0.7 and 0.8)
(Mannan & Ganapathy, 2001a)	1:1.69:0.76	0.41	7
(Teo, et al., 2007)	1:1.66:0.60	0.38	60
(Mahmud, et al., 2009)	1:1:0.8	0.35	160
(Alengaram, et al., 2010a)	1:1.2:0.80	0.35	105

Generally, good workability is seen with OPSC since OPS has a smooth surface (Shafigh, et al., 2010). Other investigators achieved higher slump values by incorporating admixtures (Alengaram, et al., 2010b). When adding different amounts of SP of 1 – 2% by weight of cement, the OPSC slump value was increased fourteen times relative to control (Mannan & Ganapathy, 2004). Other investigators also studied the flexural strength of OPSC when adding fibres to the mix, and it has been shown that the workability decreases when adding steel fibres to the mix (Mo, et al., 2017a). In a later study by the same authors (Mo, et al., 2015b) a study was done on adding acrylic fibres and showed a reduction in the workability. This is the same when adding Polypropylene-fibre (PP-fibre) according to (Yew, et al., 2015c).

Thus, there is no consensus on the effects of OPS on concrete workability. This may be owing to variations in the type of OPS used, resulting in varying volumes of added OPS (of same weight), along with different porosity and hence water absorption capabilities. However, the author of this present review cannot confirm this hypothesis, due to limited provided data on the specific characteristics of OPS that are suspected to affect workability.

2.2.3. Mix Design Ratio of OPSC

Any type of concrete needs a mix proportion recipe or a formula according to specifications. This is known by making different proportions to achieve essential properties of both fresh and hardened concrete (Kosmatka, et al., 2002). Since LWA from waste materials are typically weaker than NWA, higher cement contents must be used while water reducing

admixtures can be used to keep the w/c ratio low. To achieve different ranges of compressive strengths, trial mixes with cement is often necessary in research. The cement content is constant with relation of the strength (Chandra & Berntsson, 2002). A "structured mixture proportioning for oil palm kernel shell concrete" was conducted by (Gibigaye , et al., 2017) and concluded that the mix proportions of 1:1.60:0.96 and 1:1.53:0.99 (cement: fine aggregate: OPS) with a w/c of 0.45 made appropriate results for workability, density and compressive strength, based on recommendations by ACI and BS Code for structural LWC. Results of various researchers employing mix proportion designs of OPSC with full replacement of coarse aggregates by OPS are summarized in Table 2.5.

Table 2.5 Mix Designs of OPSC

Reference	Cement	Fine Aggregate	OPS	Water	28 Day Strength
	Kg/m³				MPa
(Okafor, 1988)	335	569.5	696.8	160.8	24.00
	314	590.32	684.52	169.56	23.50
	295	619.5	330.4	191.75	18.00
(Basri, et al., 1999)	480	820.8	369.6	196.8	24.20
(Mannan & Ganapathy, 2001b)	480	576	470.4	196.8	24.00
(Mannan & Ganapathy, 2001a)	325	552.5	552.5	211.25	7.30
	340	540.6	540.6	210.8	9.90
	480	576	470.4	259.2	10.40
	520	644.8	449.8	197.6	20.00
	520	556.4	509.6	187.2	18.75
	565	463.3	502.85	214.7	18.60
	600	492	438	246	20.25
(Mannan & Ganapathy, 2002b)	400	740	400	192	19.80
	400	756	408	180	21.30
	400	764	412	172	21.80
	400	752	404	184	19.80
	420	722.4	394.8	201.6	20.70
	420	739.2	399	189	21.20
	420	747.6	403.2	180.6	20.90
(Teo, et al., 2006b)	510	848	308	193.8	28.10
(Teo, et al., 2007)	490	842.8	294	200.9	14.50
	490	862.4	294	191.1	17.00
	500	825	290	205	15.50
	500	850	290	195	20.00
	510	877.2	290.7	178.5	24.50
	510	877.2	295.8	178.5	24.50
	510	877.2	306	178.5	25.00
	510	846.6	306	178.5	28.50
	510	836.4	306	183.6	28.50

22

Reference	Cement	Fine Aggregate	OPS	Water	28 Day Strength
		Kg/m³			MPa
	510	846.6	285.6	193.8	28.00
	520	785.2	291.2	213.2	20.50
	520	863.2	842.4	182	24.00
	530	773.8	291.5	185.5	26.50
	530	769	339	217	21.00
	550	688	292	193	27.50
	550	842	292	182	28.50
(Alengaram, et al., 2008a)	530	424	530	186	23.70
(Mahmud, et al., 2009)	596	596	477	209	26.98
(Shafigh, et al., 2011a)	500	868	360	190	39.34
(Shafigh, et al., 2011b)	500	780	420	174	42.49
(Alengaram, et al., 2011a)	560	446	560	196	22.50
	596	596	477	209	26.00
(Shafigh, et al., 2011d)	550	950	281	234	45.54
	550	950	273	234	46.15
	480	1050	295	182	47.22
	520	852	364	177	46.35
	520	746	420	177	42.75
(Shafigh, et al., 2012)	550	891	333	192	41.38
	500	726	435	177	43.25
(Yap, et al., 2013)	530	970	320	159	34.80
(Shafigh, et al., 2013b)	500	780	420	175	42.50
(Mo, et al., 2014a)	550	780	360	165	37.00
(Yew, et al., 2014a)	540	920	350	167	48.52
(Yew, et al., 2014b)	550	860	380	165	46.90
(Shafigh, et al., 2014a)	500	980	310	190	37.80
(Mo, et al., 2014c)	550	935	358	182	45.10
(Yew, et al., 2015a)	530	920	340	155	42.89
(Yew, et al., 2015b)	550	920	350	160	49.70
(Foong, et al., 2015)	550	890	370	193	46.43
(Mo, et al., 2015a)	520	940	400	170	33.30
(Yew, et al., 2015c)	520	960	330	156	40.90
(Mo, et al., 2015c)	470	850	425	200	25.30
(Islam, et al., 2015)	565	960	368	170	41.80
(Aslam, et al., 2015)	480	890	360	173	36.90
(Serri, et al., 2015a)	400	721	525	160	20.28
	375	675	567	150	19.99
	350	632	607	140	18.61
(Serri, et al., 2015b)	300	516	699	124	11.56
	300	539	692	124	9.00
	300	570	678	124	10.50
	350	595	623	140	16.50
	350	630	609	140	16.00

23

Reference	Cement	Fine Aggregate	OPS	Water	28 Day Strength
	Kg/m³				MPa
	350	666	592	140	16.70
	400	679	544	160	17.00
	400	721	525	160	18.00
	400	760	508	160	21.50
	450	764	463	180	23.00
	450	811	441	180	24.00
	450	854	423	180	22.50
	500	850	375	200	26.50
	500	899	360	200	26.00
	500	951	335	200	28.00
(Mo, et al., 2016c)	550	935	355	180	45.10
(Aslam, et al., 2016)	480	890	360	173	36.00
(Islam, et al., 2016)	565	960	368	170	40.00
	565	960	368	226	34.80
(Yahaghi, et al., 2016)	480	805	159	168	47.38
(Ahmmad, et al., 2016)	466	847	373	165	43.09
(Farahani, et al., 2017)	500	945	324	180	39.90
(Aslam, et al., 2017)	480	890	360	173	36.94
(Mo, et al., 2017a)	515	950	410	160	34.50
(Mo, et al., 2017b)	540	990	375	165	34.04
	400	840	420	180	10.04
	400	800	440	180	7.36
	400	764	460	180	10.68
	400	732	476	180	13.40
	400	700	492	180	14.46
	400	672	504	180	12.83
	450	792	396	202.5	12.92
	450	751.5	414	202.5	16.26
	450	720	432	202.5	18.23
	450	688.5	445.5	202.5	22.42
	450	661.5	463.5	202.5	11.50
(Gibigaye , et al., 2017)	450	634.5	477	202.5	11.34
	500	780	350	225	14.69
	500	740	370	225	21.74
	500	705	390	225	14.50
	500	675	405	225	14.40
	500	645	420	225	16.08
	500	620	430	225	11.90
	550	770	308	247.5	18.00
	550	726	330	247.5	18.55
	550	693	346.5	247.5	21.24
	550	660	363	247.5	14.80
	550	627	379.5	247.5	14.72

Reference	Cement	Fine Aggregate	OPS	Water	28 Day Strength
	Kg/m³				MPa
	550	599.5	390.5	247.5	14.76
(Tjahjono, et al., 2017)	500	860	273	225	16.27
(Akmal, et al., 2017)	500	800	360	225	26.00
(Traore, et al., 2018)	550	913	330	220	28.44
(Mo, et al., 2018)	540	925	380	189	39.32
(Maghfouri, et al., 2018)	550	470	466	182	40.50
(Krishnamurthy & Vandanapu, 2019)	550	553.6	415.2	302.5	10.10
	550	552.7	362.3	330	11.40
	550	433.3	371.9	357.5	13.50
(Ting, et al., 2020)	520	715	455	171.6	38.88
(Muthusamy, et al., 2021)	500	700	300	175	29.58
(Rahman, et al., 2020)	500	860	273	175	22.09
(Yew, et al., 2021)	530	900	340	186	44.59
(Maghfouri, et al., 2021)	480	819	406	163	40.50
(Loh, et al., 2021)	515	1000	290	170	25.02
(Nadh, et al., 2021)	480	715	382	240	10.40
	480	715	382	264	11.60
	480	715	382	288	13.70
	480	715	382	154	24.60
(Yew, et al., 2022)	510	905	350	153	46.50
Min	**295**	**433.3**	**159**	**124**	**7.30**
Max	**600**	**1050**	**842.4**	**357.5**	**49.70**

The data in Table 2.5 indicates that higher cement content with a low w/c ratio, higher fine aggregate content, low OPS content corresponds to a variable compressive strength, ranging from 7.3 – 49.7 MPa. Researchers have used cement contents from 295 up to 600 kg/m³. The data verifies the literature from previous sections in this review concerning the cement, sand, OPS, and water content. Yew et al. (Yew, et al., 2015b) achieved the highest strength as of this review, with OPSC with a result of 49.7 MPa in 28 days and 50.5 MPa in 56 days. Yew used 550 kg/m³ of cement, 920 kg/m³ of fine aggregates, 350 kg/m³ of unsterilized Dura-OPS, superplasticizers, and a w/c of 0.29 (ratio of 1:1.67:0.64 (cement: fine aggregate: OPS)). The OPS was crushed, heat-treated (60 °C for 0.5 hours) and used as SSD state in the mix. The mix ratio by Gibigaye et al. is similar to Yew, but only reached peak 28-day compressive strength of 21.74 MPa (Gibigaye , et al., 2017), illustrating the necessity of analysing OPS characteristics prior to application in mixes. Furthermore, histograms of the mix designs in Table 2.5 are shown in Figure 2.11 (a – c), showing the mix design distribution with respect to OPS content, w/c ratio, and fine aggregate content, respectively. Figure 2.11 (a) shows that most research employs an OPS: cement ratio less than 1, typically between 0.6 to 0.8. These are significantly high cement amounts, as typical concrete mixes contain coarse aggregates up to 3 or 4 times the weight of cement.

This poses further questions on the sustainability of OPSC: provided the goal is to be environmentally friendly by reducing the amount of waste oil palm shells, it should not result in an excessive use of cement, given cement production contribute up to 8% of global CO_2 emissions (Ellis, et al., 2020). Figure 2.11 (b) and (c) show w/c ratio of 0.4 to 0.45, and fine aggregate/cement ratio of 1.6 to 1.8 to be most used in research literature, respectively.

(a)

(b)

(c)
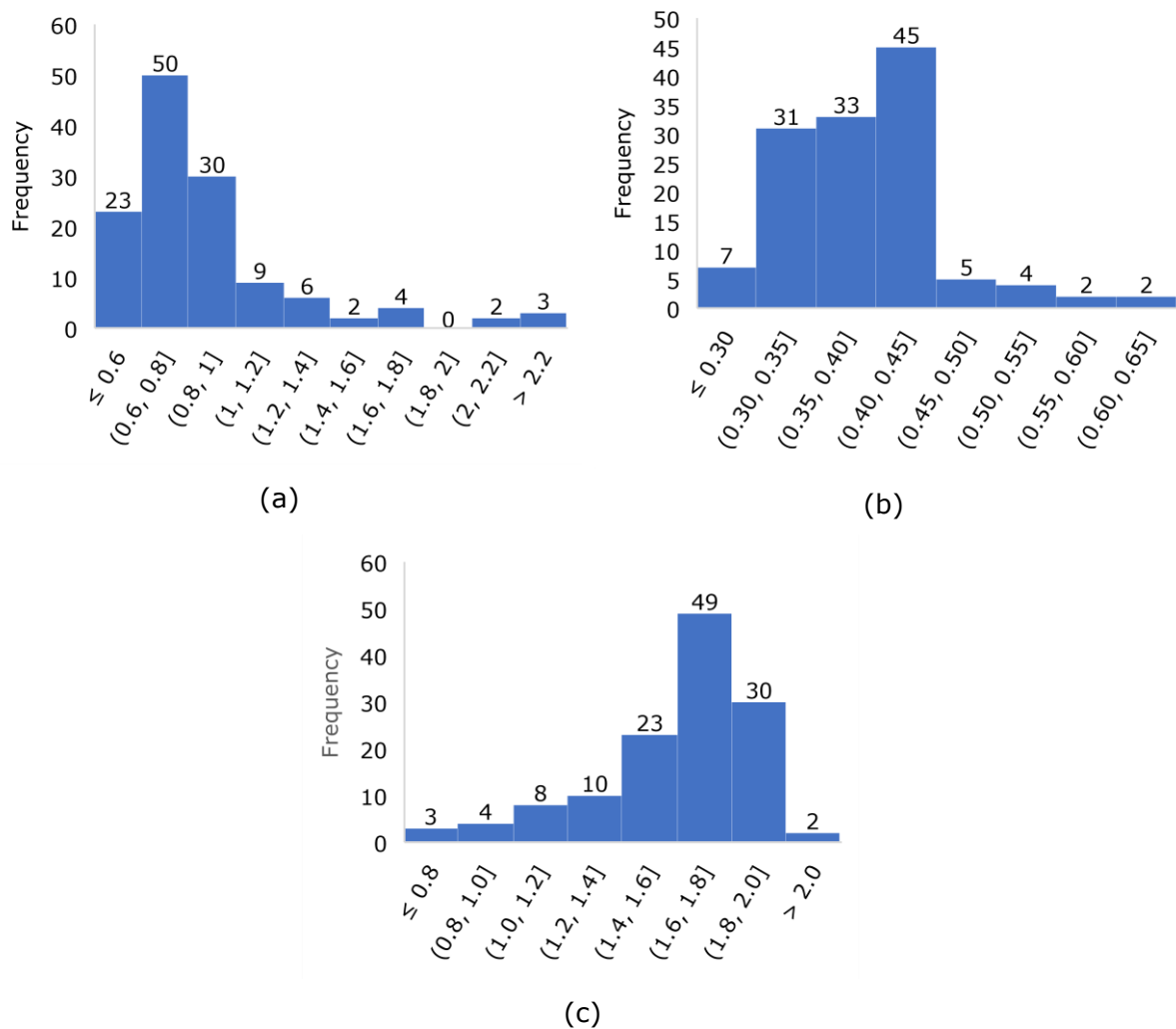
Figure 2.11 Frequency of mix materials (a) OPS: Cement ratio, (b) w/c ratio, and (c) fine aggregate/cement ratio (data from Table 2.5)

Noteworthy, much research has been done on using artificial intelligence (AI) and machine learning (ML) models to predict the compressive strength based on empirical mix design results, also using such tools on NWC with and without additive or admixtures as seen in a systematic review paper by Nunez et al. (Nunez, et al., 2021). A paper by (Zhang, et al., 2020) used the Hybrid AI model to predict the uniaxial compressive strength of OPSC. The authors claimed to have produced a tool with high prediction accuracy, with a correlation coefficient of 0.9588 made with a data set of 119 mix designs of OPSC (cement, sand, OPS, water, and superplasticizer). They had used mix designs with results at 3-, 7-, and

28-days compressive strengths varying from 7.3 – 46.5 MPa. A similar study was also conducted by (Zhu, et al., 2022) with a correlation coefficient of 0.9713 followed with another study by (Ghanbari, et al., 2023) having a correlation coefficient of 0.9821. Therefore, by using the similar amount of data from Table 2.5, ML models could potentially be used such as artificial neural networks (ANN), fuzzy logic, support vector machine (SVM), decision tree (DT) and hybrid models as tools for predicting the mechanical properties of OPSC (Chaabene, et al., 2020).

Nevertheless, based on the listed mix designs in Table 2.5, the 28-day compressive strength is plotted with respect to each mix content, and the graphs are shown in Figure 2.12 (a – d). A few mix designs were omitted as outliers, namely from (Okafor, 1988) and (Nadh, et al., 2021). As expected, OPSC shows decreasing compressive strength with increasing w/c ratio (Figure 2.12 (a)), increasing compressive strength with high cement contents (Figure 2.12 (b)), and decreasing compressive strength with increasing OPS contents (Figure 2.12 (c)) and OPS to total aggregate ratio (Figure 2.12 (d)). This is in line with established NWC and LWC mix designs (Neville, 1995) & (Chandra & Berntsson, 2002). However, an increase in OPS content significantly reduces compressive strength (Figure 2.12 (c)), understandable due to its weak strength characteristics. Of note are the low correlation values of the trendlines, with R^2 values as low as 0.16 for OPS content with respect to strength (Figure 2.12 (c)), or 0.21 for varying cement contents (Figure 2.12 (b)). This is evident in the scatter of the data points as well, where keeping the same w/c ratio or cement content gives significantly different strength performances. These rows of data points are highlighted as A1, A2, and A3 for Figure 2.12 (a), and B1, B2, and B3 for Figure 2.12 (b), respectively. For instance, B1 and B2 illustrate that a cement content of approximately 550 kg/m^3 gives 28-day compressive strengths in the range of 9 MPa to 50 MPa. Of course, these mix designs have been acquired from research literature, with different variables that are not controlled for such as OPS characteristics, type, etc. Further analysis of research data was performed using Response Surface Methodology (RSM) analysis to better capture the mix design trends in OPSC.
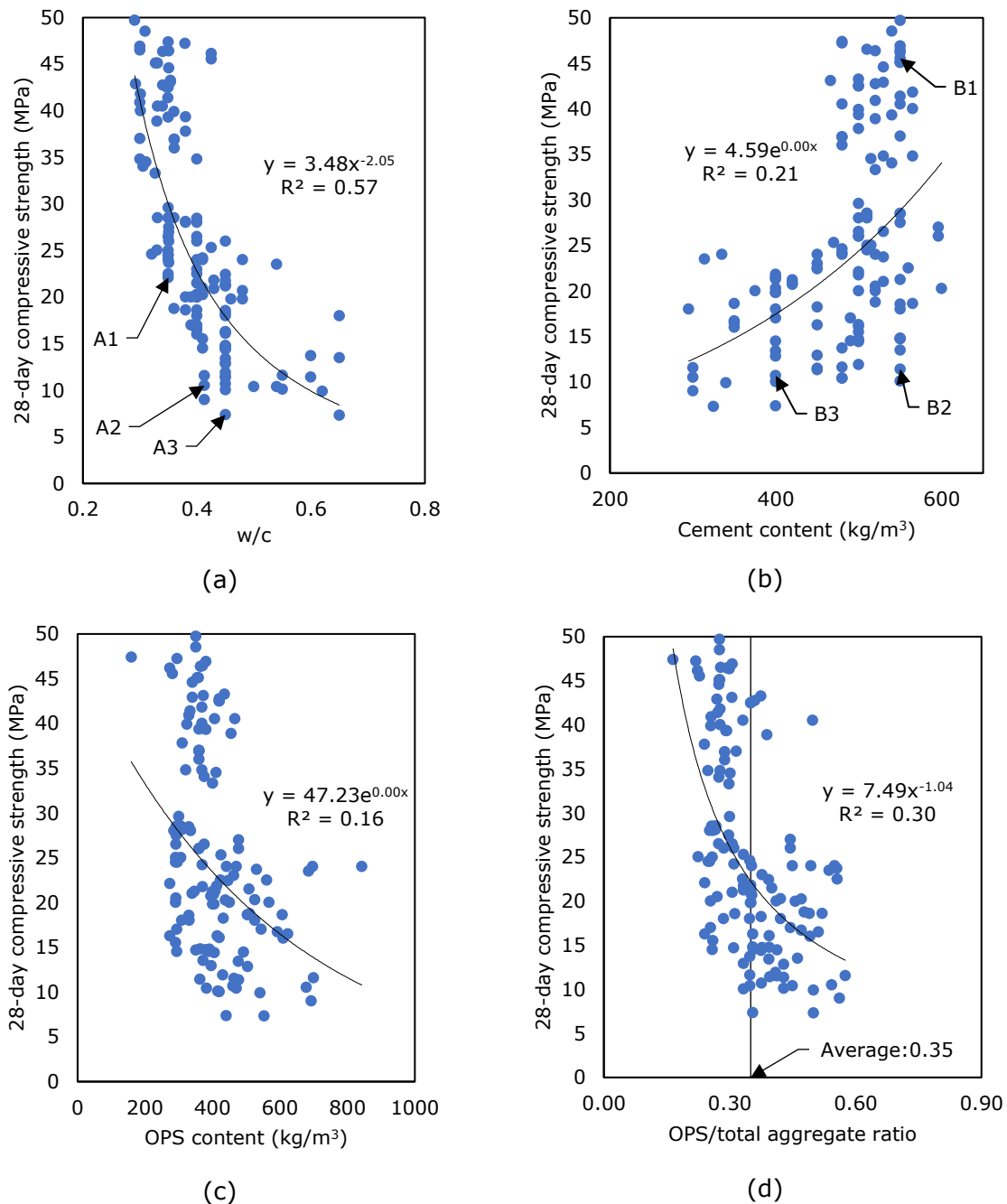
Figure 2.12 Compressive strength vs (a) w/c, (b) cement content, (c) OPS content, and (d) OPS/total aggregate ratio (data from Table 2.5)

The Design Expert software was used for obtaining RSM data, using a Central Composite Design type, quadratic model with fine aggregate: cement ratio, OPS: cement ratio, and water: cement ratio as the factors, and the 28-day compressive strength as the only response. The results from the Design Expert software were plotted in graphs shown in Figure 2.13 Figure 2.15. The ratios were selected instead of contents in kg/m^3 for easier comparison of data. The ANOVA of the quadratic model showed high Model F- value (24.63) and low p-value (<0.005), indicating the factors and response are significant, while the predicted and adjusted R^2 values were reasonably close (<0.2 difference), and with

28

minimal noise in the signal for the design model. However, the lack of fit was considerably high at 50.12, a similar issue being faced as with trendlines in Figure 2.12 (a – d). Table 2.6 shows the correlation matrix of the input factors with each other and with the overall design model intercept.

Table 2.6 Correlation matrix of the input factors

	Intercept	Fine agg. /c	w/c	OPS/c
Intercept	1.000	-0.381	0.081	0.723
Fine aggregate/c	-0.381	1.000	0.297	-0.305
w/c	0.081	0.297	1.000	-0.379
OPS/c	0.723	-0.305	-0.379	1.000

c: cement

As can be seen, the OPS: cement ratio had the highest impact on the design model intercept (correlation of 0.723), followed by the fine aggregate: cement ratio (a negative correlation of 0.381), and low correlation with the w/c ratio. Additionally, higher OPS: cement mixes clearly correlated to lower fine aggregate: cement and water: cement ratios, however higher fine aggregate: cement ratio mixes also appeared to have higher w/c values on average among the research literature data. These correlations do not lead to any conclusions regarding mix design of OPSC, instead they are included to illustrate the trends in the data incorporated in the RSM model itself. The contour plots in Figure 2.13, Figure 2.14, and Figure 2.15 show the 28-day compressive strength contours with varying water and OPS contents (as ratios of cement), for low, moderate, and high fine aggregate contents, respectively.
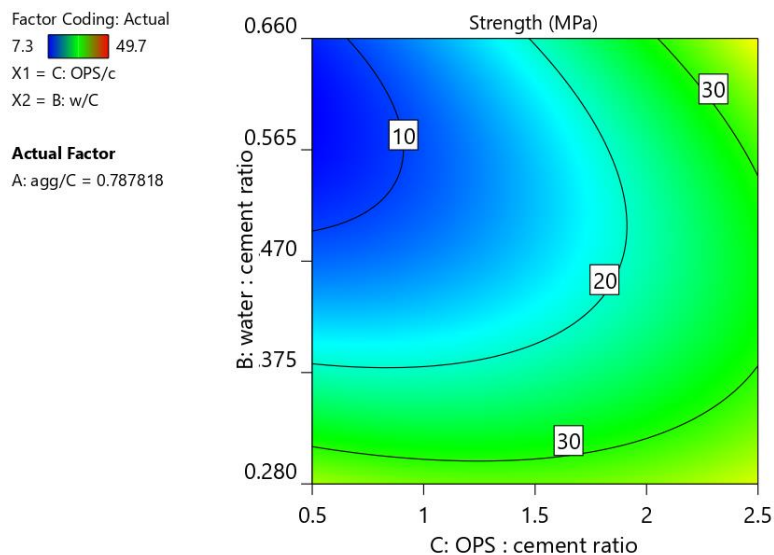
Figure 2.13 W/C vs OPS/Cement at F.A/C of 0.79

29
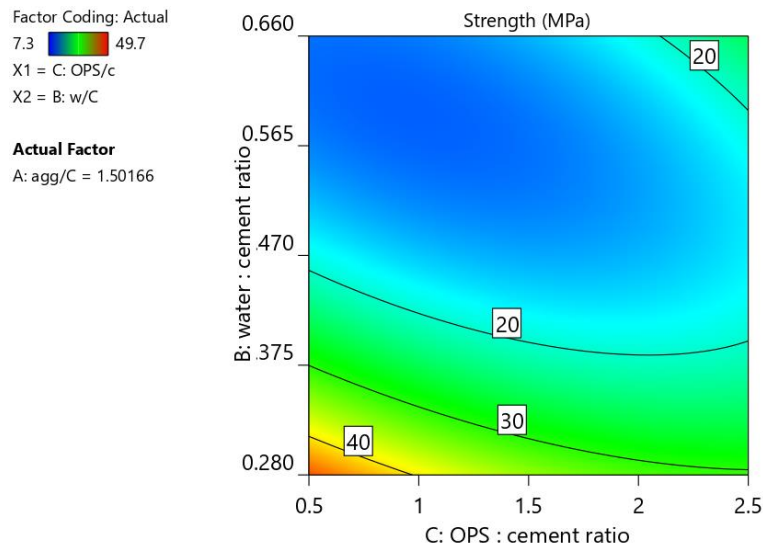
Figure 2.14 W/C vs OPS/Cement at F.A/C of 1.50
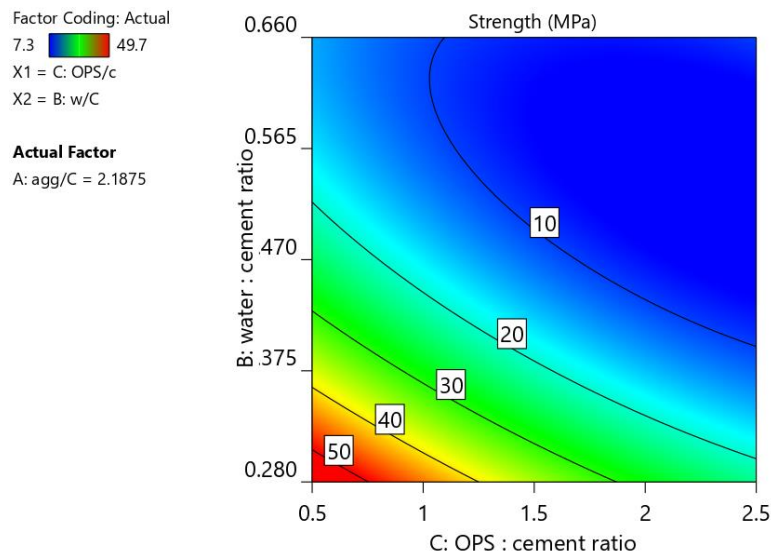
Figure 2.15 W/C vs OPS/Cement at F.A/C of 2.19

According to the RSM model, at low w/c ratios, the lower the OPS content w.r.t to cement, the higher the compressive strength, provided the fine aggregate (F.A.) content is sufficient (Figure 2.15). At higher F.A./cement ratios, compressive strengths of up to 50 MPa are theoretically possible, but with low OPS and water contents. Interestingly, at low F.A./cement ratios (i.e., less fine aggregate content or higher cement amounts), the model shows high OPS/cement ratios with extremely high w/c ratios (0.55 – 0.60), may lead to compressive strengths of up to 30 MPa (Figure 2.13). This is practically not possible and is a design limitation of RSM analysis (Myers, 1999), as high-water amounts will lead to decreasing compressive strengths. Meanwhile, moderate F.A./cement ratios (Figure 2.14) are a transitory state, reinforcing that OPS inclusion will reduce compressive strength, however 28-day compressive strengths of 30 MPa can easily be achieved for high OPS

content OPSCs, if w/c ratios are kept close to 0.29 or lower. This is easier said than done, as discussed in Section 2.1.6 and 2.2.1, respectively.

2.2.4. Density of OPSC

Density of OPSC is mostly found to be ≤2000 kg/m^3 (Hamada, et al., 2020), which is confirmed to be a structural LWC by (BS EN 206, 2021) (800 – 2000 kg/m^3). It can be determined that the density of OPSC depends on factors such as specific gravity of OPS, w/c ratio, sand content, OPS content, water absorption of OPS, and cement content (Alengaram, et al., 2013a). Of note, researchers use the 'as received" or SSD state of the OPSC when measuring its density and use these results to specify whether it is considered as a LWC or not. However, both BS (BS EN 206, 2021) and ACI (ASTM C330M-17a, 2017), requires the oven-dry density to be less than 2000 kg/m^3 and 1850 kg/m^3 to be considered as LWC, respectively.

When using different binder replacements, such as fly ash, the OPSC density decreases when increasing the binder replacement for cement (Mannan & Ganapathy, 2004) & (Shafigh, et al., 2013a). This was the same for slag content (Mo, et al., 2015a). However, when introducing 1% steel fibres, the OPSC density significantly increases by 170 kg/m^3 (Mo, et al., 2014a), though still with a density of 1900 kg/m^3. Also, when using Polypropylene (PP) fibres, the density of OPSC decreases when increasing PP fibres (Yap, et al., 2013). Nevertheless, from the research collected in this study, it can be concluded that when using OPS as a LWA in concrete, it reduces the density by 13 - 25% compared to NWC.

Figure 2.16 illustrates the change in strength ratio versus density ratio based on the highest strength and density mixes in the data collected from Table 2.5. The ratios were obtained based on the highest 28-days compressive strength and density from Table 2.5. The results illustrate improved compressive strength with increasing density of OPSC, also expected of LWC and NWC, the trendline also possessing a moderately high R^2 value of 0.51 relative to the mix design trends discussed in the previous section.

31
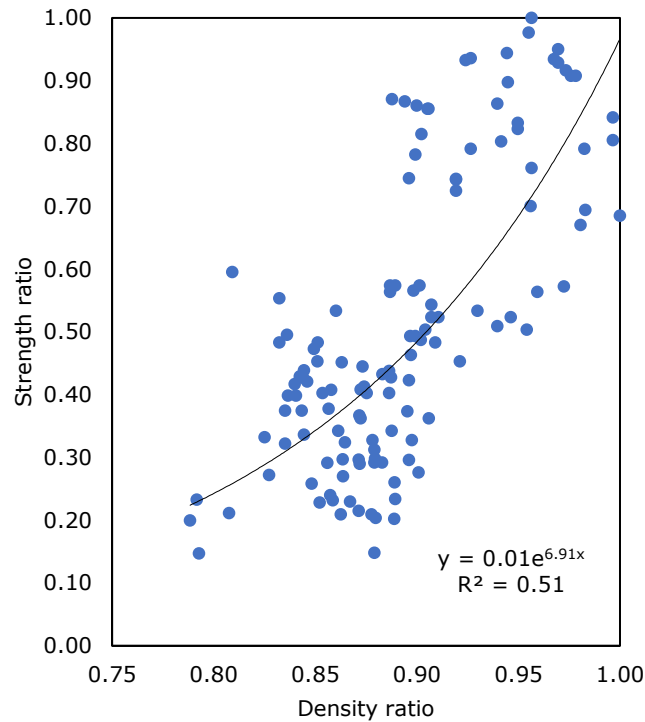
Figure 2.16 Change in strength ratio vs density ratio (data from Table 2.5)

The light weight of OPS, combined with its varying characteristics and its pre-treatments for OPSC, poses an interesting issue of how much space does it occupy in the hardened OPSC, and if that allows for different void ratios which could be contributing to the varying OPSC performances. This is further aggravated by the rough shapes of the OPS. For instance, using crushed OPS would logically reduce the voids in the OPSC mix, leading to a denser hardened structure. This may also be true for heat-treated OPS. As mentioned in Section 2.1.5, sieve analysis of Dura type OPS with similar dimensions to Tenera OPS will fail to account for the differing thicknesses of the shells. However, the latter would undoubtedly weigh less due to its relative thinness. Therefore, if OPS is added by weight to the OPSC mix, greater volume of Tenera OPS would be added, which may significantly alter its mechanical contributions to the concrete. To the authors knowledge, specific research on this issue has not been performed for OPS/OPSC, however measuring strength per unit weight of OPSC may lead to some insight regarding the variations in mix designs and resulting strengths of OPSC. Another simple alternative would be to specify mix designs in terms of both weight and volume ratios to better conceptualize the effects this may have on the density and porosity of hardened OPSC.

2.2.5. Compressive Strength

One of the most valued aspects of concrete by engineers is its compressive strength (Mehta & Monteiro, 2006). Concrete's compressive strength is in most cases associated to other hardened properties such as its flexural/splitting tensile strength, modulus of elasticity,

and other durability properties. The compressive strength of concrete is in general determined by crushing cubes or cylinders until failure occurs. The failure is fundamentally caused due to crushing and shear failure mainly assumed to generate both internal friction and cohesion to resist such failure. However, in most cases this is still understood as a complex phenomenon (Shetty, 2005). In general, for NWC, it is more or less related to the w/c ratio. However, for LWC, the type of aggregate is of large influence (Chandra & Berntsson, 2002).

For many engineers, the compressive strength of concrete samples is tested at an age of 28 days to assure the characteristic strength during the design phase. However, earlier, and later ages can also be crucial to understand its strength development (Neville, 1995). Certain codes such as from (ACI 209, 1997) and (BS EN 1992-1-1, 2014) have proposed models to predict concrete's compressive strength at any given time with a known 28-day compressive strength, see equation 2-1 and 2-2 respectively.

$$f_{cm}(t) = f_{c28} \times \left[\frac{t}{4 + 0.85t} \right]$$
(2-1)

$$f_{cm}(t) = f_{c28} \times e^{s \times \left(1 - \sqrt{\frac{28}{t}} \right)}$$
(2-2)

Where, (t)=time in days, f_{cm} (t)=the compressive strength at time (t), f_{c28}=empirical compressive strength at 28 days (≥20 MPa), and s = is a coefficient which depends on the type of cement:

- 0,20 for cement of strength Classes CEM 42,5 R, CEM 52,5 N and CEM 52,5 R (Class R)

- 0,25 for cement of strength Classes CEM 32,5 R, CEM 42,5 N (Class N)

- 0,38 for cement of strength Classes CEM 32,5 N (Class S)

According to (Okafor, 1988), OPS "performs satisfactorily" as an LWC for middle- and low-strength concrete, and the reported investigation reached a maximum of 24 – 30 MPa in 28-day compressive strength. Subsequently, many other compressive strengths obtained by researchers (Table 2.5) are higher than 18 MPa and C17/20 MPa which is confirmed to be a structural LWC as per (ASTM C330M-17a, 2017), (ACI 318M-08, 2008) and (BS EN 206, 2021) respectively. As mentioned earlier, the compressive strength decreases when the percentage of OPS coarse aggregate is increased. It can also be observed from Table 2.5 that most researchers have shown an improvement in compressive strength by increasing the fine aggregate to OPS ratio. This was investigated and confirmed by (Mahmud, et al., 2009). This may lead some credence as to better packing of OPSC by fine aggregates, especially due to the irregular concave structure of the OPS, however no research has specially examined these interactions, although different strength grades have been reported with changes in the particle size of OPS (Alengaram, et al., 2010a).

Additionally, strength also depends on the curing conditions of OPSC (Mannan, et al., 2002a). Curing OPSC via full immersion in water showed the highest compressive strength compared to curing in partial water and full and partial covering with plastic (Mannan, et al., 2002a). This was also later confirmed by (Alengaram, et al., 2010a), (Shafigh, et al., 2012) and (Maghfouri, et al., 2021). However, (Shafigh, et al., 2012) found when OPSC is water cured more than 3 weeks, no difference in mechanical strengths is observed. (Alengaram, et al., 2010a) further recommended to use all particle sizes of OPS in the mix, as removing small particles (less than 5mm) would decrease the compressive strength. Alengaram et al. concluded that OPS with small particle sizes (accounting for about 65 – 70% of the total concrete mass) have higher relative density, which accumulates for 4% of the total density of OPSC (Alengaram, et al., 2010a). This would therefore make the concrete more packed and thus decrease the concrete water absorption. It has further been reported when OPSC has a low water absorption ranging between 3.12 – 6.2%, high concrete strengths are obtained (Shafigh, et al., 2011d), confirming the earlier study by (Alengaram, et al., 2010a).

Another factor affecting the strength is the irregular shape and strength of OPS (Mannan & Ganapathy, 2004). The compressive strength depends on either the strength of the aggregate or the cement paste depending on which one fails first (Mannan & Ganapathy, 2002b). However, the bond between the OPS aggregate and cement paste also plays an important role (Okpala, 1990). Because of the smooth surface of OPS, the cement binding force is found to be inadequate (Shafigh, et al., 2011b) due to the low adhesion between the cement paste and OPS surface (Okpala, 1990) & (Mannan & Ganapathy, 2002b).

A potential method to increase de-bond properties between OPS and cement paste has been done by adding silica fume (10%) (SF) and fly ash (5%) (FA) in the mix, showing an increase in the compressive strength by 30% (Alengaram, et al., 2011a). Alengaram et al. (Alengaram, et al., 2011a) took SEM images of OPS prior and after the mix, see Figure 2.17 (a – c). The images reveal that the pores are uniformly filled when adding SF and FA compared to just cement, thus increasing the bond, and therefore increasing the compressive strength. Though, (Mannan & Ganapathy, 2001a) showed a decrease in strength with the addition of FA (10 and 15%) as cement replacement by 7% and 19% respectively. This is also confirmed by (Shafigh, et al., 2013a), (Ting, et al., 2020), (Maghfouri, et al., 2021) and (Muthusamy, et al., 2021). It is possible that the increase in compressive strength reported by (Alengaram, et al., 2011a) was obtained solely due to the SF, also confirmed in a previous study by (Mahmud, et al., 2009). Conversely, a decrease in compressive strength has been observed with GGBFS as cement replacement in OPSC (Mo, et al., 2014c), while the durability was not measured. Muthusamy et al. (Muthusamy, et al., 2015) incorporated 20% palm oil fuel ash (POFA) with cement

replacement in OPSC and presumed an enhancement of the bond between the cement paste and OPS, resulting in an increase in compressive strength by 15%. Higher content of POFA was not recommended, as it would decrease the compressive strength (Muthusamy, et al., 2015). Foong et al. (Foong, et al., 2015) found that rice husk ash (RHA) increases the compressive strength by 10% with 15% of RHA replacement with cement. Foong concluded that it might be because the RHA attributed to the strong bond at the interfacial transition zone (ITZ) cause by the pozzolanic reaction of RHA. However, no SEM images were included to confirm this hypothesis. To the authors' knowledge, no further studies investigating RHA in OPSC were available to corroborate these findings.

(a)

(b)

(c)
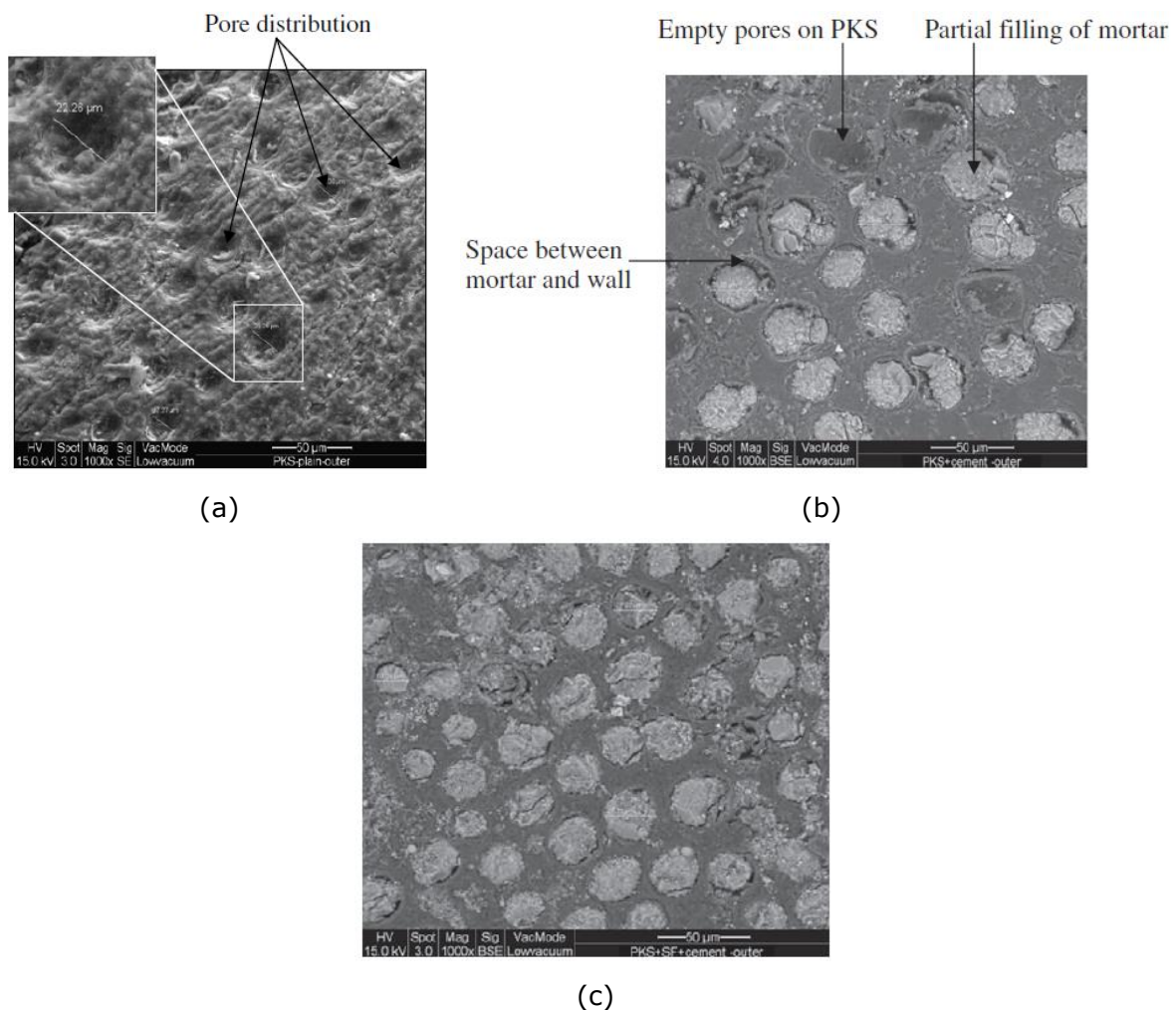
Figure 2.17 Filling of mortar in micro-pores of OPS with FA and SF (a) OPS shell prior to mixing, (b) OPS shell with only cement, (c) OPS shell with 5% FA and 10% SF cement replacement (Alengaram, et al., 2011a)

Other investigations have found an increase in bonding between OPS and cement by treating OPS with PVA solution which created a thin layer on the shells (Mannan, et al., 2006), (Chai, et al., 2014), and (Traore, et al., 2018). Mannan et al. (Mannan, et al., 2006) achieved to increase the compressive strength by 28% by treating OPS with 20% of PVA solution. However, Chai et al. (Chai, et al., 2014) could only increase the compressive

strength by 13% with the same amount of PVA solution. The main reason for this could be because Mannan exposed the OPS to very severe environment conditions by incorporating alkaline and acidic solution compared to Chai who exposed the OPS to 1 – 2 weeks of natural weathering. In contrast to Mannan and Chai, Traore et al. (Traore, et al., 2018) found that treatments of PVA decreased the compressive strength by 8%. This might be because Traore only used 5% of PVA solution by covering the OPS for only 3 minutes and was then drained at room temperature. While Chai did not mention their procedure, Mannan followed a different procedure than Traore for the treatment as described by Santos et al. (Santos, et al., 1999). However, Traore found an increase in compressive strength (25.5 MPa) by 8% with lime solution treatment of OPS. The author concluded that the lime treatment improved the adherence of OPS with the cement matrix. A different treatment of OPS was done by hot and cold alkali treatment of OPS (Nabinejad, et al., 2014). It was found that hot alkali treatment improved the mechanical properties (tensile and flexural strength) of OPSC by 49% and 33% respectively at 28 days. However, no compressive strength tests were conducted. Nano coating OPS with siliceous material showed to improve the compressive strength by 53% (Nadh, et al., 2021). Nadh mentioned that the interfacial transition zone of the nano coated OPS was reduces from 600 micrometres to 400 micrometres according to SEM images (Figure 2.18), thus creating a better bond. Another simple coating method was done by gun spraying grout formulation of 1.25 w/c on OPS prior to mixing (Yew, et al., 2021). This method proved to increase the compressive strength by 14%.
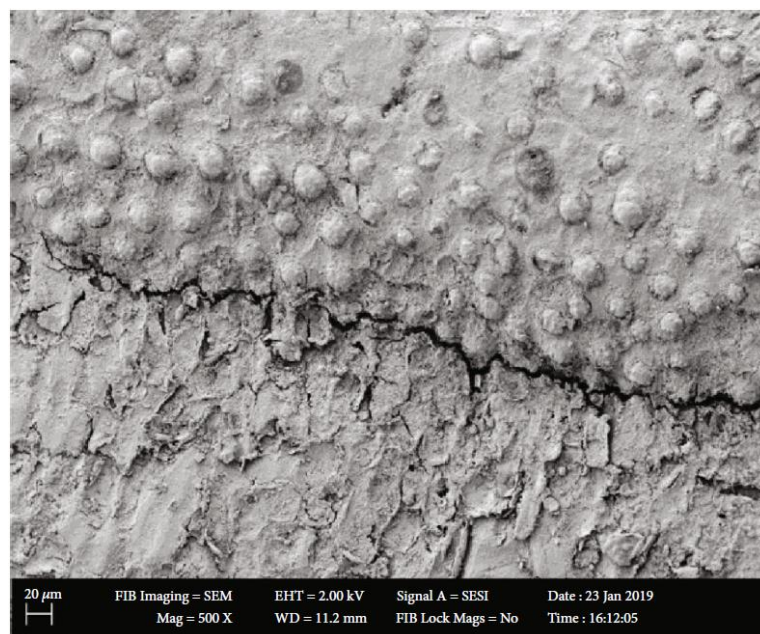
Figure 2.18 Nanocoated OPS (Nadh, et al., 2021)

In another study by (Katte, et al., 2022), a method of treating the OPS to remove oil inhabits was done to improve the strength development of OPSC by saponification-based

treatment from 2 – 20 g/L concentration of solution of potassium hydroxide. It was found that the oil content in the OPS was reduced from almost 11% to less than 2% from 2 to 20 g/L, respectively. The authors found that the optimum solution was 10 g/L which removed most of its internal oil, However, higher concentrations would damage the aggregates integrity effecting the strength of the OPSC. Furthermore, the compressive strength was increased by 81% (11 MPa vs 20 MPa) at 28 days with the optimum dosage of 10 g/L. However, all the concentrations seemed to have a negative effect on the splitting tensile strength, explained further in the next section.

2.2.6. Flexural and Splitting Tensile Strength

The flexural test measures the concrete's tensile strength in an indirect manner. Typically, the cement bonding matrix is the limiting factor for tensile strength of most concretes. Although the tensile strength of concrete in flexure is commonly neglected in strength design by engineers, it is still however important in deflection and cracking considerations at service loads (ACI 318M-08, 2008). Concrete is known to be weak in tension. When the concrete is reinforced with steel bars, tensile strength of concrete is less important. However, it is still important to determine its tensile strength, as cracks can occur by tensile stresses due to many reasons such as drying shrinkage, rusting of steel reinforcement, and temperature gradients. One such example is longitudinal tensile stress in the bottom of the pavement. Because of restraint and temperature warping, tensile stress occurs to as much as 2.5 MPa (without the addition of wheel loads) (Shetty, 2005).

In general, LWC has a lower flexural and splitting tensile strength compared to NWC. However, typically the cement bonding matrix is the limiting factor for tensile strength of most concretes. Though some LWA's such as slate, allows for better internal hydration and a stronger interfacial transition zone (ITZ), which in turn increases the tensile strength compared to NWC (Evangelista & Tam, 2020).

However, in the case of OPSC, depending on the mix ratio and content of admixtures and or fibres, it can produce high tensile strength in comparison to NWC (Alengaram, et al., 2011b). The tensile failure mechanism in OPSC occurs because of failure of bond between the OPS surface aggregate and cement matrix, and not by the OPS aggregate (Alengaram, et al., 2010c). Table 2.7 reports the tensile strength of OPSC from various researchers. Because of low stiffness and strength of the OPS, a large difference is seen between OPSC and NWC in terms of flexural strength (Alengaram, et al., 2010b).

Table 2.7 Mechanical Properties of OPSC from Various Researchers

Reference	Investigation	Flexural tensile strength (MPa)	Splitting tensile strength (MPa)	Young's modulus (GPa)
(Mannan & Ganapathy, 2002b)	OPSC vs NWC	2.75 - 4.00	1.78 - 2.41	7.00 - 7.60

Reference	Investigation	Flexural tensile strength (MPa)	Splitting tensile strength (MPa)	Young's modulus (GPa)
(Alengaram, et al., 2010c)	OPSC vs NWC	3.50 - 3.83	1.95 - 2.10	10.05 - 11.15
(Ahmed & Sobuz, 2010)	OPSC vs NWC	2.40 - 2.60	2.10 - 2.50	13.40 - 17.10
(Okafor, 1988)	OPSC mix design	4.30 – 4.90	2.00 - 2.40	-
(Okpala, 1990)	OPSC mix design	2.13 - 2.81	-	-
(Mahmud, et al., 2009)	Sand/Cement ratio + SF + FA	2.79 - 4.10	1.98 - 2.35	7.08 - 10.09
(Shafigh, et al., 2012)	Crushed OPS	4.40 – 7.00	2.80 – 3.50	-
(Alengaram, et al., 2010a)	Aggregate size + SF + FA	2.21 - 3.00	1.50 - 18.40	7.01 - 11.18
(Traore, et al., 2018)	OPS treatment	4.00 - 6.40	-	7.06 - 12.08
(Ting, et al., 2020)	FA + SP	-	1.62 - 2.82	-
(Mo, et al., 2015a)	High volume slag	-	2.33 - 2.69	-
(Mo, et al., 2014c)	GGBFS	4.03 - 5.71	2.31 - 3.51	12.6 - 17.6
(Mo, et al., 2016a)	GGBFS	-	2.30 - 2.50	5.50 - 8.30
(Mo, et al., 2016b)	Bond stress-slip behaviour + GGBFS + SP	-	2.52 - 2.99	-
(Islam, et al., 2015)	POFA	3.00 - 6.50	2.60 - 4.00	12.70 - 15.40
(Mo, et al., 2018)	Metakaolin-blended OPS	4.58 - 6.88	2.55 - 3.38	13.71 - 15.46
(Foong, et al., 2015)	Rice husk ash + manufactured sand + SP	5.20 - 5.90	3.12 - 3.45	14.10 - 17.80
(Katte, et al., 2022)	Saponification-based treatment of OPS	-	0.90 – 1.40	-
With fibres				
(Shafigh, et al., 2011a)	Steel Fibres	5.42–7.09	2.83–5.55	5.50-7.10
(Yap, et al., 2015a)	Torsion RC + Steel fibres	3.26-8.16	-	13.87-16.29
(Yap, et al., 2015b)	Steel fibre aspect ratio	3.81-6.04	2.83-3.91	13.25-15.48
(Yap, et al., 2015c)	Torsion Behave. + Steel fibres + SF	3.26-8.16	2.59-5.47	13.87-16.29
(Yap, et al., 2015a)	Torsion Behave. + Steel fibres	3.26-8.16	-	13.87-16.29
(Mo, et al., 2017b)	Shear behaviour + Steel fibre + Geo-polymer concrete + FA + AA	3.182-6.180	2.129-6.125	-
(Yap, et al., 2019)	Ductility behaviour + Steel fibres + SF + SP	3.26-8.16	-	13.87-16.29
(Mo, et al., 2014b)	Steel fibres	5.80-6.88	5.91-4.80	10.65-14.79
(Yap, et al., 2017)	Steel fibres	4.84-18.48	3.22-10.99	13.53-16.35
(Jagarapu & Eluru, 2019)	Glass fibre	-	1.0-3.2	0.55-3.25
(Yap, et al., 2013)	Fibres — PP	3.51-4.64	2.48-3.23	14.16-15.23
	Nylon	4.20-4.37	2.97-3.49	12.26-12.78
(Yew, et al., 2015c)	PP Fibres	5.75-7.64	3.35-4.12	12.04-15.36
(Yew, et al., 2015b)	PP twisted bundle fibres	5.98-6.46	3.52-3.98	17.4-15.9
(Yew, et al., 2015a)	Polyvinyl Alcohol fibres	4.17-5.49	-	15.3-16.9
(Noor, et al., 2017)	Palm oil Fibre	1.2-6.6	-	-

SF: Silica Fume, FA: Fly Ash, SP: Superplasticizer, GGBFS: Ground Granulated Blast Furnace Slag, POFA: Palm Oil Fuel Ash, PP: Poly Propylene

Increase in cement content (295, 314, up to 335 kg/m^3) improved the flexural and splitting tensile strength of OPSC at 28 days by 14% and 16%, respectively. This was in parallel with decreasing the w/c (0.65, 0.54 to 0.48) (Okafor, 1988). Similar conclusions were drawn by (Okpala, 1990) with w/c's of 0.5, 0.6, 0.7, and 0.8 at mix ratios of 1:1:2 and 1:2:4 (cement: sand: OPS). Okpala also concluded that increasing the curing age, will also

increase the flexural strength by 22%. Mannan et al. (Mannan & Ganapathy, 2002b), also confirmed when increasing the curing age from 7 to 28 days, the flexural strength increases by 46% and splitting tensile strength by 35%. However, the NWC control samples showed to have a higher flexural and splitting tensile strength by 55% and 93%, respectively, compared to OPSC. Mannan et al. concluded that OPSC has a similar behaviour to NWC under curing conditions and that the main reason for weaker strength was influenced by the diffused moisture distribution on the OPS and the weak bonding between cement matrix and OPS. However, cement replacement with 10% SF and 5% FA showed a smaller difference to NWC in flexural and splitting tensile strength by 17% and 38% respectively (Alengaram, et al., 2010c).

When using crushed OPS, OPSC is shown to have similar flexural and splitting tensile strengths compared to NWC with similar compressive strengths ranging from 34.8 – 53 MPa. Also, OPSC with higher compressive strengths have a higher flexural and splitting tensile strength (Shafigh, et al., 2012). Alengaram et al. (Alengaram, et al., 2010a) studied the OPS size and proportion in OPSC and showed that OPS sized between 2 – 10 mm (at 100% proportion) showed higher tensile strengths compared to 2 – 15, 5 – 10, 5 – 15, and 0 – 15 mm by 2%, 8%, 23%, and 12% at 28 days curing. The authors mentioned the smaller sizes had more flaky and angular surfaces which caused a better bonding with the cement matrix compared to the larger sizes. However, they concluded that OPS particles of all sizes were the best performers in both compressive and tensile strengths. Interestingly, they did not provide the particle size distribution for the 2 - 10 mm OPS aggregates. When increasing the sand-cement (s/c) ratio in OPSC (s/c: 1, 1.2, and 1.6), the flexural strength is increased by 17% and 49%, respectively, and splitting tensile strengths is increased by 5% and 24%, respectively, at 28 days. Though, the densities with s/c: 1, 1.2, and 1.6 did increase by 1% and 4% respectively. Nevertheless, it was still below the LWC requirement (< 2000 kg/m^3) (Mahmud, et al., 2009). Traora et al. (Traore, et al., 2018) found that by treating OPS with lime, sodium silicate and heat treatments, improvements in flexural strengths were 8%, 5%, and 6% compared to the control, with strength varying from 4 – 5 MPa. PVA showed no significant increase or decrease in flexural strength, although as mentioned in Section 2.2.5, the treatment was quite brief and caused a decrease in compressive strength performance. Of note, despite the filling of pores by PVA as shown in Figure 2.10, the adhesion of cement paste was not improved. The use of potassium hydroxide as a treatment for OPS in concentrations between 2 – 20 g/L was studied by (Katte, et al., 2022). Katte found that their so-called saponification-based treatment of OPS did improve the compressive strength by 81%, it reduced the splitting tensile strength by 53% (1.60 vs 0.75 MPa). The authors mention that the probable reason for their observations was that the potassium hydroxide not only removed the oil, but also

damaged the integrity of the OPS. The authors called for further investigation on this matter.

When the incorporation of FA is used as cement replacement in increments of 30%, 40% and 50%, a decrease in splitting tensile strength is observed by 10%, 27%, and 58% compared to control specimen at 28 days, respectively. However, in the long term at 90 days, the decrease was 3%, 18%, and 27%, respectively. The authors mentioned that the FA at 28 days were still smooth and spherical and is thus still in the early age of hydration as shown in Figure 2.19 (a), whereas at 90 days in Figure 2.19 (b), the smooth and rounded shape of FA were not easily noticeable, which explains the higher strength in 90 days compared to 28 days (Ting, et al., 2020). Comparable results for splitting tensile strength are observed with GGBFS as cement replacement where 20% and 60% have shown a decrease of 6% and 14%, respectively, compared to control specimen at 28 days (Mo, et al., 2015a). An earlier study (Mo, et al., 2014c) showed equivalent results, but studied GGBFS replacements at 20%, 30%, 40%, 50%, 60%, and 70% showing a decrease in splitting tensile strength by 4%, 5%, 4%, 13%, 15%, and 34% and for flexural strength by 4%, 13%, 16%, 19%, and 29% respectively at 28 days. In both studies by Mo et al. (Mo, et al., 2015a) & (Mo, et al., 2014c), the main reason for strength reduction stated was because of the delayed hydration compared to cement. Other studies by (Mo, et al., 2016a) & (Mo, et al., 2016b) observed similar tensile strength behaviours with GGBFS replacement in OPSC. Also, by using POFA as cement replacement at 5%, 10%, 15%, 20%, and 25%, the flexural strength decreased by 0.5%, 5%, 12%, 28%, and 39% and for splitting tensile strength by 0.5%, 10%, 17%, 18%, and 26% respectively (Islam, et al., 2015).

(a) FA (50%) at 28 days   (b) FA (50%) at 90 days
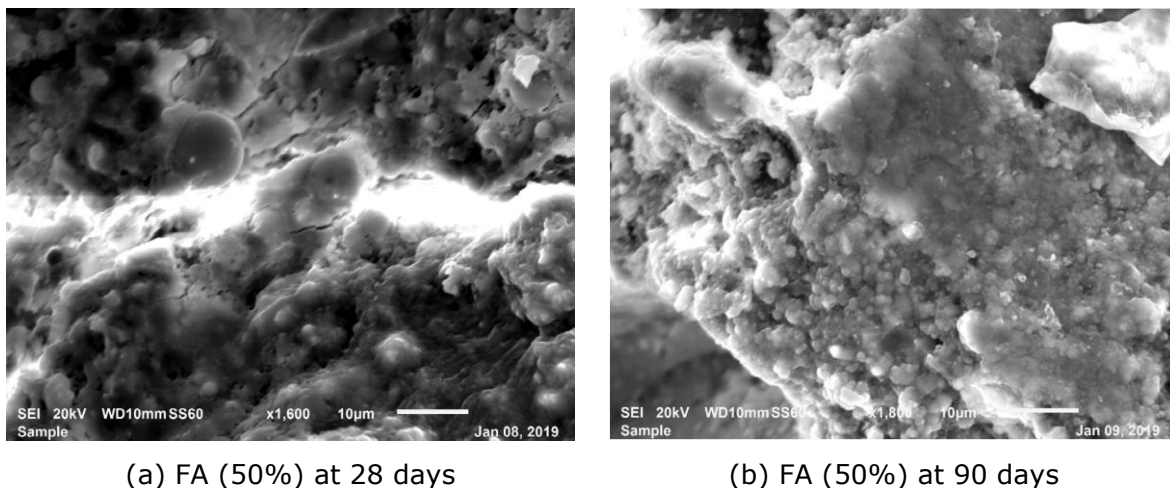
Figure 2.19 SEM of OPSC with 50% FA content at 28 and 90 days (Ting, et al., 2020)

However, by using metakaolin as cement replacement at 10%, the flexural and splitting tensile strengths were found to be improved by 44% and 50% respectively at 28 days. The

authors claimed to have increased the bonding in the ITZ between cement and OPS, though no SEM images were taken (Mo, et al., 2018). An increase was also seen when replacing 15% of RHA with cement by 15% and 28% for flexural and splitting tensile strength, respectively. The authors achieved this by also using 100% of manufactured sand. They mentioned the cause for increase in strength was due to the higher packing ability of the RHA particles (Foong, et al., 2015).

Fibres like polypropylene, nylon, steel, and other agricultural fibres have shown to improve the flexural and tensile strength as seen in Table 2.7, which proves to behave like NWC. In summary, as flexural and splitting tensile strength is incumbent on the adhesion of cement paste to the aggregates, including OPS, results between OPSC, LWC, and NWC show similar trends with or without addition of admixtures and/or additives. Also as expected, the addition of pozzolanic materials did not increase 28-day strengths significantly but showed improvements at the 90-day stage.

2.2.7. Modulus of Elasticity

Concrete is a material that is not elastic, so when it is unloaded, it will not assume its original shape. Additionally, the concrete stress-strain curve is not linear. Thus, the elastic constants Poisson's ratio and modulus of elasticity (MOE) are to a certain extend not relevant. However, for simplicity reasons, they are applied to the analysis and design of concrete structures under the assumption of elastic behaviour. For the estimation of the deformation of structures and members, the concrete's MOE is necessary (Subramanian, 2021).

Due to the non-linearity of concretes stress-strain curve, different types of methods are used to compute the static MOE such as the tangent modulus, secant modulus, and chord modulus, see Figure 2.20. However, in most cases the secant modulus is adapted, also referred as the static MOE. Another method is also known as the dynamic MOE, computed using a non-destructive technique (NDT) which finds the initial tangent modulus which in turn shows a higher MOE than the static MOE (Mehta & Monteiro, 2006).
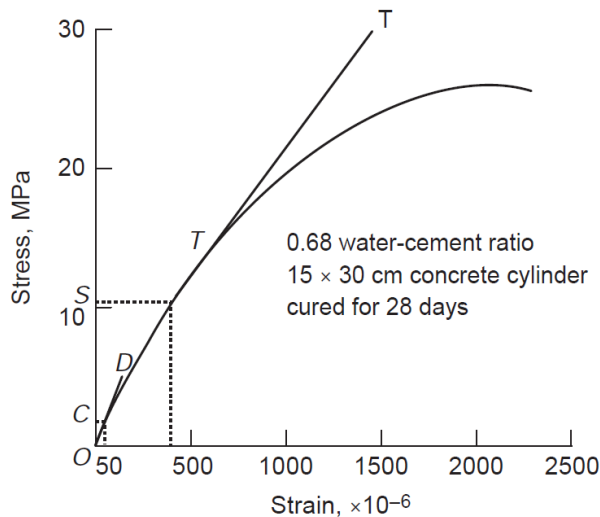
Calculating the Elastic Moduli

f_t = 26 MPa
40% f_t = 10.4 MPa = SO

Secant Modulus: Slope of the line corresponding to stress SO
$10.4/(417 \times 10^{-6})$ = 24.9 GPa

Chord Modulus: Slope of the line corresponding to stress SC $(10.4 - 1.6)/$ $(417 \times 10^{-6} - 50 \times 10^{-6})$ = 24.0 GPa

Tangent Modulus: Slope of the line TT drawn tangent to any point on the $\sigma - \varepsilon$ curve $(30 - 14.6)/(1445 \times 10^{-6} - 625 \times 10^{-6})$ = 18.8 GPa

Dynamic Modulus (Initial Tangent Modulus): Slope of the line OD from the origin $5/143 \times 10^{-6}$ = 34.9 GPa

Figure 2.20 Example for determining different types of MOE (Mehta & Monteiro, 2006)

The values for the MOE for concrete differ depending on the strength, age, type of loading and the mix design of the concrete such as the matrix, type of aggregates, the effective w/c ratio, and the volume of the cement (McCormac & Brown, 2014). The elastic modulus of the cement paste is controlled by the w/c ratio. Also, when the sand has a high density, the stiffness of the matrix increases (Chandra & Berntsson, 2002). The curing conditions are also known to effect the MOE (Kocab, et al., 2017). Generally, the MOE of NWC is higher than that of LWC because MOE of NWA is higher than that of LWA (Holm & Bremmer, 2000). For SLWC it is recommended to have a static MOE between 10 – 24 GPa (FIP, 1983). The following predicting formulas for MOEs are recommended by (ACI Committee 213R-14, 2014) and (BS EN 1992-1-1, 2014) in equations (2-3) and (2-4), respectively. The model proposed by the ACI is designed solely for LWC, whereas the BS model can be applied to concrete of any type.

$$E_c = w_c^{2.687} \times (f'_c)^{0.24} \tag{2-3}$$

$$E_c(t) = (\frac{f'_{cu}(t)}{f'_{cu-28days}})^{0.3} \tag{2-4}$$

Where, f'_{cu} is the compressive strength in MPa, W_c represents the dry density of LWC, and (t) referring to the time in days.

Most researchers from Table 2.7 have achieved a static MOE of 10 GPa or higher to be recommended as a structural LWC according to (FIP, 1983). They concluded that the value of MOE for OPSC is influenced by the OPS quantity, type of cement, w/c ratio of the mix, curing period, and bond between the OPS and the cement matrix.

42

As with NWC, it has been observed that the compressive strength of OPSC is related to the MOE. As the compressive strength increases, the MOE also increases (Aslam, et al., 2017). As explained Section 2.2.3, by reducing the OPS content, the compressive strength increases and thus leading to a higher MOE (Shafigh, et al., 2016). This is similar when the fine aggregates are increased as shown in a study by (Mahmud, et al., 2009) and confirmed by (Alengaram, et al., 2011a). Though larger size particles of OPS of 10 mm and above decrease the compressive strength, it has been shown to increase the MOE by 31% compared to OPSC with smaller sizes (Alengaram, et al., 2010a). The authors have posited that larger OPS particles possess greater toughness and hardness compared to other sizes, thereby exhibiting a higher MOE. This assertion can be attributed to the notion that the external surface of the shell potentially plays a critical role in maintaining the integrity of the shell. Consequently, when the shell is broken, its fractured edges may become more susceptible to damage.

Moist curing compared to air curing of OPSC have shown higher MOE (Islam, et al., 2015), whereas curing for longer than 28 days up to 90 days have shown 8% and 6% increase in MOE for moist cured and air cured, respectively (Mannan & Ganapathy, 2002b). Similar results have been shown by (Alengaram, et al., 2010a). Nevertheless, this might be related to the increase in cement hydration (Neville, 1995).

Other authors have used cement replacement agents such as SF, GGBFS, RHA, POFA, and metakaolin to study the MOE. SF (Mahmud, et al., 2009) & (Alengaram, et al., 2010c), RHA (Foong, et al., 2015), and metakaolin (Mo, et al., 2018) have all shown increments in the MOE. All authors claimed the agents have filled the OPS pores resulting in a better interfacial transition zone between the cement matrix and OPS. In contrast, GGBFS (Mo, et al., 2014c), and POFA (Islam, et al., 2015) have shown a decrease in MOE. Mo et al. (Mo, et al., 2014c) and Islam et al. (Islam, et al., 2015) have concluded that GGBFS and POFA, respectively, contribute to the weak bond at the interfacial transition zone of OPS and cement matrix. Mo et al. (Mo, et al., 2014c) mentioned that it might be attributed to the fact that, as pozzolans, GGBS undergoes a slower hydration process compared to the cement. Islam et al. (Islam, et al., 2015) drew a similar conclusion for POFA. This concludes that OPSC behaves in a similar matter to NWC i.e., increase in compressive strength increases the MOE and vice versa. In another study mentioned in the earlier sections by Traore et al. (Traore, et al., 2018), the authors have shown that lime treatment of OPS increases the MOE significantly by more than 64% compared to the control OPSC. However, both the compressive strengths and MOE values were far behind normal control concrete (41.8 MPa vs 25.5 MPa, 21.6 GPa vs 12.6 GPa, respectively). The authors gave a similar explanation as the above authors.

An investigation on predicting the MOE of OPSC by using CEB/FIP model code formula was done by (Alengaram, et al., 2011a). They suggested modifying the formula because it overestimated the value from 65% to 120%. The modified formula is shown in equation (2-5).

$$E_c \ (GPa) = \left[\frac{w}{2400}\right]^2 \times (f_{cu})^{1/3} \times 5.0, (R^2 = 0.95)$$
(2-5)

Where, (w) is the air-dry density of OPSC in kg/m^3, and f$_{cu}$ is to be taken as the compressive strength at 28 days in MPa.

With the above formula it predicted Alengaram's MOE with the experimental values with an error of ±1.5 GPa. This was later confirmed in a study by (Foong, et al., 2015) who had a comparable error value of ±1.5 GPa.

2.2.8. Drying Shrinkage

The ability of a material to maintain its size, shape, or dimension over time is referred to as dimensional stability. A dimensionally stable material's long-term volumetric change should be so negligible as to not affect the material's structural integrity. Shrinkage is one of the main phenomena that compromises the dimensional stability issue for concrete (Li, 2011). Freshly formed-wet concrete undergoes shrinking when exposed to ambient humidity, causing strains, even in unloaded concrete. Such shrinkage strains can have negative impacts on concrete such as manifesting into tensile stresses when restrained causing cracks due to low tensile strength of concrete. This cracking tendency is one of the significant drawbacks of concrete structures (Mehta & Monteiro, 2006).

The important elements that affect the drying shrinkage of concrete are cement paste content, w/c ratio, hydration degree, elastic modulus of aggregate, characteristics and amounts of admixtures used, time and the relative humidity of exposure, size and shape of the concrete mass, and the amount and distribution of internal reinforcement such as steel and fibres (Shah, et al., 1994). Generally, in a concrete mix, the cement paste tends to shrink whereas the aggregate restrains shrinkage. This is because of the difference of elastic modulus of the aggregate. When w/c ratio is reduced and cement content is increased, the shrinkage increases. This is significant when w/c is lower than 0.42, which leads to less moisture available internally. When the surface area to volume ratio of the concrete is high, the shrinkage is also higher. However, when the aggregate content, relative humidity, and moist exposure time (curing in tank) is increased, the shrinkage decreases.

When supplementary cementitious materials are used like GGBFS and SF, the shrinkage increases since the volume of fine pores are increased. Common tests used to observe drying shrinkage of concrete are done by the free drying shrinkage test and the bar type

test. It is also known for concrete to reach 90% of its ultimate shrinkage in 365 days (Li, 2011). The (ACI 209.2R-92, 2008) and (BS EN 1992-1-1, 2014) codes have proposed prediction models for the drying shrinkage of any concrete up to any age. The prediction models for development of drying shrinkage strain of concrete with time by both the ACI and BS codes are shown in equations (2-6) and (2-7), respectively.

$$\varepsilon_{sh}(t, t_c) = \frac{(t - t_c)^\alpha}{f + (t - t_c)^\alpha} \times \varepsilon_{shu} \qquad \text{2-6)}$$

Where, $\varepsilon_{sh}(t, t_c)$ is the shrinkage strain at a given time in days, (t) is the given age of the concrete in days, (t_c) is the starting age of drying in days, (α) is a constant taken as 1, (f) is to be found using the formula $26 \times e^{1.42 \times 10^{-2} \times \frac{V}{S}}$, and V/S is the volume to surface ratio of the specimen. The ε_{shu} is the ultimate shrinkage strain taken from known experiment results, if available, or to be found by $\varepsilon_{shu} = 780 \times \gamma_{sh,tc} \times 10^{-6}$, where $\gamma_{sh,tc}$ can be found using the formula 1.23-0.006(V/S).

$$\varepsilon_{cs} = \varepsilon_{cd}(t) + \varepsilon_{ca}(t) \qquad \text{2-7)}$$

Where, ε_{cs} is total shrinkage strain which is by summing the drying and the autogenous shrinkage strain. To find the shrinkage strain $\varepsilon_{cd}(t)$ at a specific age, it is calculated with the formula $\varepsilon_{cd}(t) = \beta_{ds}(t, t_s) \times K_h \times \varepsilon_{(cd,0)}$. Where $\beta_{ds}(t, t_s)$ is calculated with the formula $\beta_{ds}(t, t_s) = \frac{(t - t_s)}{(t - t_s) + 0.04 \times \sqrt{h_o^3}}$, where t = age of concrete at the time considered in days, t_s = age of concrete when drying begins in days, and h_o is the notional size of the specimen calculated as $\frac{2A_c}{u}$. Where (A_c) is the concrete cross-sectional area mm^2 and (u) is the perimeter of (A_c) of that part which is exposed to drying in mm. Furthermore, K_h is a coefficient depending on the notional size (h_o) as provided in Table 2.8. $\varepsilon_{(cd,0)}$ is obtained from the formula $\varepsilon_{cd,0} = \frac{0.85 \times \beta_{RH}}{10^6} \times \left[(220 + 110 \times \alpha_{ds1}) \times e^{-\alpha_{ds2} \times \frac{f_{cu}}{f_{cm}}}\right]$, where $\beta_{RH} = 1.55 \times (1 - (\frac{RH}{RH_o})^3$, RH being the ambient relative humidity in % and RH$_o$ is taken as 100%. Also, the f_{cm} is to be taken as 10 MPa and f_{cu} is the mean compressive strength at 28 days (MPa) of the sample. The coefficients α_{ds1} and α_{ds2} depend on the cement class used to make the concrete specimen taken from Table 2.9.

Finally, to find the autogenous shrinkage strain $\varepsilon_{ca}(t)$, it is to be calculated at a given age with the formula $\varepsilon_{ca}(t) = [1 - \exp(-0.2t^{0.5})] \times [2.5(f_{cu} - 10) \times 10^{-6}]$.

Table 2.8 Coefficient K_h from (BS EN 1992-1-1, 2014)

h_o	K_h
100	1.0
200	0.85
300	0.75
≥500	0.70

Table 2.9 Coefficient depending on cement class from (BS EN 1992-1-1, 2014)

Cement class	α_{ds1}	α_{ds2}
S	3	0.13
N	4	0.12
R	6	0.11

As for LWC, the values of drying shrinkage value are in the range of 0.04 – 0.15 % (Meininger, 1966). According to (FIP, 1983), the shrinkage value of LWC is normally around 50% greater than that of NWC and is greatly affected by the properties of the LWA and its content (Chandra & Berntsson, 2002). A study by (Maghfouri, et al., 2019) found that OPSC showed a 60% higher drying shrinkage compared to NWC as well as the prediction models from both (ACI 209.2R-92, 2008) and (BS EN 1992-1-1, 2014). Higher shrinkage value occurs when the LWC contains aggregates that have high rates of absorption, low modulus, high proportion of fineness, and/or require high cement contents to obtain the specified strength (Washa, 1956). However, when the LWA is saturated, internal curing occurs which could result in decrease of shrinkage (Geiker, et al., 2004).

Several authors have investigated the drying shrinkage of OPSC at different curing regimes & curing time, different mix proportions, and with different supplementary cementitious materials like FA, GGBFS, POFA and RH. As for the testing method, mainly two types were used: the free drying shrinkage test and the bar type test. However, it is difficult to relate and compare their results, since each author has used a different specimen size, different type of test, different mix proportions and different room temperature & RH. However, some indications can be related like the increase in shrinkage qualitatively. Several graphs have been plotted with drying shrinkage results of various types of OPSC being cured for different ages as seen from Figure 2.21 to Figure 2.23. Results have shown a decrease in shrinkage when lower content of OPS (425 – 365 kg/m^3) is used by 14% at 150 days, though with low water content (Mo, et al., 2015c) (Figure 2.21). This is most probably because the moisture from the OPS assisted in internal hydration, since mixed in SSD state. This was also concluded by (Aslam, et al., 2016). When OPSC was compared to NWC, it has shown that the shrinkage value is five times that of NWC which decreased after 60 days (Abdullah, 1997). However, (Mannan & Ganapathy, 2002b) mentioned that

the drying shrinkage of OPSC was 6, 27, and 14% higher than the NWC at 28, 56, and 90 days, respectively. The author further mentioned that the reason for a higher drying shrinkage at 56 days of curing was because of the loss of water at the early age when it was in the plastic stage and the surface irregularity of the OPS. This was also confirmed in a similar study by (Mo, et al., 2015c). Mannan probably resulted in less shrinkage compared to Abdullah since he used a higher fine aggregate content (sand/cement: 1.71 vs sand/cement:1). (Maghfouri, et al., 2021) had the highest shrinkage since he had the highest A/V ratio. However, even though (Islam, et al., 2016) had a higher A/V ratio compared to (Farahani, et al., 2017), Islam had lower shrinkage. This might be because Islam kept the samples in a room with higher RH (85%), therefore reducing the shrinkage.
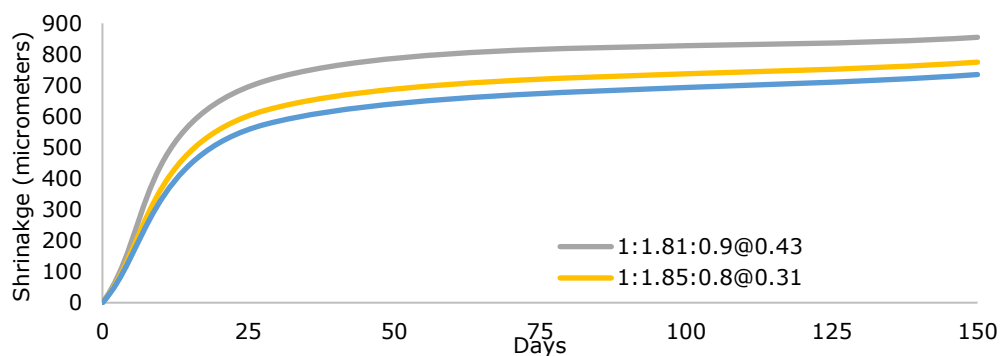
Figure 2.21 Drying shrinkage, no curing from (Mo, et al., 2015c)
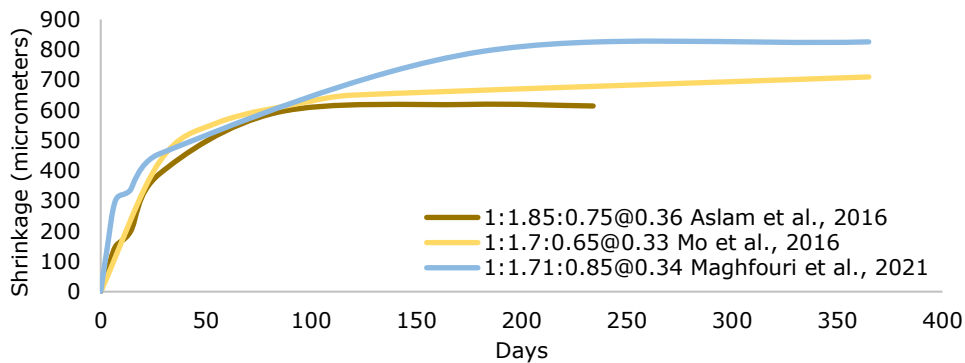
Figure 2.22 Drying shrinkage, 7 days curing

47
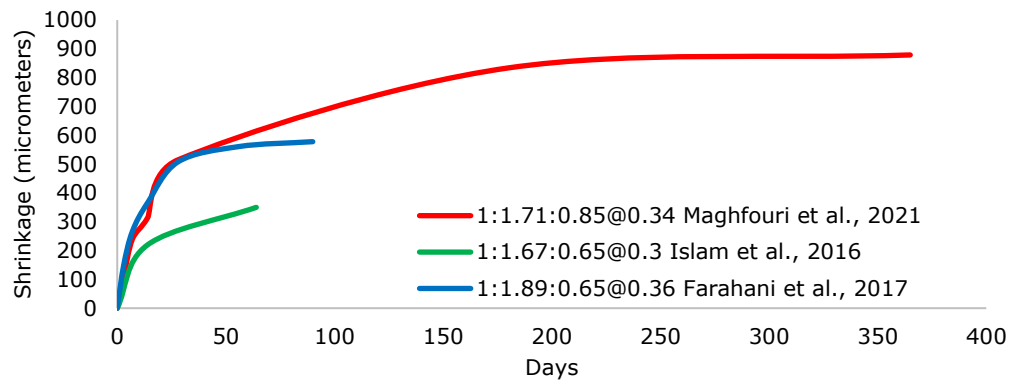
Figure 2.23 Drying shrinkage, 28 days curing

Other studies have examined the drying shrinkage effect when incorporating supplementary cementitious materials such as FA (Maghfouri, et al., 2021), POFA (Islam, et al., 2016), GGBFS (Mo, et al., 2016c), and RH+FA (Farahani, et al., 2017). Maghfouri et al. (Maghfouri, et al., 2021) incorporated 20% FA in OPSC and compared it to OPSC without FA at different curing ages of 0, 7, and 28 days as seen in Figure 2.24. It was observed that OPSC with FA content increases the long-term shrinkage (365 days) with higher curing age with 35% whereas without FA only 23%. While up to 7 days, no significant difference in shrinkage was observed for all specimen types.
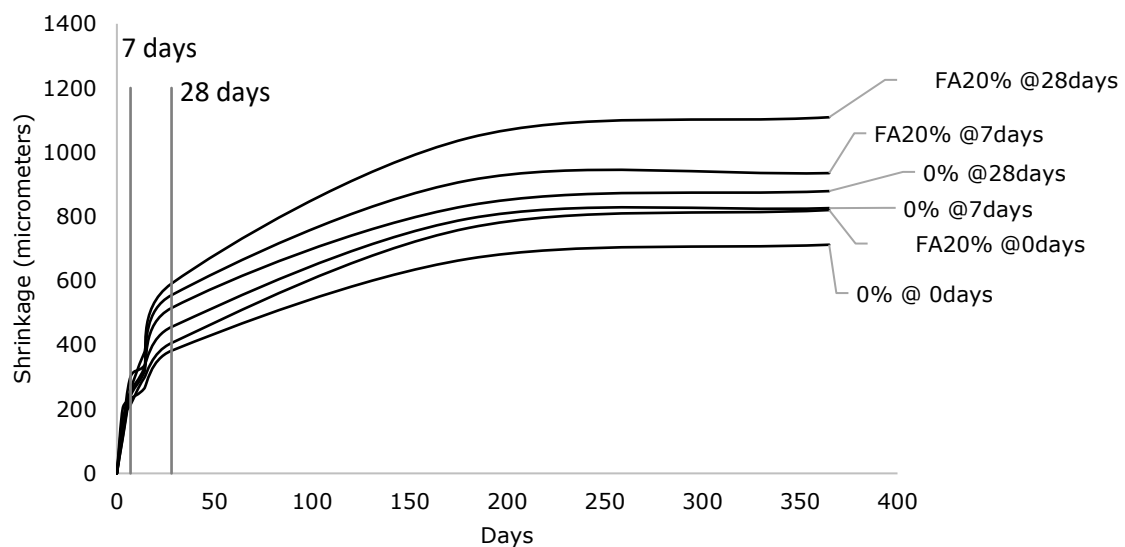
Figure 2.24 Drying shrinkage OPSC with FA (Maghfouri, et al., 2021)

Shafigh et al. (Shafigh, et al., 2013a) mentioned when OPSC is mixed with 10% of FA, no difference in drying shrinkage was observed. However, only an insignificant increase was observed when higher levels were used (30% and 50%) by 17% and 8% greater than the control specimen, respectively. An increase of drying shrinkage of OPSC was found with higher levels of POFA (10%, 30% and 50%) with a w/c ratio of 0.3 cured with 28 days by 53%, 66% and 126% respectively after 64 days. However, with a higher w/c of 0.4, OPSC

48

with 70% of POFA was found to be similar to 0% of POFA as seen in Figure 2.25 (Islam, et al., 2016).
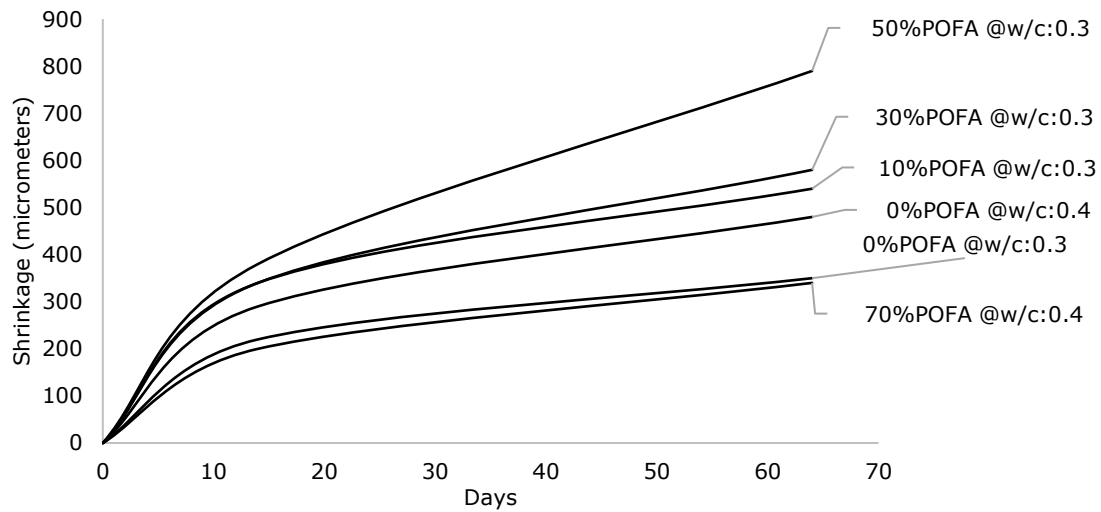
Figure 2.25 Drying shrinkage of OPSC with POFA (Islam, et al., 2016)

In a long-term study of 365 days by (Mo, et al., 2016c), it was found that OPSC without GGBFS replacement had a comparable drying shrinkage value to OPSC with 40% of GGBFS as seen in Figure 2.26. However, when the GGBFS was increased to 60%, the drying shrinkage also increased by 20%. Mo et al. mentioned the reason for this might be because the free water could escape from the pores caused by the low hydration with the presence of high GGBFS content.
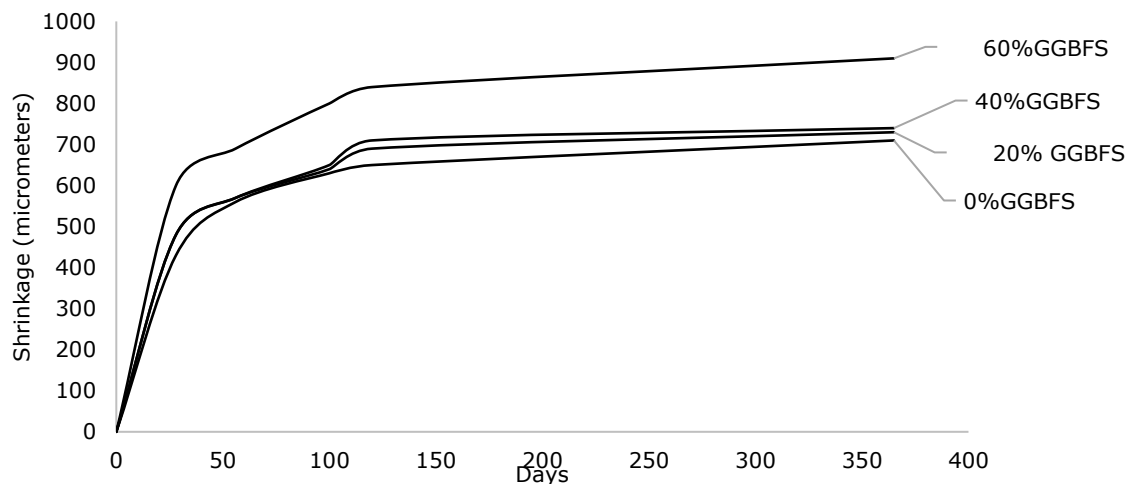
Figure 2.26 Drying shrinkage of OPSC with GGBFS (Mo, et al., 2016c)

An increase in drying shrinkage was also found when using RH and RH+FA in OPSC, especially of RH and RH+FA in OPSC at 20% and 30% replacement by 26% and 79% compared to the control, respectively. However, no significant difference was seen with 10% RH and 15% RH+FA as seen in Figure 2.27. The author further recommended when

OPSC is incorporated with 30% of RH and or RH+FA, it is not recommended to be used for constructing structural elements due to its high shrinkage value (Farahani, et al., 2017).
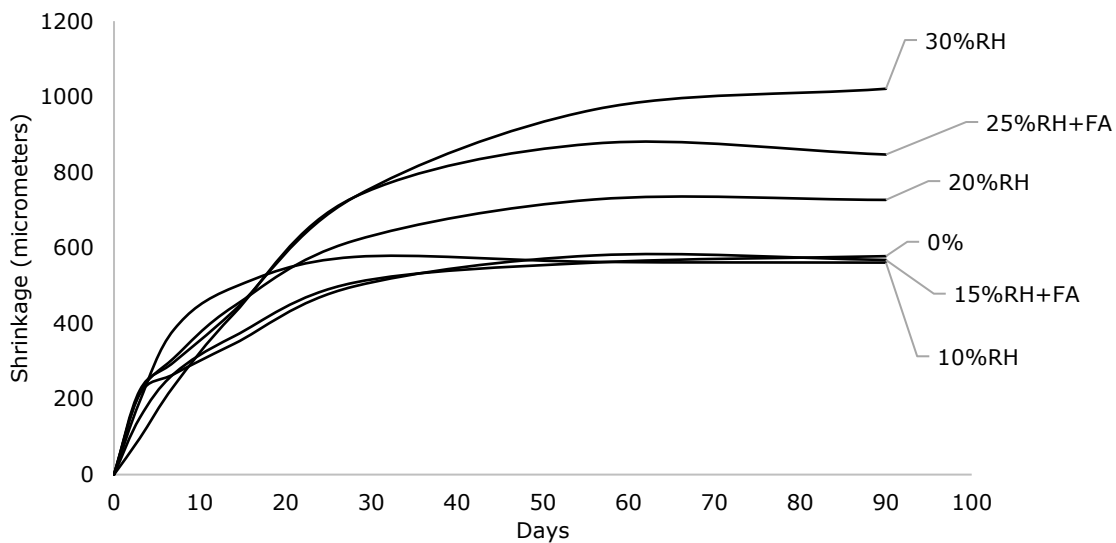
Figure 2.27 Drying shrinkage of OPSC with RH+FA (Farahani, et al., 2017)

2.3. Trends in OPSC Research

In Section 2.2, it was observed that almost no OPSC researcher covered in this review specified the variety of OPS being used in OPSC, and that the thicker Dura shell was being phased out by the thinner, albeit denser Tenera OPS, as the respective fruit type yields more oil. Furthermore, in Section 2.1.5 it was noted that the sterilization process in palm oil milling considerably reduces the hardness of OPS, which is beneficial for the stripping and oil extraction process, but renders OPS much weaker than its fresh, non-sterilized counterpart. Also in the same section, mechanical testing of OPS was performed to show a poor ability to withstand surface deformation. From these observations, the author of the present review hypothesizes that little attention has been paid to the high variance in mechanical properties of OPS, leading to poor predictor models of OPSC performance based on research literature, as detailed in Section 2.2.3 and 2.2.4.

To further support this hypothesis, a basic bibliometric analysis was performed on recent literature on OPS and OPSC, with the goal of finding trends that corroborate with the findings of this review. The term "oil palm shell" and "concrete" were searched in the Web of Science catalogue, and the abstracts of the cumulative results were exported for bibliometric analysis. The "Bibliometrix" package in R was used for capturing the relevant trends (Aria & Cuccurullo, 2017). Only English language research papers were used to ensure the abstracts were catalogable, however both research and conference papers were included in the data analysis. Figure 2.28 shows the cumulative publications of OPSC, along with 'dura', 'tenera' and 'pisifera' specific research publications. As is evident, despite the

recent rise in OPSC published research, reaching a cumulative peak of 1525 publications by the end of 2022, less than 10% of oil palm research has considered the variety of OPS important enough to be highlighted in either the title, keywords, or the abstract of the total publications. Figure 2.29 further breaks down OPSC related research, showing countries with the most cited references. Malaysia is seen as the highest, reaching 168 publications, while the second most publications are only 21, for India.

This is completely logical, but it does raise questions regarding the global utilisation of OPS as a viable LWA for LWC. Specifically, that if most research arises from a close network of academics, it is also likely that they will have a singular source of OPS and will be conducting tests at the same research facilities, with preestablished specific research interests and/or areas, namely the incorporation of OPS in concretes with various additives/admixtures. The lack of new research networks can inhibit other directions of research (Kemmelmeler, 2015), which specifically in this case is the investigation into mechanical characteristics of the OPS aggregate itself. Regarding the source of OPS, a singular source, or perhaps stockpile of old shells may cause a discontinuity between results in OPSC and the recent trend of thinner, denser shells from the Tenera variety. As the researchers do not specify the age of their OPS, the variety, or the mechanical properties such as hardness and cohesiveness, and based on the included images of OPS in the respective research publications, it is not entirely unlikely that an old, now defunct Dura variety of OPS is continually being tested. However, until new research specifies their OPS, this is all presumption and cannot be confirmed either way.
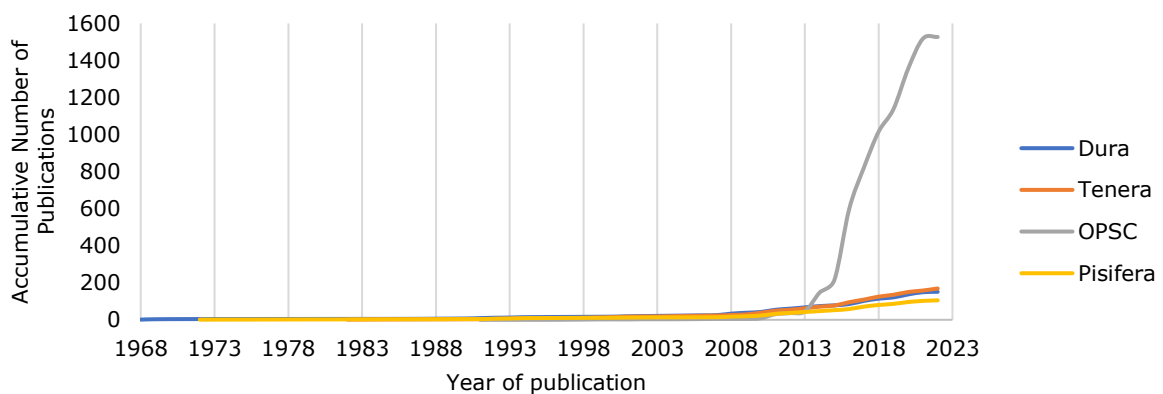
Figure 2.28 Number of publications on Dura, Tenera, OPSC and Pisifera
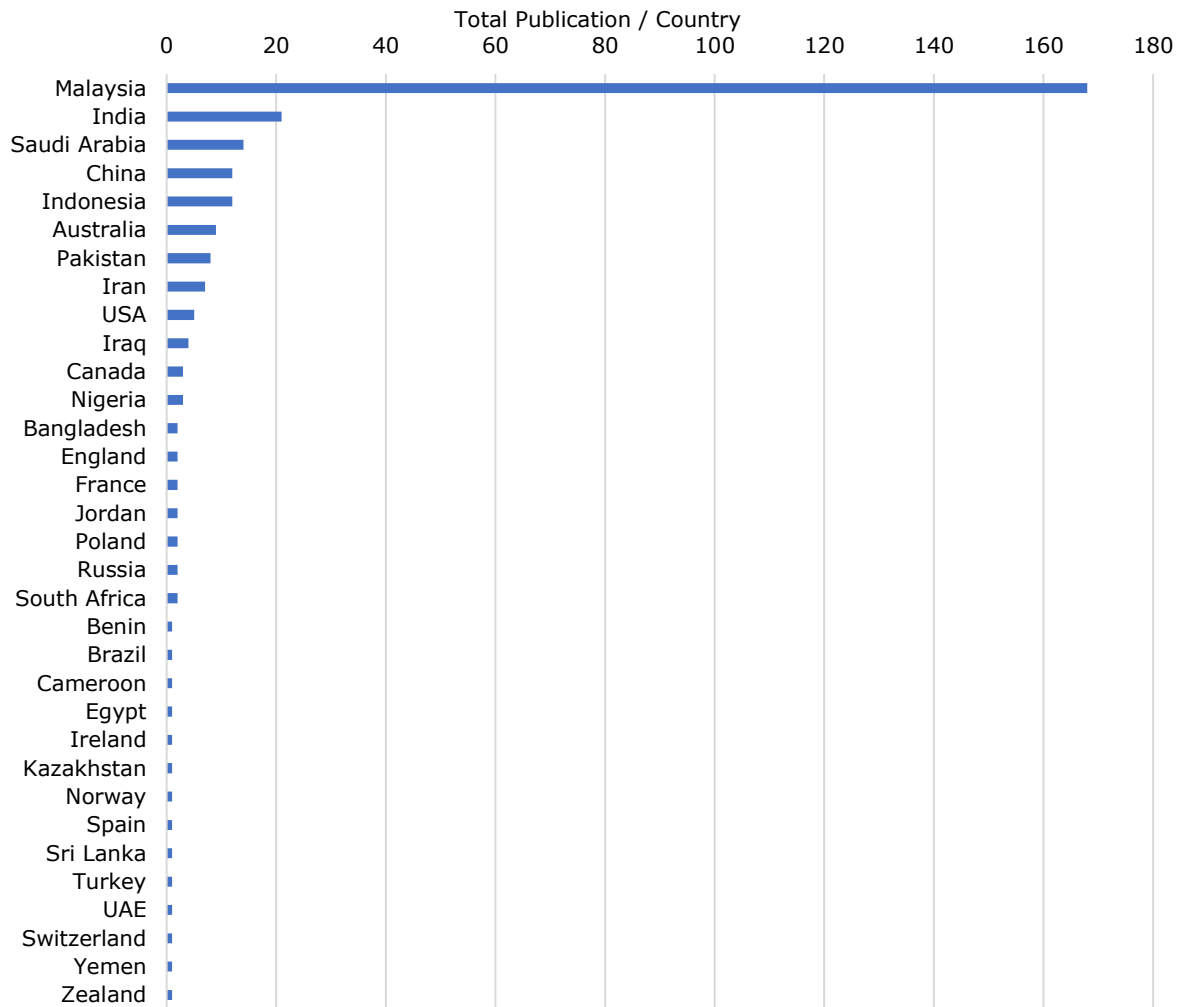
Figure 2.29 Total publications per country on OPSC

2.4. Summary

Significant research has been undertaken to incorporate OPS in concrete, with varying success. Mix designs of OPSC appear to follow typical LWC trends, and addition of pozzolanic additives or plasticizing admixtures also work as intended, making OPS use as a coarse aggregate viable in concrete. Furthermore, OPS do not affect workability significantly, which adds to the practicality of OPSC. However, the low density and high porosity of the shell is known to cause bleeding issues in the mix, alleviated by heat treatment, PVA coating, or treatment with lime. Additionally, the high porosity of OPS and possibly its prolonged sterilization in the milling process may significantly increase its water absorption capacity. As a mitigative measure, it is recommended to have OPS in an SSD state prior to mixing. The adhesion of hydrated cement paste with the surface of OPS has also been investigated, mitigated by cleaning with detergent or lime/PVA treatment. Research literature has deduced that OPS's smooth surface could be resulting in poor bonding with hydrated cement, however flexural and tensile strength results of OPSC are

more comparable to LWC, with compressive strength showing greater reductions and variabilities. This leads into some significant research omissions, which the author of the present review hypothesizes to be primary reasons behind the discrepancy in OPSC mechanical performance throughout the researched literature.

Unlike typical mineral LWA such as expanded shale, clay, or lime, the palm oil fruit is organic, and its growth is incumbent upon the environmental conditions, such as exposure to sunlight, age of ripening, etc. This also affects the palm oil kernel, also called the OPS. Research of the palm oil fruit showed that the genus of the plant bearing the fruit (dura, tenera, or pisifera) can significantly affect the OPS thickness, hardness, and porosity. With conventional LWA, high variance between coarse aggregates is not expected due to their crystalline origins, but most research on OPSC seemed to hold similar expectations with the OPS. As a result, there are glaring omissions of any mechanical tests performed on the OPS, and almost no information conveyed on mechanical properties of the shell aggregates being incorporated in OPSC. Furthermore, most literature did not specify the variety of OPS, age of the shell, storage conditions, and even the source where OPS was collected from, all of which are key parameters needed to better understand the characteristics of the aggregate being incorporated. Conversely, OPS is mostly subjected to conventional aggregate tests such as sieve analysis or crushing, which research as early as 1990 had deemed inappropriate for this aggregate. The consequence of this approach is high variable in strength results, and low precision that often fails to validate the conclusions made by research authors. Often these results are non-replicable, with similar mix designs of OPSC giving 28-day compressive strengths in the range of 9 to 50 MPa. The absence of OPS characteristics then makes any detailed critique impossible. There is also an over-reliance on standard testing methods such as ASTM, which are not intended for LWA such as OPS and often give results that are inconsequential at best and misleading at worst, such as performing sieve analysis for OPS which fails to account for the thickness of the shells, a key mechanical property. Also, for instance, the water absorption of OPSC was not determined, rather only the OPS samples. This may be overlooked for typical mineral LWA but would drastically impact the curing in OPSC. Furthermore, more specific research such as the effects of admixtures, pozzolans, and additives on OPSC is also still open for critique, as presumptions of the smoothness of OPS surface and its adhesion to the hydrated cement matrix in the ITZ remains unverified if the surface roughness and profile of OPS has not been quantified.

Over the last decade, developments in breeding of oil palm trees have resulted in considerably thinner shells, which would drastically alter the OPS mechanical properties. However, this change has not been reflected even in current OPSC research. To investigate, a simple bibliometric analysis was performed to better gauge the locations of research,

and to (roughly) infer which variety of OPS is likely being used. Results showed that most research has been conducted at only a handful of research institutions by a close network of esteemed researchers. This may introduce several biases in the aggregate collection and testing, especially if a singular source, or even stockpile, of OPS has been used to conduct research over the decades but would explain the absence of thinner shells in new research. Thus, a detailed examination and inclusion of resulting characteristics of OPS are further emphasized to ensure such biases are not prevalent. Other practical recommendations are as follows:

- Reporting mix designs by both weight and volume of OPSC constituents to account for the variability in density of OPS.
- Mean thickness measurements of the OPS to consider its potential toughness and or strength.
- Detailed information on the variety of palm oil fruit, age of parent plants, and time elapsed since extraction and sterilization of said fruit from which the OPS originates.
- Crushing of OPS for improved strength performance.
- Exploration of the use of OPS as fine aggregate, as results showed improved strength with finer OPS particles.

By following the abovementioned recommendations will allow for much more precise data regarding the mix design of OPSC, which could greatly accelerate OPSC research, as more predictable performances of OPS can allow for practical implementations of the product, which would address the sustainable and environmental issues surrounding OPS waste production.

Chapter 3. Methodology

In this chapter, the experimental setups for this study are presented, outlining the procedures adopted to achieve the study's objectives. The primary focus of this research is to create mix designs for NWC, coarse, and fine Tenera OPSC with a 28-day moist cured compressive strength of 20 MPa. The fundamental mechanical properties of these concretes are then experimentally investigated, compared, and evaluated to determine whether Tenera OPSC remains a viable solution for producing SLWC. The experimental investigation's flowchart is shown in Figure 3.1. The following sections provide a detailed explanation of the methods used in each stage, including the materials used, testing procedures, and data analysis techniques.
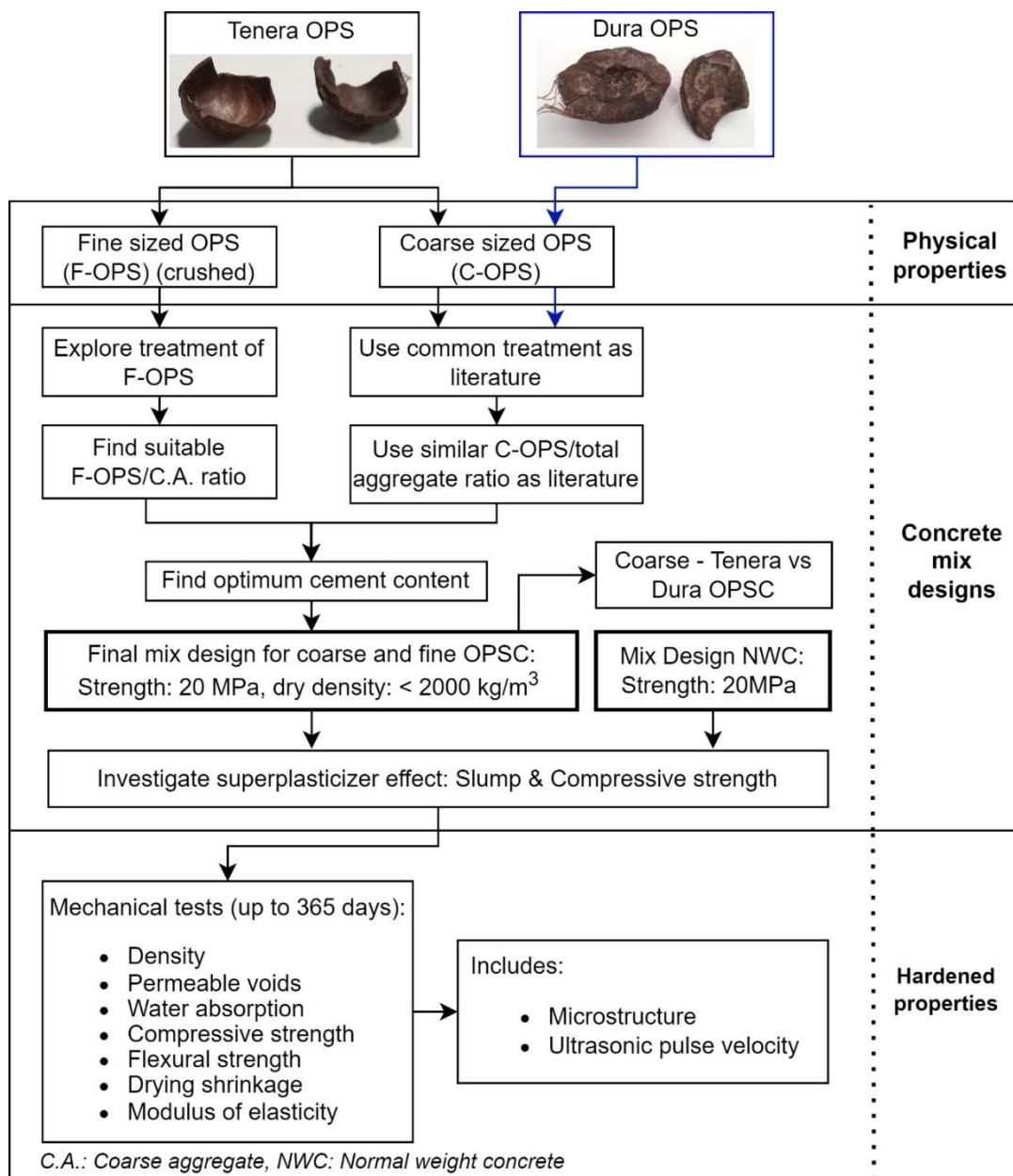
Figure 3.1 Flow Chart of the experimental study

In this chapter, Section 3.1 presents a comprehensive list and description of the materials used in this study, including the physical property tests conducted on the main materials used to produce NWC, coarse, and fine OPSC. The establishment of mix designs for NWC, coarse, and fine OPSC is described in Section 3.2, wherein a single mix design is selected for each type of concrete for the main tests throughout the study. The evaluation of the effect of superplasticizers on the concretes with the chosen mix designs is also included in this section. Section 3.4 details the methods used to evaluate fundamental mechanical characteristics, such as compressive strength, flexural tensile strength, dynamic and secant MOE, drying shrinkage, permeable voids and water absorption, ultrasonic pulse velocity (UPV), and microstructural analysis of the hardened properties on the selected mix designs. Finally, Section 3.4 outlines the methodology for batching, casting, and curing the concrete samples required for the tests in this study.

3.1. Materials and Physical Properties Tests

3.1.1. Materials for Concrete

The materials employed in this study comprise Portland cement, natural fine and coarse aggregates, Dura and Tenera OPS, potable water, and liquid superplasticizers. Further information about these materials is provided in the subsequent subsections.

3.1.1.1. Cement

The present investigation employed MS EN 197-1-CEM II/B-L 32.5N, commercially recognized as CASTLE, as the cement type. Table 3.1 presents an overview of the properties of the CASTLE brand cement. The cement bags were utilized within a two-week timeframe subsequent to delivery and were carefully stored in a sealed container. No specific analyses were conducted on the cement specimens.

Table 3.1 Castle cement properties (YTL, 2016)

Tests		Units	Specification MS EN 197-1: 2014 CEN II/B-L 32.5N	Test results
			Chemical composition	
Sulphate Content (SO$_3$)		%	Not more than 3.5	2.1
Chloride (CL)		%	Not more than 0.10	0.01
			Physical properties	
Fineness (According to Blaine)		m^2/kg	-	440
Setting time: Initial		Mins	Not less than 75	155
Soundness		mm	Not more than 10	0.8
Compressive strength (mortar prism)	: 7 days	MPa	Not less than 16	24.0
	: 28 days	MPa	$32.5 \leq x \leq 52.5$	35.2

3.1.1.2. Aggregates: Fine and Coarse Aggregate

The aggregates for NWC and OPSC consisted of both fine (river sand) and coarse (granite) materials. These aggregates were obtained from Yap Lee Hardware Trading Store, located in Semenyih, Selangor, and were readily available in the laboratory of the University of

Nottingham, as illustrated in Figure 3.2. The maximum size of the coarse and fine aggregate utilized was 20 and 5 mm, respectively. Throughout this study, the coarse aggregate from granite will be referred to as "coarse aggregate," and the river sand will be called "fine aggregate" for the sake of simplicity. Additionally, the coarse and the fine aggregates are also referred with the "conventional aggregates".

Figure 3.2 Coarse and fine aggregate

3.1.1.3.   Oil Palm Shell

Two types of OPS were used in this study. The main type of OPS used for the experiments is known as Tenera, see (a). The other type is known as Dura seen in Figure 3.3 (b). The classification for Tenera and Dura is explained later in Section 3.1.2.1. In this study, Tenera-OPS was used as coarse sized (C-OPS) and fine-sized (F-OPS) whereas Dura-OPS was used as coarse sized only. For both Dura and Tenera as C-OPS, sizes of 4.75 mm and larger were used. The Tenera-OPS was around 8 years old stored outside the laboratory in large, closed containers. The OPS was obtained from a farm in Carey Island, Klang, Selangor. The Dura-OPS was collected from Sime Darby plantation in Lukut Port Dickson Nigeri Sembilan. No information was available on the sterilization for both materials.

This study employed two types of OPS, as shown in Figure 3.3 (a) & (b). The primary type utilized for the experiments was Tenera OPS, while the other type was Dura OPS, as classified in Section 3.1.2.1. In particular, Tenera OPS was utilized as both coarse-sized (C-OPS) and fine-sized (F-OPS), while Dura OPS was used solely as coarse-sized. For both Tenera and Dura OPS, particle sizes of 4.75 mm and above were selected for C-OPS. As for the F-OPS, Tenera OPS was crushed to particle sizes of 5 mm and below.

The Tenera OPS was roughly 8 years old and had been kept in closed containers outside the laboratory. The OPS was obtained from a farm located in Carey Island, Klang, Selangor.

On the other hand, Dura OPS was sourced from Sime Darby Plantation in Lukut Port Dickson, Negeri Sembilan. Unfortunately, no information was available regarding the sterilization procedures for either of these materials.

<div align="center">(a)   (b)</div>
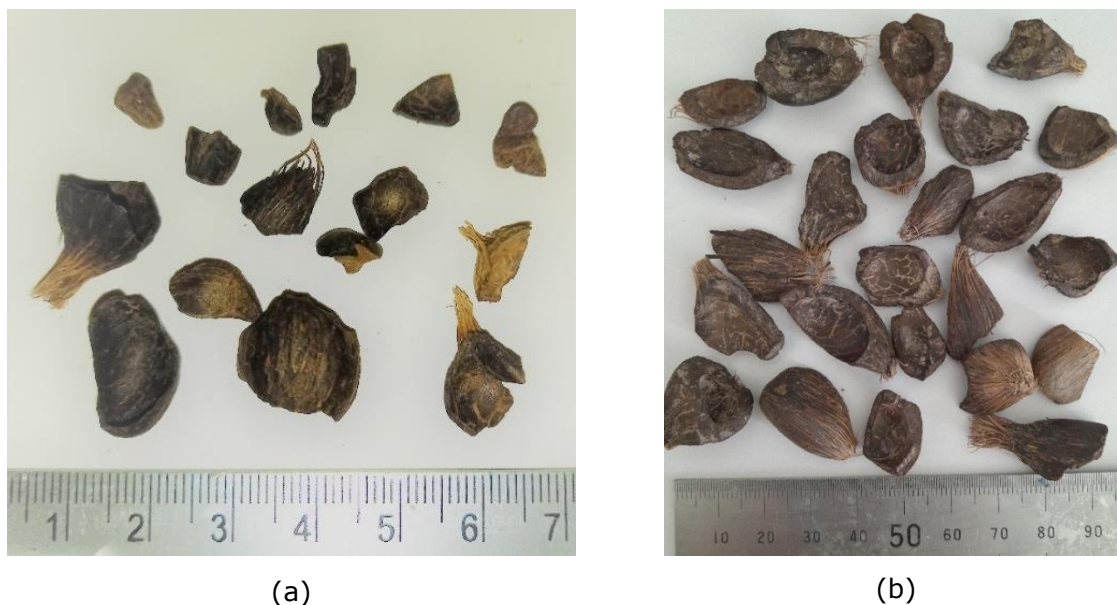
<div align="center">Figure 3.3 Coarse sized Tenera- and Dura-OPS</div>

Coarse sized oil palm shell

During OPS collection, the shells are often mixed with fibres and dirt, as illustrated in Figure 3.4 (a). Consequently, the OPS was initially sieved with a 4.75 mm sieve size to eliminate unwanted materials such as dirt and OPS fibres. To handle large quantities of OPS, a high-capacity sieve shaker was employed, as shown in Figure 3.4 (b). After the sieving process, the OPS was washed with water to remove any remaining dirt. This was achieved using a drum mixer, as depicted in Figure 3.4 (c). The drum was drained and refilled with water three times to eliminate dirt. On the fourth cycle of adding water, a detergent (1 - 2% of the total OPS weight) was introduced to remove oil, sand, fibres, and any other impurities. The process took five minutes, after which the water was drained, and the OPS was washed with water several times to eliminate the detergent. The OPS was manually inspected for oil and dirt residue and left to dry under the sun, as shown in Figure 3.4 (d), until it felt free from oil and dirt. This produced clean OPS, as seen in Figure 3.4 (e).

It was observed that drying the OPS was crucial after cleaning. When left wet and stored overnight, insects and microbes were attracted, and a repulsive odour developed. Additionally, a white substance similar to spider webbing was found on the OPS, as depicted in Figure 3.5. This can perhaps be identified as something known as white-rot fungi (Fitriyah, et al., 2022), which is further discussed in Section 4.3.2.1. Nevertheless, this was prevented by fully drying the OPS in an oven at 100˚C for 24 hours. Approximately

18 kg of uncleaned OPS was necessary to produce 10 kg of clean OPS using this cleaning process.

Before incorporating OPS into the concrete mix, the OPS was soaked in water for 24 hours and then left under the sun for a few hours (depending on the weather) to attain a saturated surface-dry (SSD) state. Visual inspection was used to confirm that the OPS had achieved SSD, although this could differ depending on the person. This treatment process was conducted using a technique similar to that used by other researchers (Hamada, et al., 2020). This similar treatment method was also used for the Dura OPS.

(a)　　　　　　　　　　(b)　　　　　　　　　　(c)

(d)　　　　　　　　　　　　　　(e)
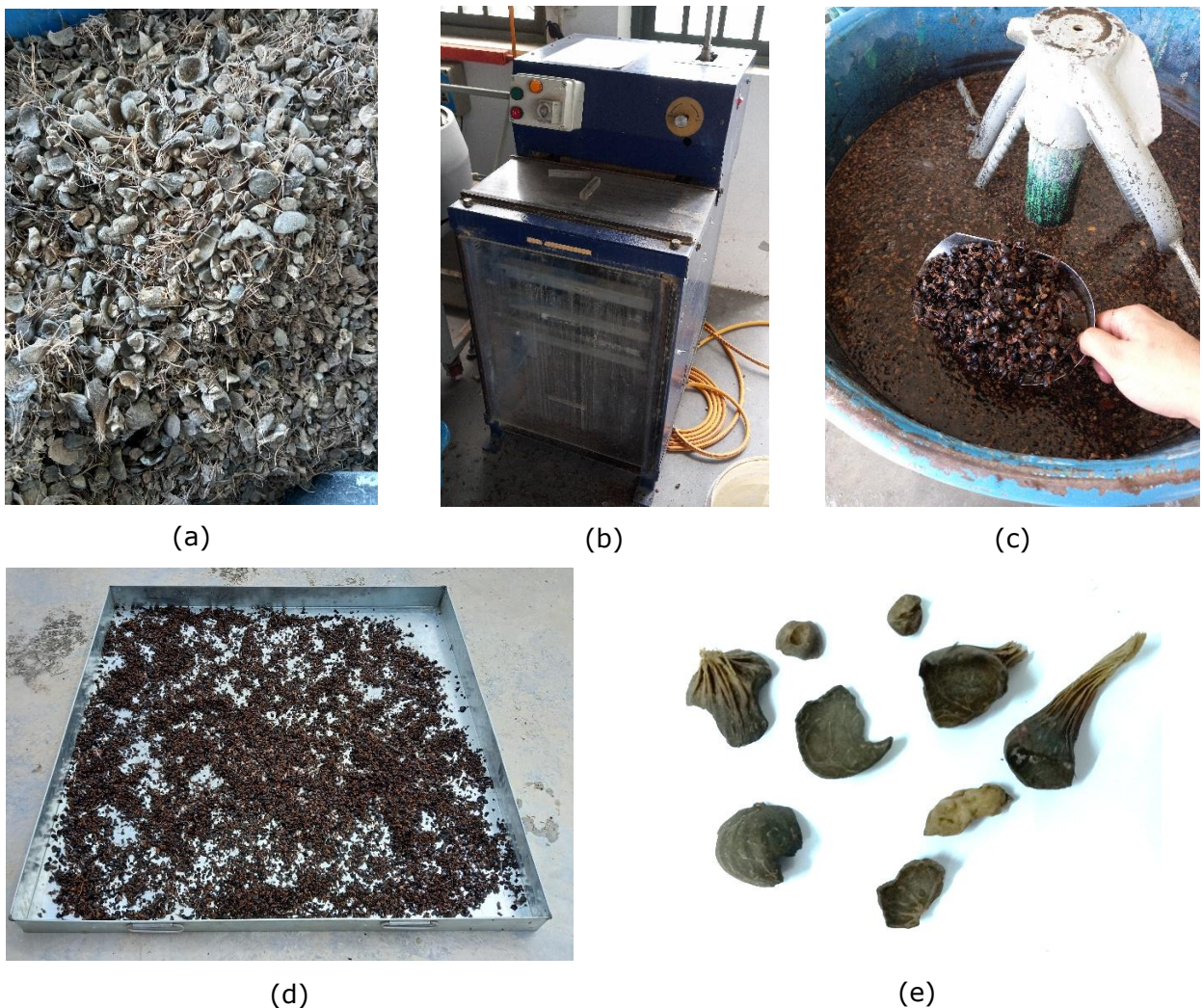
Figure 3.4 Cleaning process (a) Dirty OPS (b) Mechanical heavy duty sieve machine (c) cleaning with detergent (d) Surface drying OPS (e) Cleaned OPS

(a)

(b)

Figure 3.5 Wet OPS left overnight

Fine sized oil palm shell

The Tenera OPS collected was initially subjected to crushing using a Retch SM100 apparatus equipped with a sieve size opening of 5 mm to produce fine-sized OPS (F-OPS), as depicted in Figure 3.6 (a – c). Subsequently, the F-OPS underwent further evaluation with varying treatment methods prior to the mixing process, which is elucidated in Section 3.2.3.

(a) Raw Tenera-OPS　　(c) Crusher Retch SM100　　(c) Dirty dry F-OPS after crushing
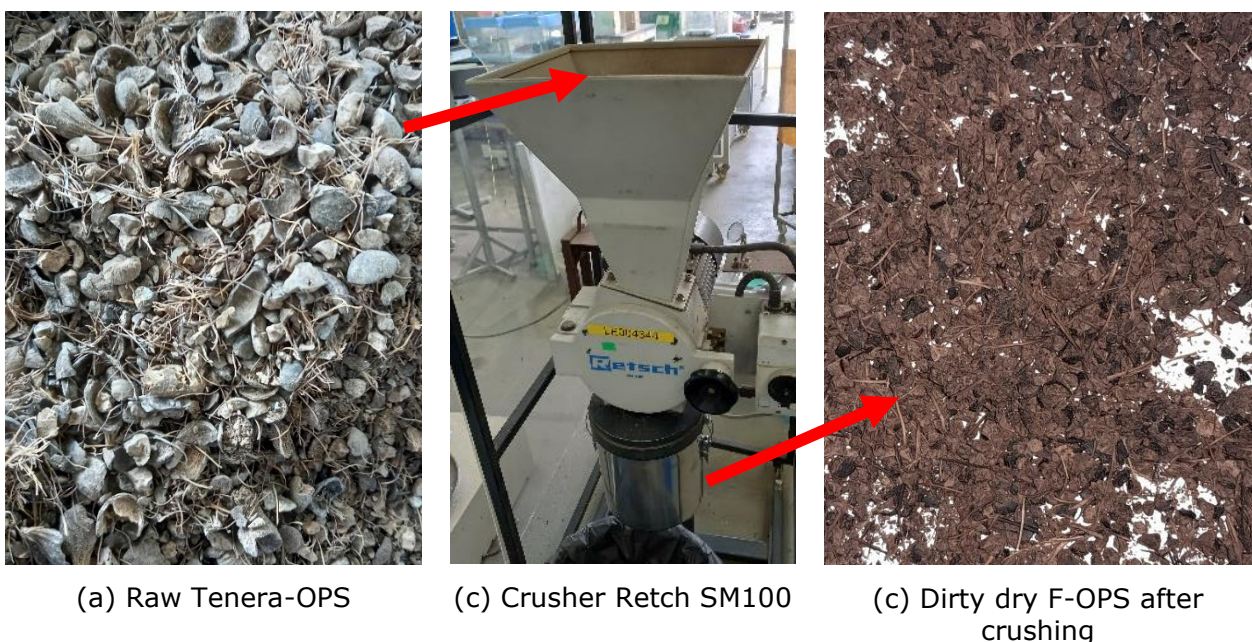
Figure 3.6 Process of producing dirty dry F-OPS

3.1.1.4.　　Water

Tap water was employed for all the mixes, and no water tests were performed as they were deemed inconsequential.

3.1.1.5.   Superplasticizer

In this study, liquid-based superplasticizers (SP) with the trade name VS 1250 NT were acquired from Sika. The SP composition comprises a polycarboxylic polyether-type polymer with a density of 1.08 kg/l. The recommended dosage, according to the product data sheet from (Sika, 2019), is 0.25 – 1.0% by weight of cement.

3.1.2.   Physical Properties

In order to determine the properties of the fine aggregate, coarse aggregates, Dura OPS, and Tenera OPS (both fine and coarse-sized), a sieve analysis was conducted along with identifying their apparent particle density, oven-dried particle density, saturated surface dry (SSD) particle density, and water absorption, as per the guidelines set by (BS EN 933, 2021) and (BS EN 1097-6, 2022), respectively. Furthermore, for the C-OPS samples of both Dura and Tenera, a measurement-indexing testing technique was proposed. The procedures utilized to obtain these properties are elaborated in the following subsections.

3.1.2.1.   Shape and texture - OPS

To provide a comprehensive analysis of the shape and other properties of the OPS, normal and microscopic images were captured. As for Tenera F-OPS, only normal images were taken.

3.1.2.2.   Dimensions

Sieve analysis

The specimens were first cleansed and subsequently dehydrated in an oven for more than one hour at 110°C, followed by air cooling. The sieve sizes employed are indicated in Table 3.2. The sieve shaker was operated for 10 minutes, and the mass was measured for each sieve pan. The cumulative weight passing (%) was calculated from the data and plotted against the sieve size using a logarithmic scale (base 10). In addition, the fineness modulus was computed according to (BS EN 12620, 2008) by summing the cumulative mass percentages retained and dividing the total by 100.

Table 3.2 Sieve opening sizes

Coarse size (mm)	Fine size (mm)
20.0	5.00
14.0	2.36
12.5	1.18
10.0	0.60
5.0	0.30
-	0.15

Measurement indexing method

The thickness of OPS as coarse size was measured using a digital electronic vernier calliper gauge micrometre, see Figure 3.7. First, the samples were divided in sizes by sieves of 14

mm, 10 mm, and 5 mm. Then, for each divided size, the height, width, and thickness measurement of the shells were taken as seen in Figure 3.7 (a), (b), and (c) respectively. A variety of measurements were taken from a handful of the sample of the most common shapes. For each set of sieves, the minimum and maximum of length, width, and thickness were measured. This test was only done for both Dura and Tenera OPS as coarse sized (C-OPS).

| (a) | (b) | (c) |
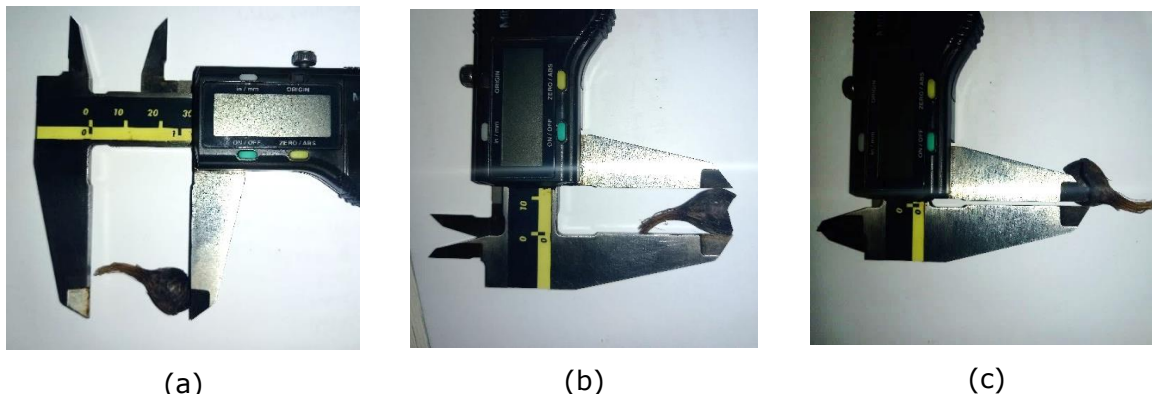
Figure 3.7 (a) Height OPS (b) Width OPS (c) Thickness OPS

3.1.2.3.   Density and water absorption

Coarse sized

The conventional coarse aggregates were subjected to a series of procedures prior to conducting the experiments. Initially, the aggregates were dried in an oven at a temperature of 110°C for 24 hours. After this, they were immersed in water for 24 hours to attain a fully saturated state and weighed in water using a specialized weight balance, see Figure 3.8. The samples were then removed and placed on a soft, absorbent cloth to achieve an SSD state, and their weight was recorded. Based on the values of fully dry, saturated in water, and SSD states, the apparent, oven-dried, SSD particle density, and water absorption were determined using the formulas provided in (BS EN 1097-6, 2022) and presented in Appendix A. Similar techniques were employed for Dura and Tenera OPS, with the exception that they were dried to an SSD state outdoors, as explained in Section 3.1.1.3.

Figure 3.8 Balance with wire basket

Fine sized

The conventional fine aggregate was first soaked in water for 24 hours and then dried with an air-dryer until an SSD state was achieved. The SSD state was observed by using a small conical mould with a tamper, see Figure 3.9 (a). The sample was put into the mould until filled and tamped 21 times by realising the tamper 1 cm above the sample. This process was repeated until the sample was similar to as seen in Figure 3.9 (b). when the sample was determined to be in an SSD state, it was either directly used in the mix or kept in a sealed bag to retain its internal moisture.

The sample was then put in a pycnometer and water was added until it was filled. The weight was taken of each element (sample, pycnometer with and without water and sample). The sample was then fully dried in an oven for 24 hours at 105°C. For F-OPS, this was done in the same manner. With these values, the apparent particle density, oven-dried particle density, SSD particle density, and water absorption were found. The formulas for these calculations are shown in Appendix A obtained from (BS EN 1097-6, 2022).

(a)

(b)
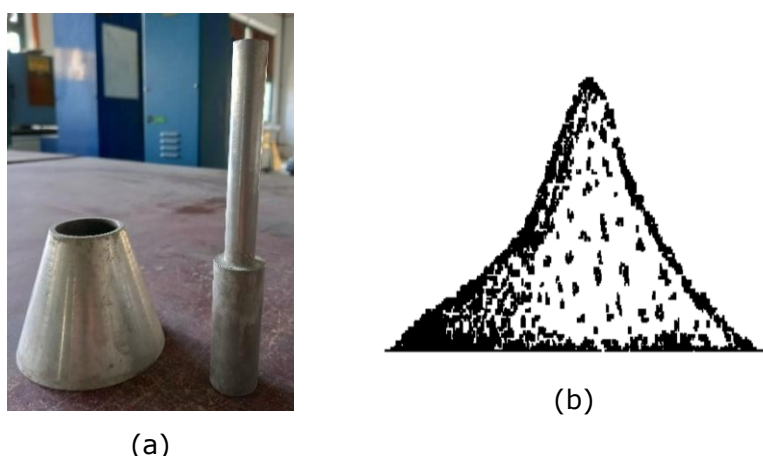
Figure 3.9 (a) Metal conical mould with tamper and (b) examples of surface-dry state
(BS EN 1097-6, 2022)

3.2. Concrete Mix Designs

This section describes the methods used to produce mix designs for NWC, coarse, and fine OPSC in sub-sections 3.2.1, 3.2.2, and 3.2.3, respectively. The mix designs were produced by applying the weight method. For the weight method, the sum of the total weight of all the materials were set equal to a known or a desired density in kg/m^3 based on previous data. Another very well-known method is the absolute volume method, known as the basis of the ACI method (ACI 211.1-91, 2009) of proportioning NWC is however, not useful for designing LWC (Mehta & Monteiro, 2006). Though the ACI also proposes a mix guideline for LWC from the report (ACI 211.2-98, 2004), this was proven not to be suitable as mentioned in Section 2.2.3. Therefore, for comparability reasons, the weight method was utilized for all three concretes by the trial-and-error basis whereas, only for the NWC, the

guideline from (Teychenné, et al., 1988) proposed by the BS standard was employed (BS EN 206, 2021). The mixes were aimed to maintain a balance between the required properties (compressive strength and dry density) of the concretes and economy.

All three mix designs were aimed to reach a cured compressive strength of 20 MPa at 28 days for comparison. As for coarse and fine OPSC, their dry density was targeted to be below 2000 kg/m^3 to produce LWC. The proportion for these mixes were adjusted to achieve an optimum mix proportion used throughout this entire study. Additionally, in Section 3.2.4, the incorporation of SP was investigated to evaluate its effect with the selected mix design for coarse and fine OPSC and compared to NWC. The detailed methodologies for the mix designs are explained in the coming subsections.

3.2.1. NWC

The NWC was prepared using cement, fine aggregate, coarse aggregate, and water. NWC concrete cube samples of 100x100x100 mm^3 were casted for mix trials to achieve a desired 28-day compressive strength of 20 MPa (cured). The guideline used for choosing the mix ratio for NWC was from the BRE (Teychenné, et al., 1988), see Appendix B. The NWC was made as a reference concrete and is in conformity with (BS EN 480-1, 2014). Table 3.3 shows the trial mix ratios chosen for NWC. The chosen mix ratio used throughout this research was NWC 1, and the details of the results are explained in Section 4.2.1.

Table 3.3 Trial Mix design NWC

ID	Cement	Fine Aggregate	Coarse Aggregate	Water	w/c
		Kg/m^3			
NWC 1	350	605	1175	217	0.60
NWC 2	238	828	1144	190	0.80
NWC 3	365	715	1160	160	0.44
NWC 4	365	715	1160	150	0.38

3.2.2. Coarse OPSC

The treatment method for the C-OPS used in the coarse OPSC was done in the most common way as done by researchers in the literature; the C-OPS treatment method followed the most popular methodology found in the literature, which sets for cleaning the C-OPS with a detergent and using it as SSD state before mixing, see Section 3.1.1.3. To be able to compare Dura OPSC from literature, similar mix designs used for Dura OPSC were adapted as a basis and was further modified to reach the desired compressive strength with Tenera coarse OPSC used in this study.

The coarse OPSC was prepared using cement, fine aggregate, Tenera C-OPS, and water. The target 28-day compressive strength of 100x100x100 mm^3 size moist-cured OPSC was 20 MPa. The mix ratios chosen for trail mix is shown in Table 3.4. Similar mix designs from

(Gibigaye , et al., 2017) and (Basri, et al., 1999) have also been used to compare Tenera to Dura OPS in concrete. The mixes A – G were all kept with a target density of 1800 kg/m³. Therefore, as the cement was increased, the other materials were decreased subsequently. The mixes A – G were based on mix designs ranging from 20 – 22.5 MPa taken from Table 2.5. it was found that the highest frequency for OPS to total aggregate ratio occurs around 35%, see Figure 3.10 and Appendix C. This 35% was also found to be the average from all the mixes in Table 2.5 and shown in Figure 2.12 (d). Therefore, for comparison reasons, the 35% ratio was adapted for the mixes A – G. The selected mix ratio used throughout this study was MIX G, and the details of the results are explained in Section 4.2.2.

In Addition, coarse OPSC made with Dura OPS was also tested with the mix design from (Gibigaye , et al., 2017), (Basri, et al., 1999) and Mix G from Table 3.4 for comparison. The Dura OPS was cleaned with a detergent and utilised in SSD state prior to mixing.

Table 3.4 Mix design by weight for OPSC

OPSC Reference/ID	Cement	Fine Aggregates	C-OPS	Water	w/c
	Kg/m³				
Tenera OPSC					
(Gibigaye , et al., 2017)	450	688	446	203	0.45
(Basri, et al., 1999)	480	821	370	197	0.41
Mix A	850	296	153	306	0.36
Mix B	950	300	161	390	0.41
Mix C	950	312	168	371	0.39
Mix D	950	336	181	333	0.35
Mix E	950	355	191	304	0.32
Mix F	1050	221	119	410	0.39
Mix G	1050	283	152	315	0.30
Dura OPSC					
(Gibigaye , et al., 2017)	450	688	446	203	0.45
(Basri, et al., 1999)	480	821	370	197	0.41
Dura-Mix G	1050	283	152	315	0.30
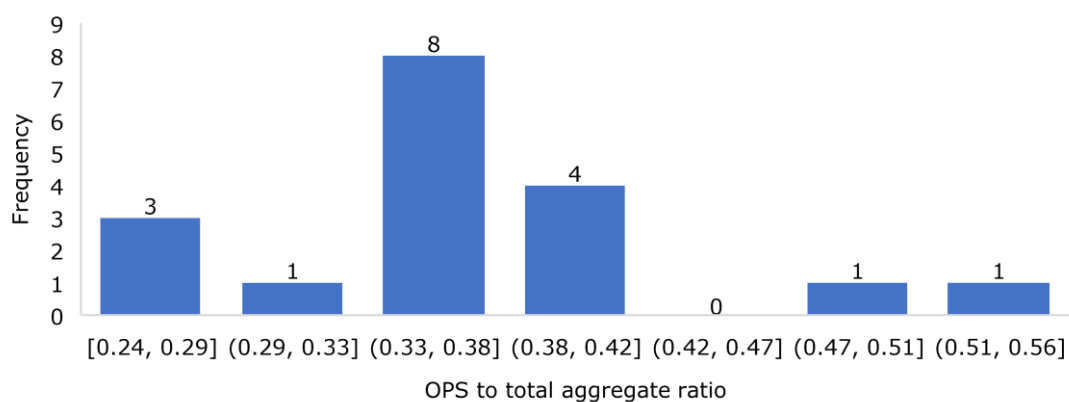
Figure 3.10 Frequency of OPS to total aggregate ratio for strengths of 20 – 22.5 MPa taken from Table 2.5

3.2.3.   Fine OPSC

Since, to the authors knowledge, no previous study is found on using OPS as fine aggregate (F-OPS) in concrete, at first, different treatment methods were explored for F-OPS in mortar cubes tested at age of 7 days. The suitable treatment was chosen based on its compressive strength, outlined in sub-section 3.2.3.1.

Based on the chosen treatment method, different F-OPS to coarse aggregate ratios (F-OPS/C.A.) were studied to see the influence on permeable voids and dry density. Based on the selected F-OPS/C.A. ratio, different cement contents were studied to achieve the final optimised mix design with a 28-days compressive strength of 20 MPa for fine OPSC described in sub-section 3.2.3.2.

3.2.3.1.   Treatment methods for F-OPS

In this innovative approach, various treatment methods were thoroughly selected and applied to fine-sized Oil Palm Shells (F-OPS) before the mixing process. The selection of these treatments draws from a comprehensive analysis of the existing literature and introduces novel treatments introduced in this study. The novel treatments were mainly originated from observations made during on the F-OPS in the lab. For experimentation, F-OPS was incorporated into mortar samples, cast in 50x50x50 mm³ moulds, following a mix ratio of 1:2 (comprising 600 kg/m³ of cement and 1200 kg/m³ of fine aggregate) with a water-cement (w/c) ratio of 0.45. The F-OPS was used as a 10% replacement for the fine aggregate, as illustrated in Figure 3.11. To evaluate the effects of these treatments, compressive strength tests were conducted precisely at the 7-day mark after a period of moist curing. To provide a basis for comparison, control specimens devoid of F-OPS were also meticulously prepared, in accordance with the guidelines outlined in (BS EN 480-1, 2014). For a comprehensive overview of the treatment methods applied to F-OPS, refer to Table 3.5.

Figure 3.11 Moulds for mortar cubes

With this investigation, the best treatment method selected was "Detergent cleaned-SSD-top filtered-retained at 1 mm", which was primarily based on the compressive strength. Table 3.6 defines the specific treatment-methodology in detail. The selected treatment method was used for the further experiments throughout this study. The details for the results of Table 3.5 is explained in Section 4.2.3.

Table 3.5 Treatment methods for mortar F-OPS

Treatment type	Information	Reference
Control	Control mortar without OPS	-
Dirty-Dry	The OPS is unwashed and used as dry condition	Proposed*
Dirty-wet	The OPS is unwashed and used as wet state condition	Proposed
Dirty-Dry-1 mm retained	The OPS is unwashed, used as dry condition and sieved up to 1mm.	Proposed
Dirty-Wet-1 mm retained	The OPS is unwashed, used as wet-state condition and sieved up to 1mm.	Proposed
Dirty-Dry-Hexane	The OPS is unwashed, used as dry-state condition and treated with hexane solution.	
Dirty-wet-Hexane	The OPS is unwashed, used as wet-state condition and treated with hexane solution.	(Sun, et al., 2016)
Dirty-Dry-Ethanol	The OPS is unwashed, used as dry-state condition and treated with ethanol solution.	
Dirty-wet-Ethanol	The OPS is unwashed, used as wet-state condition and treated with ethanol solution.	
Wet-Sonicated	The OPS is unwashed, used as wet-state condition and sonicated for 15 min. at 35Khz.	Proposed
Detergent cleaned-wet	The OPS was washed with a detergent and used as wet-state condition.	Proposed
Detergent cleaned-PVA20%	The OPS was washed with a detergent and treated with a 20% PVA solution for 1 day.	(Chai, et al., 2014) & (Mannan, et al., 2006)
Detergent cleaned-PVA10%	The OPS was washed with a detergent and treated with a 10% PVA solution with spray.	(Traore, et al., 2018)
Dirty-wet-top filtered	The OPS is unwashed, used as wet-state condition and the floating particles on the top were removed.	Proposed

Treatment type	Information	Reference
Detergent cleaned-wet-top filtered-heat treated	The OPS was washed with a detergent, used as wet-state condition, the floating particles on the top were removed, and heat treated.	(Yew, et al., 2014a)
Detergent cleaned-wet-top filtered-cement treated	The OPS was washed with a detergent, used as wet-state condition, the floating particles on the top were removed, and treated with cement.	Proposed
Detergent cleaned-SSD-top filtered-retained at 1 mm	The OPS was washed with a detergent, used as SSD-state condition, the floating particles on the top were removed and, sieved up to 1mm.	Proposed
Control with same amount added for cement treatment F-OPS	The cement content was increased with the same amount used for the treatment of F-OPS (no F-OPS was added)	Proposed

* The idea was proposed by the author of this research.

Table 3.6 Treatment methods for F-OPS

Treatment type	Method
Dirty	The C-OPS used prior to crushing was in its delivered dirty state. After the crushing process, the F-OPS was used as is, see Figure 3.12.
Dry	The F-OPS was kept in an oven at 105°C for 24 hours. The F-OPS was cooled down in an airtight vessel prior to mixing.
Wet	The F-OPS was kept in water for 24 hours and was drained on a sieve size of 0.075 mm. The sieve was shaken to remove any excess of water and the F-OPS was used shortly after in the mix, see Figure 3.13.
SSD	The F-OPS was kept in water for 24 hours and then put on a sieve size of 0.075 to allow the water to drain. The F-OPS was allowed to dry until an SSD state was achieved. The inspection for an SSD condition was done as mentioned in Section 3.1.2.3 see Figure 3.14.
Retained at 1 mm	The dry F-OPS was put on a sieve with opening size of 1 mm. The passing material was discarded whereas the retained F-OPS was used for the mix, see Figure 3.15.
Hexane	The as received F-OPS after crushing was kept in a 15% solution of Hexane for 24 hours. The idea was to remove as much oil as possible and clean the surface. The F-OPS was dried for 24 hours in room temperature prior to mixing. Sun et al. used this method to extract left over palm oil from OPS (Sun, et al., 2016).
Ethanol	The as received F-OPS after crushing was kept in ethanol for 24 hours. Like the hexane treatment, this was also done for cleaning purposes. The F-OPS was dried for 24 hours in room temperature prior to mixing. Sun et al. used this method to extract left over palm oil from OPS (Sun, et al., 2016).

Treatment type	Method
Sonicated	The F-OPS was kept in a thin glass bottle and put in a sonicator device for 15 minutes at 35 KHz. The purpose was to remove dirt from the F-OPS.
Detergent cleaned	The F-OPS was first put in water and drained using a sieve size of 0.075 mm. This process was repeated until the water was clear with the F-OPS. After removing the water, a household detergent was added to the F-OPS with water and hand washed. The water with detergent was drained again using a sieve size of 0.075 mm and repeated until the water was clear, see Figure 3.16.
PVA 10% & 20%	10% and 20% of Polyvinyl alcohol (PVA) was added to warm water and was kept on the hot plate with a magnetic stirrer for 24 hours at 80°C, see Figure 3.17 (a). The 10% solution was put in a spray bottle, see Figure 3.17 (b), to spray over the F-OPS until it was homogeneously distributed and allowed to dry for 1 day prior to mixing. The 20% solution did not work with the spray pump since it was too thick. Therefore, small amounts were poured on the F-OPS until a homogeneous distribution was achieved and allowed to dry 24 hours prior to mixing.
Top Filtered	When the F-OPS was put in water, an amount tended to float while most sunk to the bottom, see Figure 3.18. The floating particles were observed to be very soft and felt similar to a sponge when squeezed. These floating particles were removed after allowing the F-OPS to be in water for 24 hours with a sieve, see Figure 3.19. The sunken particles were used in the mix.
Heat treated	The F-OPS was heated at 60°C for 30 minutes prior to mixing. The method was replicated from (Yew, et al., 2014a).
Cement treatment	Dry cement was poured over F-OPS in a wet state condition with a ratio of 0.43 (cement/OPS). It was found that a ratio of 0.43 allowed the cement to fully cover all the F-OPS. The cement-treated-F-OPS was then allowed to dry for 1 hour prior to mixing, see Figure 3.20.

Figure 3.12 Dirty dry

Figure 3.13 Wet state method – water removal

(a)

(b)

Figure 3.14 SSD method F-OPS (a) cone and (b) acceptable form of SSD state

(a)   (b)

Figure 3.15 Retained at 1 mm – discarded material
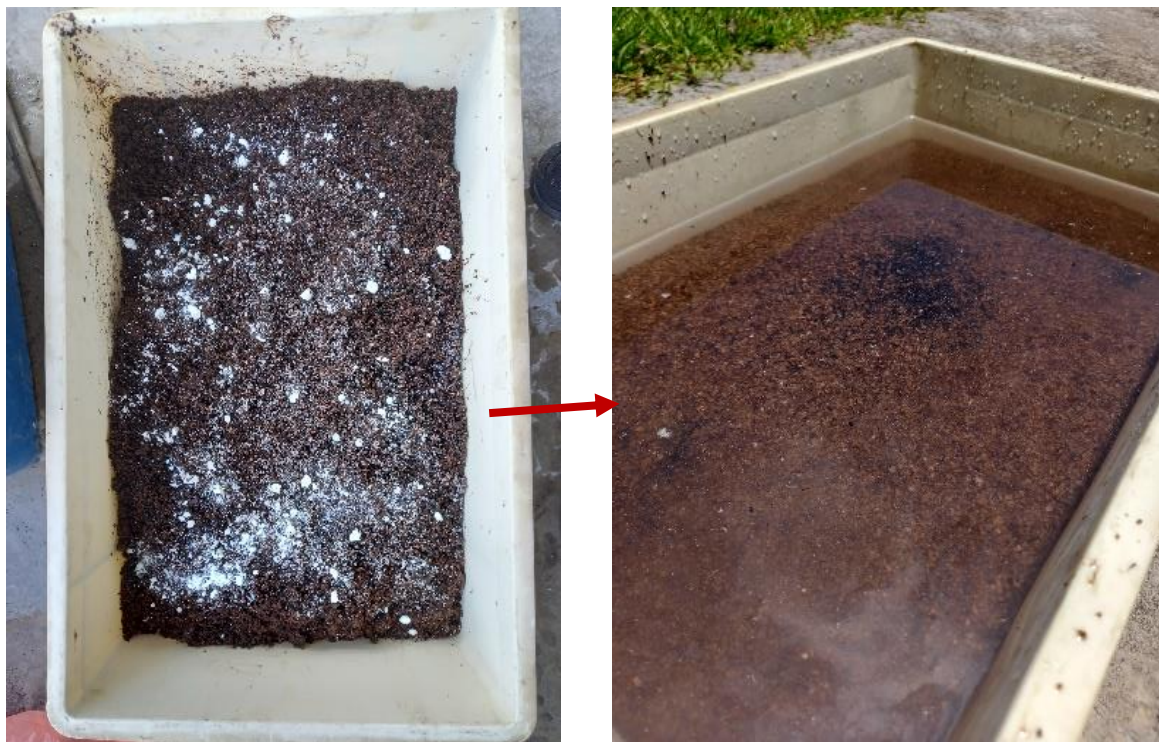
(a)   (b)

Figure 3.16 (a) Cleaning with detergent and (b) after cleaning

(a)   (b)

Figure 3.17 (a) PVA solution method and (b) spray pump

(a)   (b)

Figure 3.18 Top filtered (a) before and (b) after 24 hours

<div align="center">(a)   (b)   (c)   (d)</div>
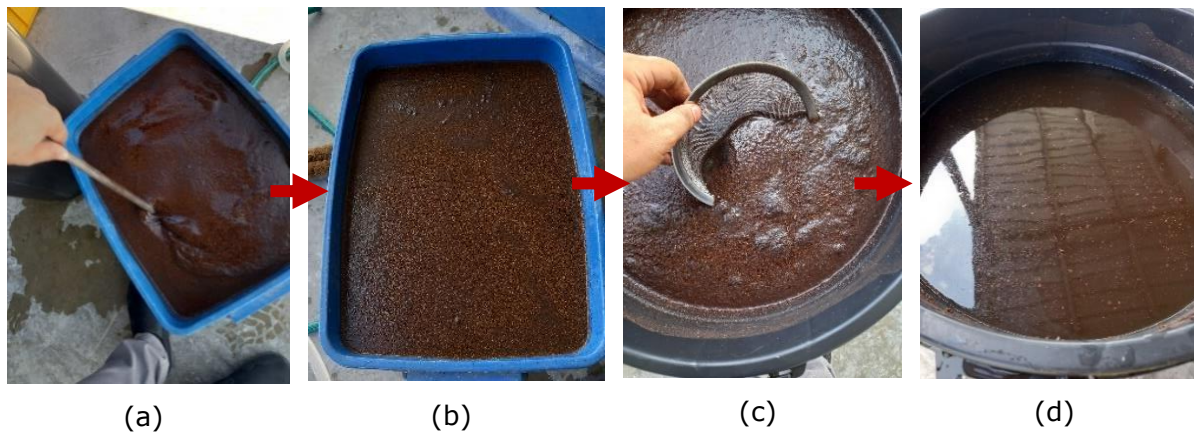
Figure 3.19 Method for Top filter F-OPS in large amounts, (a) initially mixed thoroughly, (b) left for 24 hours, (c) top particles removed with a sieve until (d) no more floating particles were observed.

<div align="center">(a)   (b)</div>
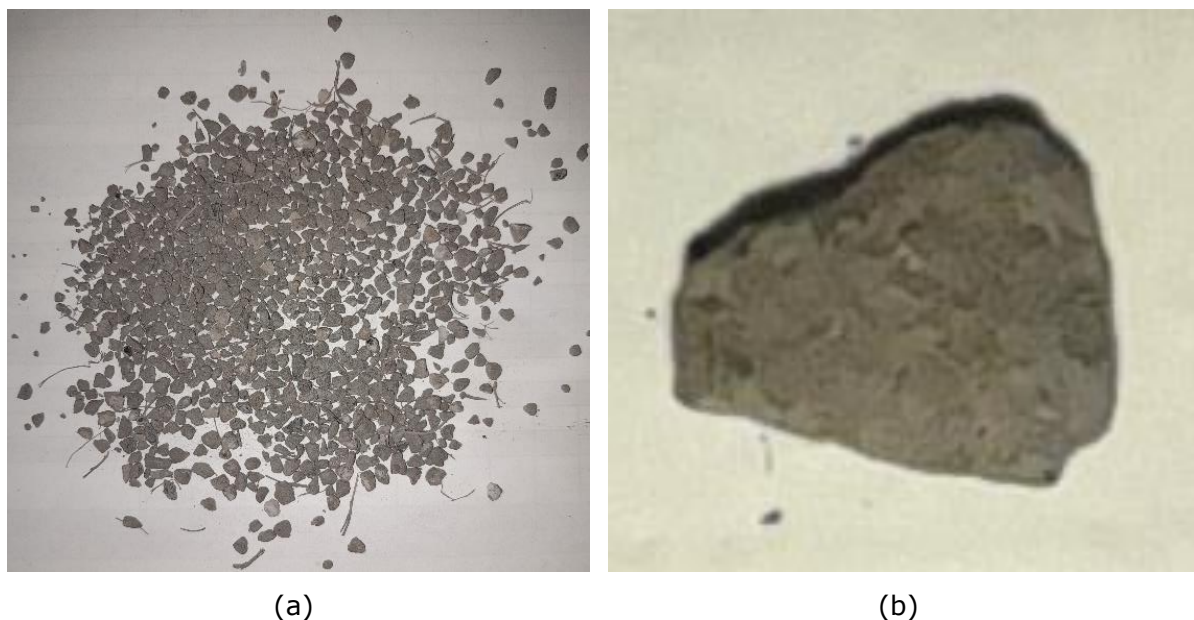
Figure 3.20 (a) cement treated F-OPS and (b) grain of F-OPS treated with cement

3.2.3.2. Mix design fine-OPSC

Based on the chosen treatment method mentioned in the previous section (3.2.3.1), fine OPSC was made with different F-OPS to coarse aggregate ratios (F-OPS/C.A.) of 0.1, 0.2, 0.3, 0.4 and 0.5 to study its permeable voids and dry density, see Table 3.7.

The one with a dry density of ≤2000 kg/m^3 and lowest permeable voids was found at a F-OPS/C.A. ratio of 0.1 and chosen for further investigating the optimum cement content. The details of the results for Table 3.7 is explained in Section 4.2.3. With the chosen F-OPS/C.A. ratio of 0.1, cement contents of 350, 400, 450, 500, 550, 600, 650 and 700 kg/m^3 were then tested for their 28 days compressive strength, see Table 3.8.

Table 3.7 F-OPS:CA ratio tests: mix proportions

F-OPS/C.A. Ratio	Cement	F-OPS	C.A.	Water
			Kg/m³	
0.1	600	99	991	210
0.2	600	182	908	210
0.3	600	252	838	210
0.4	600	311	779	210
0.5	600	363	727	210

C.A.: Coarse Aggregate

Table 3.8 Fine-OPSC mix design – cement content

F-OPS/C.A. Ratio	Cement	F-OPS	C.A.	Water
			kg/m³	
	350	130	1298	123
	400	124	1236	140
	450	118	1175	158
	500	111	1114	175
0.1	550	105	1052	193
	600	99	991	210
	650	93	930	228
	700	87	868	245

3.2.4.   Superplasticizer Investigation

Superplasticizers (SP) are recognised for their ability to increase workability of concrete while maintaining the same water content. They are also recognised for their ability to decrease water content without compromising workability to achieve higher strengths (Mollah, et al., 2000).

This investigation aims at studying the influence of SP dosage on Tenera coarse and fine OPSC and compare to control concrete with a similar grade strength of 20 MPa by using the same mix designs as those selected in the previous subsections. Two methods were mainly adopted to study the influence of SP dosage on strengths:

1. SP dosages were added to the concrete mixes whilst keeping the w/c constant to study the effect on the workability, compressive strength, and water absorption.

2. SP dosages were added whilst reducing w/c and keeping the slump constant to the original mix without SP to investigate the effect on the compressive strength.

3.2.4.1.   Addition of superplasticizer with constant w/c

In this method, the influence of SP on the concretes were investigated whilst keeping the w/c constant. The primary objective was to track changes in workability using a slump test

in accordance with (BS EN 12350-2, 2019). Though other workability testing methods are available, the slump test is known to be the simplest, cheapest, and most widely used test globally (Kovler & Roussel, 2011). Also, according to (BS EN 934-2, 2012), the workability can be observed either by slump of flow test. However, the typical purpose of the flow test is for self-compacted concrete (Neville, 1995), which is outside the scope of this study. Additionally, the compressive strength and permeable voids in accordance with (BS EN 12390-3, 2019) and (ASTM C642 - 13, 2013) respectively were tested at ages 7 and 28 days under separate SP dosages of 0.1, 0.3, and 0.5% by weight of cement, see Table 3.9. The concrete samples were also sliced for microstructural analysis, see Section 3.3.7.

Table 3.9 Addition of SP with constant w/c

	Control	SP (%)		
NWC	0.0	0.1	0.3	0.5
Coarse OPSC	0.0	0.1	0.3	0.5
Fine OPSC	0.0	0.1	0.3	0.5

3.2.4.2.　　Addition of superplasticizer with decrease of w/c

To investigate the impact on the compressive strength at 28 days (moist cured), the SP dosage of 0.4% and 1.0% was added while the w/c was simultaneously decreased in this approach. In this setup, all the components were initially dry mixed. The SP dosage was then added to a small amount of water that was added to the dry mixed components, which was then gradually increased until, when measured by visual inspection, the workability matched that of the original mix without SP. The total amount of water added was then recorded. Finally, the concrete cubes were cured for 28 days and tested for their compressive strength. In addition, UPV tests were also performed in accordance with (BS EN 12504-4, 2021) by using a Pundit NDT device, see Section 3.3.8.

3.3. Hardened Properties Tests

The selected mix designs for the three concrete types were tested with for their hardened properties by investigating their density, permeable voids and water absorption, compressive strength, flexural tensile strength, dynamic and static modulus of elasticity, and drying shrinkage. The methodology for each investigation is shown in sub-sections 3.3.1 – 3.3.6, respectively. In addition, microstructural analysis was also done by slicing concrete samples and inspecting the internal surface visual and microscopic inspections described in sub-section 3.3.7. Furthermore, ultrasonic pulse velocity (UPV) tests were also used throughout different experiments and described in sub-section 3.3.8. the concretes were mainly exposed to two types of curing regimes: curing in a water tank and air curing. More information on the curing regimes is expounded upon in Section 3.4.

Tests were done at ages 3, 7, 28, 56, 90, 180, 270, and 365 days. Additionally, tests were also conducted at 1 and 14 days, to measure the dynamic and secant modulus of elasticity as well as drying shrinkage. Samples were tested under curing and air curing regimes. Number of cube, cylinder, and prism specimens used for testing is presented in Table 3.10. The above-mentioned tests are further explained in the coming sub-sections.

Table 3.10 Mechanical tests – number of samples

Test type		Cubes	Prisms	Cylinders	Sample x Test Day x 2 (cured & air cured)
Density		2	-	-	32
Permeable voids & water absorption		2	-	-	32
Compressive strength		3	-	-	48
Flexural tensile strength		-	3	-	48
Modulus of elasticity	Dynamic	-	-	2	2*
	Static	-	-	3	48
Drying shrinkage		-	2	-	2*

Two samples were used since the test was non destructive

3.3.1. Density

The density was measured for the NWC, coarse, and fine OPSC samples exposed to a cured and air cured regime. The density of the concretes was found by following the procedures from (BS EN 12390-7, 2019). The SSD and as received density for curing and air curing, respectively, was measured by using a single specimen for each concrete type up to 365 days. However, for the dry density of the concretes, two separate cube specimens were used at each age of 3, 7, 28, 56, 90, 180, 270 and 365 days. To ensure the correct volume was used to calculate the dry density, each specimen was measured for their dimension in accordance with (BS EN 12390-1, 2021). Subsequently, the mass of each specimen was divided by its volume.

The SSD density was found by weighing the specimen after surface drying it by an absorbent cloth for the cured specimens. For the air cured specimens, the weight was taken as received. The air cured specimens were exposed to an outdoor environment in a room with open windows. For the dry density, the specimens were kept in an oven at 110 °C for 48 hours. The specimens were weighed in two sets, after 24 and 48 hours, to ensure the mass change was less than 0.2%. Before weighing the specimens, they were kept in an airtight vessel until they were cooled to room temperature.

3.3.2. Permeable Voids and Water Absorption of Concrete

Concrete cubes of 100x100x100 mm^3 were used to determine the permeable voids and water absorption in accordance with (ASTM C642 - 13, 2013). Two types of curing regimes were used for the specimens tested in this investigation, cured in water tank and air cured. The procedure was done in the following matter:

1. The cubes were extracted from their respective curing regimes and subsequently subjected to a temperature of 110°C in an oven for a period of 48 hours.

2. The specimens were weighed in two sets, after 24 and 48 hours, to ensure the mass change was less than 0.2%. Before weighing the specimens, they were kept in an airtight vessel until they were cooled to room temperature.

3. The samples were placed in water for a period of 48 hours and were then surface dried and weighed.

4. Then, the samples were put on steel rods in a large steel pot filled with water. The steel pot was put on an electric heater to be boiled at 100°C for 5 hours, see Figure 3.21.

5. After boiling, the samples were allowed to cool down for a period not less than 14 hours to a temperature of 20 – 25°C.

6. After cooling, the immersed apparent weight was found by using the special balance, see Figure 3.8. Then the SSD weight was measured by drying the surface moisture with an absorbent cloth.

With the oven dry-, SSD-, Boiled SSD- and, apparent weight, the following were found:

- Water absorption (%) (after immersion and after immersion & boiling)

- Bulk density (kg/m^3) (dry, after immersion and after immersion & boiling)

- Apparent density (kg/m^3)

- Volume of permeable pore space (voids) (%)

The formulas for these calculations are shown in Appendix A.
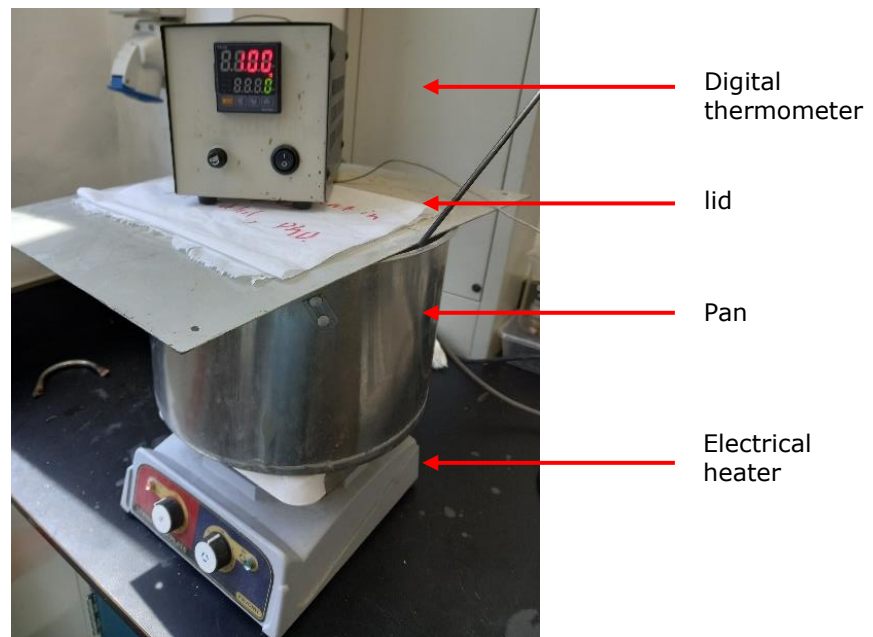
Figure 3.21 Boiling concrete

3.3.3. Compressive Strength

Concrete and mortar cube samples of 100x100x100 mm^3 and 50x50x50 mm^3, respectively, were tested in a concrete compressing machine. All settings were set following the standard in (BS EN 12390-3, 2019). For each set, three samples were surface dried with an absorbent cloth and tested. Finally, an average was taken from all three results to find the average compressive strength in N/mm^2. The ramp rate was set at 3 kN/sec. Tor this test, a Servocon testing machine was used, see Figure 3.22.

Figure 3.22 Concrete compressive machine

3.3.4. Flexural Tensile Strength

Prisms of 100x100x500 mm^3 were used to test their flexural tensile strength using the flexural beam test instrument under a two-point loading in accordance with (BS EN 12390-5, 2019), see Figure 3.23. The prisms were surface dried with an absorbent cloth prior to testing. The formula used for calculating the flexural tensile strength is shown in Appendix A.

Figure 3.23 Flexural testing instrument

3.3.5. Modulus of Elasticity

The modulus of elasticity (MOE) was tested for NWC, coarse and fine OPSC in this study. Both the dynamic and secant method were used in this investigation. The secant MOE is also known as the static MOE. The methods are explained in the following sub-sections.

3.3.5.1. Dynamic modulus of elasticity

Cylinders of H:300xD:150 mm was used to test the dynamic MOE by means of using a non-destructive technique (NDT) in accordance with (BS 1881-209, 1990). A Resonance Frequency Meter device was used as seen in Figure 3.24 (a). The dynamic MOE was tested for samples in cured and air cured regimes. More information on the cured and air cured regimes are available in Section 3.4. The specimens used for this test were also used for the static MOE.

3.3.5.2.   Secant modulus of elasticity

In this method, three cylinders of H:300xD:150 mm were used to determine the secant MOE in accordance with (BS EN 12390-13, 2021). Two cylinders were tested under the compressive test to determine the average compressive strength (f_c) used to define the stress levels of the test cycle for the determination of secant MOE. The third cylinder was used to determine the secant MOE, see Figure 3.24 (b). The loading cycles were performed as seen in Figure 3.25. Prior to testing, gauge studs were fixed on the face of the samples with epoxy. A digital micrometre, see Figure 3.26 (b), was used to measure the strain by using the gauge studs at every load cycle.

(a)   (b)
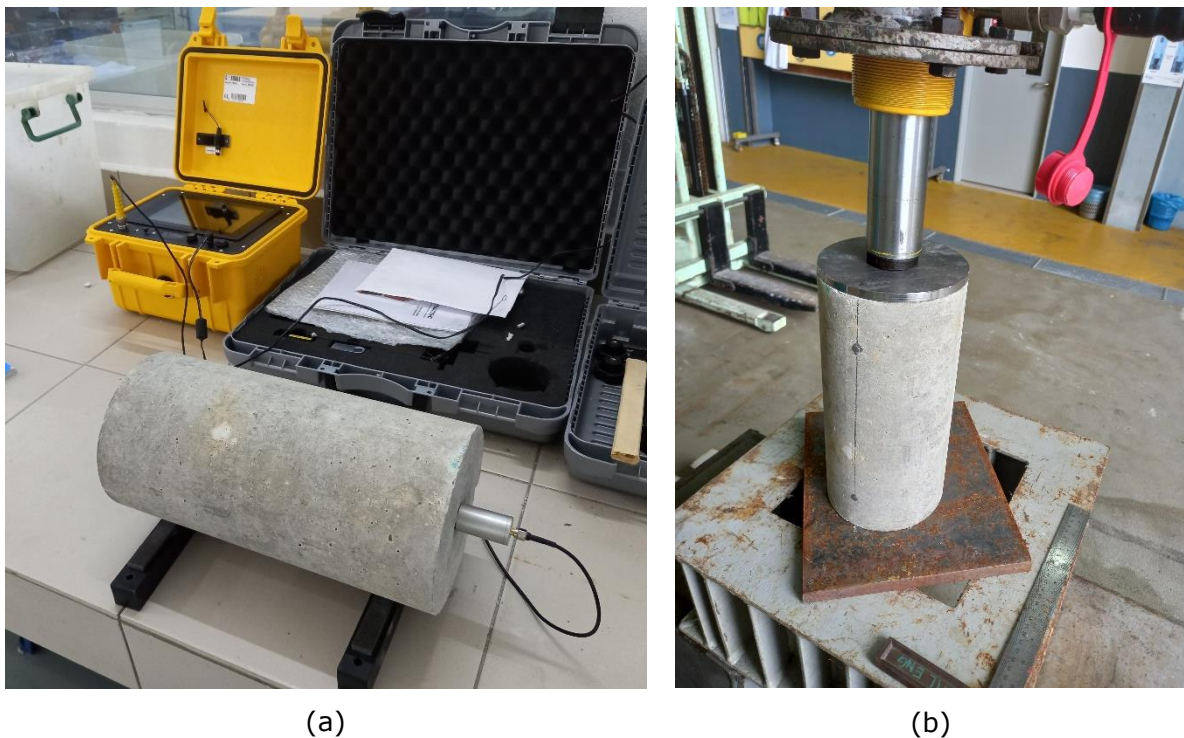
Figure 3.24 (a) Resonance frequency meter device and (b) secant MOE test set up
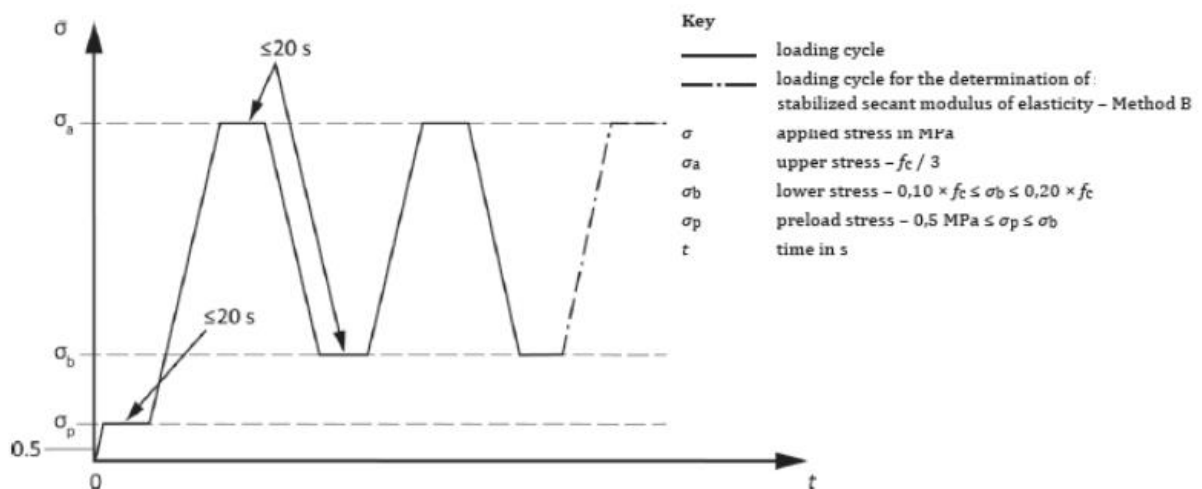
Figure 3.25 Cycle for the determination of secant MOE (BS EN 12390-13, 2021)

3.3.6. Drying Shrinkage

Prisms of 100x100x500 mm^3 were casted to be tested for the drying shrinkage. After demoulding the samples (after 24 hours), demec gauge studs were fixed to the sample by using epoxy on two sides of the prism, see Figure 3.26 (a). Then, the specimens were kept in a controlled room environment of 20 – 25°C and RH 50 – 70% and were placed on steel rods to allow free air circulation in accordance with (BS ISO 1920-8, 2009). The demec gauge studs were read using a digital micrometre with a precision of 0.001 mm seen in Figure 3.26 (b). The formula used for calculating the drying shrinkage at a given time is shown in Appendix A. Two prisms were used for each type of concrete.

Demec gauge studs

(a)   (b)
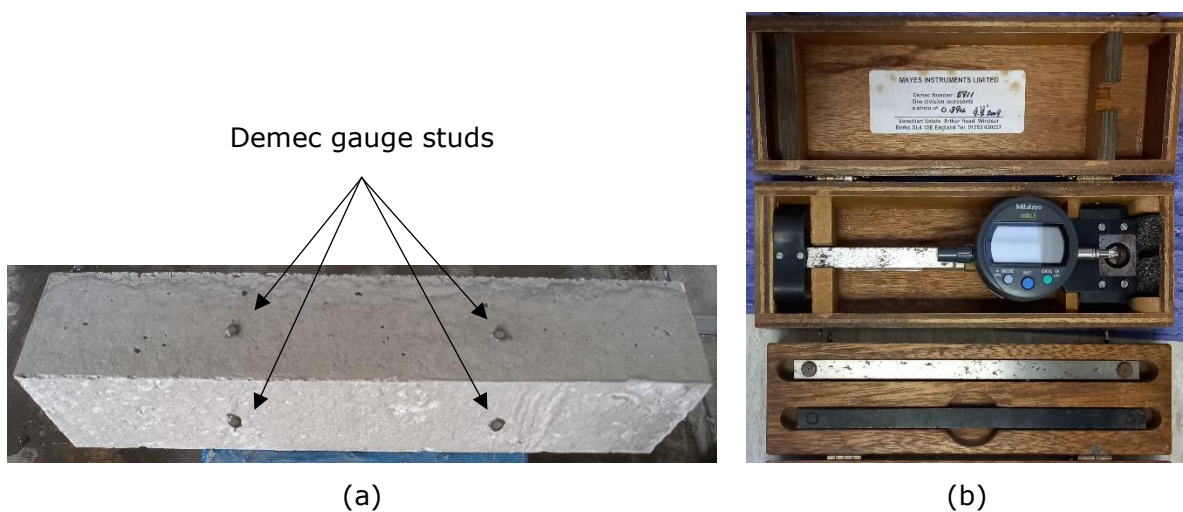
Figure 3.26 (a) Prism for drying shrinkage (b) Digital micrometre

3.3.7. Microstructure Analysis

The concretes were cut into slices using a concrete slicer to examine their internal structure. The examination of the internal structure of the sliced face was done in two methods. The first method comprised scanning the sliced samples and analysing the samples with the visual eye-spectrum. The second method involved studying the sliced concrete samples at the microscopic level using a microscope. The slicing of the concretes and the microscope method are explained in the following subsections.

3.3.7.1. Slicing of Concrete

Samples of cubes 100x100x100 mm^3 were sliced with a rotary concrete cutter as seen in Figure 3.27. The samples were scanned with a normal printer scanner with a resolution of 400 dpi. This was done to visually inspect samples for homogenous distribution of the mixing materials and inspect the interface between OPS and the cement matrix. This inspection was done for all three concrete types i.e., NWC, coarse, and fine OPSC.

Figure 3.27 Concrete slicer

3.3.7.2. Microscopy

A microscopy test was used for visual examination of the sliced concretes. An Olympus microscope BX53M was used with an including software package to capture snapshots and measure lengths on the images using a connected PC, see Figure 3.28. The microscope has a zoom capability of 5, 10, 20, 50, and 100x.

Figure 3.28 Olympus microscope BX53M

3.3.8.   Ultrasonic Pulse Velocity

The ultrasonic pule velocity (UPV) was utilised alongside the other aforementioned investigations. The UPV apparatus produces ultrasonic vibration pulses that are transmitted between two electro-acoustic transducers with the specimens held in between. This kind of testing is primarily carried out to evaluate the quality of the concrete. However, it is noteworthy that UPV results for concretes with comparable grade strengths can vary. This can be primarily attributed to the various aggregate types and content used, which have a significant impact on the relationship between strength and UPV. Age and moisture content are two additional variables that impact the relationship (Neville, 1995). As a result, only individual comparisons between each type of concrete were made in this study using the UPV results.

A Pundit NDT device was used to measure the UPV in accordance with (BS EN 12504-4, 2021) seen in Figure 3.29 (a). The testing procedure was carried out as per manufacturer's manual instructions. Before any testing, a water-based gel was applied to the two electro-acoustic transducers. The device was initially calibrated using the included calibration rod, see Figure 3.29 (b).

(a)   (b)
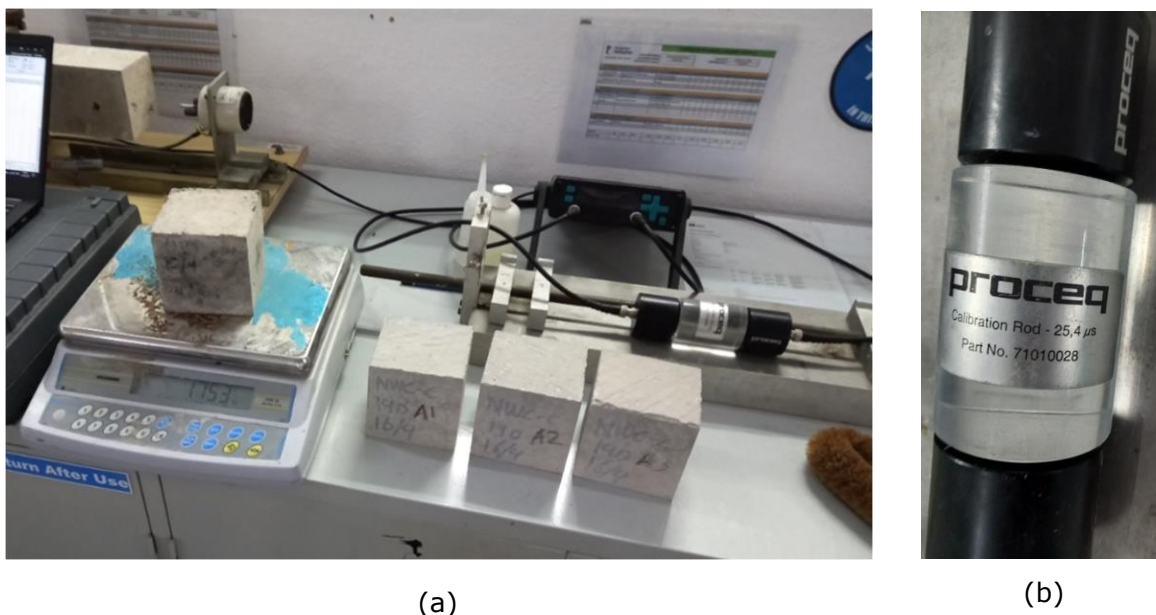
Figure 3.29 (a) UPV testing set up (b) Calibration rod between the two electro-acoustic transducers

3.4. Concrete Batching, Casting, and Curing

All concrete samples were batched conform to (BS 1881-125, 2013) according to their mix design. For the NWC, fine aggregate and cement were first dry mixed and ½ of the coarse aggregates were added and allowed to mix in a mix drum. Then ¾ of water was added while mixing. At last, the rest of the water and coarse aggregates was added. For the

coarse OPSC, this was done in a similar manner, however, all the water and C-OPS was added. As for the fine OPSC, this was done in the same manner as for NWC (F-OPS instead of fine aggregate).

Before casting the mix into the moulds, slump tests were performed in compliance to (BS EN 12350-2, 2019). The mould sizes used were 100x100x100 mm³ for concrete cube samples, H:300xD:150mm for cylindrical concrete samples, 100x100x500 mm³ for concrete prism samples and, 50x50x50 mm³ for mortar samples. All moulds were cleaned and applied with oil before casting. The moulds were kept on a mechanical shaker to prevent air being entrapped (5 – 10 seconds/layer) and poured in three layers. All specimens were cast together and demoulded after 24 hours ± 1h.

After demoulding, the specimens were put into a curing tank (26 °C ± 4) for their designated curing days in accordance with (BS EN 12390-2, 2019), see Figure 3.30. Air cured samples were kept in a room with open windows to simulate outside environments, or in a controlled environment, as specified.

Noteworthy is that the specimens in the air cured regime were exposed to Malaysian outdoor environmental conditions with relative humidity falling within 10% to 90% and with mean annual temperature of 25.4 °C (MET Malaysia, 2022). Also, the cubes were kept in a room with open windows on two sides of the room only, therefore exposed to some air circulation. It is therefore expected that the specimens would undergo very low moisture reduction, thus allowing for continuation of hydration (Neville, 1995).

Figure 3.30 Curing tank

Chapter 4. Results and Discussions

The findings from the methodological approach mentioned in Chapter 3 are presented in this chapter divided into three main sections followed by a summary section. The first part discusses the physical properties of the materials in Section 4.1. Then, the results of the mix designs and SP investigation for the NWC, coarse, and fine OPSC are discussed in Section 4.2. The final section discusses the overall hardened property findings of the three types of concretes in Section 4.3.

4.1. Physical properties of Materials

In the following subsections, the physical properties of the conventional fine and coarse aggregates, Dura OPS, and Tenera as C-OPS and F-OPS are discussed. The characteristics discussed in three subsections are:

- the shape and texture of OPS,

- dimensions,

- density, and water absorption.

4.1.1. Shape and Texture - OPS

Shape and texture of any aggregate plays a key role in understanding the effects of workability, bonding, and compressive strength in concrete (Li, 2011). The shape and texture of Dura and Tenera as C-OPS and F-OPS are explained in the coming sub-sections.

4.1.1.1. Shape

The most common shapes found in Dura and Tenera C-OPS are shown in Figure 4.1 (a) and (b) respectively. The images show that their thicknesses differ most noticeably. The shapes for both Dura and Tenera C-OPS was found to be similar to the description given for Dura mentioned in Section 2.1.5, i.e., flaky, circular, angular, and/or polygonal. However, in addition to the aforesaid shapes, Tenera OPS with sizes of ≥10 mm was found to have a half-hollow-spherical shape as seen in Figure 4.2 (a). This is because Tenera OPS is thinner than Dura OPS while having similar sizes. This type of shape was found to be disadvantageous in concrete from this study as is explained later in Section 4.2. Also, the Tenera OPS were found to have two common shapes, top and side shapes as seen in Figure 4.2 (b). This is because in the cracking process (see Section 2.1.2), the shells are broken in two patterns as illustrated on an unbroken-OPS in Figure 4.2 (c). Other broken smaller sizes could be due to handling and storing of the OPS. The Tenera OPS was found to be extremely brittle, capable of being broken between two fingers. In a separate test, the cracking strength of Tenera OPS was found to be much weaker than Dura OPS seen in Appendix D. Although another type of test known as the aggregate crushing value is used

for coarse aggregates to observe its indirect strength, this was stated as unsuitable to be used for OPS in one of the earliest research's in OPSC by (Okafor, 1988) and (Okpala, 1990). Both Okafor and Okpala found that the results for OPS gave a value superior to that of the conventional coarse aggregate, which is deemed to be erroneous. Okafor explained that the OPS did not crush to much fine particles, but exhibited cracking of the OPS, with fragments large enough to be retained at sieve size of 2.36 mm, therefore showing inaccurate values. Okafor deemed it to be necessary to find a more appropriate testing method. Okpala gave a similar impression and conclusion on the aggregate crushing value test. The aggregate crushing value is also observed to be insensitive to weak aggregates by (Neville, 1995). Nevertheless, this type of testing is mostly considered important for pavement structures (Li, 2011).

(a)   (b)
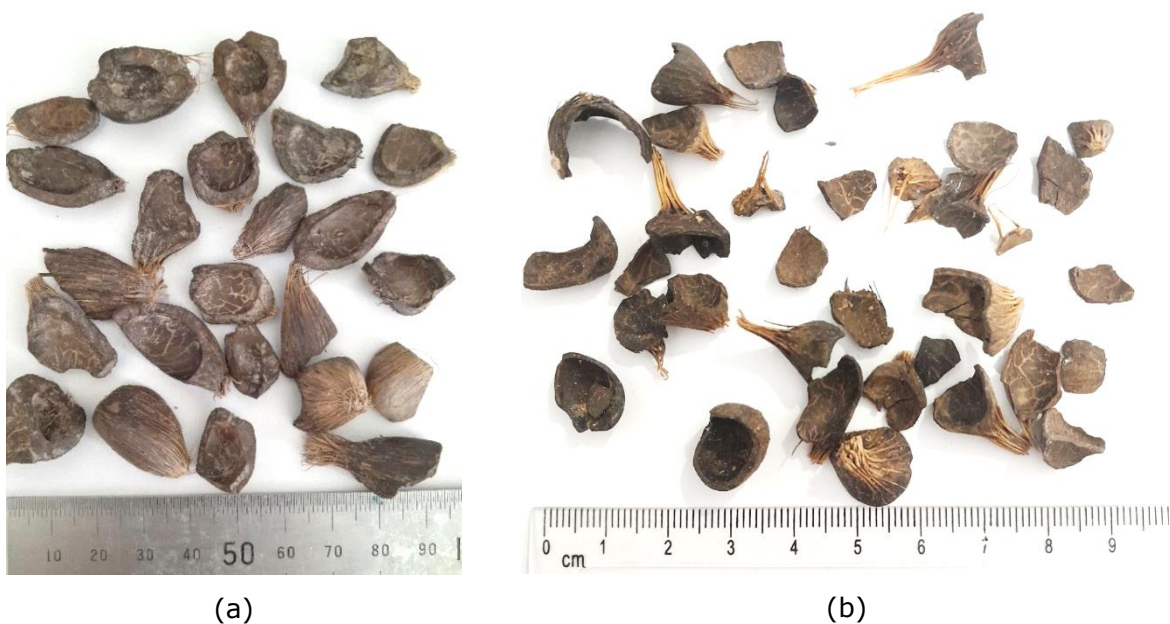
Figure 4.1 (a) Dura OPS and (b) Tenera OPS

86

(a)

(b)   (c)

Figure 4.2 (a) Half-hollow-spherical shapes, (b) Common Tenera OPS shapes and (c)
Unbroken OPS shell with cracking pattern, horizontal or vertical

As for Tenera F-OPS, given that it was only crushed to smaller sizes with a similar treatment applied as C-OPS (see Section 4.2.3), the texture is therefore found to be the same as that of C-OPS. However, the crushing process eliminated the half-hollow-spherical shape (Figure 4.2 (a)) and resulted in spiky and irregular shapes as seen in Figure 4.3.

(a)   (b)
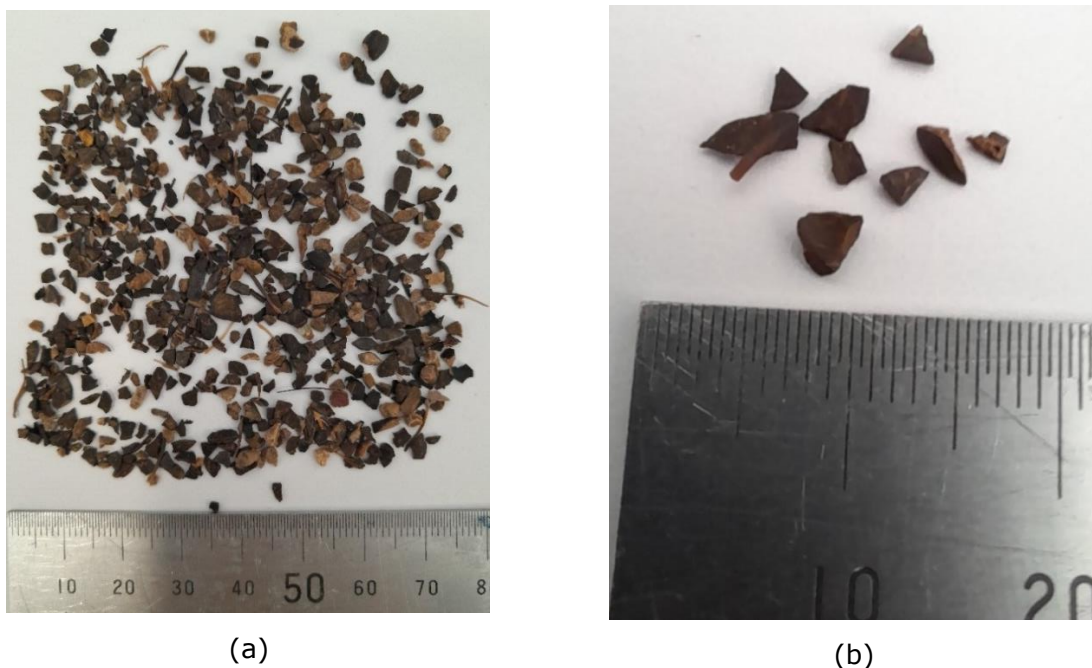
Figure 4.3 Tenera F-OPS

4.1.1.2.   Texture

Though the texture of Dura OPS was reported to be fairly smooth on both the inner and outer surface of the shell, from microscopic images taken of Tenera OPS samples, the inner

side seemed to have a smoother surface than the outer side as seen from Figure 4.4 (a & b). Furthermore, the shells are mostly varying from dark to light brown in colour. Similar to Dura OPS, the edges are also observed to be spiky and rough-broken. Also observed was that many shells have large number of fibres that go along the outer surface of the shell and accumulate on the top as lose strands as seen in Figure 4.1 (b). During the cleaning procedure explained in Section 3.1.1.3, the fibres were not eliminated. However, the fibres could be removed effortlessly by pulling or pealing them and are found to be very weak in contrast to traditional fibres used in concrete such as steel and plastic fibres.

(b)   (c)
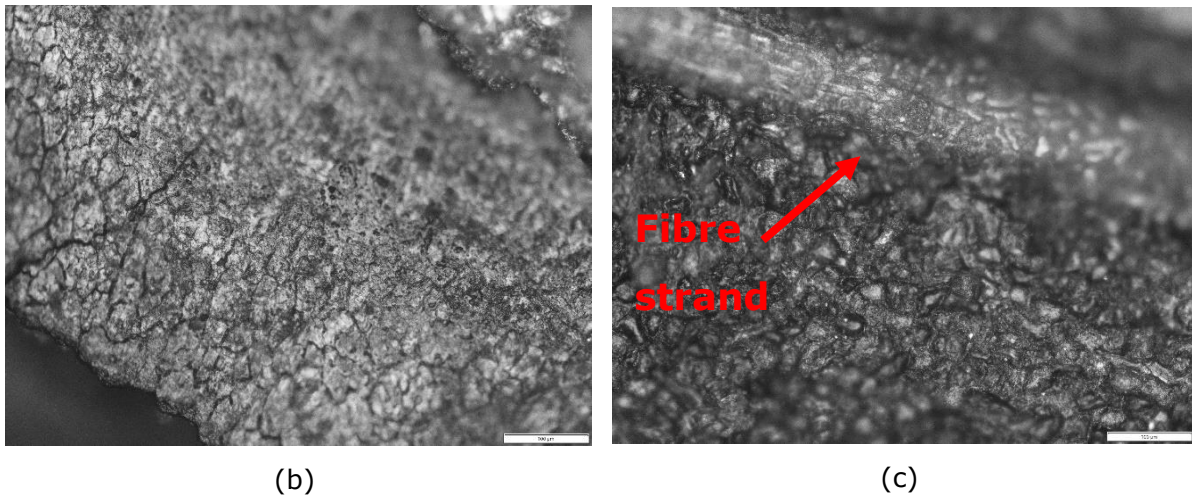
Figure 4.4 (a) Inner shell 20x (b) Outer shell 20x

4.1.2.   Dimensions

The dimensional size of the aggregates for this study was analysed through the conventional method known as the sieve analysis and a measurement indexing-method proposed in this study. The proposed measurement indexing-method was used for the Tenera and Dura as C-OPS only.

4.1.2.1.   Sieve analysis

This particular test was performed to obtain the grading curve (particle size-distribution) of Tenera C-OPS for comparison to Dura C-OPS from this study and from the literature (Section 2.1.5). The grading curves obtained from the sieve analysis for the materials used in this study have been plotted in Figure 4.5 (a).

Figure 4.5 (c) shows general recognized size-distribution curves for aggregates. In reference to Figure 4.5 (c), it is thus observed that the normal coarse aggerates and both Tenera and Dura as C-OPS have a similar uniform-graded size distribution. The river sand shows a well-graded curve while the F-OPS shows a lesser amount at and after 1 mm sieve size. This is accurate, since the F-OPS was filtered up to 1 mm sieve in the treatment process as is mentioned later in Section 4.2.3.1. It is therefore expected that the fine OPSC would require higher cement content than the NWC.

A uniform graded size distribution basically means that at the vertical falling line between the two curves, the sizes are dominating the other size aggregates. For the conventional coarse aggregates and the Tenera C-OPS, the dominating sizes are found to be between 10 – 20 mm and 4.75 – 12.5 mm, respectively. As for the well-graded curve, it is in general a desired grading to produce concrete where a wide range of all sizes are available with a smooth distribution (Li, 2011). However, an ideal grading curve cannot be set as a rule for every kind of concrete i.e., NWC and LWC. As long as a workable concrete is achieved, any kind of grading, within certain limits, would be ideal. When an aggregate sample has a well-graded curve, less voids are available and thus reducing the paste requirement. This is important since in the case of NWC, the paste is known to be the most vulnerable material in concrete because it is more permeable and weaker than conventional aggregates (Neville, 1995).

(a)

(b)

(c)
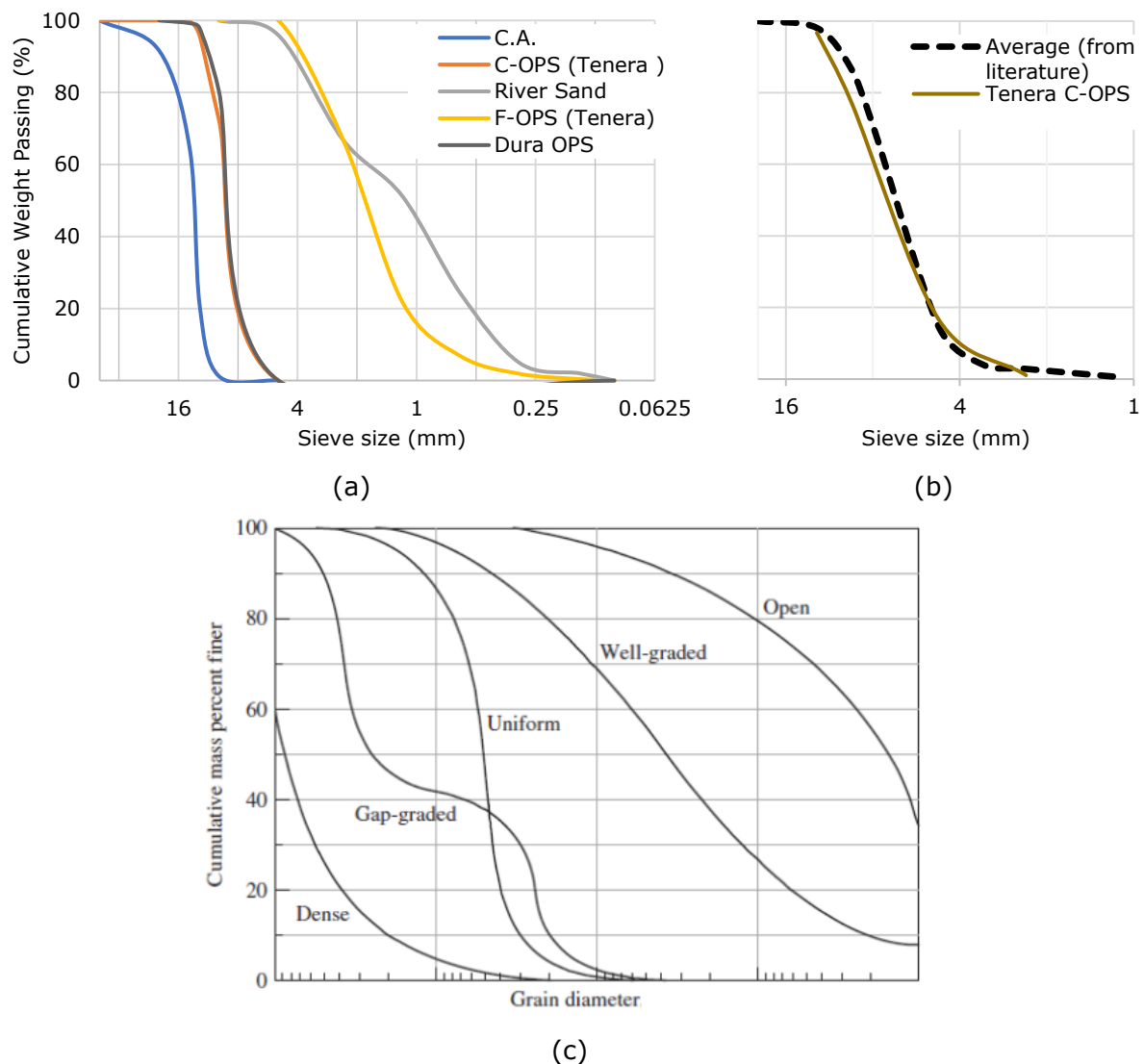
Figure 4.5 (a) Grading curve of materials used in this study, (b) Tenera C-OPS used in this study compared to average grading of Dura C-OPS from literature, and (c) grading curves (Li, 2011)

89

What is most notable, from Figure 4.5 (b), is that the grading curve of Tenera C-OPS used in this research is very close to the average grading curve of Dura C-OPS found from the literature (Section 2.1.5), though having a thinner shell thickness, as is explained later in Section 4.1.2.2. This was similar to the grading curve for Dura C-OPS used in this study, see Figure 4.5 (a), while the thickness between Tenera and Dura OPS was found to be significantly different by 57%, see Section 4.1.2.2. This comes to show that only performing a sieve analysis for OPS as coarse-sized is unreliable for comparison to other research and might not be an appropriate test for defining its physical dimension/size. Hence, these results have proven the hypothesis previously made in Section 2.1.5. Therefore, in the next subsection, the thickness, size, and shape of Dura and Tenera as C-OPS is examined in order to develop a more reliable indexing method for use in future references to distinguish between the various OPS varieties, i.e., Dura and Tenera.

The type of grading is also known to influences the cement requirement to produce a workable concrete; the available voids between the aggregate's particles would demand more paste to fill out the concrete mixture. A mentioned earlier, a well-graded aggregate would contain minimum voids, thus requiring minimum paste. Also, since the price of aggregates are roughly a tenth that of cement, a well-graded aggregates will act as a basis for an economical concrete (Shetty, 2005). More on the influence of C-OPS and F-OPS grading on cement content based on the mix design procedure in this study is further explained in Section 4.2. The size and shape of aggregates are also known to affect the mechanical properties of concrete (Mehta & Monteiro, 2006), which is further expanded upon in Section 4.3.

In addition to the grading curves, the fineness modulus' (FM) have also been obtained for the conventional fine aggregate and Tenera F-OPS seen in Table 4.1. For any aggregate sample, the FM is used to check constancy and as an index to define the fineness or coarseness of the material (Mehta & Monteiro, 2006) as seen in Table 4.2. Though the FM is only intended for fine aggregates according to (BS EN 12620, 2008), the FM was also calculated for Tenera C-OPS to compare to Dura C-OPS from literature. The FM of Tenera C-OPS appears to be in the lower bound from the values reported for Dura C-OPS from the literature in Table 2.3 (FM: 5.78 – 6.41). This might be since the Tenera C-OPS is fragile due to its low thickness which is broken down to smaller sizes due to handling. Nevertheless, the FM of the aggregates in Table 4.1 should not be compared to each other, since each are from different material substances (Li, 2011). However, these values are to be used for further comparison as reference in future experiments. As for F-OPS, the FM shows to be on the barrier of the limits from Table 4.2. The main reason for this is because the treated F-OPS was filtered at 1 mm sieve size i.e., anything below 1 mm was discarded, thus showing a high FM value.

Table 4.1 Fineness modulus of aggregates

	River Sand	F-OPS (Tenera)	C-OPS	
			Dura	Tenera
Fineness Modulus	2.30	4.00	6.32	5.98

Table 4.2 Fine aggregate limits for fineness modulus (BS EN 12620, 2008)

Definition	Fineness Modulus
Fine sand	0.6 – 2.1
Medium sand	1.5 – 2.8
Coarse sand	2.4 – 4.0

4.1.2.2.   Measurement indexing-method

It was seen from the previous section that a sieve analysis test for Dura and Tenera C-OPS gave a matching size distribution curve whilst having different thicknesses, thus giving a misleading interpretation of their actual dimension. It is therefore important to be able to state the physical dimensions of any OPS with a practicable method which can achieve distinguishable results between different samples. Dura and Tenera as C-OPS was examined for its dimension with a method proposed in this study.

The dimensions of Dura and Tenera as C-OPS are shown in Appendix E and the averages are shown in a form of a bar chart seen in Figure 4.6. The same samples that were used for the sieve analysis in Section 4.1.1 were also used for this testing procedure. The bar chart shows how smaller or larger Dura OPS is to Tenera OPS stated in percentages. This was done separately in terms of their average thickness, length, and width for each divided size (>14mm, 10 – 14mm, and 5 – 10mm). The average differences between the Dura and Tenera for all sizes greater than 5 mm are shown in Figure 4.6 (b). Moreover, the minimum and maximum thicknesses of Dura and Tenera OPS are shown in Table 4.3.

(a)   (b)
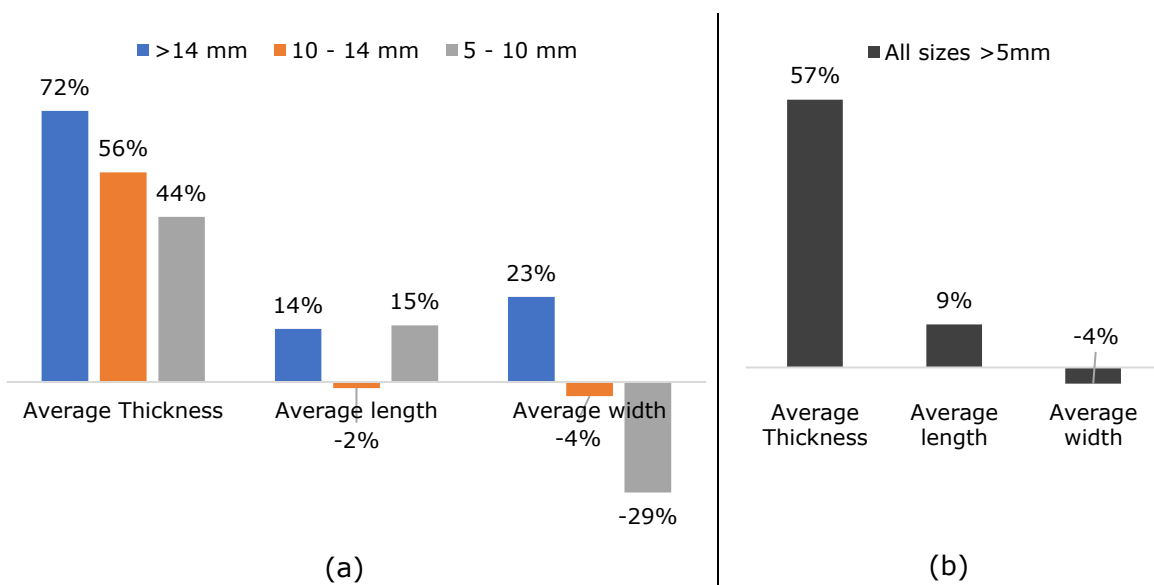
Figure 4.6 Dimension differences between Dura- and Tenera-OPS (+ve and -ve values indicate how larger and smaller Dura is to Tenera respectively)

From Figure 4.6, only a small difference is seen in the average length and width which are 9% larger and 4% smaller than Tenera OPS, respectively. Its longer length and smaller width demonstrate that Dura OPS is slenderer than Tenera OPS. However, this is mostly in the case for sizes between 5 – 10 mm. Furthermore, the most notable difference is the average thickness of Dura OPS by being 57% larger than Tenera OPS. Though the method used, shown in Figure 4.6, is not a common practice, the author believes that this type of measurement-indexing of OPS may be a more reliable method to sieve analysis. As analysed earlier, the sieve analysis failed to differentiate between Dura and Tenera OPS by showing a similar grading curve. While using this suggested method, the results presented in a bar chart directly distinguished between the two different varieties of OPS.

From the literature, maximum thickness sizes of up to 8 mm have been reported for Dura OPS, whereas Tenera OPS was measured to have a thickness between 0.11 – 2.74 mm with an average thickness of 1.12 mm, see Table 4.3. The Dura OPS in this study showed similar thicknesses compared to the literature. Based on its measured thickness, the OPS used in this study can be designated as Tenera variety OPS (Lai, et al., 2012).

Table 4.3 Minimum and Maximum thicknesses of Tenera and Dura C-OPS

Retained at (mm)	Tenera-OPS Thickness		Dura-OPS Thickness	
	Min.	Max.	Min.	Max.
14	0.34	2.03	1.57	8.04
10	0.54	2.49	0.85	6.33
5	0.11	2.74	0.43	4.01

The first publication on Tenera OPS in concrete was mentioned in a paper by (Yew, et al., 2014b). Yew et al. studied both Dura and Tenera OPS as original- and crushed-sizes with maximum thicknesses of 12.5 and 9.5 mm, respectively. Apart from a sieve analysis test, the authors did not quantify the difference in the thickness between their Dura and Tenera OPS. However, by a close observation from their provided images, their Tenera OPS seem to be thicker than the Tenera OPS used in this study and described by (Lai, et al., 2012), though thinner than their Dura OPS as seen in Figure 4.7. Yew et al. continued using the same images throughout later studies (Yew, et al., 2014a), (Yew, et al., 2015a), (Yew, et al., 2015b), (Yew, et al., 2015c), (Yew, et al., 2021), and (Yew, et al., 2022). They did not measure the thickness in any of their studies. This would therefore create complications for future comparison studies. This emphasises the significance of the suggested method used in this study, demonstrated in Figure 4.6. Nevertheless, the thicker type of Tenera OPS used by Yew et al. is most probably a mix-variant hybrid known to be consisting of 50% Tenera, 25% Dura and 25% Pisifera (Woittiez, 2019). Besides Yew et al., no other study by any other author has been found on Tenera OPS in concrete.
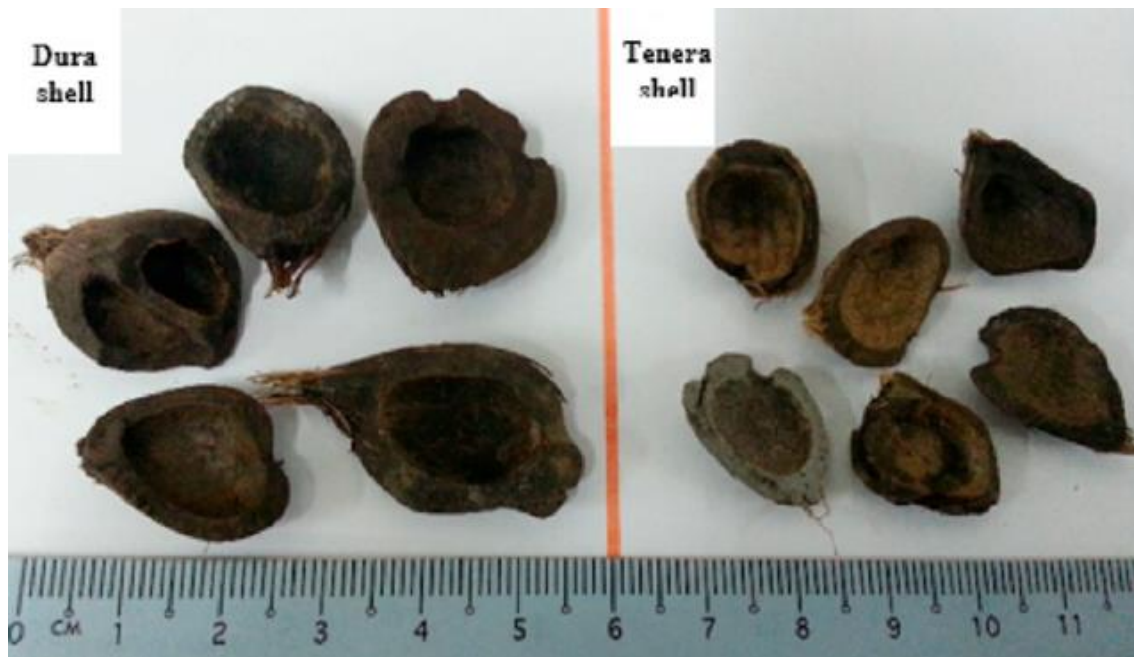
Figure 4.7 Dura and Tenera OPS from studies by (Yew, et al., 2022)

4.1.3. Density and Water Absorption

The Loose bulk-, apparent particle-, oven-dried particle-, SSD particle-density and water absorption of the materials are shown in Table 4.4.

Table 4.4 Properties of aggregates

| Test | Unit | River Sand | Coarse Aggregate | Tenera | | Dura OPS |
				C-OPS	F-OPS	
Dry Loose Bulk Density		1350	1567	442	572	505
Oven dried particle density	kg/m^3	2690	2610	930	910	1130
Apparent particle density		2750	2650	1300	1310	1450
SSD particle density		2710	2620	1220	1220	1350
Water absorption	%	0.72	0.60	30.65	34.28	19.26

The values in Table 4.4 are further used for correlating their properties to the mechanical behaviour of the concrete explained in Sections 4.2 & 4.3. Information about the density and water absorption can be a preliminary-identifying observation of how the aggregate sample will behave in concrete in terms of strength; an aggregate of low density is expected to develop a concrete of low strength and density, where the reverse is also true (Chandra & Berntsson, 2002). The density of aggregates is also a crucial factor for designing concrete mixes when using the absolute volume method. However, in this study only the mix by weight method was used for the mix designs as was explained in Section 3.2.

Furthermore, more details regarding the materials' density and water absorption are discussed in the subsections that follow.

4.1.3.1.   Density

The Tenera C-OPS shows a slight lower dry loose bulk density value compared to Dura OPS from the literature seen in Table 2.3 (500 – 600 kg/m³). This is also confirmed by the results of Dura OPS used in this study by being 12.5% lower. This is a predictable outcome given that Tenera is thinner than Dura and has a size distribution similar to Dura OPS, as shown in Section 4.1.2.1 and Figure 4.5 (b) respectively. In other words, the bulk volume of Tenera C-OPS contains more void space. Consequently, higher paste would be necessary for C-OPS (Neville, 1995), which is further discussed in Section 4.2.2.

F-OPS demonstrated a dry loose bulk-density value that was within the range of Dura OPS values found in literature and for the Dura OPS used in this study. Although C-OPS and F-OPS are made of the same material composite, F-OPS resulted to be 29% higher in dry loose bulk density owing to its more compacted, or less void space, crushed state. A density increase was also observed by (Shafigh, et al., 2011b) by crushing Dura-OPS from original sizes of 12.5 mm to 9.5 mm.

Though the dry loose bulk-density of Tenera F-OPS was higher than Tenera C-OPS, the oven dried particle-density of C-OPS is slightly higher than F-OPS, 930 vs 910 kg/m³ (2%) respectively. This might be due to entrapped content found in OPS such as palm oil in the impermeable volume spaces of the unbroken shells (Sundalian, et al., 2021). This might also explain why the apparent particle density of F-OPS is slightly higher than C-OPS, 1310 vs 1300 kg/m³, respectively. This may imply that F-OPS is cleaner in the aggregate solid compared to C-OPS. Nevertheless, both Tenera C-OPS and F-OPS fall under the lightweight aggregate class by having a loose bulk density not exceeding 1200 kg/m³ or particle density not exceeding 2000 kg/m³ following the (BS EN 13055, 2016). The loose bulk density of Tenera C-OPS and F-OPS were both found to be 72% and 58% lighter compared to the conventional coarse and fine aggregates used in this study, respectively.

4.1.3.2.   Water absorption

Dura and Tenera as C-OPS used in this study were both found to have water absorption values that were within the range of Dura OPS values found by other researchers from literature (Table 2.3, 18.7 - 33.3%). However, the Tenera C-OPS and F-OPS showed a higher water absorption by 57% and 78% compared to the Dura OPS used in this study. Also, Tenera F-OPS showed a higher water absorption by 12% compared to Tenera C-OPS. A honeycomb structure with a size of around 17 µm were found at the broken edges of F-OPS samples seen in microscopic examinations, see Figure 4.8. As a result, the higher water absorption is explained because water would enter through the broken shell-sides. This might also explain the reason for the lower oven dried particle-density of F-OPS compared to C-OPS. A similar observation was also found by (Alengaram, et al., 2011a)

with broken OPS, by giving a similar explanation that the smaller particles have larger number of pores at the broken edges.

Nevertheless, for both Tenera as C-OPS and F-OPS, a higher water absorption was found compared to the conventional fine and coarse aggregates used in this study by 51 and 48 times, respectively. In general, most LWA have higher water absorption compared to NWA (Newman, 1993).
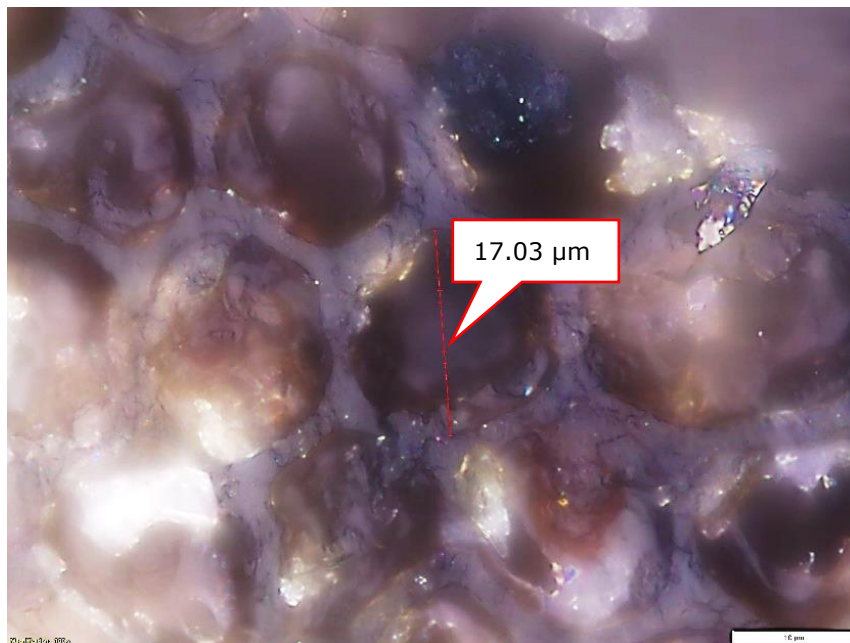
Figure 4.8 Microscopic image of broken edge OPS at 100x

4.1.4.   Concluding remark

In this part, the physical properties of the materials used to produce the concretes in this study were investigated. Furthermore, Dura and Tenera OPS was also analysed for its shape, texture, and a proposed measuring indexing-method. The following can be summarized for the investigations:

- Tenera as C-OPS is found to have similar shape features as Dura, i.e., flaky, circular, angular, and/or polygonal, though the most apparent difference being the difference in thickness. The lower thickness of Tenera results in a weak half-hollow-spherical shape not found for Dura OPS. The broken-down F-OPS is found to be spiky and irregular in shapes. The texture of Tenera is found to be like Dura, though the inner surface of Tenera is found to be smoother than the outer.

- It was found that the Tenera C-OPS has a uniform-graded size distribution like the conventional coarse aggregate where the F-OPS was found to have a well-graded

size distribution. Also, both Tenera and Dura as C-OPS were found to have a similar grading curve, though with different thicknesses, which concludes the sieve analysis to be an unreliable method to differentiate between different OPS species. Furthermore, F-OPS was found to have an FM of 4.00 being 74% more than the conventional fine aggregate, therefore being defined as "coarse sand".

- Since the conventional sieve analysis was found to unsuitable for OPS, the proposed measurement indexing-method in this study successfully differentiated between the Tenera and Dura type OPS. The results showed that the Dura type is 57% larger in average thickness and is slenderer than Tenera OPS. The Dura type was found to have thicknesses ranging from 0.43 – 8.04 mm and the Tenera type 0.11 – 2.74 mm. Furthermore, the main OPS type used in this study is identified as 100% Tenera species attributed to its thickness.

- Tenera F-OPS was found to have a similar dry loose bulk density as Dura C-OPS, though 29% higher than Tenera C-OPS. The lower density of Tenera C-OPS is found to be caused by its half-hollow-spherical shape creating high void space, thus expected to have a higher cement demand in concrete. The Tenera F-OPS was observed to be 2% lower in oven dried particle density compared to Tenera C-OPS. The hypothesis behind this is that the internal oil trapped in the OPS pore space is released when the OPS is broken down to fine sized particles, therefore being more permeable. This is further evident from the higher water absorption resulted for the F-OPS being 12% more than the C-OPS. Both Tenera C-OPS and F-OPS were also found to be 59% and 78% higher in water absorption compared to Dura C-OPS used in this study, demonstrating to have a higher pore volume space.

- Both Tenera C-OPS and F-OPS were found to be withing the limits of LWA being <1200 kg/m^3 in accordance with the BS standard.

4.2. Concrete Mix Designs

The main goal of this study was to achieve a compressive strength of 20 MPa after 28 days of moist curing for NWC, coarse, and fine OPSC. This strength was chosen specifically because it meets the minimum criteria for establishing an SLWC following (BS EN 206,

2021). It was also a requirement for both the OPSCs to keep their dry densities below 2000 kg/m^3 in order to stay within the bounds of LWC. The NWC was used as a control in accordance with (BS EN 480-1, 2014).

Sections 4.2.1, 4.2.2, and 4.2.3 present detailed results and discussions for NWC, coarse, and fine OPSC, respectively, followed by a discussion section to compare the concretes in Section 4.2.5. Despite the fact that SP is commonly used in concrete by researchers and industry, it was investigated separately in Section 4.2.4 with the selected mix designs for NWC, coarse, and fine OPSC. Moreover, the selected mix designs for the three types of concretes established in these investigations were investigated further for their fundamental mechanical properties in Section 4.3.

4.2.1. NWC

Table 4.5 shows the results obtained for the NWC. It is well known that cement is significantly more expensive than aggregates (Mehta & Monteiro, 2006). As a result, the primary goal was to achieve a concrete strength of 20 MPa while using the least amount of cement possible. This was accomplished using a cement content of 350 kg/m^3 (NWC 1). The NWC 1 was used primarily as a control for coarse and fine OPSC, with cement content serving as the primary criterion for comparison, as is discussed further in Section 4.2.4. Though a high w/c ratio was used for NWC 1, this was mainly attributed to the fact that a fine aggregate with a low FM was used, see Section 4.1.2.1.

Table 4.5 Trial mix results for NWC

ID	Cement	Fine Aggregate	Coarse Aggregate	Water	w/c	28-day strength
	Kg/m^3					MPa
NWC 1	350	605	1175	217	0.62	20.12
NWC 2	238	828	1144	190	0.80	12.16
NWC 3	365	715	1160	160	0.44	22.33
NWC 4	365	715	1160	150	0.41	28.24

4.2.2. Coarse OPSC

In this investigation, both Tenera and Dura as C-OPS were studied with different mix designs. Initially, Tenera C-OPS was tested with Mix A – G, seen in Table 4.6, by investigating their moist cured compressive strength at 28 days. In Mix A – G, the cement content was mainly increased where the C-OPS to total aggregate ratio was kept constant at 0.35 for all mixes, see Section 3.2.2. The effect of cement content on the compressive strength is shown in Figure 4.9. It can be seen, as expected, that with the increase of cement content, the compressive strength also increased. This was a similar observation with Dura OPSC from the literature as was shown in in Figure 2.12 (b). From Mix A – G, Mix G was selected based on the criteria to produce a SLWC for further investigations

throughout this study, i.e., compressive strength of 20 MPa and dry-density <2000 kg/m³. The results for Tenera OPSC are further elaborated in Section 4.2.2.1.

To compare Tenera to Dura as C-OPS in OPSC, two mix designs were taken from literature to produce OPSC made with Tenera and Dura C-OPS in this study seen in Table 4.6. Also, the selected Mix – G for Tenera OPSC was used with Dura C-OPS for further comparison. The results and discussions are shown in Section 4.2.2.2.

Table 4.6 Trial mix results for coarse-OPSC

Tenera OPSC	Original strength	28-day strength	SSD Density
	MPa	MPa	kg/m³
Mix A	-	13.56	1921
Mix B	-	16.64	1928
Mix C	-	17.64	1909
Mix D	-	15.66	1954
Mix E	-	16.94	1959
Mix F	-	18.64	1909
Mix G	-	20.24	1997
(Gibigaye , et al., 2017)	22.42	5.70	-
(Basri, et al., 1999)	24.20	8.77	-
Dura OPSC			
(Gibigaye , et al., 2017)	22.42	13.56	1871
(Basri, et al., 1999)	24.20	14.61	1946
Dura-Mix G	20.24	31.23	2018
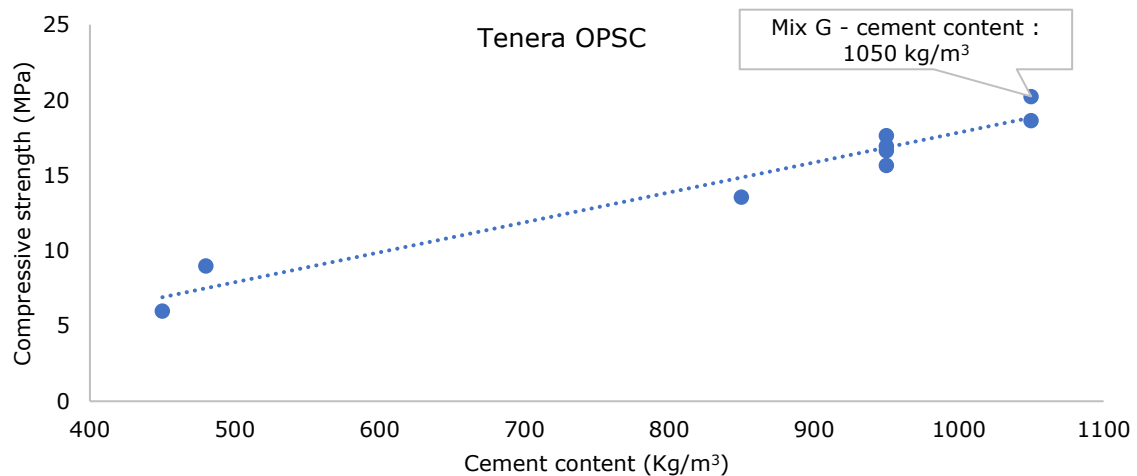
Figure 4.9 Cement content influence on compressive strength Tenera coarse OPSC

4.2.2.1.   Tenera OPSC

From Figure 4.9, a compressive strength of 20.24 MPa was achieved with a cement content of 1050 kg/m³, which is deemed to be high (Kosmatka, et al., 2002). Sliced cubes of the Tenera OPSC samples from Mix – G indicate why such high cement content is demanded, see Figure 4.10. The sliced samples show that the OPS is well distributed, and no signs of segregation is observed. However, by taking a closer look at the OPS in the red dotted boxes in Figure 4.10 (a – c), the shells with a half-hollow-spherical shape, see Figure 4.10 (d), seem to take large amounts of cement matrix to fill in the shells i.e., the cement

matrix is enclosed inside the shells. OPS is very well known to have a weak bond with cement matrix (Hamada, et al., 2020). It can therefore be assumed that the cement matrix inside the shell essentially does not contribute to the strength because it is entrapped inside the shell and only weakly bonded to the inside of the shell i.e., the concave side. From Section 4.1.1 it was also observed that the inner side of the Tenera shell was smoother than the outer, thus expected to have an even weaker bond. The outer side of the shell (convex side) is also assumed to have a weak bonding with the cement matrix which therefore causes OPS to only act as a barrier with no bonding mechanism between the cement matrix from the inner to the outer, thus creating a weak link. This is evident in Figure 4.11, taken from samples destructed by compressive strength test, where imprints of the convex sides of OPS are seen in larger amounts compared to leftover-OPS with its concave side facing the camera.

(a)

(b)

(c)

(d)
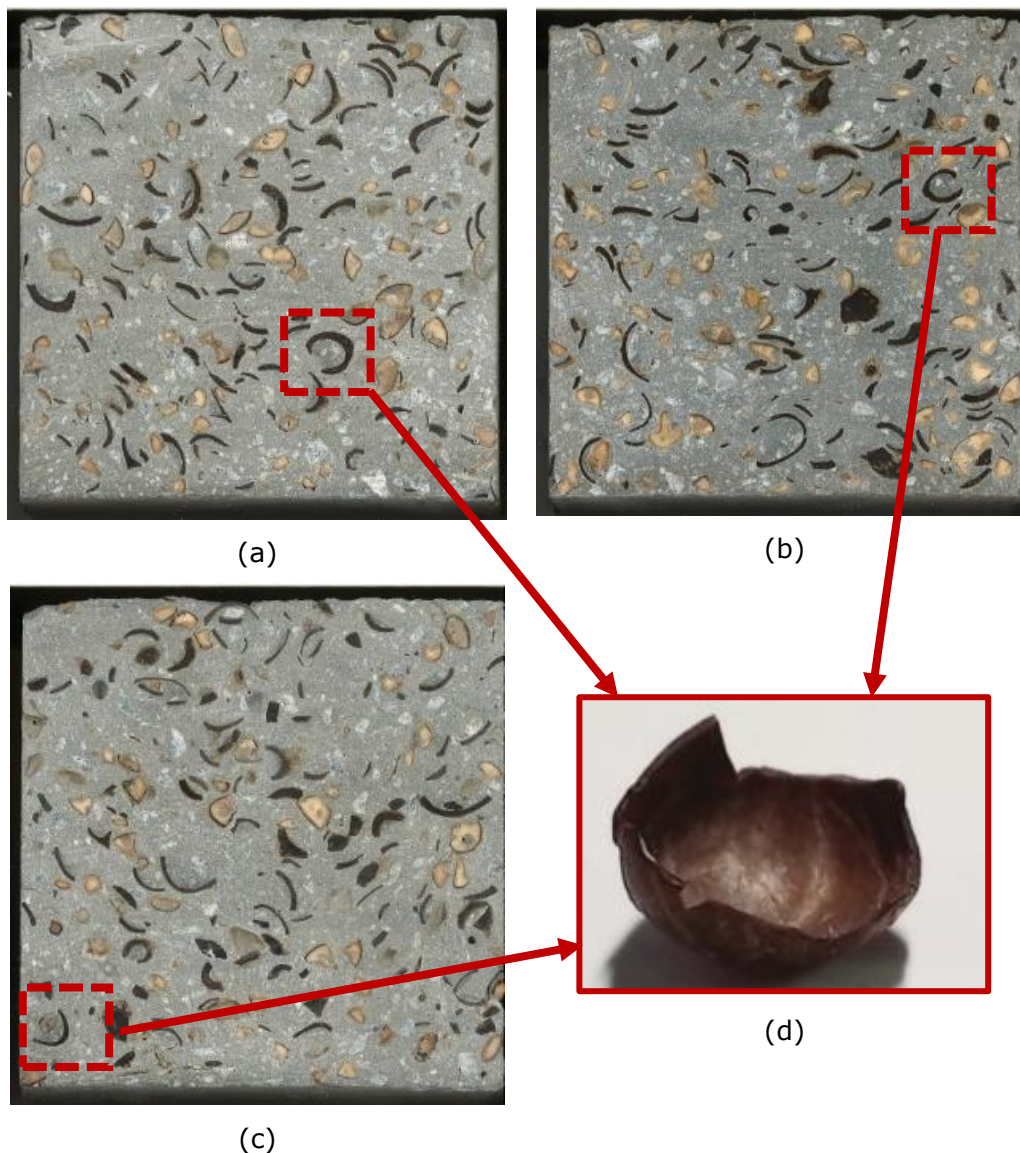
Figure 4.10 (a – c) Sliced cubes of Tenera OPSC and (d) common shape of Tenera OPS
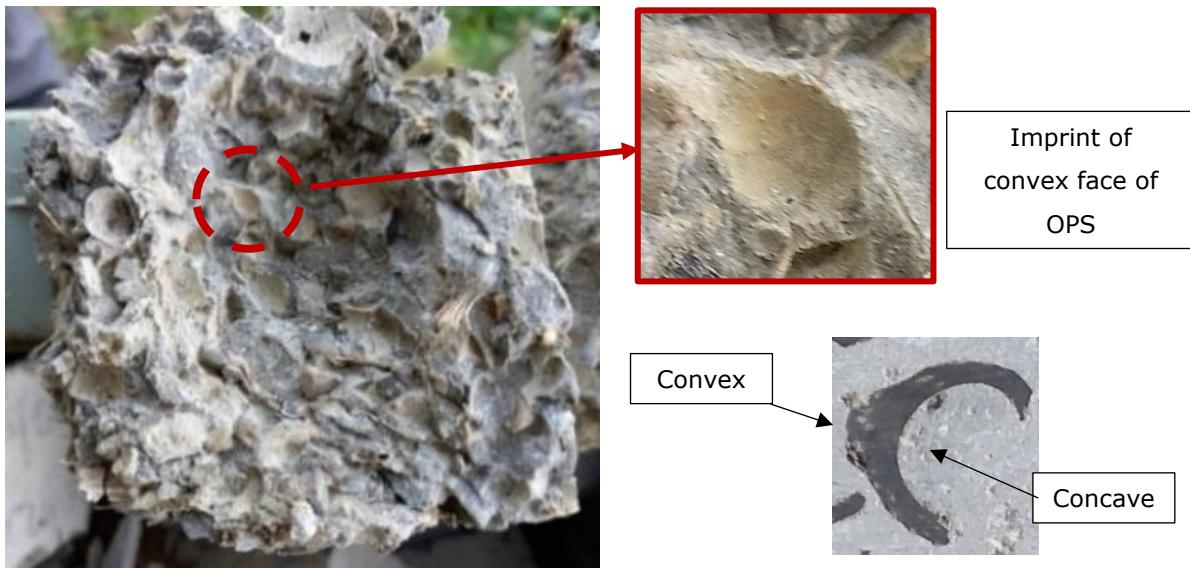
Figure 4.11 Inner face of destructed Tenera OPSC cube sample

Further observations from the sliced samples from Figure 4.10 were analysed by taking microscopic images at point of contact between the OPS and the cement matrix where it further revealed the bonding mechanism of the materials in the hardened mix shown in Figure 4.12. It is apparent from the images that there is a void space of 29 – 42 μm between the OPS and the cement matrix on the outside where no such large void was observed on the inner side.

Interfacial void between OPS and cement matrix
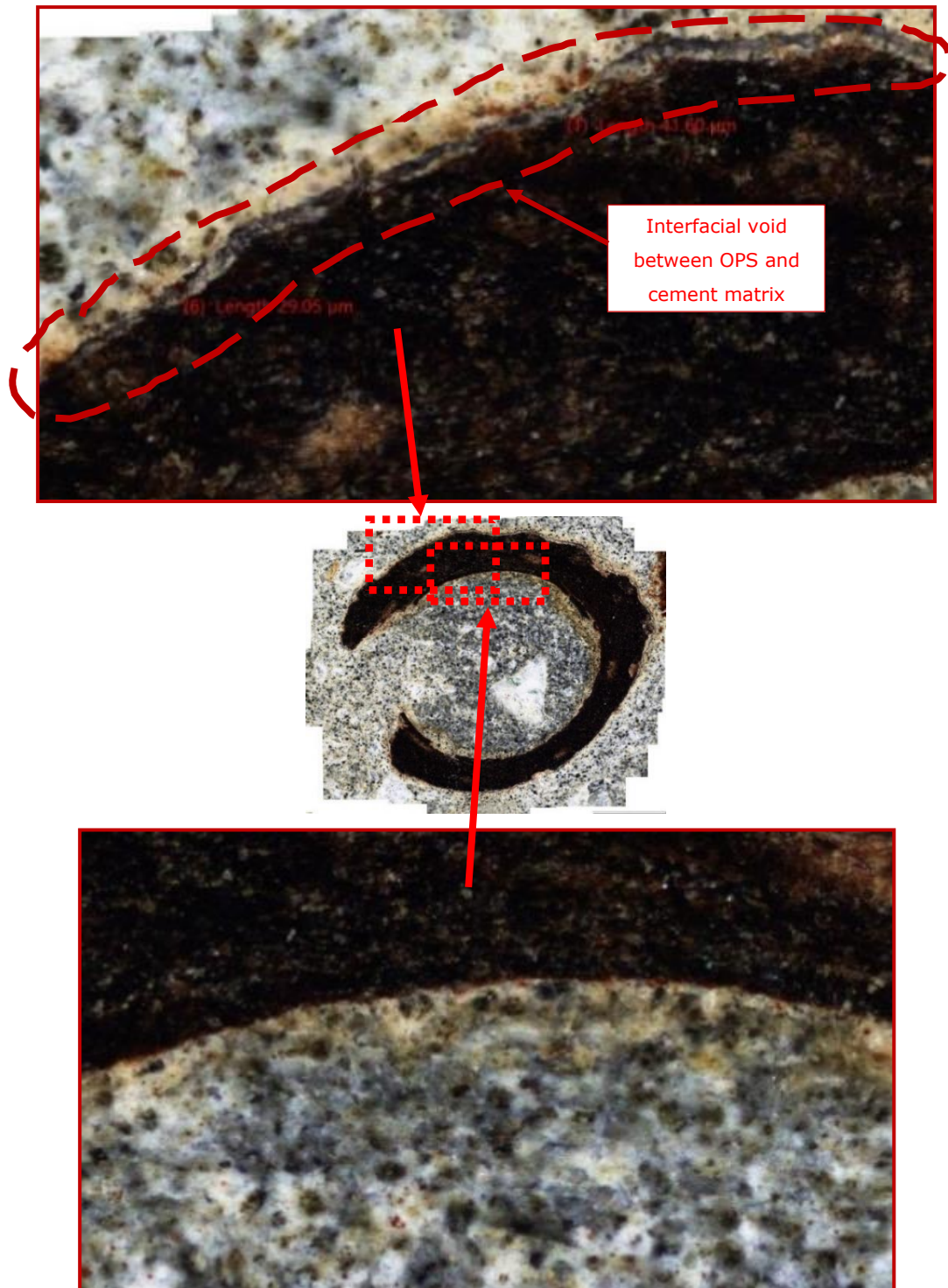
Figure 4.12 Microscopic images of sliced Tenera OPSC (20x scanned images)

Though difficult to observe quantifiably as to why this has happened, Figure 4.13 illustrates what might be occurring withing 24 hours after casting. Figure 4.13 (a) illustrates a swollen OPS sample by being in an SSD state in the liquid state mix. Then Figure 4.13 (b) shows that the OPS shrinks and de-bonds from the cement matrix causing the void space, which can be attributed to self-desiccation due to the hydration of cement absorbing the internal water in the OPS. This swell and shrink effect of the OPS is also found in wood materials

when changed from moisture state to dry state (Stamm & Hansen, 1937). To verify that the internal water from the OPS is absorbed by the hardened cement matrix, one can take a closer look at the images in Figure 4.12, where it can be seen that the surrounding cement matrix has a yellow/brown colour representing the palm oil residue from the OPS.

| (a) | (b) |
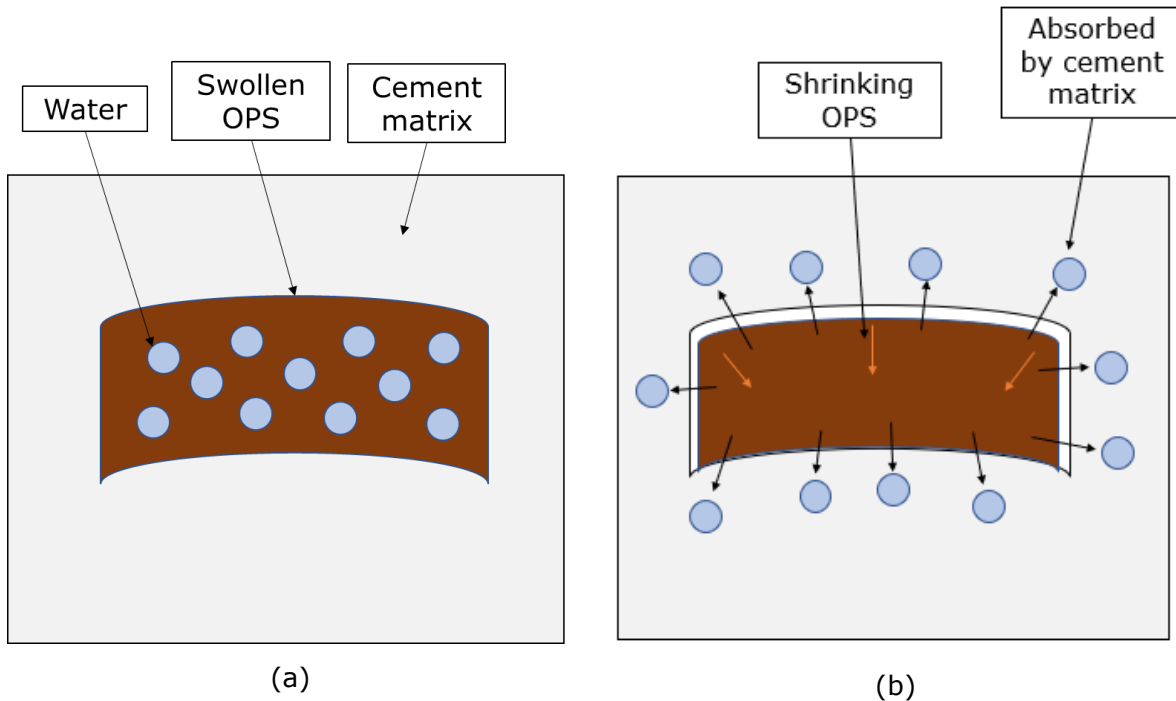
Figure 4.13 (a) When mix is in liquid state, (b) Cement matrix hardened < 24 hours

Also, to demonstrate the swelling and shrinking effect of the OPS in the concrete, a sliced OPSC sample was kept in water for 24 hours where then microscopic images were taken of an OPS sample as seen in Figure 4.14 (a). Then the same sample was allowed to dry in an outside environment for 24 hours where then microscopic images were taken from the same OPS sample seen in Figure 4.14 (b). The two images evidently show the swelling (when kept in water) and shrinking (when allowed to dry) of the OPS. Therefore, it can be concluded from this study that Tenera OPS shrinks during the hardening process of the concrete, which then causes the cement matrix to lose all its bonding mechanism with the OPS and is perhaps the main reason behind the high cement demand.
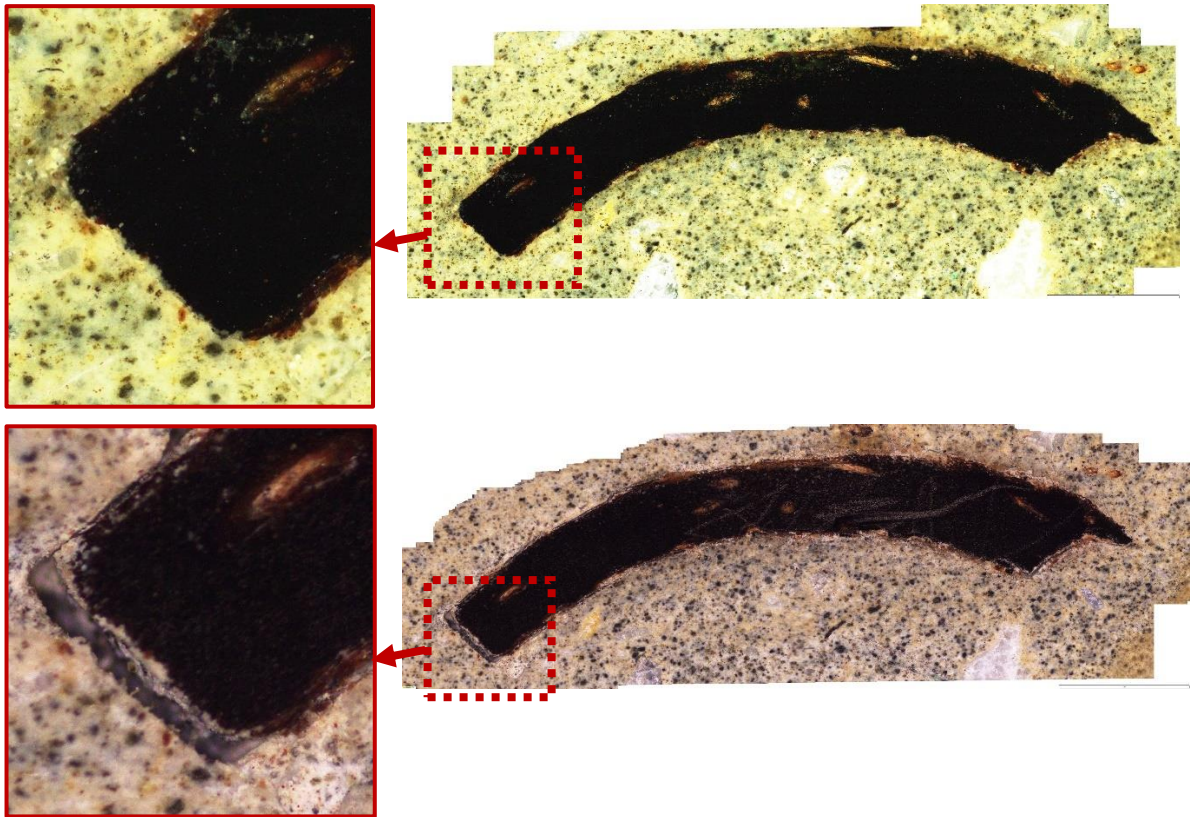
Figure 4.14 (a) After 24 hours in water and (b) after 24 hours drying (the difference in colour is due to presence and absence of moisture)

When Tenera OPS was used in a dry state prior to mixing rather than SSD state by applying Mix - G, a similar swelling-shrinking effect was also observed. This was done in the following matter: the Tenera OPS was first weighted when in SSD state according to mix design Mix – G and was then kept in an oven from 24 hours to allow it to fully dry to have the same volume and was then used to make the OPSC. Samples were used for compressive strength test after 28 days moist curing and others were sliced for microstructural analysis. Though from the sliced samples similar void spaces where found between the dry-state OPS and the cement matrix as SSD-state OPS, a reduction by 39% was found in the compressive strength, see Figure 4.15. This might indicate when OPS is used in an SSD state it allows for internal curing, i.e., helps with hydration. This behaviour has also been found for other LWA, where in a review by (Ma, et al., 2019) concluded that the pre-wetting of LWA show better internal curing effects than dry LWA. Nonetheless, since this is outside the scope of this study, it is recommended to investigate this for future studies.

103
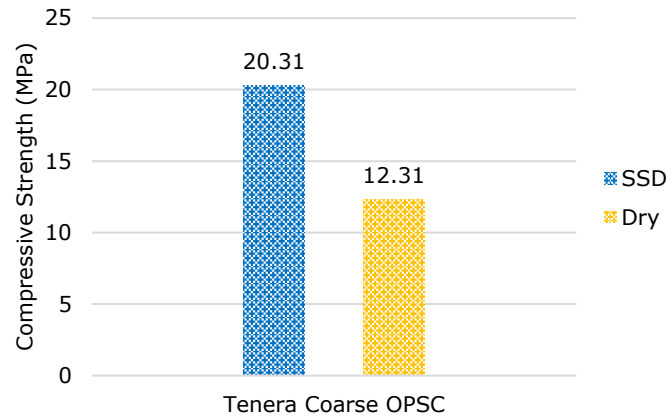
Figure 4.15 Coarse OPSC made with Tenera C-OPS in SSD- vs dry-state using Mix G

4.2.2.2.   Dura OPSC

One can easily recognize that a cement demand of 1050 kg/m^3 is remarkably high for producing a 28-day compressive strength of only 20 MPa. Therefore, the mix designs taken from (Gibigaye , et al., 2017) and (Basri, et al., 1999) were also tested with both Dura and Tenera OPS for comparison in this study. The mix designs made for Dura OSPC by (Gibigaye , et al., 2017) and (Basri, et al., 1999) produced a 28 days compressive strength of 22.42 and 24.2 MPa respectively in their work. However, when used with Tenera OPS, it resulted to have a far less compressive strength of 5.70 and 8.77 MPa being 75% and 64% lower respectively, see Figure 4.16. Since the same mix design is used, the high strength reduction could therefore be mainly due to the following parameters being different by the type of cement, fine aggregate, and coarse aggregate (OPS). The difference in material properties used by (Gibigaye , et al., 2017), (Basri, et al., 1999), and in this study is shown in Table 4.7.

Table 4.7 Material properties differences

Material	Cement	Fine aggregate (Type, FM)	Coarse aggregate
This study	Type II	River sand, FM 2.30	Tenera OPS
(Gibigaye , et al., 2017)	Type II	(Unknown), FM 2.40	Dura OPS
(Basri, et al., 1999)	Type I	Mining sand, FM 2.56	Dura OPS

Though (Basri, et al., 1999) used OPC (Type I), in this study and by (Gibigaye , et al., 2017), Type II cement was used. However, Type I and II are known to have a minimal difference in strength development at 28 days (Li, 2011), see Figure 4.17. Therefore, the different cement types are most probably not the cause for the high difference in strength. As for the fine aggregate, (Basri, et al., 1999) used mining sand with a FM of 2.56 and (Gibigaye , et al., 2017) did not mention what type of sand but mentioned the FM to be 2.40 where in this study river sand was used with a FM of 2.30. Though the FM are slightly different, they all fall in the range of medium sand (FM 1.5 – 2.8), see Table 4.2. The FM is known to mostly effect the slump; however, the same w/c ratio was used with Tenera

OPSC. Therefore, the fine aggregate is also deemed not to be a crucial factor behind the high difference in strength. Which leaves the only possible cause to be the different OPS variety of Dura and Tenera used as coarse aggregate. To verify this, Dura OPS was used with the mixes from (Gibigaye , et al., 2017), (Basri, et al., 1999), and Mix – G with the results shown in Figure 4.16. It can be clearly seen that with Dura OPS higher strengths of 18.23, 19.61, and 31.23 MPa by being 320%, 224%, and 65% higher than Tenera OPSC was achieved with mix designs of (Gibigaye , et al., 2017), (Basri, et al., 1999), and Mix – G respectively. It can therefore be concluded that OPSC mix designs used with Dura OPS are not suitable with Tenera OPS and that the physical alternations of the thickness of Tenera OPS reduces the compressive strength of OPSC by significant amounts. This highlights the significance of this study's reinvestigation of Tenera OPS's fundamental mechanical properties as an aggregate replacement in concrete.
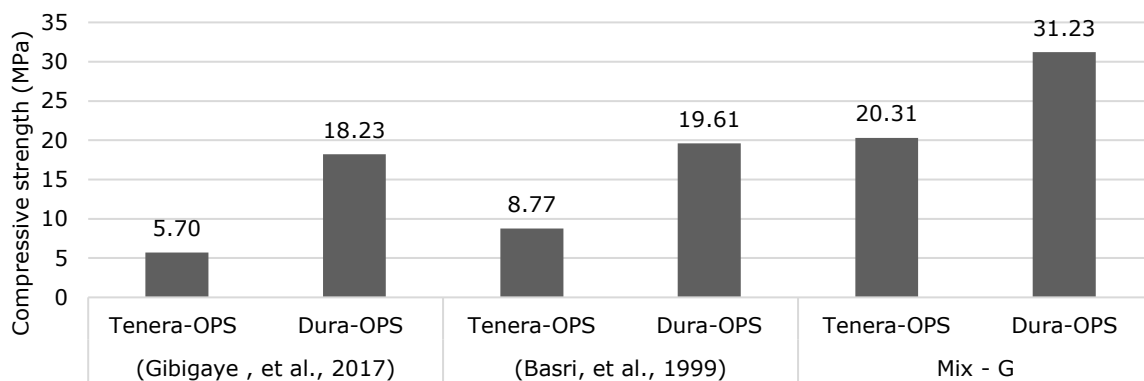
Figure 4.16 Compressive strength at 28 days of Dura vs Tenera OPSC made with different mix designs
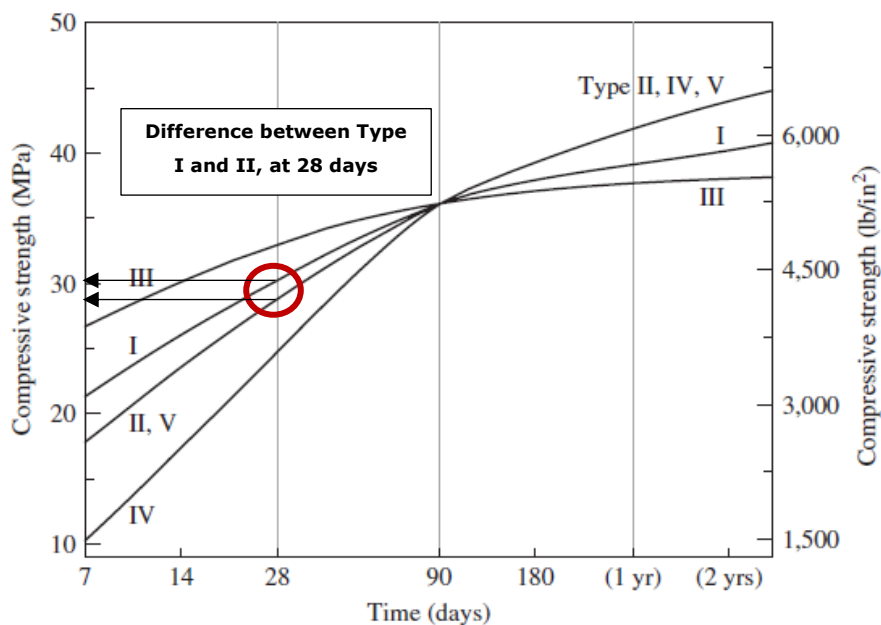
Figure 4.17 Strength development of cement pastes with different types of cement (Li, 2011)

105

4.2.3. Fine OPSC

To the best of the authors' knowledge, no research is conducted on producing OPSC from fine-sized OPS. Therefore, a variety of treatment techniques of F-OPS in mortar cubes were investigated by testing its compressive strength, with the results shown in Section 4.2.3.1. The selected treatment with F-OPS was tested in concrete with varying F-OPS to coarse aggregate ratios discussed in Section 4.2.3.2. Then, with the selected F-OPS to coarse aggregate ratio, different cement contents were investigated with the aim of producing a 28 days moist cured concrete with a compressive strength of 20 MPa and a dry density of <2000 kg/m^3 to produce a SLWC in accordance with (BS EN 206, 2021).

4.2.3.1. Treatment of F-OPS in mortar

F-OPS was initially tested in mortar cubes to investigate its compressive strength, a similar methodology as done by (Kabeer & Vyas, 2018) with marble powder and many other researchers with different types of waste-based materials presented in a review paper by (Brahami, et al., 2022). It is well recognised that increasing the bonding mechanism between cement and aggregate results in improved mechanical properties (Neville, 1995). Because OPS is an organic material derived from wastelands, it is expected that chemicals and other substances will be adhered to its surface, affecting the cement's ability to bond with it. Nonetheless, as discussed in Section 2.2.5 of the literature, pre-treating OPS prior to mixing increases the mechanical properties of concrete. As a result, in this study, some new methods in addition to some pre-treatment methods previously investigated with Dura OPS, were explored with F-OPS. Table 4.8 and Figure 4.18 show the various treatments applied to F-OPS and the resulting 7 days compressive strengths of mortar sample cubes.

Table 4.8 F-OPS treatment results

ID	Treatment type*	7 Days Compressive strength (MPa)
1	Control	20.95
2	Dirty-Dry	7.39
3	Dirty-Dry-1 mm retained	9.12
4	Dirty-Dry-Hexane	8.31
5	Dirty-Dry-Ethanol	6.63
6	Dirty-wet	12.69
7	Dirty-Wet-1 mm retained	13.68
8	Dirty-wet-Hexane	9.58
9	Dirty-wet-Ethanol	13.22
10	Dirty-wet-top filtered	15.04
11	Sonicated-wet	13.41
12	Detergent cleaned-wet	14.16

ID	Treatment type*	7 Days Compressive strength (MPa)
13	Detergent cleaned-wet-top filtered-heat treated	13.80
14	Detergent cleaned-wet-top filtered-cement treated	19.13
15	Control with same amount added for cement treatment in ID 16	26.43
16	Detergent cleaned-PVA20%	11.89
17	Detergent cleaned-PVA10%	13.74
18	Detergent cleaned-SSD-top filtered-retained at 1 mm	17.51

*More information on the treatment type is shown in Table 3.6
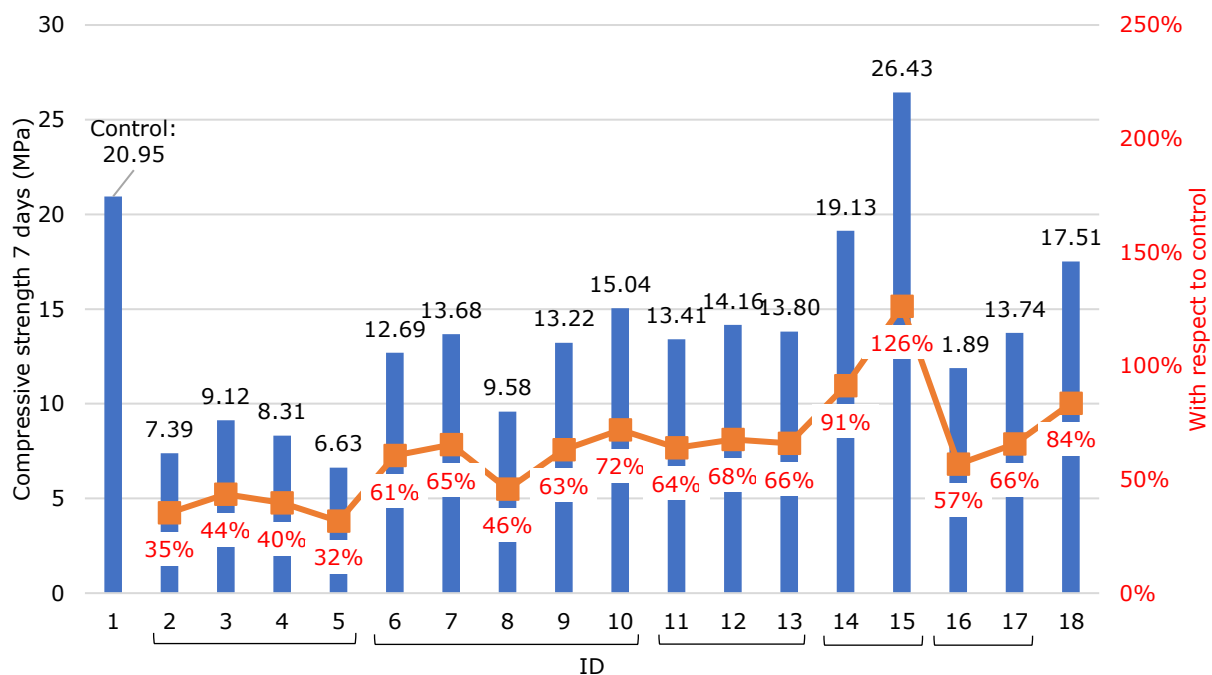
Figure 4.18 Treatment F-OPS-mortar results

The control sample (ID 1) showed a compressive strength of 20.95 MPa which is in accordance with (BS EN 480-1, 2014). ID 2, 3, 4, and 5 performed the lowest with strengths of 7.39, 9.12, 8.31, and 6.63 MPa, respectively. The common treatment was that they were kept in their dirty and dry state. Out of these three, the hexane solution (ID 4) showed a small higher strength, whereas the ethanol solution (ID 5) performed the weakest. However, ID 3 performed the best among the dirt-dry samples without any solution, rather by just removing any particles below 1 mm size. As was shown earlier in Figure 3.15, the discarded materials were observed to be clayey materials with OPS fibres. A decrease in the compressive strength with the addition of clay with aggregate replacement in concrete was also shown in a study by (Désiré & Léopold, 2013). The clay by-product found on OPS's surface is most probably accumulated when the palm oil fruit

107

bunches are cut from the tree and fall on the soil surrounding the tree and after the milling process (see Section 2.1.2), the OPS is dumped onto clayey soil landfills (JPM, 2022). Thus, based on ID 2 – 5, ID 3 was selected for further investigations.

This was done by using the samples in a wet state instead of dry in ID 6, 7, 8, and 9 showing higher results of 12.69, 13.68, 9.58, and 13.22 MPa, respectively. The higher strength results are perhaps caused by the water removing further dirt from the surface of the samples. This is most probably because a lesser volume of F-OPS in wet state is weighted compared to dry state as the F-OPS becomes denser when used as wet state. Nevertheless, in ID 7, by having the samples wet (kept in water for 24 hours), by removing particles smaller than 1 mm showed, again, showed the highest strength among ID 6 – 9. On the other hand, the ethanol solution performed better in wet state than dry state where the strength was comparable to ID 7. Since ethanol is known to fully stop the hydration of cement (Neville, 1995), the higher strength might be because all the ethanol solution was removed when kept in water for 24 hours, also proving that it can clean the OPS. However, by being 3% lower in strength compared to ID 7 without any addition of a chemical, ID 7 can hence be deemed to be a better choice. Therefore, based on the results from ID 2 – 9, it can be determined that discarding particles below 1 mm and not using F-OPS in dry state is the better treatment so far.

It was also found when removing any floating particles (top filtered), keeping the sample wet and in its dirty state (ID 10), the strength outperformed all treatments in ID 2 – 9. However, when cleaning the sample by means of sonication (ID 10) or detergent cleaning (ID 11) the strength was further improved by 6% and 11.6% respectively compared to dirty wet (ID 6). Therefore, in this comparison case, the cleaning of the sample is found to be of essence, particularly by using the detergent method (ID 11). Thus, so far, it can be stated that the wet, detergent cleaned, 1 mm retained, and top filter treatment method (ID 11) shows the best result among ID 2 – 12.

From ID 13 (heat treatment of F-OPS), no significant difference in strength was observed. However, by treating the F-OPS with cement (ID 14), it seemed to achieve the highest strength among ID 2 – 13 by having a 91% strength with respect to the control (ID 1). Still, this idea might just be deceiving, since adding cement to the surface of the sample and then adding it in the mix actually decreases the amount of F-OPS by making the samples denser and increases the amount of cement in the mix concurrently. To scrutinise this, the same cement amount added in ID 14 was added in ID 15 without using it as a treatment on F-OPS and certainly showed to have increased the strength even more than the control sample (ID 1) by 26%. As a result, the idea of cement treatment is proven to be inaccurate. It was also found that the cement on the F-OPS with the cement treatment method did not bond to the surface of the F-OPS. This was observed with an F-OPS grain

treated with cement, after 24 hours, by rubbing the surface resulted in the cement being removed easily as is depicted in Figure 4.19 (a – c).

| (a) | (b) | (c) |
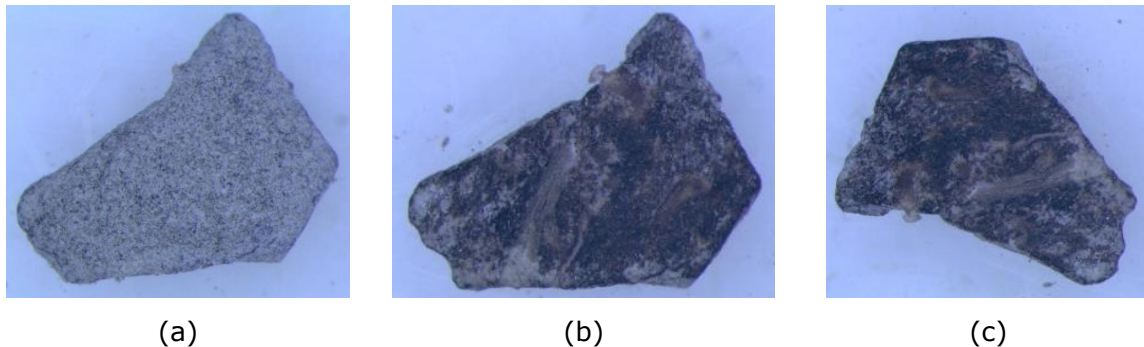
Figure 4.19 (a) Cement treatment on F-OPS grain after 24 hours (b) rubber off front-face and (c) rubber off back-face

Another attempt was by treating the F-OPS with PVA solutions of 10% and 20% in ID 17 and ID 16, respectively. However, both ID 17 and ID 16 showed to have a lower strength to a comparable sample of ID 12 (cleaned with detergent & in a wet state). Though the PVA solution turned hard when dried, it turned to liquid when in contact with the mixing water. Furthermore, the 20% PVA solution caused all of the F-OPS to stick together as a bulk, making mixing difficult, as shown in Figure 4.20 (a – c).

| (a) | (b) | (c) |
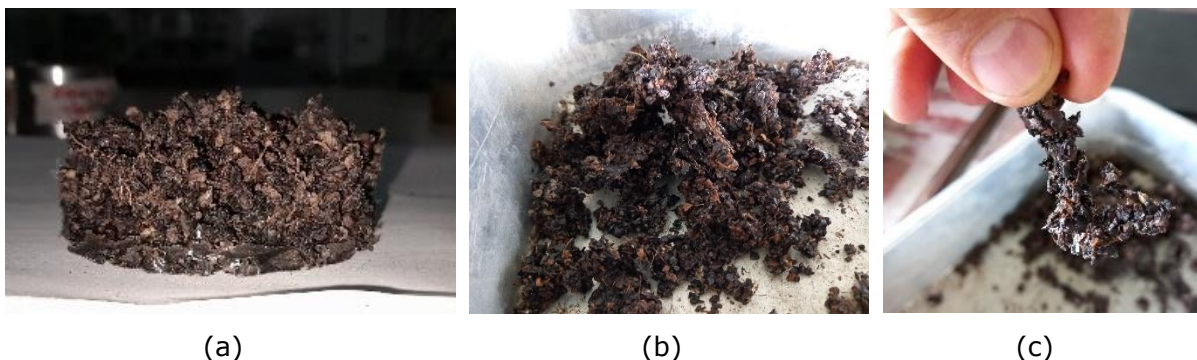
Figure 4.20 (a) 20% of PVA solution, (b) broken down, and (c) F-OPS particles stuck to each other after breaking down

Nevertheless, by:

- ➢ cleaning the F-OPS using a detergent (**Detergent cleaned**),

- ➢ using the F-OPS in an SSD state (**SSD**),

- ➢ by filtering/removing the top floating particles when keeping the F-OPS in water (**Top filtered**), and

- ➢ by discarding particles less than 1 mm size (**1 mm retained**)

the highest compressive strength of 17.51 MPa was achieved (ID 18) among the other treatment methods and being 84% with respect to the control sample (ID 1). It can therefore be concluded that the best treatment method among the treatment methods used in this study was ID 18 and selected for further investigations in the coming sections.

4.2.3.2.   Mix-design

From the previous investigation, the "Detergent cleaned – SSD - top filtered - retained at 1 mm" was chosen as the suitable treatment method for F-OPS. This treatment method for F-OPS was further investigated by utilising it as fine aggregate in concrete to produce fine OPSC. In the first investigation, the cement and the water content were fixed while different F-OPS to C.A. ratios were tested for their dry-density and permeable voids. Then with the selected aggregate ratio, different cement contents were investigated to achieve a compressive strength of 20 MPa at 28 days moist cured. The results and discussions for these investigations are further elaborated in the coming subsections.

Aggregate ratio

In this investigation, five mixes made with F-OPS to C.A. ratios of 0.1, 0.2, 0.3, 0.4, and 0.5 were made and the results with permeable voids (%), dry-density, and compressive strength at 28 days moist cured have been plotted in Figure 4.21.
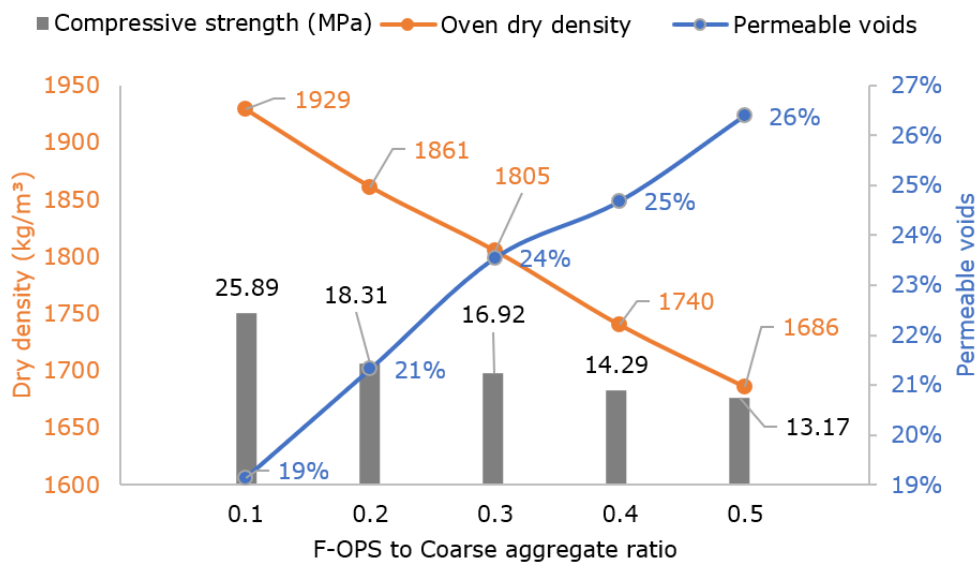
Figure 4.21 Influence of F-OPS: C.A. ratio on dry-density, permeable voids, and compressive strength at 28 days

From Figure 4.21 it can evidently be seen that with the increase of F-OPS content (higher F-OPS: C.A. ratio) an increase is seen in the permeable voids from 19.1 – 26.4% and a decrease in the dry-density of the concretes from 1929 – 1686 kg/m^3. This is the opposite behaviour observed with NWC, as demonstrated in a study by (Lin, 2020), who also investigated the fine to coarse aggregate ratio with conventional aggregates. However, for fine OPSC, this is expected since F-OPS has a lower density and a higher water absorption

than the conventional aggregates. Also notable was the compressive strength increase with the decrease in F-OPS to C.A. ratio. This similar behaviour was also found for OPSC made with Dura C-OPS as was previously analysed in Section 2.2.3, i.e., C-OPS and fine aggregate instead of F-OPS and coarse aggregate, respectively. Since the criteria for producing a LWC is having a dry-density of <2000 kg/m^3, from Figure 4.21 all the F-OPS: C.A. ratios are withing the limit of LWC. Also, from scanned images taken of sliced samples of each ratio, it can be seen that no segregation or visible voids are detected, see Table 4.9, with the exception of at the ratio of 0.5. This might have had happened because the mortar (OPS and cement) easily slides through the coarse aggregate or most probably because a lack of coarse aggregate being present. Also, like Tenera OPSC, a void space was also found at the interfacial zone between the cement and F-OPS, see Figure 4.22. However, the void spaces found with F-OPS was between 3 – 8 μm where C-OPS showed larger void spaces of 29 – 42 μm. The decrease in void space is most probably due to the elimination of the large sizes and arch shapes found in C-OPS.

Nevertheless, it is well known when concrete absorbs less water, better mechanical and durability properties are expected (Li, 2011). Since at a ratio of 0.1 the permeable voids were at the minimum of 19.1% among the other ratio's, the ratio of 0.1 has therefore been selected for further studying different cement contents in the next part.

Table 4.9 Slice samples of F-OPS/C.A. ratio

F-OPS/C.A. ratio	Sliced samples
0.1	

F-OPS/C.A. ratio	Sliced samples
0.2	
0.3	
0.4	
0.5	
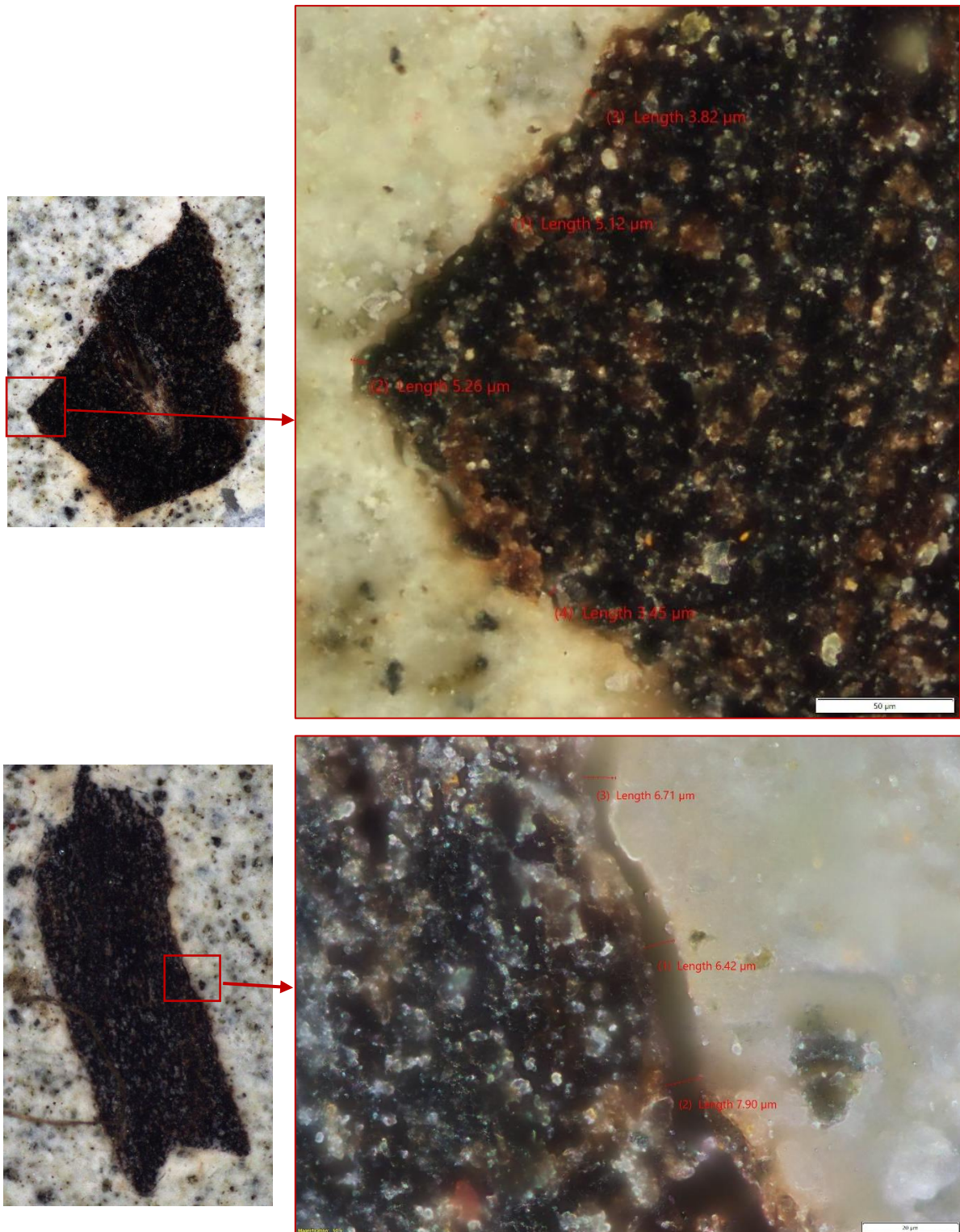
Figure 4.22 Microscopic images of F-OPS in concrete (50x zoom)

Cement content

With the chosen F-OPS: C.A. ratio of 0.1, it was further experimented with different cement contents from 350 – 700 kg/m^3 with the results shown in Table 4.10 and plotted in Figure 4.23. Results indicate that with the increase of cement content, an increase is observed in the compressive strength of up to 26.07 MPa at a cement content of 700 kg/m^3. At a

113

cement content of 350 kg/m^3, it produced a concrete with deficient cement as seen in Figure 4.24. However, it was found that at a cement content of 400 kg/m^3, the desired compressive strength of 20 MPa was achieved by being the closest. One might counter that the concrete is expected to be very lean and therefore unworkable with such a high coarse aggregate content, however, due to the smooth surface of the F-OPS, it was observed that the F-OPS positively affected the workability. This was also the conclusion of other studies, as explained in Section 2.2.2. Therefore, the mix design with a cement content of 400 kg/m^3 was selected for further investigations throughout this study.

Table 4.10 Cement content influence on compressive strength

Ratio F-OPS/C.A.	Cement	F-OPS	Coarse aggregate	Water	28-day Compressive strength	Dry-Density
	kg/m3				MPa	Kg/m³
	350	130	1298	123	12.06*	-
	400	124	1236	140	20.85	1994
	450	118	1175	158	22.15	1981
0.1	500	111	1114	175	22.83	1969
	550	105	1052	193	25.11	1962
	600	99	991	210	25.89	1929
	650	93	930	228	26.15	1916
	700	87	868	245	26.07	1889

*Produced permeable/honeycomb concrete: low cement
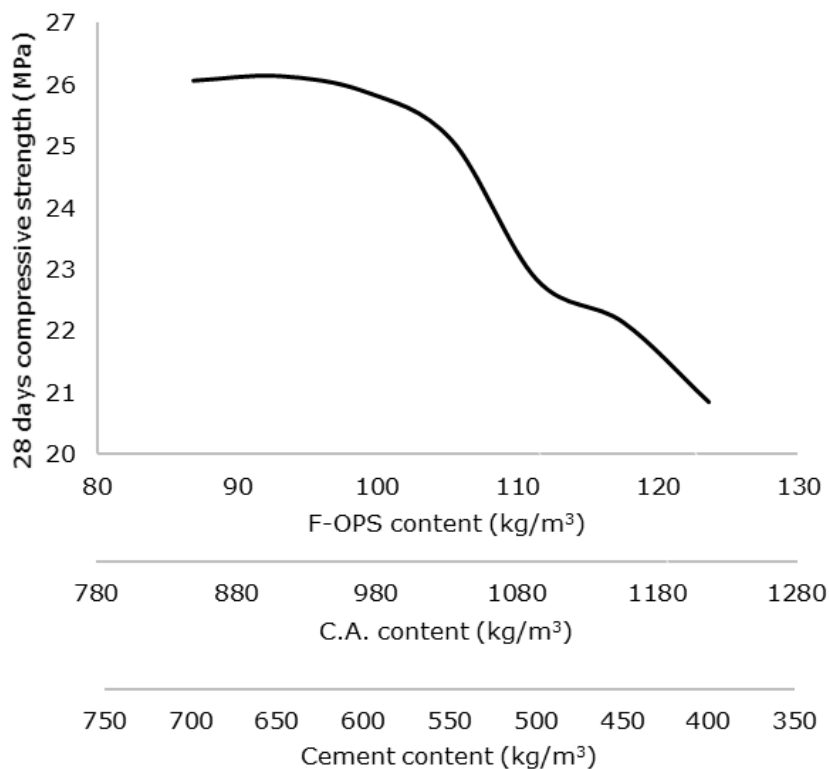
Figure 4.23 Influence of F-OPS, C.A., and cement content on compressive strength

114

Figure 4.24 Deficiency in cement content at 350 kg/m^3

4.2.4. Superplasticiser Investigation

Demand for low cost and high strength concrete is increasing in contemporary civil structures. Superplasticizer (SP) is frequently used to increase the concrete's workability by also using a low water-to-cement ratio (w/c) to achieve high strength and low permeability (Neville, 1995), (Chang, 2004), and (Haach, et al., 2011). According to research, if a polycarboxylate ether (PCE) based plasticizer or superplasticizer is used, concrete can maintain good flowability at a w/c as low as 0.16 and reach a compressive strength higher than 150 MPa (Hirschi & Wombacher, 2008). Not only does the addition of SP improve the flowability of the concrete, but the particle dispersion (or de-agglomeration) also significantly homogenizes the concrete mix. The packing density of solid particles in a cement paste may further be increased by SP, according to some research (Kwan & Fung, 2012).

Nevertheless, no study has been conducted on the influence of SP in Tenera OPSC with the use of Tenera OPS apart from a study conducted by (Okafor, 1991) using Dura OPS as coarse aggregate. However, Okafor employed a second-generation SP made of sulphonated naphthalene formaldehyde. The most prevalent type of SP currently being used in the industry is third generation polycarboxylate SP, also used in this study, which is known to be more efficient and less expensive than first- and second-generation SP (Mailvaganam, et al., 1999). There is very few research on the application of Tenera OPS in concrete. It is therefore vital to re-investigate the utilisation of Tenera OPS as aggregate in concrete and with the incorporation of the third generation polycarboxylate SP to validate its functionality in Tenera OPSC. The results and discussions are elaborated in the subsections 4.2.5.1 and 4.2.5.2, respectively.

4.2.4.1. Influence on workability with constant w/c

In this method, the influence of SP on the concretes were investigated whilst keeping the w/c constant. The workability (slump test), the water absorption, permeable voids, and

compressive strength at ages 7- and 28-days were tested under SP dosages of 0.1, 0.3, and 0.5% by weight of cement with the results presented in Figure 4.25 - Figure 4.29.

From Figure 4.25, all three types of concrete displayed a comparable value of slump at 0.1% of SP dosage and showed little change by 2.6, 3.9, and 6.3% for NWC, coarse and fine OPSC, respectively. The slump values for both coarse and fine OPSC at an SP dosage of 0.1% were found to be 50 mm and 63 mm, respectfully. Therefore, falling in the range of SLWC slump values of 50 – 70 mm (Mehta & Monteiro, 2006). However, a noticeable difference between 0.1 – 0.3% is seen where both OPSCs perform similarly in terms of slump increment but no discernible change was seen for NWC. At a dosage of 0.3% of SP, the slump values were found to be 74, 233, and 195 mm for NWC, course and fine OPSC, respectively. However, at 0.5% of SP dosage, all three types collapsed in slump test (showing 300 mm). As for the NWC, similar values for slump changes with a similar mix design from this study was shown by (Paktiawal & Alam, 2021) who used SP dosages from 0.15 – 0.55%. Similar trends have also been observed for Dura OPSC by (Okafor, 1991), (Mannan & Ganapathy, 2004) and (Alengaram, et al., 2010b). Also, the effect of using OPS as coarse or fine sized does not results in different slump effects as was also concluded by (Alengaram, et al., 2010a) who used crushed and uncrushed Dura OPS.

It can therefore be concluded that coarse and fine OPSC demand smaller amounts of SP dosage as compared to NWC regarding increasing slump values. This might be due to the fact that OPS, either used as coarse or fine aggregate, has a smoother surface compared to the that of conventional aggregates (coarse and fine) identified by (Shafigh, et al., 2010).
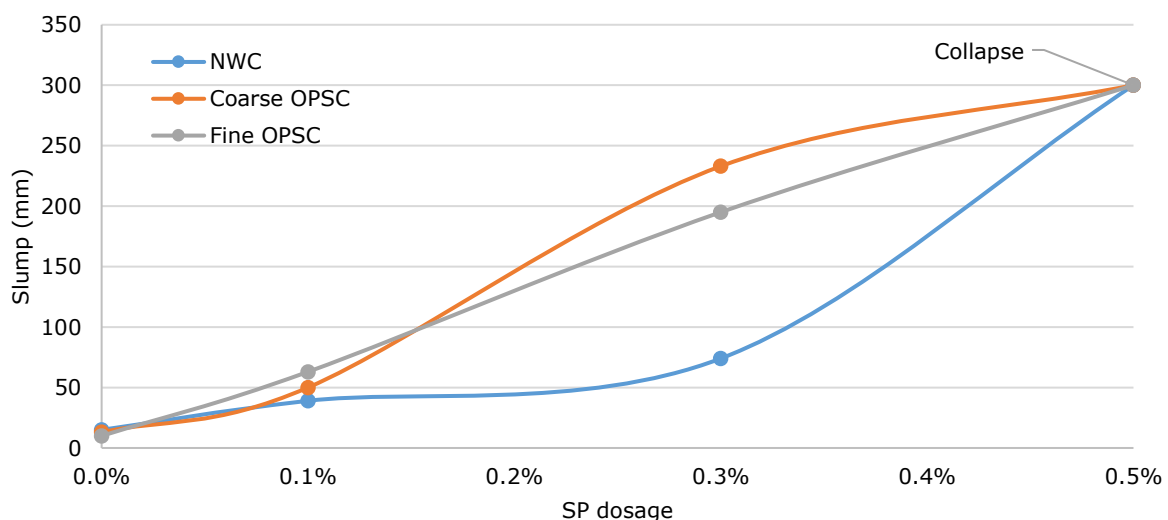
Figure 4.25 Influence on slump with increase of SP dosage

For all three concrete's types, a reduction in the compressive strength (compared to 0% SP dosage) was seen at ages 7 and 28 days with the increment of SP dosage seen in Figure

4.26 and Figure 4.27, respectively. Therefore, the addition of the type of SP used in this study seemed to have an adverse effect on the compressive strength. This might be caused by the effect of segregation as explained later referring to images taken from the sliced sample in Table 4.11. The compressive strength at age 7 days for fine OPSC was observed to have the least decrease in strength with the increment of SP dosage compared to NWC and coarse OPSC with a maximum of 5% decrease at 0.3% of SP dosage. The NWC compressive strength decreased in a linear manner up to a maximum of 14% at 0.5% SP dosage, while the coarse OPSC showed the highest decline in compressive strength by 28% at 0.3% of SP dosage. In contrast to NWC decreasing further at 0.5% SP dosage, both coarse and fine OPSC showed a smaller decrease in compressive strength at SP dosage of 0.5% compared to 0.3%. This might be due to the segregation of the OPS at the higher dosage of 0.5% as seen from the figures in Table 4.11. No notable segregation was found in NWC, and little segregation seen for coarse OPSC, while fine OPSC showed high segregation of F-OPS aggregates mainly floated to the top. However, it is not possible to tell whether the fine aggregates in NWC and coarse OPSC have also segregated.

A similar reduction pattern in compressive strength was observed at age of 28 days compared to 7 days for all three concrete types. However, both coarse and fine OPSC decreased further in compressive strength by 34% and 18% respectively at a dosage of 0.5% compared to 14% for NWC. NWC had a similar decrease rate at 7 days of 8%, 12%, 14% and at 28 days 10%, 12%, and 14% at SP dosages of 0.1%, 0.3%, and 0.5% respectively showing that the hydration continued in a linear manner. This can be better observed from Figure 4.28, showing that NWC has a similar increase rate of 27 – 30% between 7 and 28 days with all dosages. Both coarse and fine OPSC demonstrated a similar trend as NWC up to 0.3% SP dosage but then at a higher dosage of 0.5%, the hydration seems to halt after 7days for fine OPSC while only a 10% increase from 7 to 28 days compressive strength is seen for coarse OSPC compared to 29% for NWC.

Accordingly, it can be concluded that 0.3% of SP is the optimum dosage for both coarse and fine OPSC, producing slump values of 233 mm and 195 mm and reducing the compressive strength at 28 days by 28% and 8% for coarse and fine OPSC, respectively, while having no effect on the hydration process up to 28 days. But perhaps a lower dose than 0.3% is recommended for fine OPSC to prevent segregation.
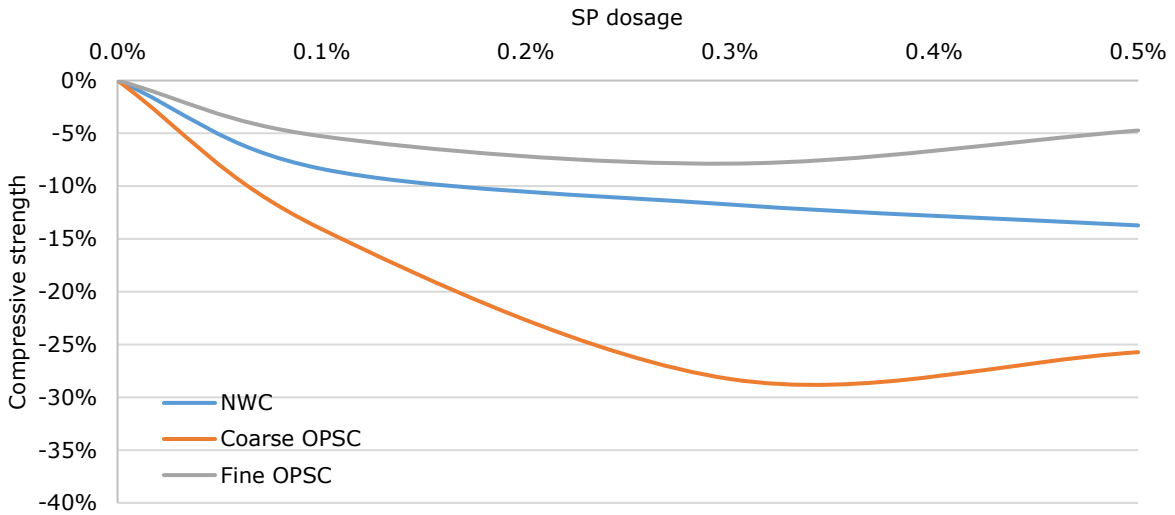
Figure 4.26 Influence on 7 days compressive strength with increase of SP dosage
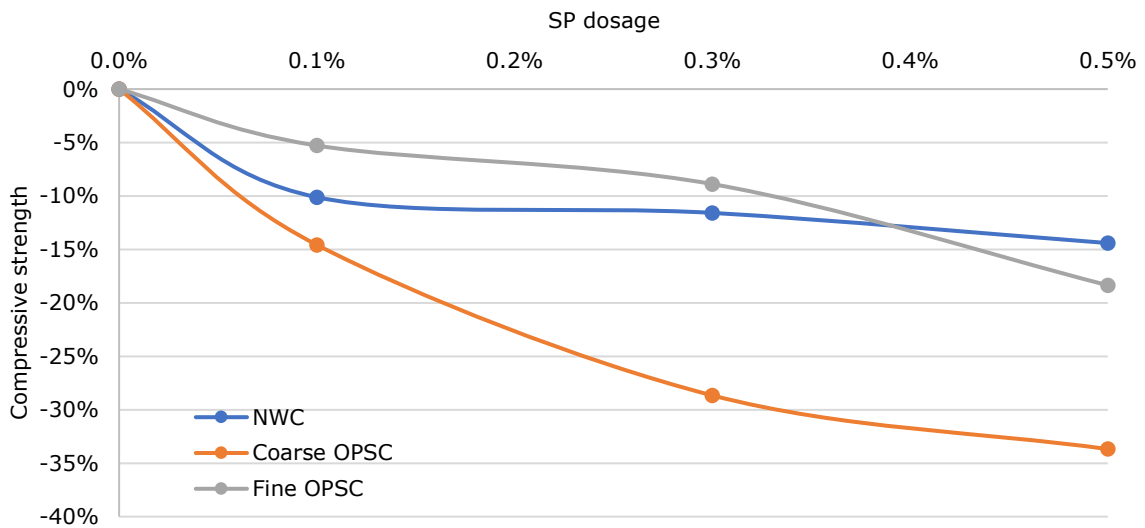
Figure 4.27 Influence on 28 days compressive strength with increase of SP dosage
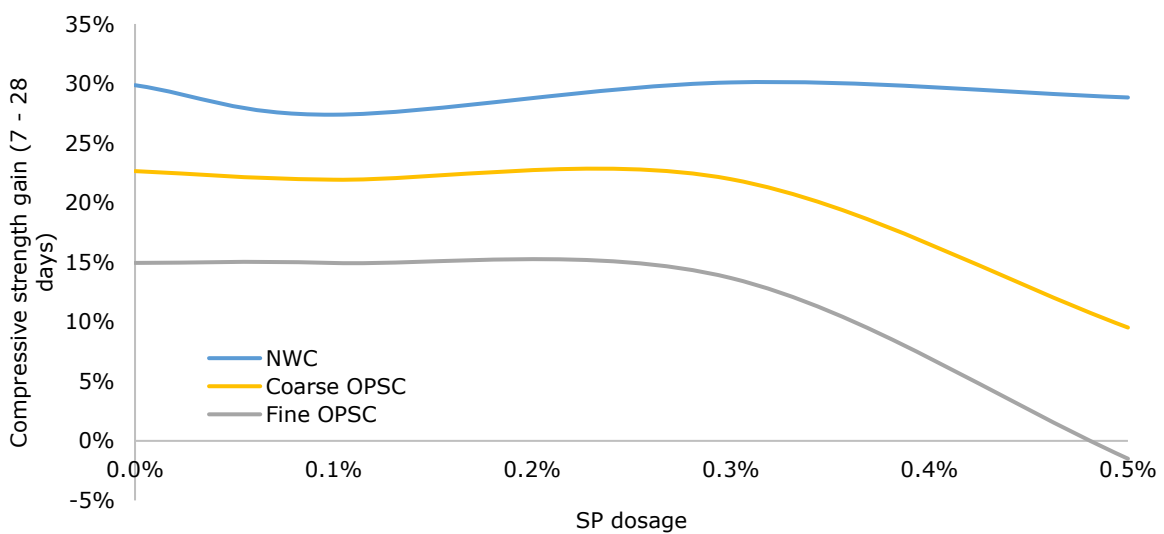
Figure 4.28 Increase rate from 7- to 28-days at different SP dosages

118

Table 4.11 Sliced samples with different SP dosages
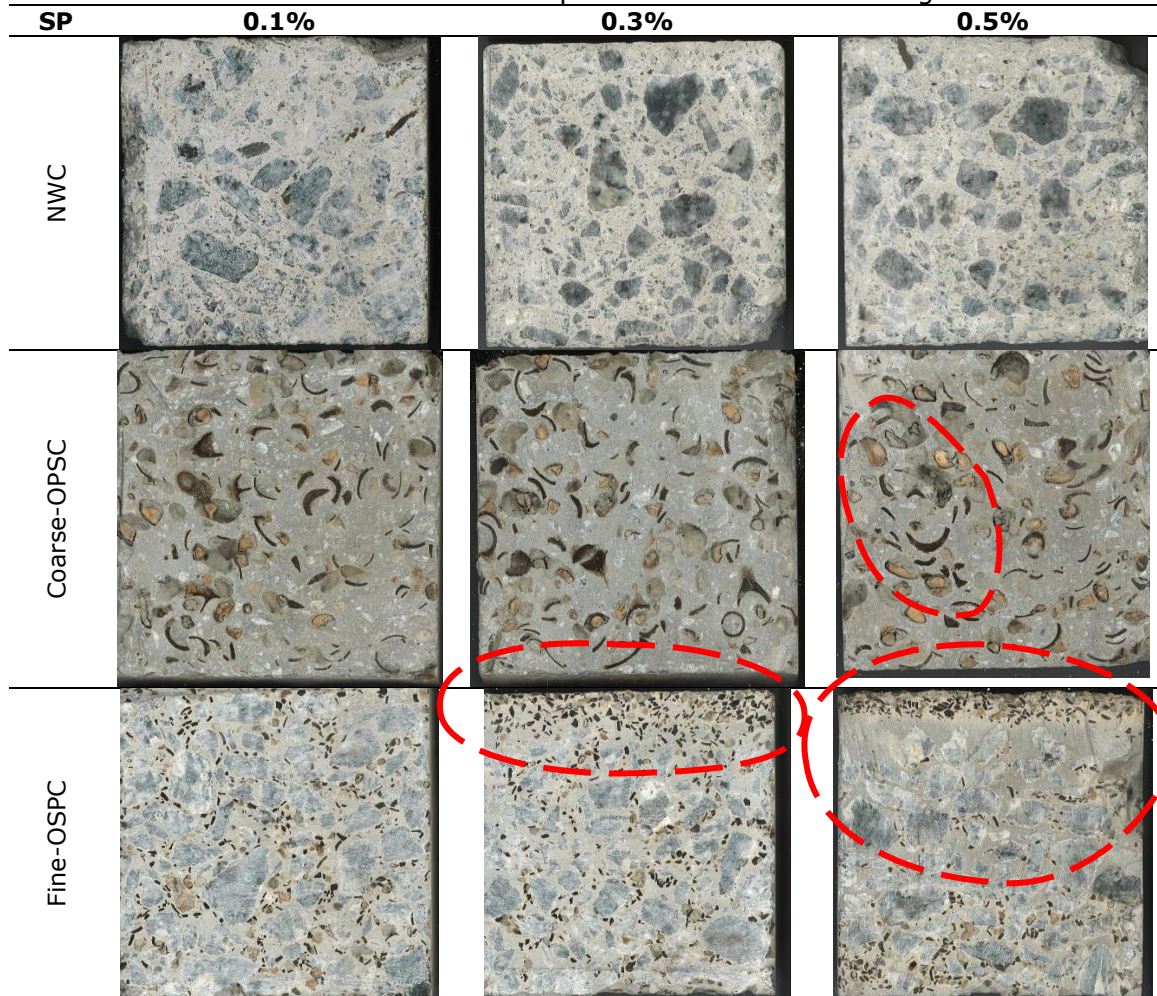
The influence on water absorption with increase of SP dosage of all three type concretes is seen in Figure 4.29. While NWC had the lowest values, coarse OPSC had values that were nearly twice as high as those of NWC and fine OPSC. In contrast to coarse and fine OPSC, NWC exhibits no changes in water absorption or permeable voids, with average values of 7.7% and 17.43%, respectively for all SP dosages. Both coarse and fine OPSC showed an increase in both water absorption by 0.6% and 24.1% respectively and permeable voids by 6.1% and 11.6% respectively with increase of SP dosage. The segregations found in the OPSCs (see Table 4.11), especially in fine OPSC, probably explains the reason behind the higher increase in water absorption and permeable voids. Since OPS has a high-water absorption rate, the OPS aggregates segregated to the top surface allows water to penetrate the concrete at a higher rate. Similar findings were observed by Teo et al., who suggested that the porous OPS's high water absorption may have led to more air being trapped in the concrete paste, which in turn increased the water absorption (Teo, et al., 2007).
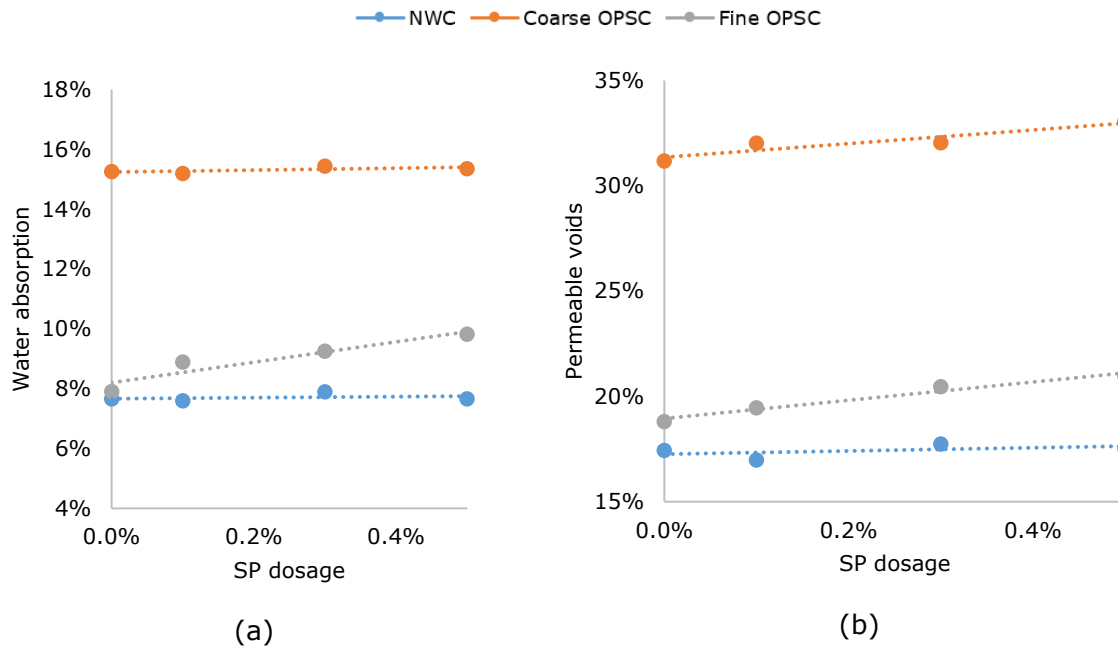
Figure 4.29 Influence on (a) water absorption and (b) permeable voids with increase of SP dosage

4.2.4.2.   Influence on compressive strength by reducing w/c

In this method, an SP dosage of 0.4% and 1.0% was added whilst the w/c ratio was lowered concurrently to investigate the influence on the compressive strength at 28-days. The selection of these dosage was merely based on the recommended dosage as prescribed in the manual of the product provided by the manufacturer (Sika, 2019). The UPV test was also conducted on the samples as an additional test. The results for this investigation are presented in Figure 4.30 - Figure 4.33. In this setup, all the materials were first dry mixed. Then a small amount of water, with the designated SP dosage, was added and increased gradually until a water amount for efficient compaction by a mechanical shaker was observed. The change in w/c with the control and addition of SP dosage is shown in Table 4.12.

Table 4.12 Change in W/C with the addition of SP dosage

SP dosage	NWC	Coarse OPSC	Fine OSPC
		w/c	
0.0%	0.62	0.30	0.35
0.4%	0.41	0.20	0.21
1.0%	0.29	0.14	0.17

The w/c decreased in a comparable manner for all three concrete types with the increase of SP dosage as seen in Figure 4.30 (a). For the NWC, compressive strength increased with the reduction of w/c (and addition of SP dosage) in a linear manner as seen from Figure 4.30 (b). However, this trend was not observed for the coarse and fine OPSC. In fact, it indicated that a dosage of 0.4% does not increase the compressive strength for both the

OPSCs, see Figure 4.31 (a). However, only at 1.0% SP dosage, a slight increase of 11% for both OPSCs is observed compared to 66% for NWC as seen in Figure 4.31 (b). It can therefore be concluded that lesser amounts (≤1%) of SP dosage is not as effective in both the OPSCs as was observed for the NWC and therefore higher dosages are probably necessary.

(a)   (b)
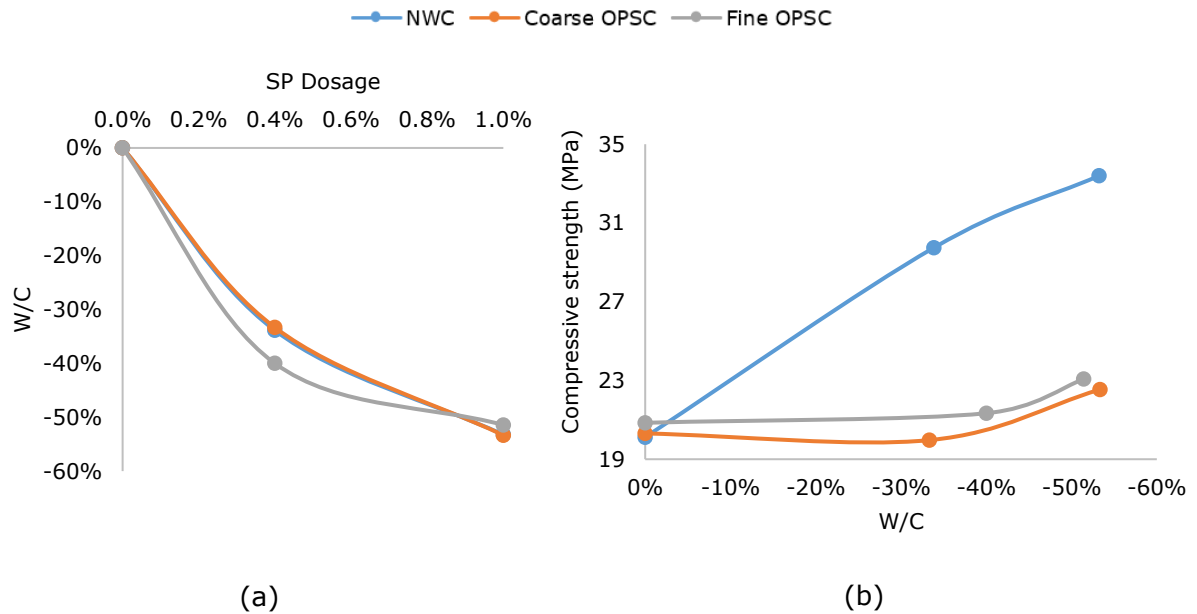
Figure 4.30 Decrease rate of W/C with addition of SP

(a)   (b)
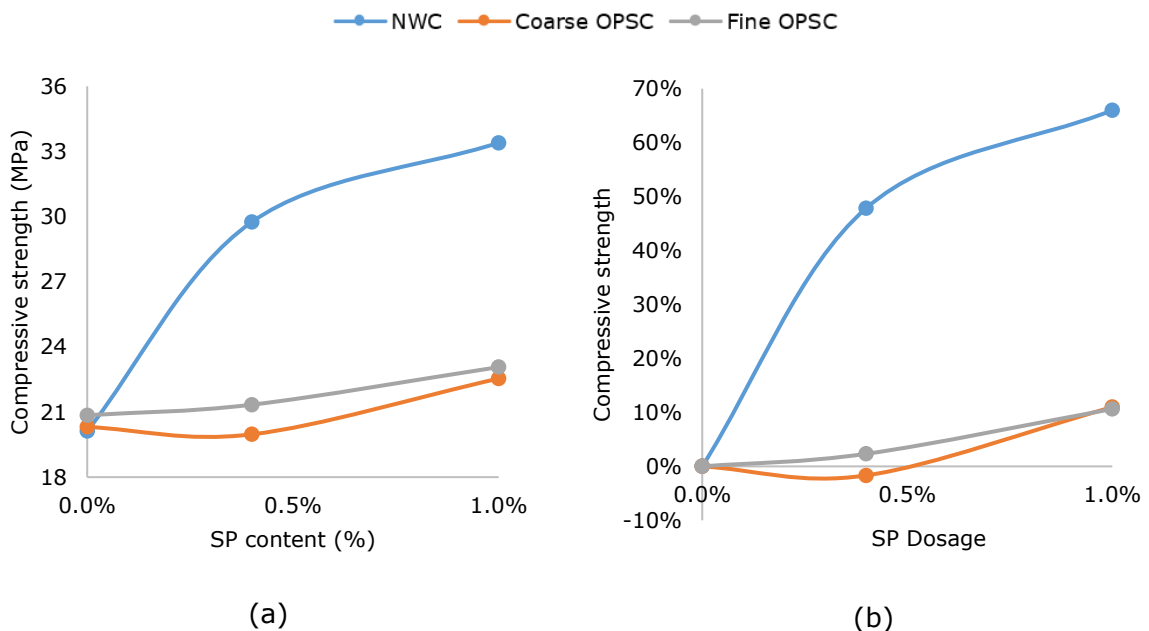
Figure 4.31 Influence on compressive strength with addition of SP dosage

Another interesting observation was the change in density with the addition of SP for all three concretes as seen in Figure 4.32. The NWC increased its density by 2.9% and 4.4% with the addition of 0.4% and 1.0% SP dosage, respectively. A similar, yet lower, increase

can be seen for coarse OPSC of 1.7% and 2.1% and for fine OPSC of 1.6% and 2.2%. However, for both OPSCs, it can be observed that after an SP dosage of 0.4%, the density increase seems to decline compared to NWC. This might be due to the difference cement contents of the mixes. A similar increase of 2.3% in density was observed by (Cartuxo, et al., 2015) with the incorporation of 1% SP dosage for concrete made with 100% fine recycled concrete aggregates. Cartuxo, et al. justified this by concluding that by lowering the w/c of the mixes, the higher density of the other materials replaces the lowered density of water relative to the materials. An additional justification may also be that SP causes the cement grains to proper disperse when w/c is reduced instead of flocculation without SP therefore causing a better packing, consequently increasing its density (Bjornstrom & Chandra, 2003).
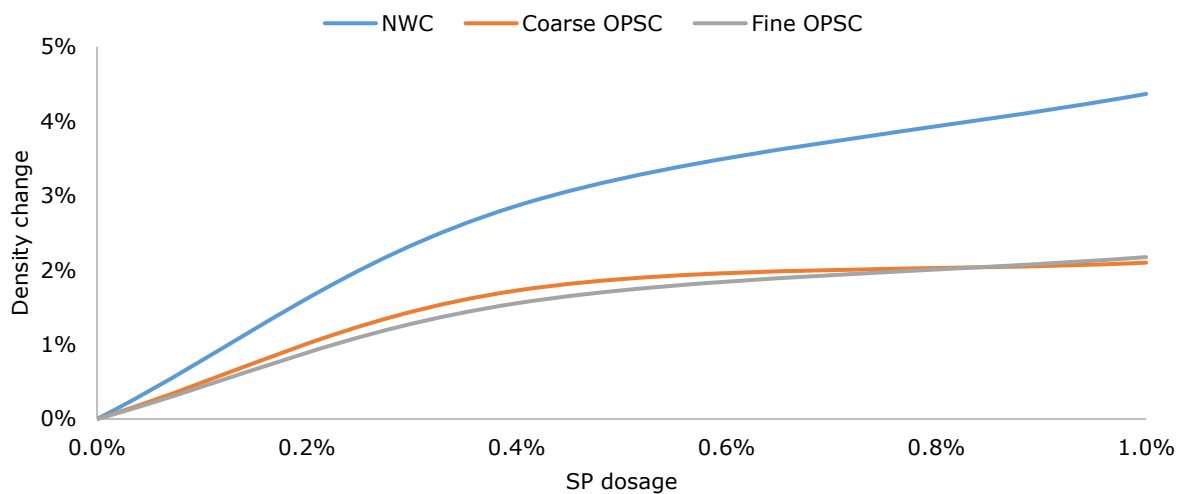
Figure 4.32 Influence of SP dosage on density

The change in packing of the concretes can also be observed by the results of the UPV test, which basically measures the time of travel of an ultrasonic pulse. A higher value (km/s) would indicate a better packed concrete (Shetty, 2005). This was confirmed in a study by (Guo, et al., 2017) where they observed the increase in UPV values (km/s) with the decrease of air voids. Certainly, the UPV values for all the three types of concretes increased with the increment of SP dosage (and reduction of w/c), see Figure 4.33 (a). The values for the NWC changed from good to excellent by 16% and 22% for SP dosages of 0.4% and 1.0% respectively. However, this was lower for the coarse OPSC by an increase of 9% and 11% and the fine OPSC being the lowest by 1% and 4%.

As for the relationship between the compressive strength and UPV, strong correlations were found for NWC ($R^2=1.00$) and fine OPSC ($R^2=0.99$) and a low correlation for coarse OSPC ($R^2=0.31$). Therefore, the increase of UPV can be associated with the increase in the density, as was shown in Figure 4.32, due to the increase of compactness/packing of the materials.
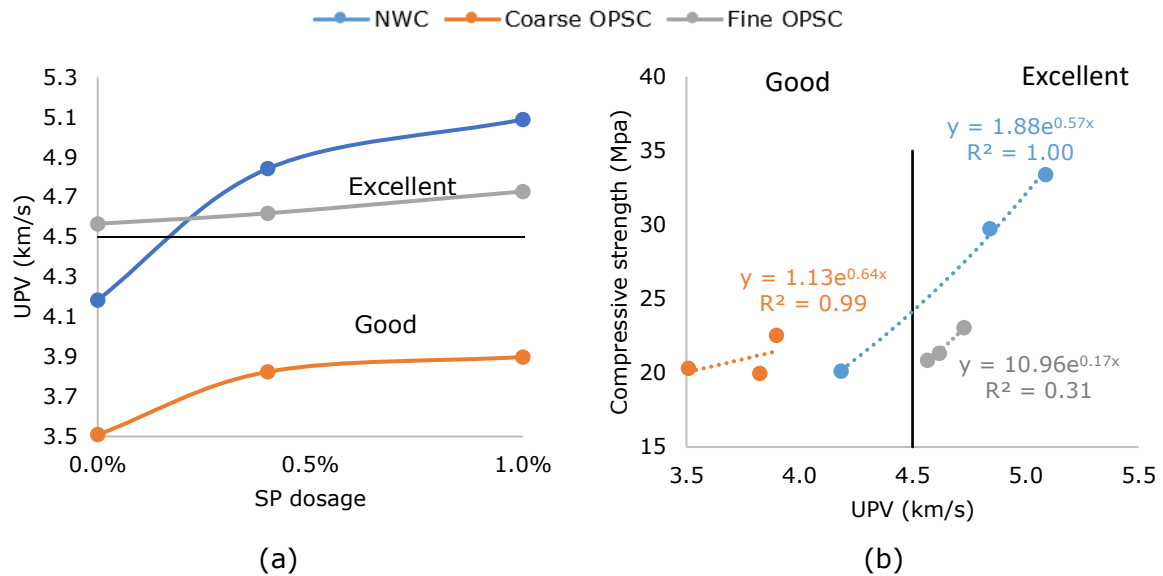
Figure 4.33 (a) Influence of SP dosage on UPV and (b) Compressive strength vs UPV

4.2.5. Concluding remark

4.2.5.1. Mix design comparison

The preceding sections studied the production of NWC and two SLWC types with a similar grade strength of 20 MPa, primarily for comparative purposes. The BRE guideline, as recognized widely and detailed in (Teychenné, et al., 1988), was used for the NWC production. On the other hand, for the SLWC types, namely coarse and fine OPSC in this study, no such guideline or equivalent was employed. According to a comprehensive study by (Mannan & Ganapathy, 2001a), even the ACI method for SLWC (ACI 211.2-98, 2004) is not a reliable guideline for producing OPSC. As such, this study focused on the trial-and-error practice (Kosmatka, et al., 2002) for both coarse and fine OPSC.

The methodology employed to produce coarse OPSC differed from that of fine OPSC due to the lack of available data on the latter, as detailed in Section 2.2.3. The primary objective of this study was to investigate the differences between Dura and Tenera as C-OPS in concrete, and to achieve this, certain parameters from the literature were re-examined with Tenera coarse OPSC for comparison purposes. Ultimately, a final mix design was attained mainly by increasing the cement content. For the production of fine OPSC, a more comprehensive investigation was carried out to fulfil the second objective of this study, by exploring various treatment methods, aggregate ratios, and cement contents to arrive at a final mix design to the best of the authors' ability.

Table 4.13 displays the selected mix designs for NWC, coarse, and fine OPSC which achieved a similar strength of 20 MPa, with the material contents illustrated in Figure 4.34. It can be clearly identified that the coarse OPSC consumed the largest amount of cement, approximately three times that of NWC. While using OPS as fine-sized aggregate compared

123

to coarse-sized, clearly resulted in reducing the cement content by 263%. Though both coarse and fine OPSC demanded an increase in cement content by 200% and 14% compared to NWC, a higher cement content for LWC is expected because of LWA being weaker than NWA (Newman, 1993). The cement content used for the fine OPSC is found to be within the typical range for LWC (Mindess, et al., 2003). However, the cement content for coarse OPSC is found to be practically unviable. High cement contents are also known to negatively affect other mechanical properties such as the shrinkage (Neville, 1995) which is expounded upon in Section 4.3.5.

Nevertheless, Figure 4.34 also reveals that both coarse and fine OPSC used similar volumes of OPS, 8% and 7%, respectively. Also, by looking at the difference in terms of OPS content and bulk density of Tenera C-OPS and F-OPS in Table 4.14, C-OPS is 23% higher in terms of OPS content, while it is 23% lower in density compared to F-OPS, therefore being similar in volume. In conclusion, Tenera fine OPSC is a more viable option for LWC due to the reduction in cement content. However, additional mechanical property evaluations are necessary, which are discussed in Section 4.3.

Table 4.13 Final mix designs

ID	Cement	Fine Aggregate	Coarse Aggregate	Water	w/c	28-day strength	Slump	Dry-Density
	Kg/m3					MPa	mm	Kg/m³
NWC	350	605	1175	217	0.62	20.12	15	2141
Coarse OPSC	1050	283	152*	315	0.30	20.24	42	1672
Fine OPSC	400	124**	1236	140	0.35	20.85	10	1994

*C-OPS, **F-OPS
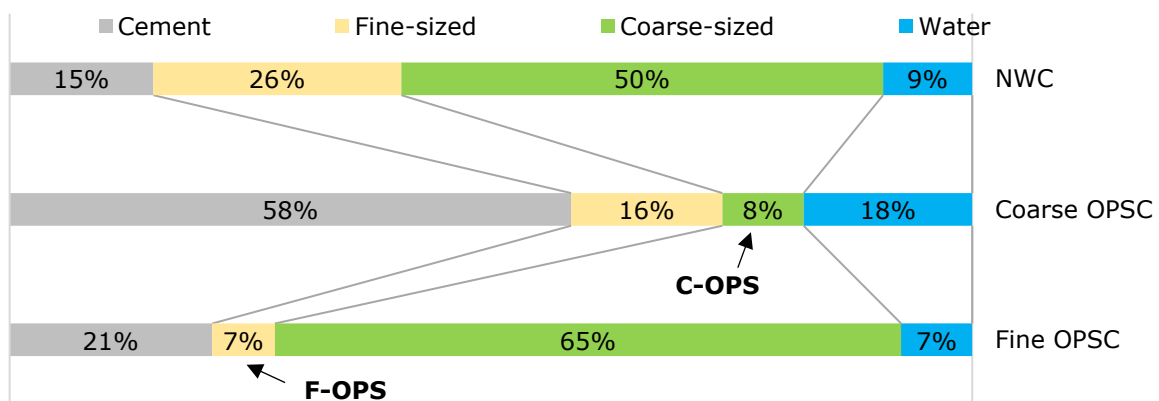
Figure 4.34 Material contents

Table 4.14 Difference in Tenera OPS content – Coarse vs fine OPSC

	Content	Loose Bulk density
	Kg/m³	
F-OPS	124	572
C-OPS	152	442
Difference	23%	-23%

124

Based on the findings of this section, the reduction in cement content for fine OPSC can be attributed to several factors, including the elimination of the half-hollow-spherical shape of C-OPS (see Figure 4.11), the rougher surface of F-OPS compared to C-OPS, and the use of granite as a more effective coarse aggregate. The half-hollow-spherical shape of C-OPS was found to create weak links and void space in the cement matrix, whereas the rough surface of F-OPS provided a better bonding effect as was also concluded by (Shafigh, et al., 2012) and (Yew, et al., 2014b). The use of granite as a coarse aggregate was also found to be beneficial, as it is stronger than Tenera C-OPS, has better bonding with cement, absorbs less water (0.60% vs 30.65%), and does not swell or shrink like C-OPS. It can therefore be summarized, that the utilization of Tenera OPS as fine sized aggregate in OPSC is preferred over coarse OPSC due to the aforementioned factors.

4.2.5.2.   Superplasticizer

It was found that a maximum SP dosage of 0.3% is optimal for both coarse and fine OPSC when the w/c is constant, but a lower dosage is suggested for fine OPSC to prevent segregation. Coarse and fine OPSC require less SP than NWC for a given slump.

However, when the w/c is reduced, SP dosages up to 1.0% are less effective than for the NWC, and higher dosages may be required. The SP used in this investigation does not appear to function as effectively with both the OPSCs as it did with the NWC, likely due to chemical interference from the similar lignin composition of both materials (i.e., OPS and SP). Subsequently, further investigation is recommended to understand this matter, and as a result, SP was not used in further investigations in this study, i.e., the hardened properties of the concretes.

4.3. Hardened Properties

In the previous sections, the physical properties of the materials used to produce the three types of concretes were investigated followed by studying different mix designs to produce similar grade strengths. Additionally, it was ascertained that using SP did not function as well as it did with NWC and was therefore decided to not utilize SP for the investigations conducted in this section.

The density, permeable voids and water absorption, compressive strength, flexural tensile strength, modulus of elasticity, and drying shrinkage tests with early ages up to 365 days were tested and the results are discussed in this section for the selected mix-designed concretes from Section 4.2. Samples were tested under curing and air curing regimes, see Figure 4.35. In order to enhance reader comprehension and provide a concise summary of the findings, a separate section of concluding remarks is included after each type of test, unlike the previous sections in this chapter.
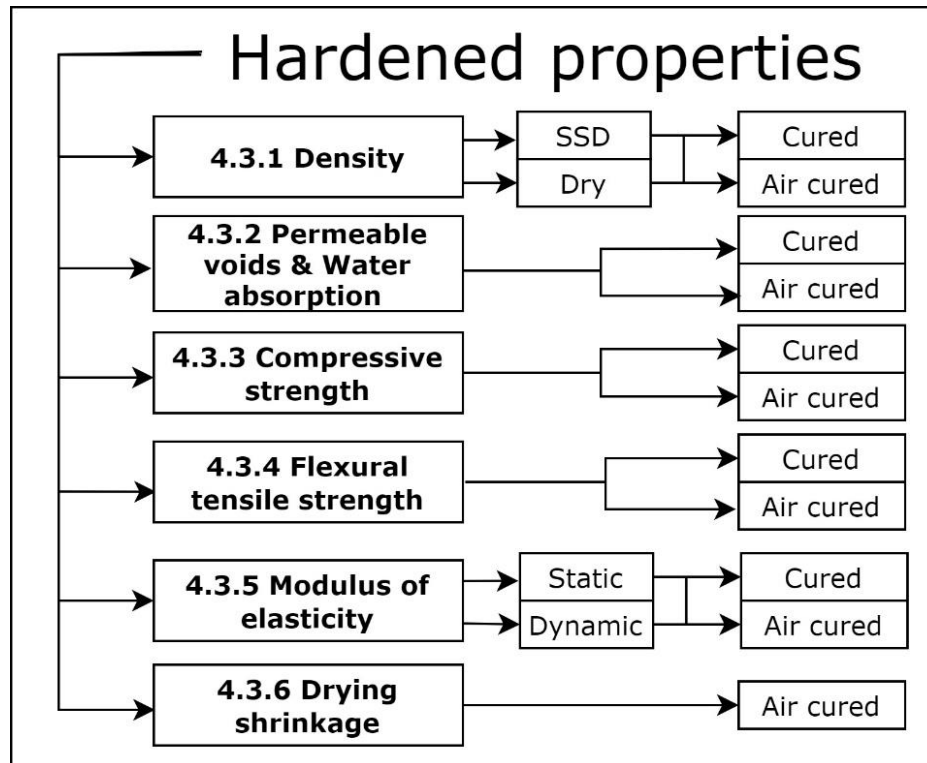
Figure 4.35 Flowchart hardened concrete properties

4.3.1. Density

In this investigation, the density of NWC, coarse, and fine OPSC over time was measured. The specimens were subjected to cured and air-cured regimes. The SSD and as-received density of the cured and air-cured specimens, respectively, were measured for each concrete type up to 365 days and discussed in Section 4.3.1.1. Likewise, the dry density of the concretes was measured and discussed in Section 4.3.1.2 with a concluding remark in Section 4.3.1.3.

4.3.1.1. SSD and as-received density

In this investigation, the SSD and as-received densities were measured from a single specimen for each concrete type. For the SSD density, a specimen was kept in a curing tank and taking out to measure its SSD density and was returned for further measurements at later ages. As for the as-received density, this was done in a similar way, though it was kept in an outside environment under a roof.

The results for the SSD and as-received densities of the cured and air-cured specimens are presented in Figure 4.36. The density change rate over time is seen in Figure 4.37. Similar trends were observed in the SSD and as-received density results between all the three concrete types. The SSD densities for the cured specimens increased by 1.5%, 3.2%, and 1.7% for NWC, coarse and fine OPSC, respectively, from age 1 up to 365 days, ranging from 2306.9 to 2340.8 kg/m^3, 1936.5 to 1997.9 kg/m^3, and 2114.3 to 2150.5 kg/m^3.

Hence, the SSD density of coarse OPSC increased approximately twice as much as that of NWC and fine OPSC. This could be due to the high-water absorption of OPS reported in the previous sections. Although the fine OPSC is also made with OPS, it showed a lower increase in SSD density than coarse OPSC, but a slightly higher increase than NWC with a difference of only 0.2%. The difference between the coarse and fine OPSC is probably due to the higher content of coarse aggregate in the latter. The conventional coarse aggregate has lower water absorption compared to the C-OPS in coarse OPSC, hence making the concrete less permeable.
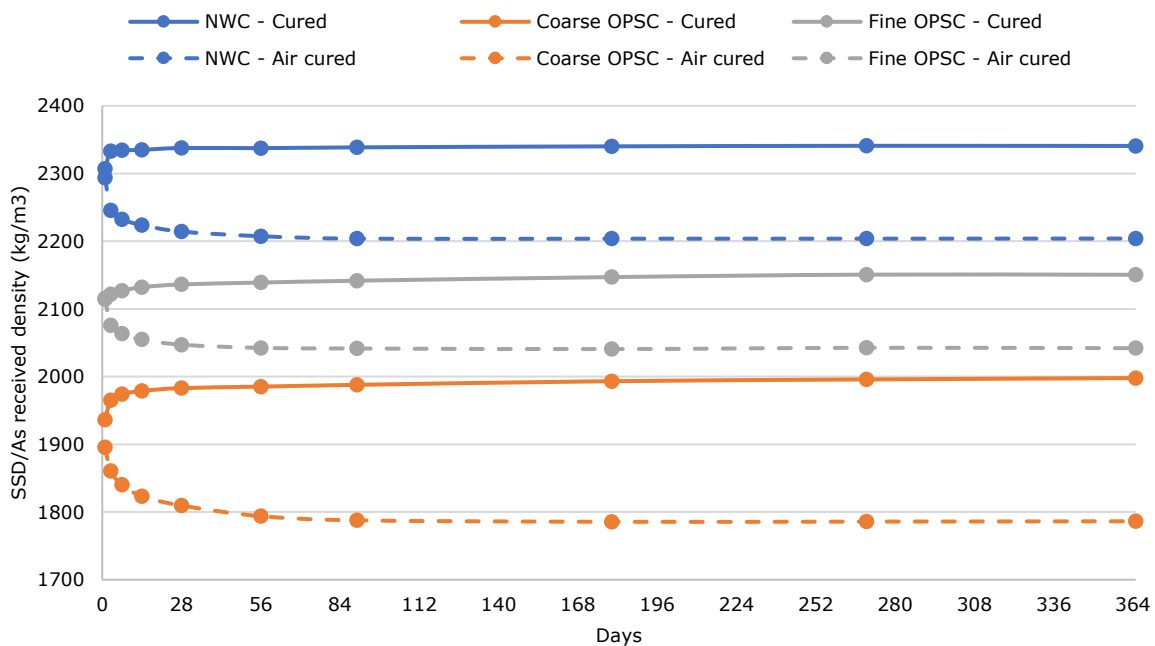
Figure 4.36 SSD density and as received density of NWC, coarse, and fine OSPC over time for cured and air cured specimens respectively (continues lines are the SSD density and dashed lines are the as received densities)

The as-received densities for the air-cured specimens decreased similarly for the three concretes. The as-received densities for NWC, coarse, and fine OPSC decreased by 3.9%, 5.8%, and 3.4%, respectively, from 1 to 365 days, ranging from 2293.9 to 2204.0 kg/m^3, 1895.6 to 1786.3 kg/m^3, and 2115.6 to 2042.0 kg/m^3 as shown in Figure 4.36 and Figure 4.37. The fine OPSC showed the smallest difference between cured and air-cured density of 108.4 kg/m^3, followed by NWC and coarse OPSC being 136.8 and 211.5 kg/m^3, respectively, indicating a smaller pore volume for fine OPSC. Further discussions on this matter can be found in Section 4.3.2. Nevertheless, the three concrete types demonstrated a typical behaviour in both their cured and air-cured states.
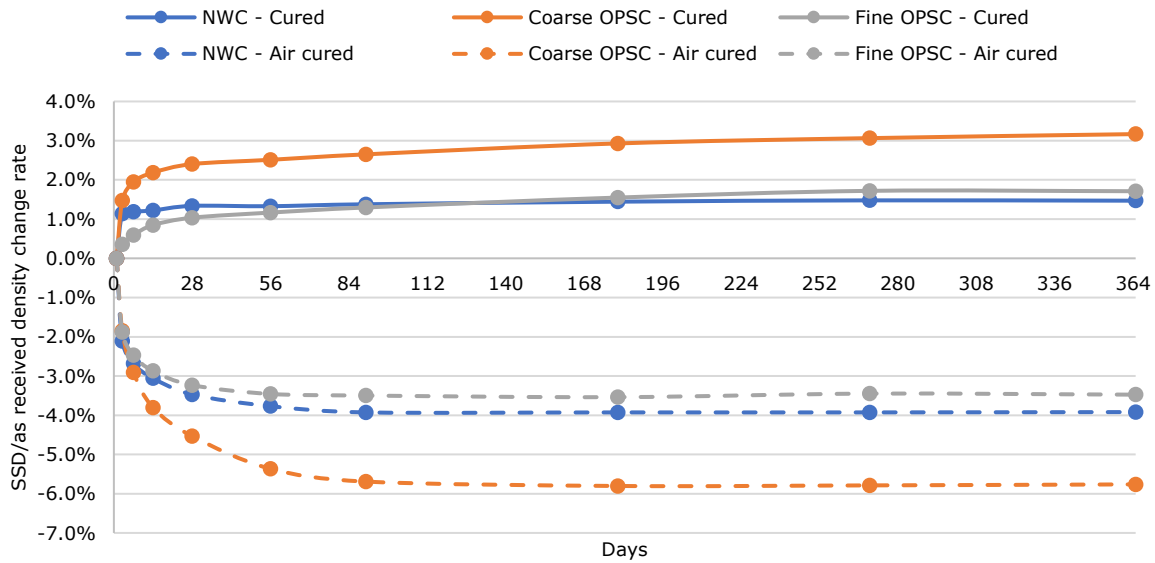
Figure 4.37 SSD density and as received density change rate of NWC, coarse, and fine OSPC over time for cured and air-cured specimens respectively

4.3.1.2. Dry density

The results for the dry densities for the concretes in cured and air cured regimes are plotted in Figure 4.38 and Figure 4.39, respectively. In this investigation, a slightly different approach was taken to observe the change in dry density over time for the concretes in this study. In the previous section, one specimen was used for each concrete type at each curing regime, resulting in a smooth change in density and acceptable trends. However, for the dry density, to adhere to the hydration process, individual specimens were utilized for each designated age, as resubmerging the samples in water, or exposing them to air cure after oven drying would disrupt the hydration process by extracting its internal water.

Noteworthy, to obtain the dry density of any specimen, the SSD density for the cured specimen and the as-received density for the air-cured specimen was first measured followed by placing it into an oven to obtain the dry density. Then the specimens were kept in water for 48 hours to finally measure its SSD density. This procedure was adhered in accordance with (BS EN 12390-7, 2019) as described in Section 3.3.1. Therefore, since different specimens were used, some irregularities among the data points were observed in Figure 4.38 and Figure 4.39 for the cured and air-cured specimens, respectively. Although the dimensions were measured separately for each specimen, since all three concretes have four different materials, it is practically impossible to have exactly the same amount of each material in each separate specimen. However, to the best of the authors ability, all the specimens were kept on the same shake-table and similar amounts of concrete was poured into the moulds for every layer.

For the dry densities, with the linear trend lines over time plotted in a $\log_2$ graph for the concretes in both cured and air-cured regimes, a trivial change could still be observed. A small increase is observed for the NWC while a slight decrease is seen for the coarse and fine OPSC for the cured specimens. However, for the air cured specimens, all three concretes are observed to increase in their dry density. Nevertheless, an attempt was made to quantitatively show the change in dry density over time, however, no acceptable trend could be recognized as seen in Figure 4.40 (a) & (b).
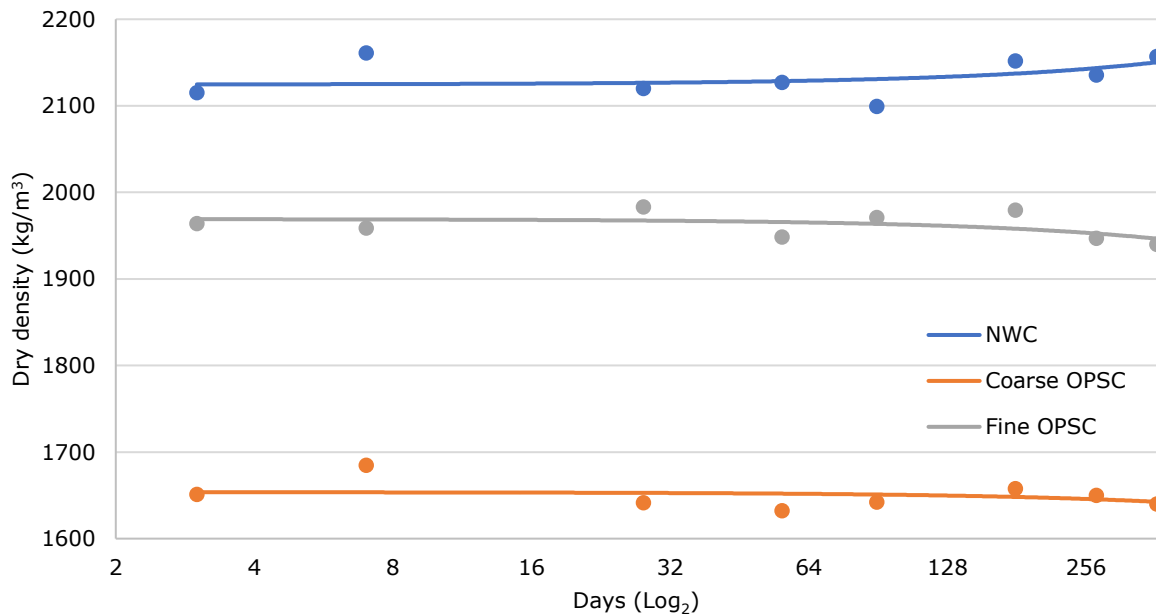
Figure 4.38 Dry density of cured specimens for NWC, coarse, and fine OPSC over time
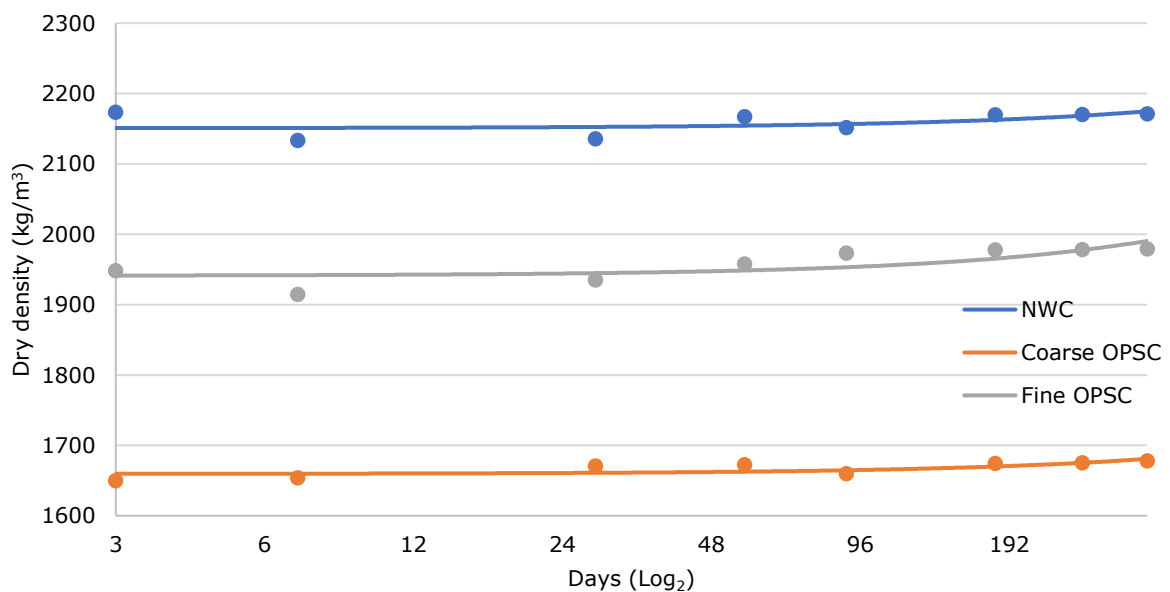
Figure 4.39 Dry density of air-cured specimens for NWC, coarse, and fine OPSC over time

(a)   (b)
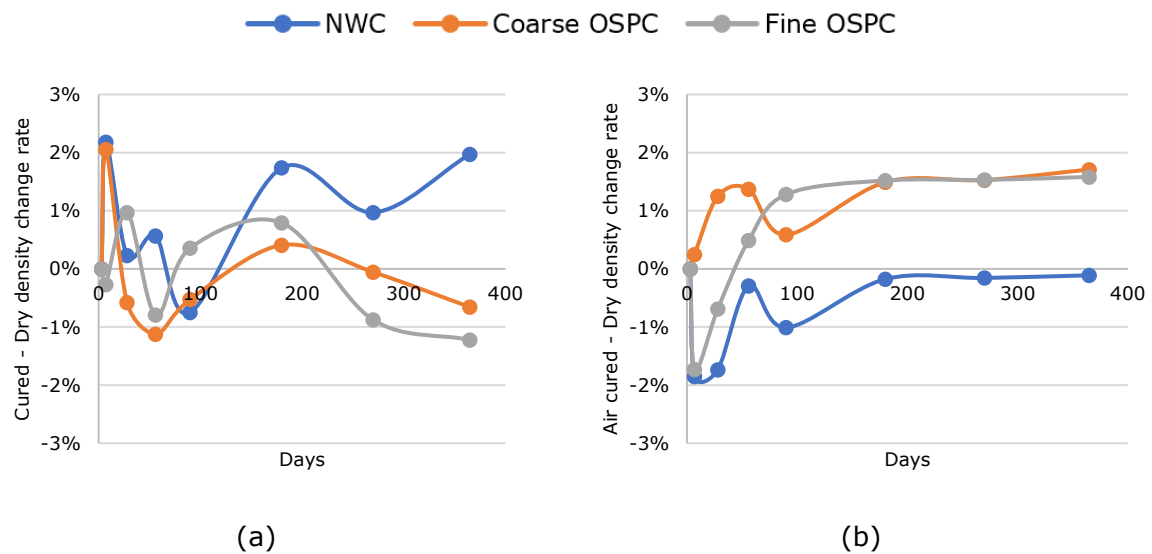
Figure 4.40 Dry density change rate for (a) cured and (b) air-cured specimens

It is well known when concrete is subjected to a cured regime, it is expected to absorb more water and thus hydrate further causing its weight to increase. This is due to increase of calcium silicate hydrates (CHS) or water being entrapped due to closing of pores (Li, 2011). The increase in dry density for the concretes exposed to air-cured regimes is most probably due to the high humidity levels in Malaysia reaching up to a RH of 90% (MET Malaysia, 2022), allowing the internal water to stay withing the internal pores for the continuation of the hydration process and entrapping water. This does seem to be the case for the NWC in both cured and air-cured regimes, except for the coarse and fine OSPC in the cured regime, as mentioned earlier. This contrary behaviour is rather an unexpected observation. However, by recalling the images taken of the OPS when left wet overnight, see Figure 3.5 in Section 3.1.1.3, the white substance can actually be related to something known as white-rot fungi (Fitriyah, et al., 2022). This was also seen in damp OPS samples left for over 6 months in a closed container, see Figure 4.41. This was found for both coarse and fine sized OPS. However, this rotting was not observed internally in the any of the two OPSCs, though only observed for the coarse OPSC on the outer surface seen in Figure 4.42.

130

Figure 4.41 Rotting of Tenera OPS left damp for over 6 months

Figure 4.42 White-rot fungi on outer surface of coarse OPSC

As mentioned earlier, one of the main composition of OPS is lignin (Sundalian, et al., 2021). White-rot fungi are known as organisms degrading lignin by depolymerizing and mineralizing lignin into carbon dioxide (CO_2) and water (H_2O) with the presence of moisture (Cerro, et al., 2021), therefore decomposing the OPS. This decomposition process due to white-rot fungi is known to cause formation of cavities inside the cell wall and cracking patterns (Brischke & Alfredsen, 2020). As the process continues over time, the lignin-rich middle lamella (i.e., outer wall of OPS) would be left behind as a skeleton of wood structure with low strength properties (Kim & Singh, 2000). To put it into simpler words, the OPS as both coarse and fine sized aggregates in concrete subjected to a cured regime decays and subsequently loses its weight over time, thus probably explaining the decline in dry density when exposed to a cured regime. The rotting effect of the OPS in concrete exposed to a cured regime can be further proven by the fact that the dry densities increased for the OPSCs as it did with NWC when exposed to an air cured regime. Since a lignin-based material can only be exposed to rotting due to moisture presence (Setherton, 2022), the OPS in the coarse and fine OPSC is therefore expected to stay intact and retain its weight, thus allowing for a similar behaviour as the NWC by increasing in density over time.

However, another explanation for the decline in dry density of the cured OPSCs could be due to the extraction of palm oil observed on the outer surface only for the specimens exposed to a cured regime after oven drying, see Figure 4.43 and Figure 4.44. The orange-brownish palm oil was found to be dry and brittle. Nevertheless, this was found for both the cured fine and coarse OPSC and on ages later than 28 days and increasing gradually with age. The probable explanation for this might be as the OPSCs cures in water, the palm oil gradually reaches closer to the surface as the concrete is also swelling. This can be reasoned since the particle density of palm oil is known to be less than that of water (Tan & Nehdi, 2012). This was also proven from microscopic images taken of the sliced OPSCs shown in Figure 4.12, in Section 4.2.2.

All in all, along the white-rot fungi, the dry density of the cured specimens probably also decreased due to the extraction of palm oil during the oven drying process. Nevertheless, it is difficult to quantifiably measure the exact amount of palm oil being extracted, as it is also difficult to measure the amount of palm oil present in the OPS. Also, since the author of this study did not anticipate such observation prior to doing such experiments, it is therefore recommended that further studies are done in the future on this matter.
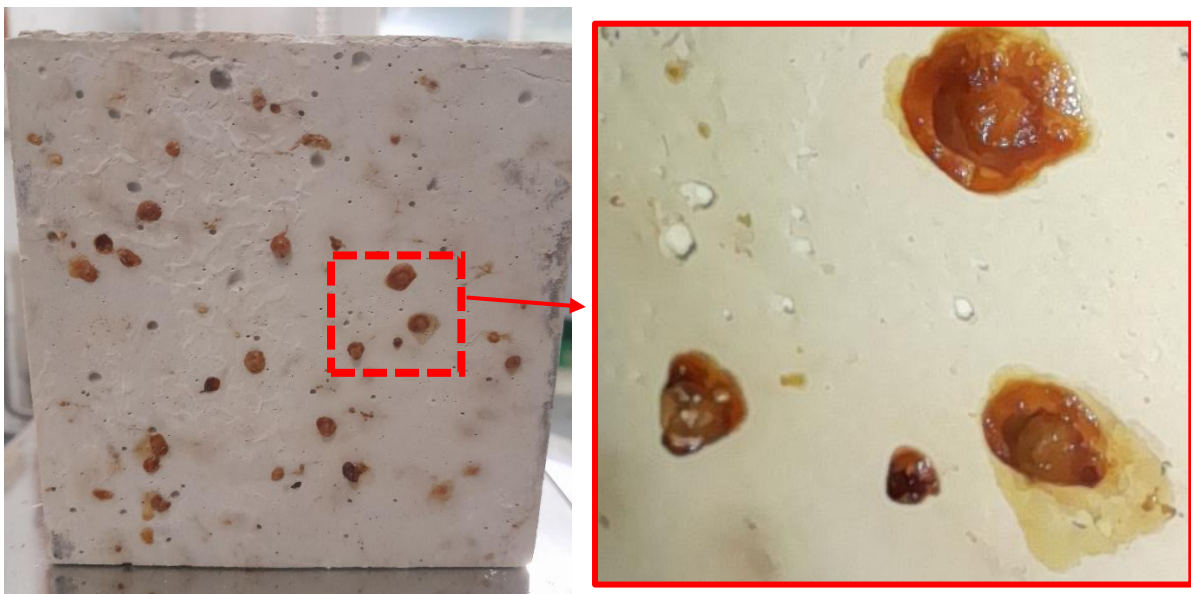
Figure 4.43 Palm oil extraction in coarse OPSC after oven drying at 90 days
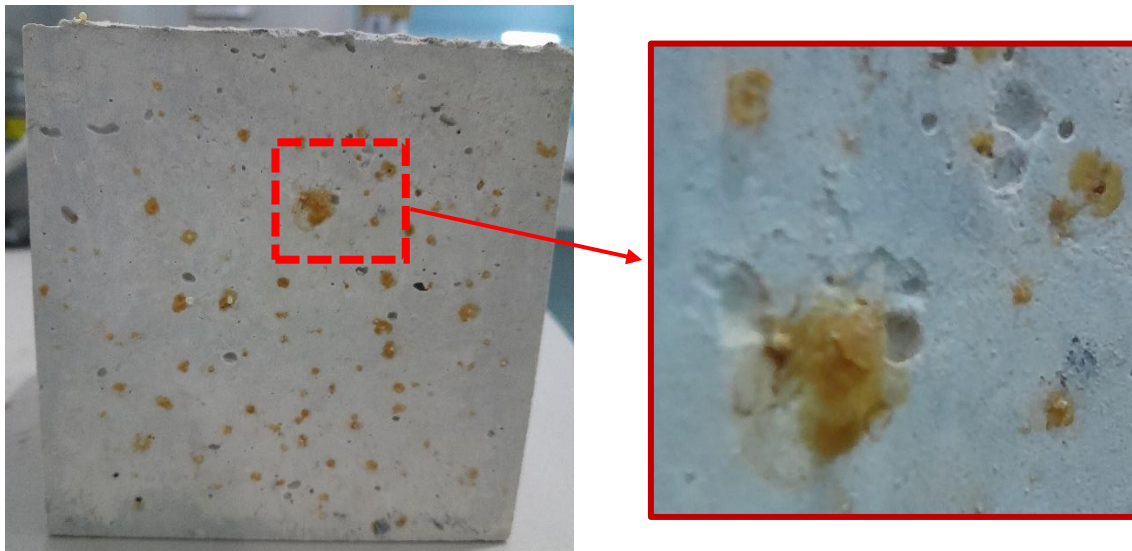
Figure 4.44 Palm oil extraction in fine OPSC after oven drying at 270 days

Also, for the same cured specimens used to find the dry density, an interesting observation was seen for the SSD density when extracting them out of the curing tank prior to oven drying and SSD density after oven drying when immerged in water for 48 hours, see Figure 4.45. For the NWC, an increase was seen for both the first and second SSD density over time, which is a normal and expected behaviour. However, for both OPSCs while an increase was seen in the SSD density from the curing tank, a decrease was observed in SSD density after drying process. By referring to the previous images from Figure 4.43 and Figure 4.44, the yellow/brownish substance believed to be the palm oil has most probably blocked pathways for water intrusion when re-immerged in water for the second time after oven drying, consequently resulting in a decrease in SSD density. While this does not directly affect the dry density of the OPSCs, a notable difference would be expected in the water absorption discussed in Section 4.3.2.
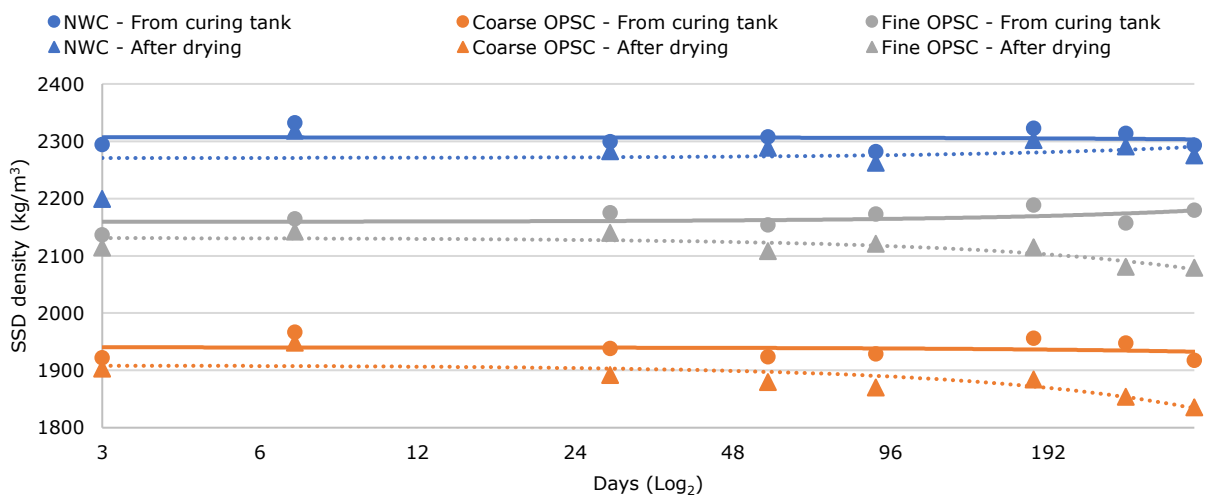
Figure 4.45 SSD density of specimens - before oven drying and after oven drying for concretes in cured regime

133

4.3.1.3.   Concluding remark

In this investigation, the density of the concretes was measured over time in cured and air-cured regimes. This was done in two parts. The first part investigated the SSD and as-received density from singular specimens for each concrete. The second part used individual specimens for each age to find the dry density for each concrete type.

For the first part, one of the main findings were that the SSD of the cured concretes and the as-received of the air-cured concretes behaved as expected by increasing in SSD density and decreasing in as-received density over time. The increase change of the coarse OPSC was found to be double that of the NWC and fine OPSC for the cured specimens and a decreasing change of slightly less than double for the air-cured specimens. The coarse OSPC observed the largest difference between SSD and as-received density followed by the NWC and fine OSPC as last. This was mainly found to be attributed to the permeability of the concrete, which is further discussed in Section 4.3.2.

However, a contrary behaviour was observed when the dry densities were measure between the cured and air-cured regimes between the NWC and both OPSCs. While the NWC increased in its dry density for both cured and air-cured regimes, both OPSCs only increased in the air-cured regime while decreasing in their dry density in cured regimes. The following reasons were hypothesized for this observation:

- Due to the rotting of the OPS when exposed to moisture over time, i.e., curing regime.

- Due to extraction of palm oil after oven drying; reducing its weight and or blocked the pores.

Though, the first hypothesis being difficult to examine quantitatively, images taken of the OPS subjected to moist outside the concrete were proven to be exposed to white-rot fungi, which is known to decompose the lignin-based material. Also, only found with the coarse OPSC, the same white-rot fungi were also found only on the outer surface of the specimens after removal from the water tank. This rotting is known to decay the OPS and consequently decrease its the weight over time. However, whether this white-rot fungi were present when the OPSCs were in the water tank is yet to be studied. It is therefore recommended to further look into aquatic fungi (Money, 2016).

As for the palm oil extraction after oven drying, this was only noticed at ages of 28 days and later for fine and coarse OPSC. It is reasoned that the palm oil seeps out of the specimen gradually over time in the water tank due to the difference in particle density between the water and the palm oil, the latter being higher. Subsequently, when it is

exposed to an oven drying process, the palm oil further seeps to the surface leaving behind a yellow/brownish brittle substance, which is identified to be most probably the palm oil.

The aforementioned reasons are the most apparent reasons found for the decline in dry density for the cured OSPCs. However, it is highly recommended that further analysis into the white-rot fungi, observed in the OPS, is further studied to better understand the matter. Perhaps a method to prevent the white-rot fungi from cultivating in the OPS while curing the specimens would be the most ideal solution. To achieve this, perhaps a water-based liquid formulation, such as Nano waterproofing, could be applied to prevent moisture penetration in the OPS. If after such treatment no decline is found in the dry density, then perhaps the hypothesis from this study could be further bolstered. Nevertheless, this does require testing specimens up to an age of 365 days. Also, caution must be exercised when introducing new chemicals that may have detrimental impacts on cement.

As for the yellow/brownish substance found on both the OSPCs, it should not affect the OPSCs on a mechanical scale, as such test would not be performed on oven dried specimens. However, perhaps chemical analysis to investigate if the palm oil extracted from the OPS into the cement matrix has any effect on the hydration process would be a recommendation for a further study.

Nevertheless, the NWC and fine OPSC were found to have a higher average SSD and dry density compared to the coarse OPSC with a difference of 18% & 22% and 8% & 13%, respectively. Both OPSCs are categorized as LWC since their average dry densities are below the BS standard of 2000 kg/m^3 (BS EN 206, 2021). The coarse OPSC is classified as the density-class D1.8 while the fine OPSC is classified as D2.0 according to Table 14 in (BS EN 206, 2021), though no further specifications are provided in the code regarding these density classes.

4.3.2. Permeable Voids and Water Absorption of Concrete

With sufficient permeability in concrete, water and oxygen are able to penetrate and corrode reinforcement in concrete, causing many problems during the life span of the concrete structure. Therefore, the permeability of concrete highly affects the long-term durability of structure. The permeability is mainly established by the presence of microcracks and pore structure in the concrete matrix (Chia & Zhang, 2002). One method for representing the durability of concrete is the water absorption characteristic of concrete which provides an indication of the open pore volume by capillary action or sorptivity (Khatib & Mangat, 1995).

The (ASTM C642 - 13, 2013) was adapted in this study to determine the permeable voids and water absorption. By knowing the permeable voids and water absorption, a good indication of the durability of concrete can be determined by comparing the three

concretes, where lower values indicate better durability than higher (Neville, 1995). Concrete exposed to curing and air-cured regimes were tested separately and also compared in the following subsections followed with a concluding remark.

4.3.2.1.   Cured regime

Similar to the dry density investigation, for both the permeable voids and water absorption individual samples were used for each age of testing for the same reason explained in Section 4.3.1. The following sub-sections discuss the results for the permeable voids and water absorption discretely.

Permeable voids

To better observe the change in results over time, a semi-log$_2$ graph of the permeable voids for the three concretes are plotted in Figure 4.46 with linear trend lines. The NWC, coarse, and fine OPSC showed permeable void values ranging from 15.9 – 17.7%, 29.0 – 31.2%, and 17.4 – 19.8%, respectively. The coarse and fine OPSC showed to be 80.0% and 8.2% higher in average permeable voids compared to the NWC, where the coarse OPSC showed 66.6% higher average permeable voids to the fine OSPC. Also notable, the NWC, coarse, and fine OPSC showed a decrease of 11.3%, 7.0%, and 12.2%, respectively, in permeable voids over time (3 – 365 days). This behaviour can be related to the SSD density of the samples increasing over time discussed in Section 4.3.1. The increase in density and decrease in permeable voids over time is most probably related to the increased hydration process closing or blocking the pores. However, this doesn't necessarily mean that the concretes have become less permeable. This might also be due to the fact that as the concrete continues to be cured in a water tank, more water penetrates into the concrete which was not able to be removed during the oven drying. Although following the procedure from the (ASTM C642 - 13, 2013), it describes that as long as a smaller change of 0.2% or less is observed between 24 and 48 hours, the weight of the specimen can be considered dry.

Nevertheless, the lower decrease value for coarse OPSC may be due to the high void space found between the OPS and cement matrix, see Section 4.2.3. Also, since fine OSPC decreases just slightly higher than the NWC, this indicates that fine-sized OPS do not have a negative effect as is with coarse sized OPS. The decrease in permeable voids over time was also found by (Teo, et al., 2010) with ages from 3 – 90 days. Teo, et al. found the permeable voids of their OPSC with dura OPS at 28 days to be an average of 20.5% and reduced to 17.5% at 90 days (14.6% change), therefore being more similar to fine OPSC than coarse OPSC from this study. Furthermore, the permeable voids found for fine OPSC were comparable to other LWCs with permeable voids ranging from 8.6 – 22.5% (Maltais, et al., 2006).
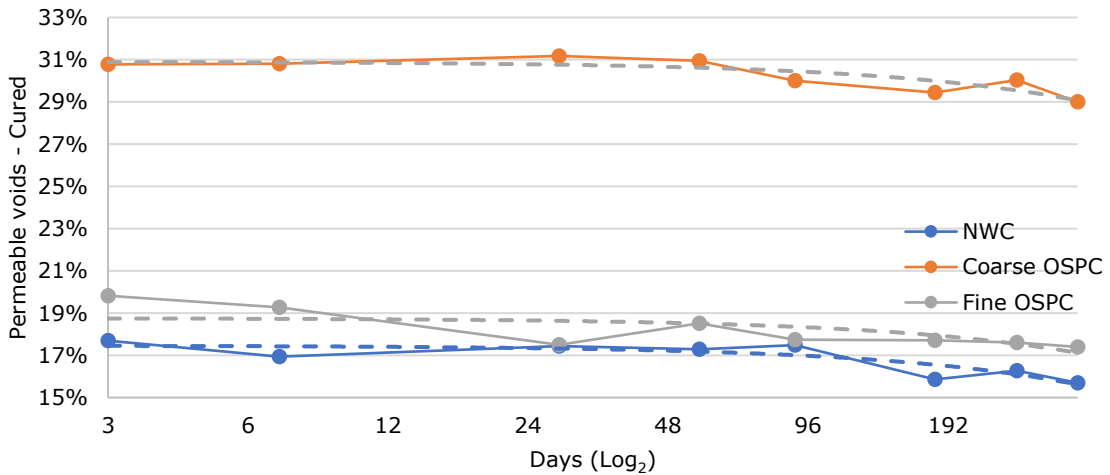
Figure 4.46 Permeable voids of cured NWC, coarse, and fine OPSC (the dashed lines are linear trendlines)

Water absorption

As mentioned in Section 3.3.2, the water absorption was measured in two stages. The first stage comprised submerging the samples in water at room temperature and was tested after the oven drying. For the second stage, the specimens were submerged in boiling water at a temperature of 100°C for 5 hours. This led the investigation to have two different water absorption results, i.e., at room temperature and after boiling.

As, for the water absorption from room temperature, a comparable behaviour is observed as the permeable voids where all three concretes observed a decrease over time, see Figure 4.47. The water absorption range, average and decrease values measured at room temperature and after boiling is shown in Table 4.15.
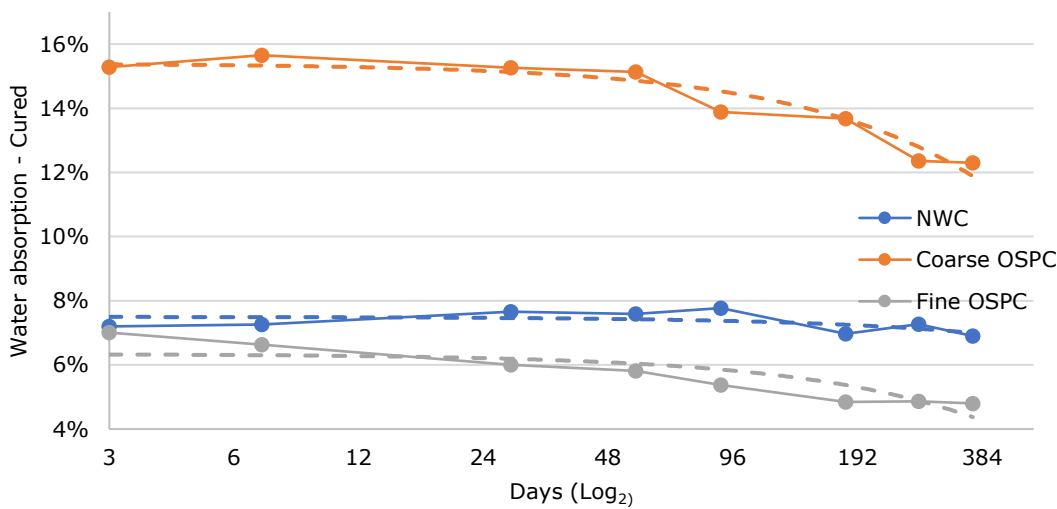
Figure 4.47 Water absorption at room temperature of cured NWC, coarse, and fine OPSC (dashed lines are linear trend lines)

137

Table 4.15 Water absorption tabulated results from 3 – 365 days (cured)

	Room temperature	Boiled
	Average	
NWC	7.3%	7.8%
Coarse OPSC	14.2%	18.1%
Fine OPSC	5.7%	9.5%

In general, with the same explanation given for the permeable voids, the reason for the reduction in water absorption is due to the continued hydration process due to the exposure of moist in a curing tank (Kearsley & Wainwright, 2001). To be more precise, the decrease in water absorption of concrete over time can be attributed to the formation of calcium silicate hydrates (C-S-H) and secondary minerals such as calcium carbonate and calcium hydroxide. These minerals play a significant role in reducing porosity, consequently enhancing the material's durability (Neville, 1995).

It can be seen that at room temperature, the fine OPSC has the least value of water absorption by being 23% and 60% less than the NWC and coarse OPSC, respectively. However, in the case of after boiling, the NWC showed the lowest value followed by fine OSPC and coarse OSPC being the highest. Although the values are of the same specimens tested at each day, the difference in water absorption can be explained due to the different testing methods, as mentioned earlier. For the water absorption after boiling, the specimens undergo a higher pressure when kept in water at 100 °C, where for the water absorptions it is at normal room temperature, thus making the water be absorbed due to capillary action or sorptivity (Khatib & Mangat, 1995). Also, water is known to become less viscous at higher temperatures (Li, 2022). This can therefore explain that water molecules are able to penetrate greater displacement withing the concretes at higher temperatures (Abdul kreem, 2012). However, this still does not explain why this is not observed with the NWC. This might probably be due to the following reason. When dry cement mixes with the SSD state OPS aggregate particles, a layer of cement paste forms on the surface. This layer has a low water-to-cement ratio, which makes the concrete uneven and creates a structure that is more permeable (Chandra & Berntsson, 2002). Therefore, water would permeate easier when exposed to boiling temperatures. The difference between the room temperature and after boiling effect on the water absorption can be seen in Figure 4.48 (a – b). Also, the water absorption after boiling for both OSPCs is shown to cease declining after the age of 90 days. Though for the NWC an average difference of 7% is observed between the room temperature and after boiling water absorption, the coarse and fine OPSC it is 27% and 68% in average, which gradually increases over time, see Figure 4.49. Furthermore, since the water absorption decrease, over time, for the OSPCs are higher than the NWC, this would suggest a presence of higher amount of moisture within an enclosed space in the OPSCs. This would further indicate a better internal hydration process for the continuity of strength development which is further discussed in Section 4.3.3.

Another explanation could also be that the boiling of the OPSCs facilitates the removal of the internal palm oil withing the OPS aggregates. This hypothesis agrees with the behaviour found and discussion for the density behaviour of the OPSCs compared to the NWC in Section 4.3.1.

(a)

(b)

(c)
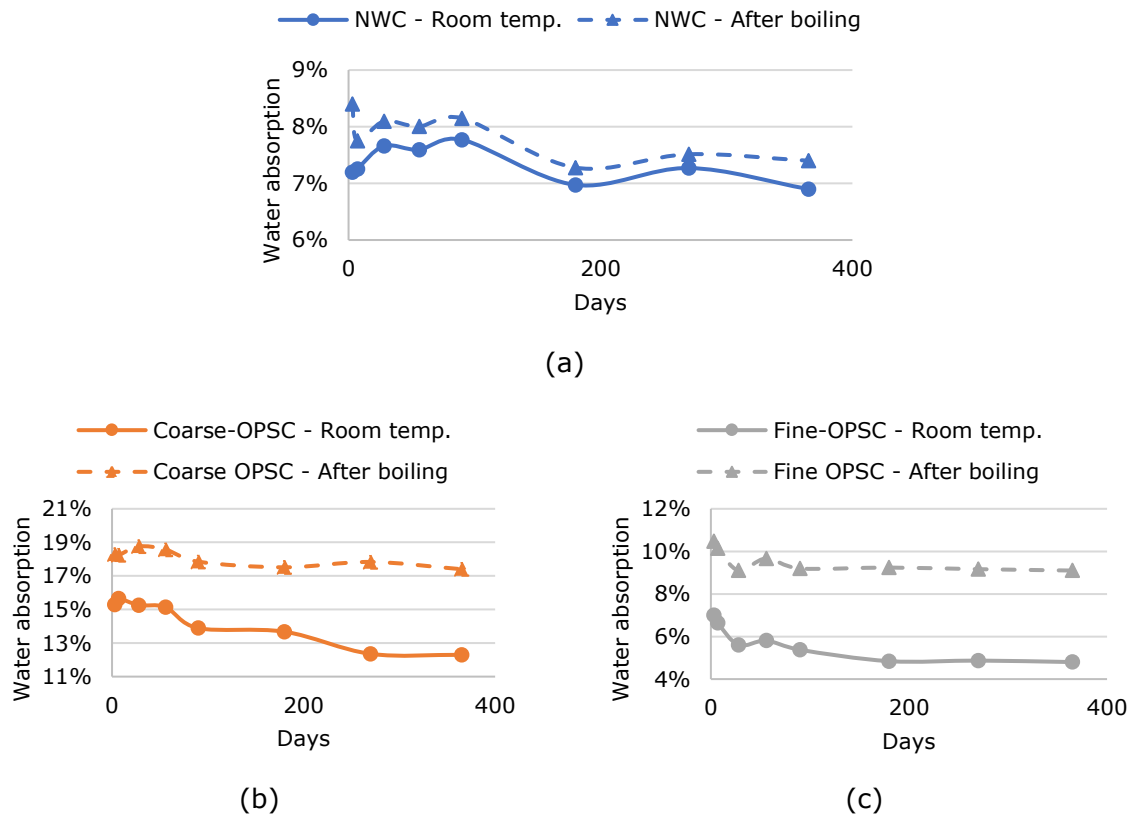
Figure 4.48 Water absorption at room temperature and after boiling, (a) NWC, (b) coarse, (c) fine OPSC
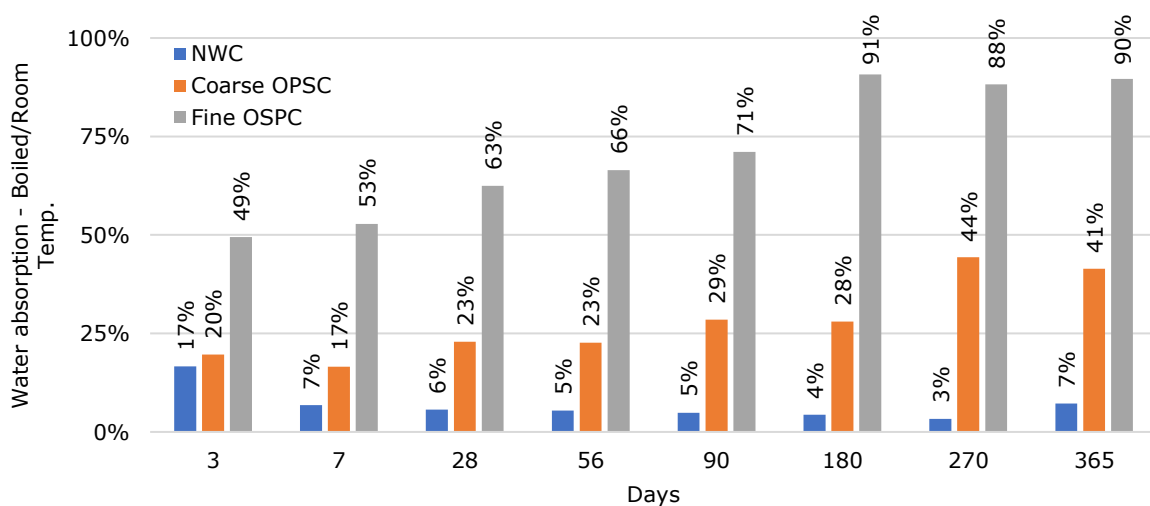
Figure 4.49 Difference between the water absorption of the concretes exposed to room temperature and boiling temperature water.

139

4.3.2.2. Cured vs air cured regime

In this part, the NWC, coarse, and fine OPCS exposed to an air-cured environment were tested for their permeable voids and water absorption and compared to the specimens exposed to a cured environment discussed earlier. The main goal of this investigation was to identify a similar trend or difference in change of permeable voids and water absorption over time, as was observed with the cured specimens.

Permeable voids

The permeable voids for the air cured specimens are shown in Figure 4.51 and the difference between the cured and air cured specimens for the NWC, coarse, and fine OPSC are shown in Figure 4.50 (a), (b), and (c), respectively. From the graphs, it can be seen that a relative similarity is seen between the cured and air cured specimens, both declining in a similar trend. It can therefore be assumed that curing the specimens don't necessarily have any impact on the permeability of the concretes. It was also found that the average permeable voids values of the cured and air cured concretes were found to be similar as seen in Table 4.16. The average permeable voids of the air cured NWC was found to be higher by 1% than that of the cured specimens. This is expected with the absence of moisture for the continuity of the hydration process. However, on the contrary, both OPSCs exposed to air cured regime were 1% lower in average permeable voids than that of the cured specimens. However, the average difference is only 0.2%. Nevertheless, when the difference between the cured and air cured permeable voids are plotted in a scatter graph with a linear trend line from 3 – 365 days for all three concretes, a downward trend is observed indicating that the cured concretes continue to decrease their permeable voids.

(a)

(b)

(c)
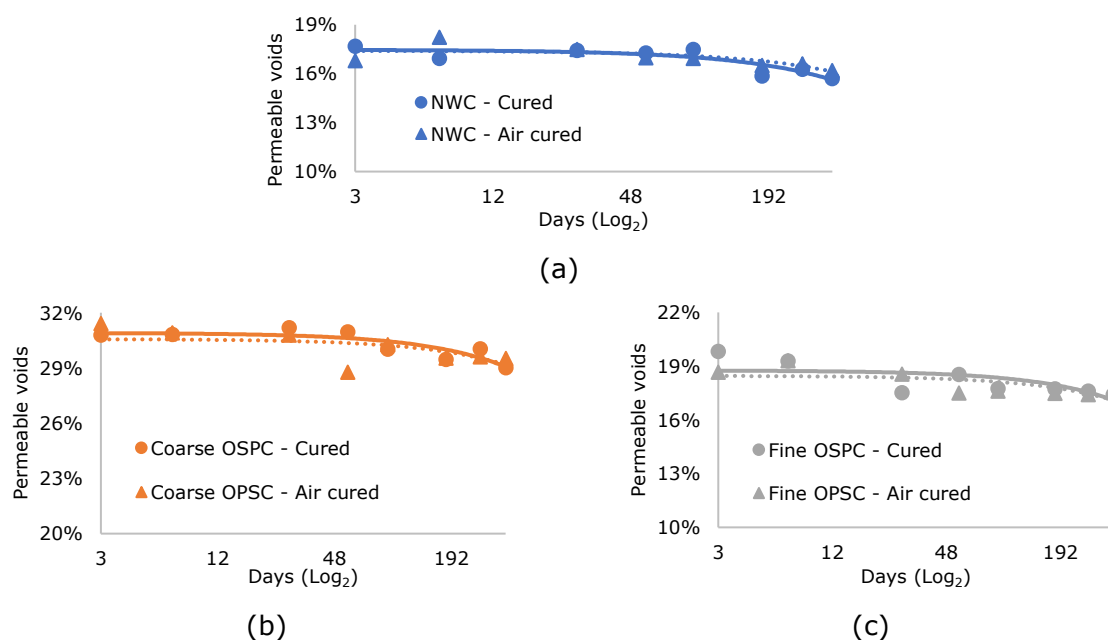
Figure 4.50 Cured vs air cured - Permeable voids of (a) NWC, (b) coarse OPSC, and (c) fine OPSC

140

Table 4.16 Average permeable voids for cured and air cured concretes from 3 – 365 days

| | Average permeable voids | |
	Cured	Air cured
NWC	16.8%	17.0%
Coarse OPSC	30.3%	30.1%
Fine OSPC	18.2%	18.0%
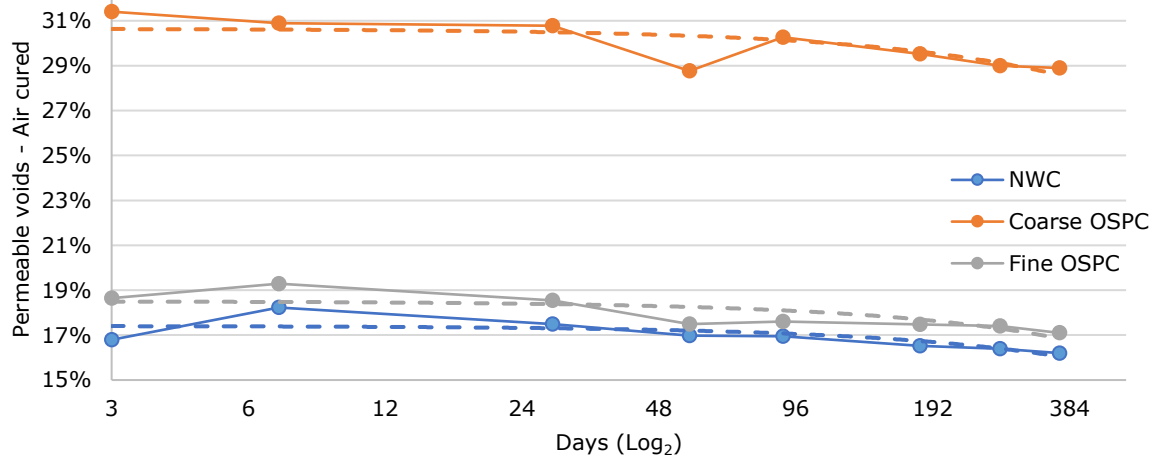
Figure 4.51 Air cured - Permeable voids of NWC, coarse, and fine OPSC
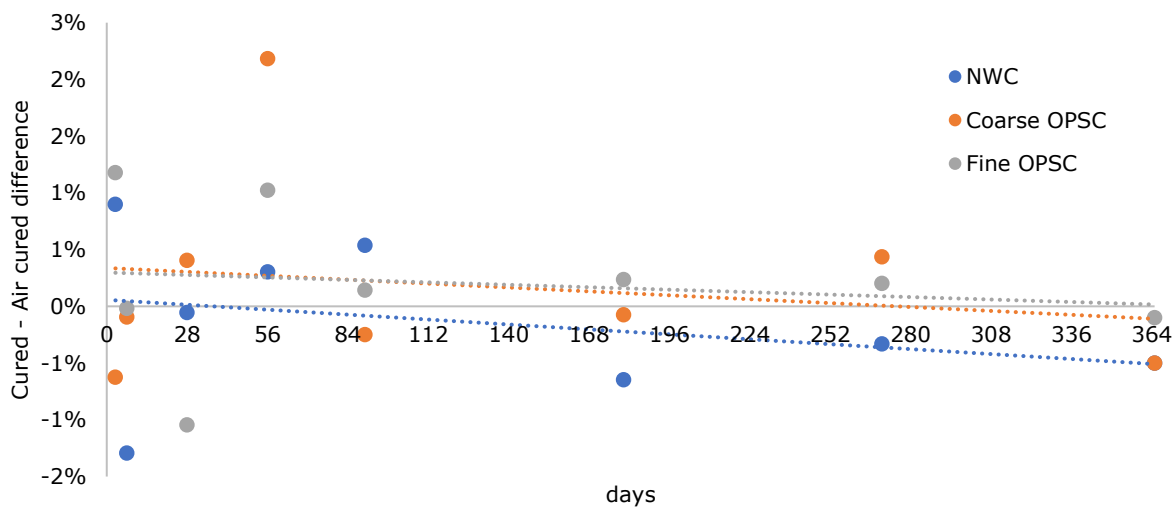
Figure 4.52 Permeable voids cured - air cured difference for NWC, coarse, and fine OPSC over time

Water absorption

The water absorption results for the air cured specimens are shown in Figure 4.53 and compared to the cured specimens in Figure 4.54 (a), (b), and (c) for the NWC, coarse, and fine OPSC, respectively, with tabulated results shown in Table 4.17.

In all three cases, the air cured water absorption is slightly higher than the cured specimens. As explained earlier, when concrete is exposed to an air curing regime, the internal moisture evaporates as was shown in Section 4.3.1 clarified by the reduction in

density. Therefore, the concrete results being dry and porous allowing water penetration to be higher. Conversely, in a cured regime, the continuously presence of moist aids the hydration process and stronger bonds are allowed to form within the cement matrix, consequently making it less permeable to water (ACI Committee 308, 2008).

The fine OPSC showed the lowest average (3 – 365 days) water absorption at room temperature being 18% and 61% lower than the NWC and coarse OSPC, respectively. Whereas after boiling, the fine and coarse OPSC were 12% and 130% higher than that of the NWC. As mentioned earlier for the cured specimens, the high temperature water penetrates into the OPS replacing the palm oil and therefore showing higher water absorption for the boiled samples compared to the room temperature samples. Therefore, the water absorption after boiling might be a biased testing method for OPSC.

Table 4.17 Water absorption tabulated results from 3 – 365 days

	Cured		Air cured	
	Room temp.	Boiled	Room temp.	Boiled
	Average			
NWC	7.4%	7.9%	7.5%	7.9%
Coarse OPSC	14.5%	18.2%	15.5%	18.0%
Fine OPSC	5.8%	9.6%	6.5%	8.8%
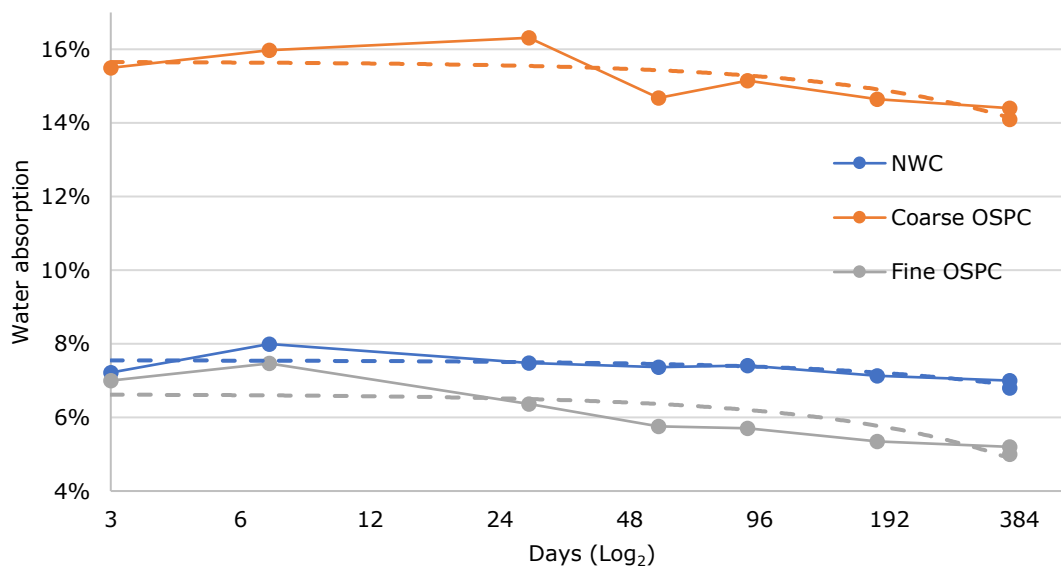
Figure 4.53 Air cured – water absorption of NWC, coarse, and fine OSPC

(a)

(b)

(c)
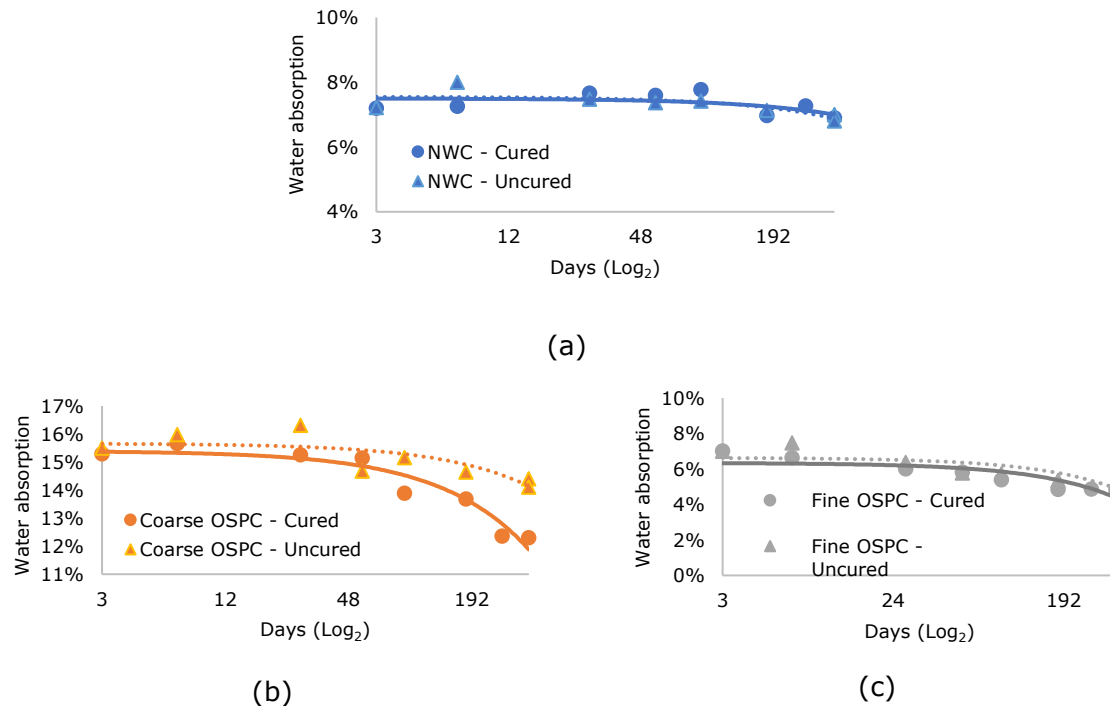
Figure 4.54 Cured vs air cured – water absorption of (a) NWC, (b) coarse OPSC, and (c) fine OSPC

4.3.2.3.   Concluding remark

In this investigation, the permeable voids and water absorptions of the NWC, coarse, and fine OPSC in a cured and air cured regime were tested from a period from 3 up to 365 days. The primary purpose of testing in both regimes was to ensure the reliability of the results obtained. For both the regimes, the values decreased over time as expected. The decrease was mainly anticipated due to the continuation of the hydration process closing in on the pore structure of the concretes. Although a smooth quantifiable decrease value could not be established due to the use of different specimens for each day, the plotted linear trend lines demonstrate a clear decline. The average values for permeable voids and water absorption presented in Table 4.18 provide a comprehensive overview of the properties of these materials over a period of up to 1 year. The air cured specimens also showed a decrease in permeable voids and water absorption over time, though slightly higher than the cured specimens. Thus, confirming the reliability behaviour of the cured regime. This was mainly attributed due to the fact that the air cured concrete is more porous and less hydrated, making it easier for water to penetrate into it. In contrast, water cured concrete has a denser and more hydrated structure, which can make it more resistant to water penetration. Also, the confirmation of the declining behaviour by testing in both cured and air cured regimes was deemed necessary since one might argue that the concretes might still have moisture in the concretes the longer it is cured.

143

The difference in the results mainly point that the NWC and fine OSPC have relatively similar permeable voids and water absorption values while the coarse OPSC showed almost double the values. Some argue that the conventional water absorption testing method, as used in this study, might not be applicable to most LWCs for comparing to NWC (Li, 2011). This is mainly reasoned due to the fact that the LWA used as highly porous and therefore indicate higher results. For the NWC, the coarse and fine aggregates have a very low water absorption (≤1%), and therefore the pore space is mainly in the cement and the interfacial transition zone (Dalton, et al., 2023). However, although with the non-availability of a particular test for LWC, the corresponding 28-day values do have a similar compressive strength. Also, though the mix design of the fine OPSC used a similar volume of F-OPS aggregate as the C-OPS aggregate in the coarse OPCS, the fine OPSC yet showed lower permeable voids and water absorption. Therefore, limited to the samples in this study, the results are considered acceptable for comparison. Furthermore, additional studies could explore the effect of different environmental conditions on the permeable voids and water absorption properties of these concretes.

Table 4.18 Average permeable voids and water absorption of concretes from 3 – 365 days

	Permeable voids	
	Cured	**Air cured**
NWC	16.8%	17.0%
Coarse OPSC	30.3%	30.1%
Fine OSPC	18.2%	18.0%
	Water absorption (room temp.)	
NWC	7.3%	7.3%
Coarse OPSC	14.2%	15.1%
Fine OSPC	5.7%	6.0%

4.3.3. Compressive Strength

The NWC, coarse, and fine OPSC have been tested for their compressive strength at ages 3, 7, 28, 56, 90, 180, and 365 under curing and air curing regimes. The results and discussions are divided into three subsections. At first, the cured samples are discussed followed by a section comparing the cured and air cured specimens. In the third part, the empirical values obtained in this study are compared to prediction formulas introduced in Section 2.2.5 followed by a concluding remark section.

The main objective of this investigation was to understand the compressive strength behaviour of the OPSCs and compared to the NWC under cured regimes and compare them to air cured regimes up to an age of 365 days. The same batch made for the cured regime was casted for cubes tested under air cured regimes. Although some researchers, such as (Mannan, et al., 2002a), tested specimens by partially curing and partially air curing them, in this study only the two most common methods were investigated.

4.3.3.1. Cured regime

In this section the compressive strength of NWC, coarse, and fine OPSC exposed to a cured regime are discussed. Firstly, the compressive strength of the concretes up to 1 year are compared for discussion. Second, the stress-strain graphs of the concretes are discussed and compared. At last, the UPV results for the concretes are discussed.

Compressive strength

The main objective for the three concrete types was to achieve a moist cured compressive strength of 20 MPa at 28 days. Therefore, the main differences are found in earlier and later ages, see Figure 4.55 and Table 4.19. Figure 4.55 also depicts the strength development of the concretes with respect to their 28-day compressive strength. The graph allows for comparison of the concrete mixtures in two periods, from early ages (3-28 days) and from later ages (28-365 days).

At 3 days, the coarse OPSC had already attained a strength of 70% with respect to its 28-day strength, while fine OPSC and NWC exhibited strengths of 69% and 64%, respectively. However, at 7 days, the strength of fine OPSC significantly surpassed that of the other two mixtures, with a ratio strength of 87%, followed by 82% for coarse OPSC, and 77% for NWC. Thus, in general, concluding that fine OPSC attained the highest early strength development among the concretes.
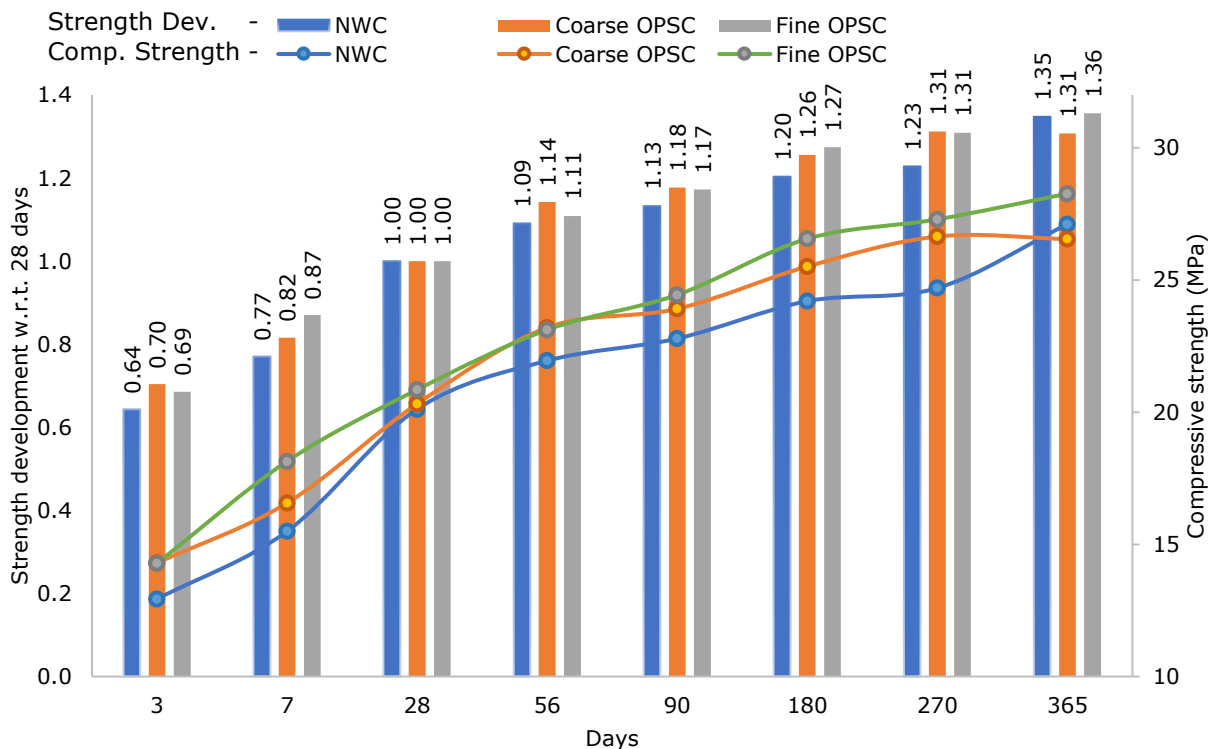
Figure 4.55 Compressive strength of NWC, coarse, and fine OPSC at different ages with ratio with respect to their 28 days compressive strength

As for ages after 28 days up to 365 days, the fine OPSC developed the highest compressive strength reaching a compressive strength of 28.26 MPa at 365 days followed by the NWC and coarse OPSC as last with 27.11 MPa and 26.65 MPa, respectively. Overall, the fine OPSC indicated to be 4% and 6% higher in compressive strength at 365 days compared to NWC and coarse OPSC, respectively.

Table 4.19 Compressive strength of NWC, coarse, and fine OPSC

Day	NWC	Coarse OSPC	Fine OPSC
	Compressive strength (MPa)		
3	12.93	14.30	14.28
7	15.49	16.56	18.14
28	20.12	20.31	20.85
56	21.95	23.20	23.12
90	22.79	23.91	24.44
180	24.20	25.51	26.56
270	24.70	26.55	27.29
365	27.67	26.65	28.26

From Figure 4.56, the compressive strength ratio between the coarse and fine OPSC to NWC is plotted over time. From the graph it is evident that the compressive strength of both OPSCs surpasses that of NWC by 10 – 11% at 3 days. However, after 7 days, the fine OPSC exhibits a superior strength compared to both NWC and coarse OPSC by 17% and 10%, respectively, suggesting a higher strength development at early age. At 28 days, all three concretes reach a comparable strength of approximately 20 MPa, as per the design objective of this study.
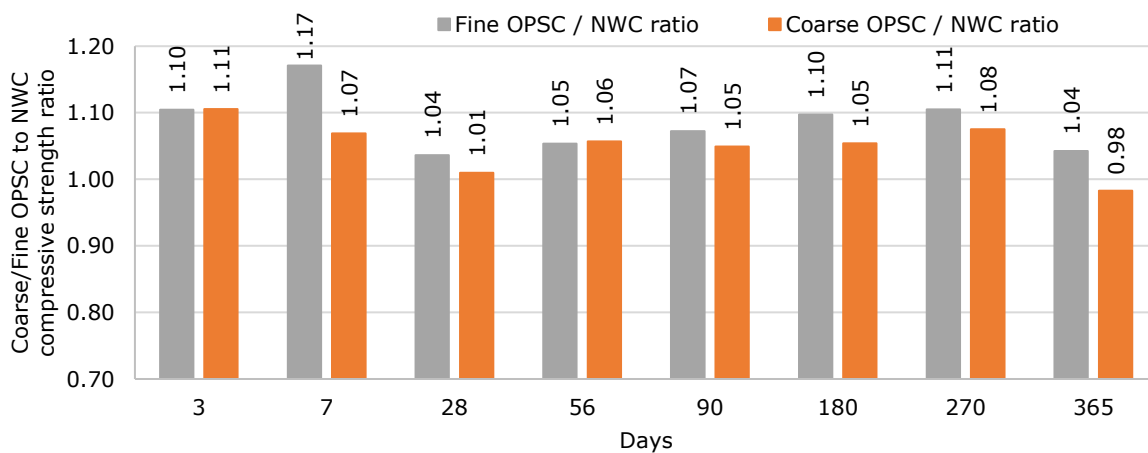
Figure 4.56 Coarse and fine OPSC to NWC compressive strength ratio over time

The observed higher strength development in both OPSCs can be attributed to their better internal curing capacity owing to the presence of reserve water in the aggregate pores (Newman, 1993), as discussed in Section 4.2. Furthermore, the improved bonding effect between the cement and conventional coarse aggregate in fine OPSC, in contrast to coarse OPSC employing C-OPS, can be considered as a probable reason for its higher strength development.

Regarding the strength-to-density ratio, also referred to as the specific strength, both OPSCs exhibit a higher specific strength compared to NWC, with coarse OPSC demonstrating the highest specific strength, see Figure 4.57. This result is expected since NWC has a higher density, yet comparable strengths to both OPSCs. The discrepancy between fine and coarse OPSC can also be explained by the fact that coarse OPSC has a lower density, resulting in a higher specific strength. In average, the coarse OPSC is 35% and 15% higher in specific strength compared to NWC and fine OPSC, respectively.
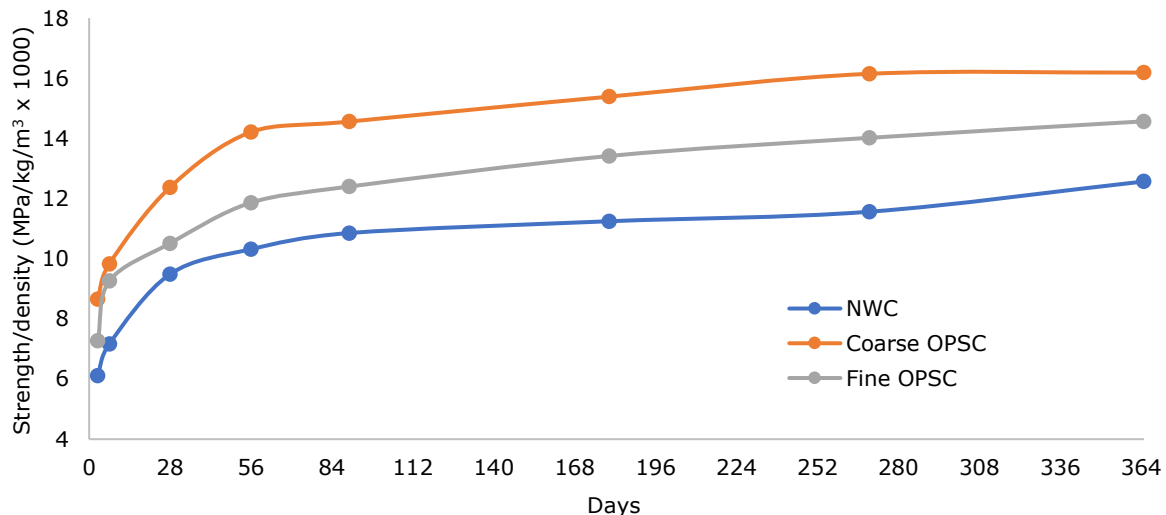
Figure 4.57 Strength/density ratio of concretes over time

Stress-strain analysis

The relationship between stress and strain in compression is a critical feature of concrete that enables the prediction of the behaviour of concrete structural elements. The stress-strain curve provides essential information regarding several properties of a particular type of concrete, including the various forms of modulus of elasticity, peak stress strain, and ultimate strain (Shafigh, et al., 2014a). The ultimate or peak strain of NWC is normally in the range of 0.0030 – 0.0050 (Pillai & Menon, 2006), though for design purposes a value of 0.0030 (MsCormac & Nelson, 2006) or 0.0035 (Ray, 1995) is assumed.

The stress-strain curves for NWC, coarse, and fine OPSC are presented in Appendix F in Figure F.1 – Figure F.3, respectively, from ages 3 up to 365 days. The average of the peak strains from 3 – 365 days for the coarse and fine OPSC was found to be 0.0023 and 0.0026, respectively, which is only slightly less compared to 0.0027 for NWC, indicating both OPSCs to be slightly more brittle. However, the only distinct difference can be seen at the early ages of the concretes, where the NWC exhibits the highest deformation. The lower average deformation of the OPSC is most likely due to the absence of bonding mechanism between the cement and C-OPS and F-OPS aggregates of the coarse and fine OSPC, respectively, due to the high void spaces. Also, the steepening of the curves as the concrete ages in the

147

graphs imply an increase in the brittleness of the concrete. This behaviour is a normal and expected characteristic of concrete (Neville, 1995), which has been observed in all the three types of concrete. Additionally, due to concretes viscous nature, early-age concretes exhibit more ductile behaviour than mature concretes, which are more brittle. As a result, all three concretes exhibit inelastic behaviour, mainly due to the transition zone. The transition zone is porous, and therefore, more deformation occurs within this zone than within the cement matrix and aggregate under the same load, resulting in greater deformation (Li, 2011). Though from the earlier sections, a void space was found in the transition zone in the coarse and fine OPSC, one might expect larger deformation in the OPSCs compared to the NWC. However, since both OPSCs exhibited a higher strength development than the NWC, it therefore explains the lower deformation in early ages, i.e., the OPSCs are therefore more brittle than the NWC in early ages. At age of 365 days, the NWC, coarse, and fine OPSC reduced their strains to 0.0018, 0.0021, and 0.0023, respectively. Nevertheless, a better comparison for the stress-strain behaviour of the concretes at each age can be seen in Appendix F in Figure F.4 (a – h).

In Appendix F in Figure F.4 (a – h) depicts a discernible difference in strain between the NWC and the OPSCs at each respective age. Though the strains of the concretes were found to be quite similar at later ages, however, both the OPSCs exhibit a slight change or jump in strain as stress increases, with rough lines on their curves suggesting the propagation of cracks from early loading (Li, 2011). The curves initially become less steep then abruptly go steeper just before a strain of 0.001 (mm/mm) and after 20-30% of the ultimate compressive strength for both OPSCs types at ages 7 days and beyond. While this behaviour is also observed in the NWC and is expected according to (Mehta & Monteiro, 2006), it is more pronounced in the OPSC types, as indicated by their less-steep lines. This strain initiates microcracks in the interfacial transition zone surrounding the OPS, leading to the distribution of internal loading from the cement matrix to the OPS. As the OPS is much weaker than the surrounding cement matrix, abrupt cracking of OPS explains the noise in the curves afterward. This explanation is better illustrated in Figure 4.58. The changing slopes on the graph from line 1 to 8 indicate the sudden changes explained earlier. These sudden changes are believed to be caused by the abrupt closing-in of the cement matrix on the void spaces shown in the illustrations from A – B, resulting in a change from less steep to steeper slopes to less steep, and so on, until failure. Nevertheless, although a difference is observed between NWC and both OPSC types, no significant difference exists between the coarse and fine OPSC, suggesting both undergo a similar behaviour.
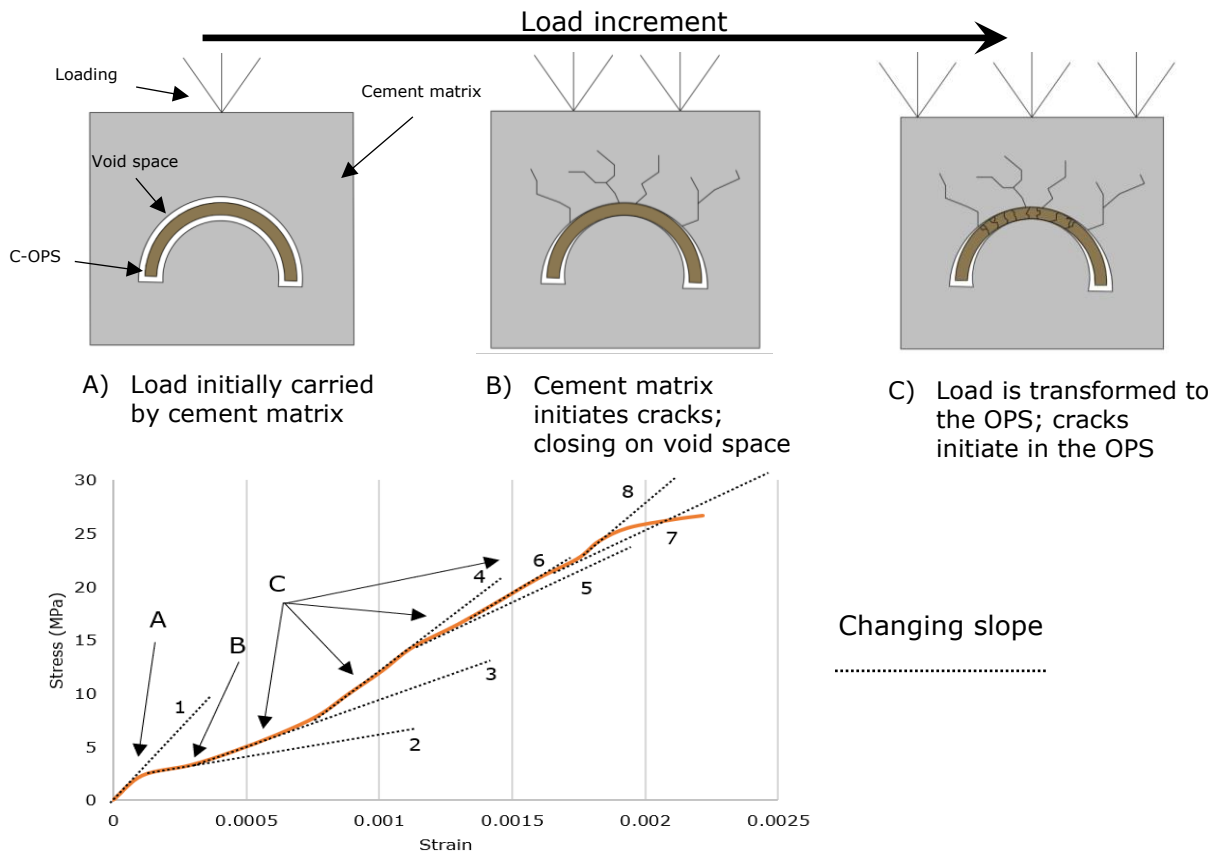
Figure 4.58 Schematic internal crack propagation of OPSC due to load increment

UPV analysis

For each set of concrete type at different ages, the UPV was measured on the cubes prior to testing, with the results shown in Figure 4.59 (a). The grading of UPV was classified based on the (BS 1881-203, 1986) standard. According to Figure 4.59 (b), all three concrete types had a 'Good' grading in early ages, but the NWC and fine OPSC improved to 'Excellent' from 7 and 28 days onwards, respectively. The UPV values increased over time for all three types of concrete by 18%, 12%, and 15% for NWC, coarse, and fine OPSC from 3 to 365 days, with NWC showing the highest values, followed by fine OPSC and coarse OPSC with the lowest values. However, the average difference from 3 – 365 days of the UPV between fine OPSC and NWC was only 4%, while the difference between coarse OPSC and NWC was 23%, indicating that the internal quality of fine OPSC better than that of coarse OPSC. However, the lower UPV results for coarse OPSC could be due to higher void spaces between coarse OPS and the matrix, as well as the use of C-OPS as coarse aggregate. On the other hand, the use of granite as coarse aggregate in fine OPSC may have contributed to higher UPV results.

149

(a)   (b)
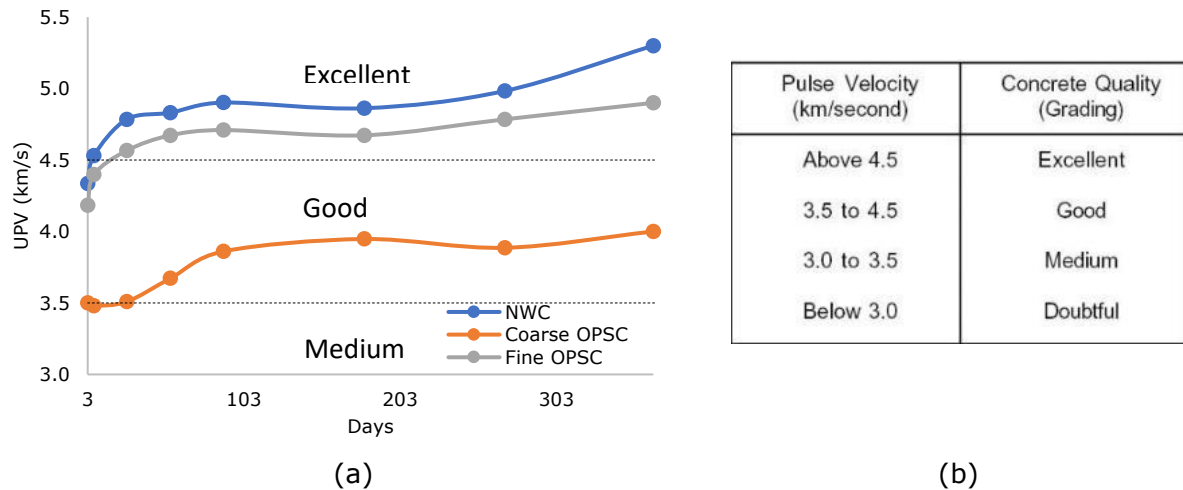
Figure 4.59 (a) UPV of cured concretes over time and (b) grading of UPV according to (BS 1881-203, 1986)

Furthermore, the fine OPSC exhibited the strongest coefficient of correlation factor between their compressive strength and UPV having R^2 = 0.94 followed by the NWC having an R^2 = 0.88 and the coarse OPSC R^2 = 0.81, see Figure 4.60. The lower corelation for the coarse OSPC since it exhibits a sudden change after 28 days.
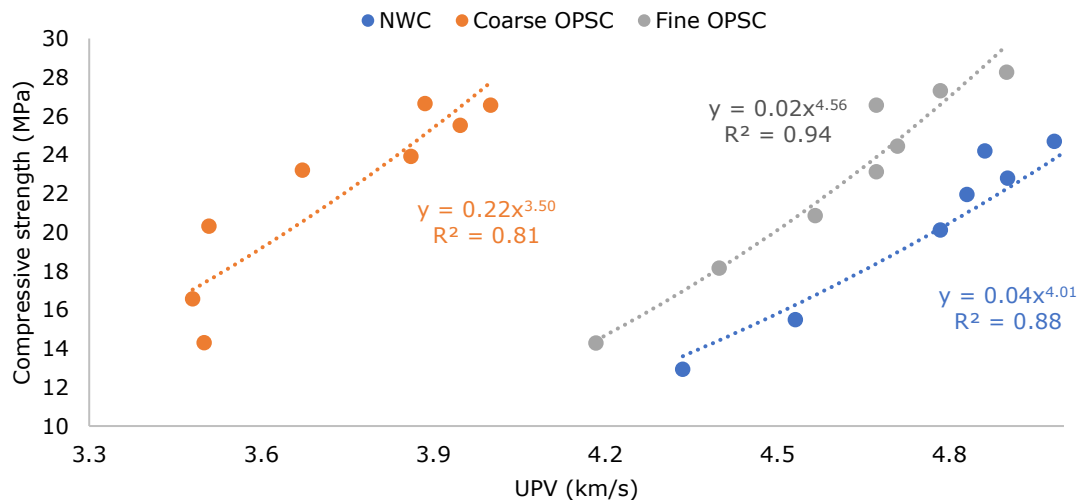
Figure 4.60 Compressive strength vs UPV

4.3.3.2.   Cured vs air cured regime

The main goal of in this investigation was to compare the compressive strength, stress-strain, and UPV behaviour of the air cured concretes with cured regimes over a period of 365 days. The batch used for the cured regime was also utilized to cast cubes that were subsequently subjected to air curing conditions.

Compressive strength

Noteworthy is that the specimens in the air cured regime were exposed to Malaysian outdoor environmental conditions with average relative humidity falling within 10% to 90% and with mean annual temperature of 25.4 ºC (MET Malaysia, 2022). Also, the cubes were kept in a room with open windows, therefore exposed to minimal air circulation. It is therefore expected that the specimens would undergo slow moisture reduction, thus allowing for some degree of continuation for hydration (Neville, 1995). In fact, from the density observations in Section 4.3.1, all the three concretes exposed to air curing were observed to have a slight increase in their dry density over time. This was mainly concluded to be attributed to the increase in hydration closing in on the pores with presence of internal moisture due to exposure to high humidity. In general, concrete is expected to have better mechanical properties when exposed to curing regime to maintain ideal conditions for temperature and humidity in concrete after placement and completion (Zeyad, et al., 2022). Consequently, appropriate curing methods can promote cement hydration and produce more hydration with the cement, which is advantageous for the growth of long-term strength. Effective curing regimens can also improve the microstructure of concrete, which helps to increase durability (Wang, et al., 2023).

The NWC and fine OPSC exhibited an expected behaviour where the air cured specimens showed lower compressive strength values to the cured regime, see Figure 4.61 and Figure 4.62. At 3 and 7 days, the air cured NWC showed similar results to the cured regime with an air cured to cured compressive strength ratio of 0.97 and 0.96, respectively. However, the strength development lowered down to 0.77 at 365 days. The fine OPSC exhibited a similar behaviour, though at 3 and 7 days the air cured to cured compressive strength ratio was 0.98 and 0.97, respectively, thus slightly higher than the NWC. At 365 days, the ratio of the fine OPSC was also higher being 0.86. in general, the lower strength of the air cured specimens is contributed to the reduction of internal moisture subsequently halting the cement hydration. As for the slightly higher ratio found for the fine OPSC, this is most probably due to the presence of internal moisture in the OPS contributing to internal curing.
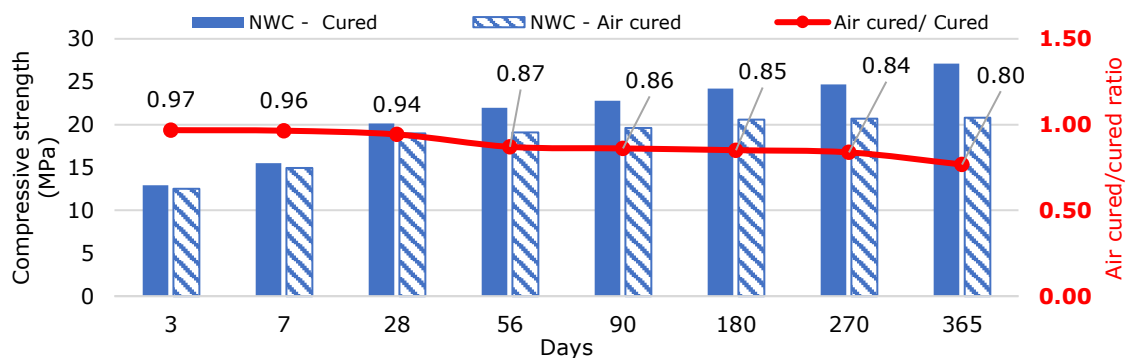
Figure 4.61 Moist cured vs air cured compressive strength of NWC
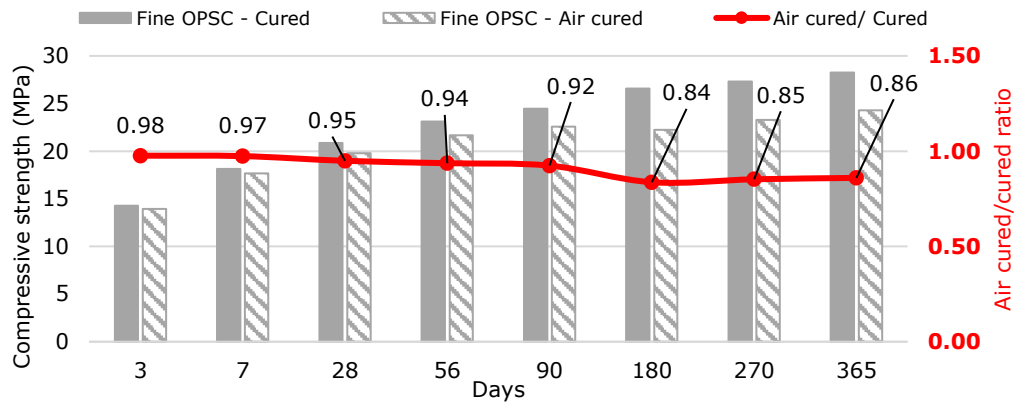
Figure 4.62 Moist cured vs air cured compressive strength of fine OPSC

However, only the coarse OPSC specimens showed a slight increase in strength under air-curing conditions at earlier ages, up to 28 days as depicted in Figure 4.63. An increase of 21% was observed at 3 days and 11% at 7 days for coarse OPSC, indicating a reduced strength development only after 28 days in the air cured specimens. Two possible reasons can explain this behaviour. Firstly, internal moisture in C-OPS may suffice to continue the hydration process up to 28 days. It was found in Section 4.3.6 that the coarse OPSC exhibited the highest water absorption of 15.5% in average among the concretes being more than twice higher than NWC and fine OPSC. The first explanation would indicate that it would at least have a similar behaviour to the cured specimens. Therefore, an additional explanation could be the absence of high moisture (i.e., curing tank) which allows the C-OPS to be stiffer in a dry or not moist state. This hypothesis could be possible since OPS has a similar composition to wood known to be more flexible and weaker in a moist state (Pestka, et al., 2018). Hence, it is possible that C-OPS mechanically aids in resisting higher compressive strength during the initial hardening of the concrete until the cement reaches its final hydration process. As demonstrated in Figure 4.63, this observable fact appears to take place at and after 56 days, where the air cured to cured ratio declined to 0.91, and the compressive strength of the air cured specimens ceased to develop in strength.
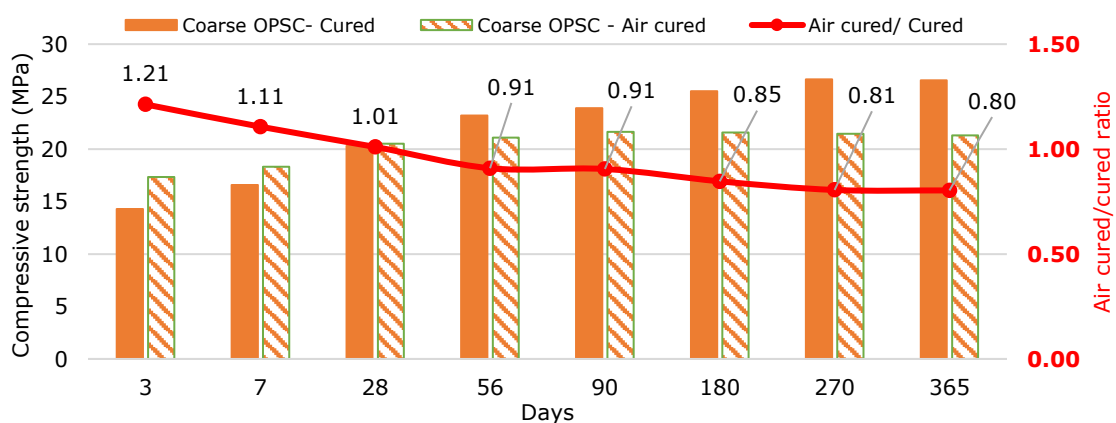
Figure 4.63 Moist cured vs air cured compressive strength of coarse OPSC

152

Stress-strain analysis

Another notable difference between the cured and air cured NWC, fine, and coarse OPSC is the stress-strain behaviour over time, as shown in Appendix F in Figure F.5 – Figure F.7, respectively. A significant difference observed is the compressive strength of the concretes, which has already been discussed earlier. However, another interesting aspect is the difference in strain between the cured and air cured specimens.

For the NWC in Appendix F in Figure F.5, the air cured specimens exhibit a slightly higher strain before failure, with an average strain of 0.0040 compared to an average of 0.0027 for the cured specimens. This indicates the air cured specimens to be a third less brittle compared to the cured specimens. This behaviour is expected and can be mainly attributed to the curing process. The use of the same materials and mix content in both cases leads to differences in the microstructure due to the curing conditions. Water-cured specimens age more rapidly due to faster hydration, resulting in a denser and more compact microstructure that is more susceptible to cracking under applied loads, resulting in greater brittleness. On the other hand, air cured specimens have lower early-age strength development, which results in a less dense and more porous microstructure that can accommodate more deformation before fracture (Kosmatka, et al., 2002).

In regard to the fine OPSC, seeAppendix F in Figure F.6, a comparable change in behaviour with respect to strain between the cured and air cured specimens was observed, as with NWC. Nevertheless, an average strain of 0.0026 and 0.0034 was recorded for the cured and air cured specimens at all ages, respectively, indicating a 24% reduction in brittle failure, approximately half that of NWC. This effect can be attributed to the greater internal hydration taking place in the OPSC, facilitated by the water present in the OPS, as previously discussed.

However, in the case of the coarse OPSC, see Appendix F in Figure F.6, the change in strain between the air cured and cured specimens was observed to be very minimal for each age. The average strain for the cured and air cured specimens were found to be 0.0026 and 0.0027 respectively, showing a difference of only 4%, thus having the smallest difference among the three concrete types. This could be attributed to a similar explanation as that for the fine OPSC, where the coarse OPSC most likely had better internal curing, which was also evident from the higher compressive strength in early ages for air cured specimens. Although both coarse and fine OPSC had a similar amount of OPS content in terms of volume, as mentioned in Section 4.2, it was also found that the coarse OPSC had a double amount of water absorption compared to the fine OPSC.

In the preceding section, the stress-strain graphs for each cured concrete at different ages revealed that both OPSCs exhibited slightly higher deformation than the NWC and that the

slope of the line changed due to the close-in effect on the void space at the interfacial transition zone. Figure F.7 in Appendix F depicts the stress-strain graphs of the cured specimens over time, along with those of the air cured specimens. In general, it can be observed that a similar difference behaviour is displayed by the air cured specimens as the cured specimens with the OPSCs compared to the NWC, albeit with varying stresses.

UPV analysis

The UPV results for the cured and air cured specimens of the concretes are plotting and compared in Figure 4.64 (a) & (b), respectively. Though both the NWC and fine OPSC progressed to excellent as the concretes cured from 7 and 28 days, respectively, in the air cured regime they progressed to excellent after 180 and 365 days, respectively. In average, the UPV difference between cured and air cured was 9%, 3%, and 6% for the NWC, coarse, and fine OPSC, respectively. The lower UPV for air cured specimens is expected with the unavailability of moisture for the continuation of the hydration process. A difference can also be observed with the relation between the UPV and compressive strength with the cured and air cured specimens in Figure 4.65 (a) & (b), respectively. The lower difference between the NWC and OPSCs shows that the OPSCs are less affected than the NWC, especially the coarse OPSC. This was also shown in the compressive strength results for the air cured specimens for the coarse OPSC.

Nevertheless, lower coefficient of correlation factors of $R^2 = 0.70$, $R^2 = 0.66$, and $R^2 = 0.65$ for NWC, coarse and fine OPSC, respectively, were found compared to the cured specimens. This is merely reasoned to be caused by the smaller change in UPV of 15%, 6%, and 7% from 3 – 365 days, for NWC, coarse, and fine OPSC, respectively.
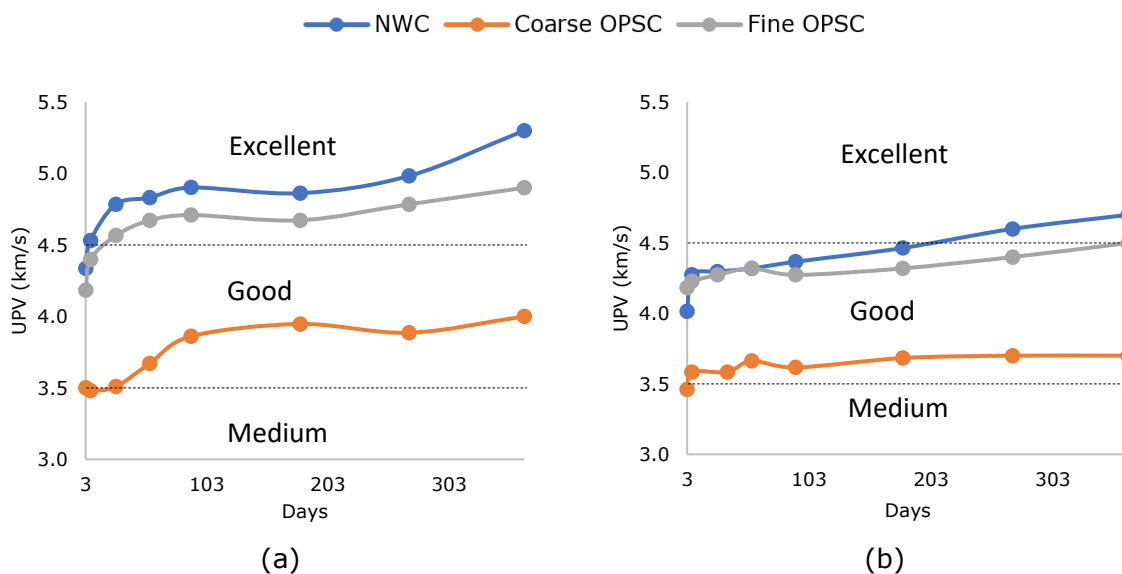
Figure 4.64 UPV results for the (a) cured (b) air cured concretes
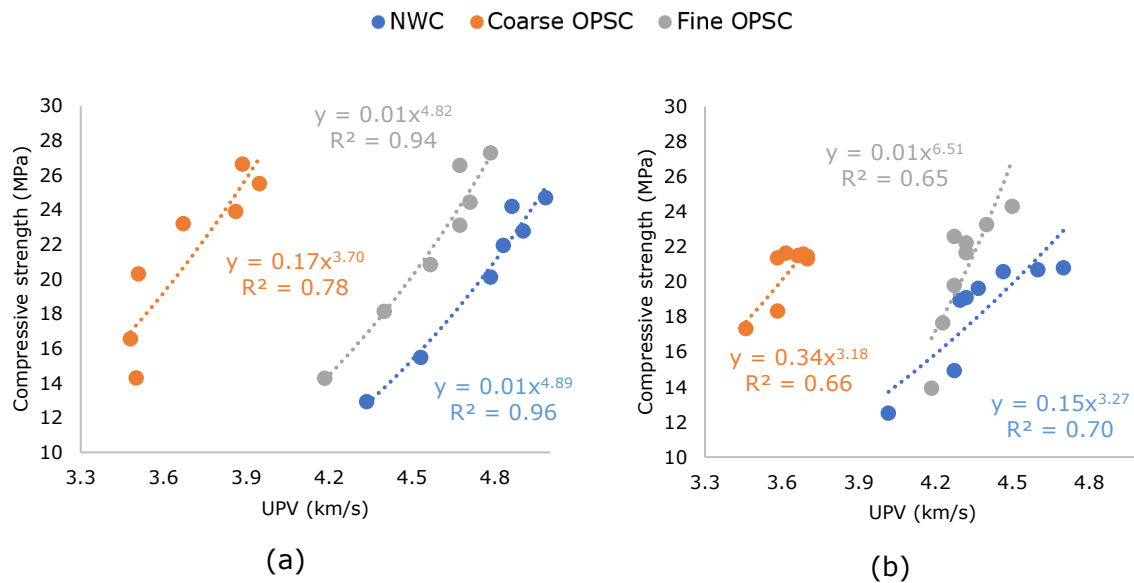
Figure 4.65 Compressive strength vs UPV for the (a) air cured (b) cured concretes

4.3.3.3. Prediction models - compressive strength

In this investigation, two models (equations (2-1 & (2-2) mentioned in Section 2.2.5 were used to predict the compressive strength of the cured and air cured NWC, coarse, fine OPSC from ages 3 up to 365 days. The predicted compressive strengths have been plotted along the empirical values of the concretes in Figure 4.66, Figure 4.68, and Figure 4.70, respectively. According to the ACI and BS codes, the models are suitable for high, normal, and lightweight concretes. Both codes consider the age and the known 28 days compressive strength as inputs into the models where only the BS also includes a coefficient which depends on the type of cement used. However, the curing method is not mentioned.

For NWC, both prediction models from (ACI 209, 1997) and (BS EN 1992-1-1, 2014) predicted the compressive strength over time for the cured specimens with acceptable estimates, see Figure 4.66 (a). A comparison with the predicted to empirical ratio over time can be seen in Figure 4.67 (a). Both BS and ACI model show slight lower prediction values from early ages from 3 - 7 days and higher accuracy values from 28 days onwards, see Table 4.20 and Table 4.21 for cured and air cured regimes, respectively. While an average prediction to empirical ratio of 90.1% and 81.3% is shown for BS and ACI from 3 to 7 days, respectively, a higher average of 98.8% and 95.8% is shown from 28 – 365 days, respectively, for the cured specimens. Therefore, implying that both models have high a prediction accuracy from 28 days onwards and can be therefore verified as acceptable prediction models. However, the BS model shows better results than the ACI which underestimated the empirical values by only 1.2% compared to 4.2% for the ACI model. However, for the NWC air cured specimens, this did not seem to be to case

155

demonstrating an average ratio of 109.1% and 105.6% between 28 – 365 days. Therefore, indicating a higher over-estimation by both models.

(a)   (b)
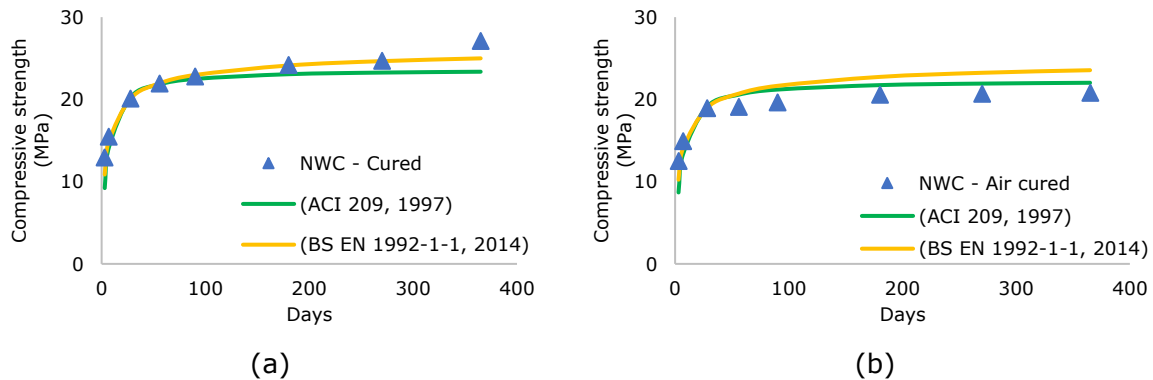
Figure 4.66 Compressive strength of (a) cured and (b) air cured NWC with prediction models from ACI and BS

(a)   (b)
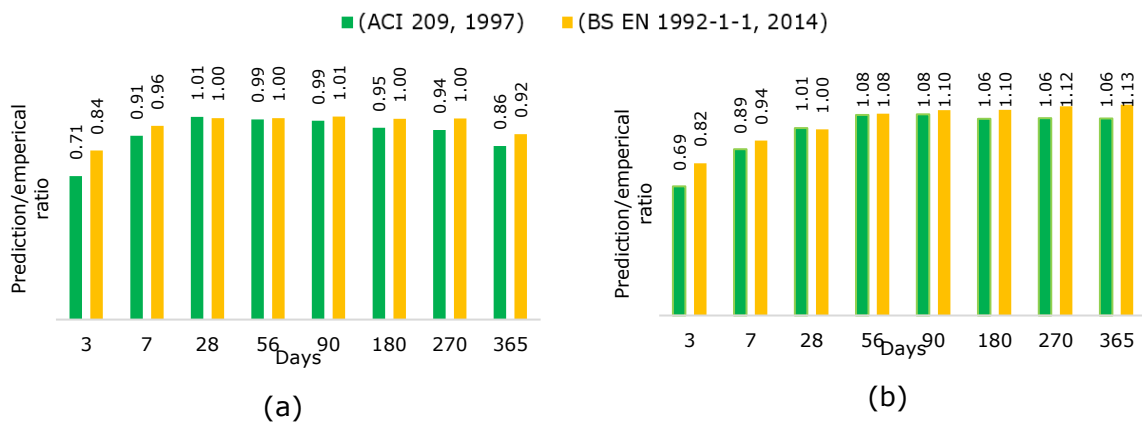
Figure 4.67 Predicted values to empirical results ratio for (a) cured and (b) air cured NWC

Table 4.20 Compressive strength prediction model to empirical ratio for cured regime

Day's range	NWC		Coarse OPSC		Fine OSPC	
	ACI	BS	ACI	BS	ACI	BS
Average (All)	92.1%	96.6%	88.8%	93.5%	88.2%	92.9%
Average (3-7 days)	81.3%	90.1%	75.7%	72.3%	73.9%	70.6%
Average (28-365 days)	95.8%	98.8%	93.2%	100.6%	93.0%	100.3%

Table 4.21 Compressive strength prediction model to empirical ratio for air cured regime

Day's range	NWC		Coarse OPSC		Fine OSPC	
	ACI	BS	ACI	BS	ACI	BS
Average (All)	99.1%	103.8%	97.1%	101.0%	92.1%	97.3%
Average (3-7 days)	79.3%	87.9%	66.5%	79.0%	71.9%	68.7%
Average (28-365 days)	105.6%	109.1%	107.3%	108.3%	98.8%	106.8%

Comparable trends were observed for the cured coarse OPSC as with the NWC, see Figure 4.68 and Figure 4.69. While lower ratios of 72.3% and 75.7% for BS and ACI models, respectively, were shown for the cured specimens during the early stages (i.e., 3 - 7 days), more acceptable values of 100.6% and 93.2%, for BS and ACI model respectively, were

shown from ages 28 days and later, see Table 4.20. Therefore, indicating that the BS model also has a higher prediction accuracy than that of the ACI model.

Moreover, consistent with NWC, both the BS and ACI models overestimated the empirical results for the air cured coarse OPSC by 8.3% and 7.3%, respectively, as shown in Table 4.21, but to a lesser degree than in NWC, being 9.1% and 5.6%, respectively. This is most probably due to the internal curing effect of the coarse OPSC discussed in the previous sections.

As in the case of cured fine OPSC, the BS and ACI models showed the lowest accuracy in early ages from 3 – 7 days of 68.7% and 71.9% respectively. This was also from ages 28 – 365 days only for the ACI model being 93.0% while showing a higher accuracy with the BS model being 100.3%. Also, for the air cured fine OPSC, lower accuracy was shown from 3 – 7 days of 68.7% and 71.9% and better accuracies for 28 – 365 days being 106.8% and 98.8% for the BS and ACI model, respectively.

Out of the three concretes, it appears that in general, the BS model was able to predict the compressive strength of the cured NWC, coarse, and fine OSPC with the most accurate values from 28 – 365 days with an error of 1.2%, 0.6%, and 0.3% as compared to the ACI model being 4.2%, 6.8%, and 7.0%, respectively. This is probably due to the fact that the BS model incorporates a coefficient for the cement type being used.

(a)   (b)
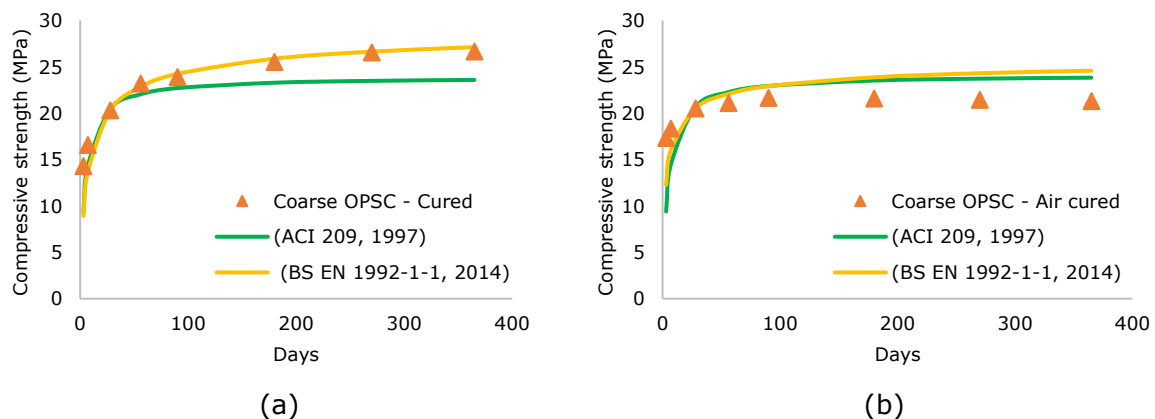
Figure 4.68 Compressive strength of (a) cured and (b) air cured coarse OPSC with prediction models from ACI and BS

(a)   (b)
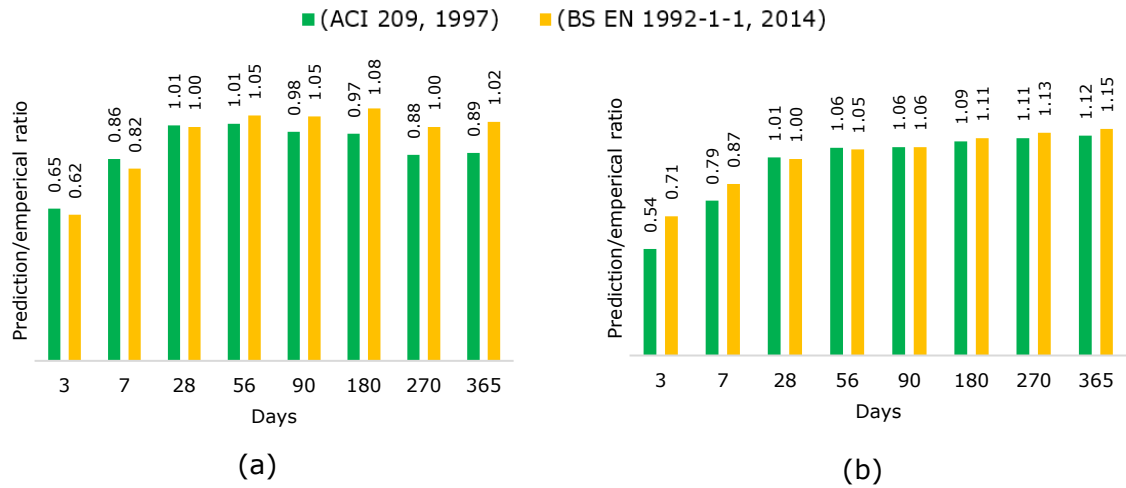
Figure 4.69 Predicted values to empirical results ratio for (a) cured and (b) air cured coarse OPSC

(a)   (b)
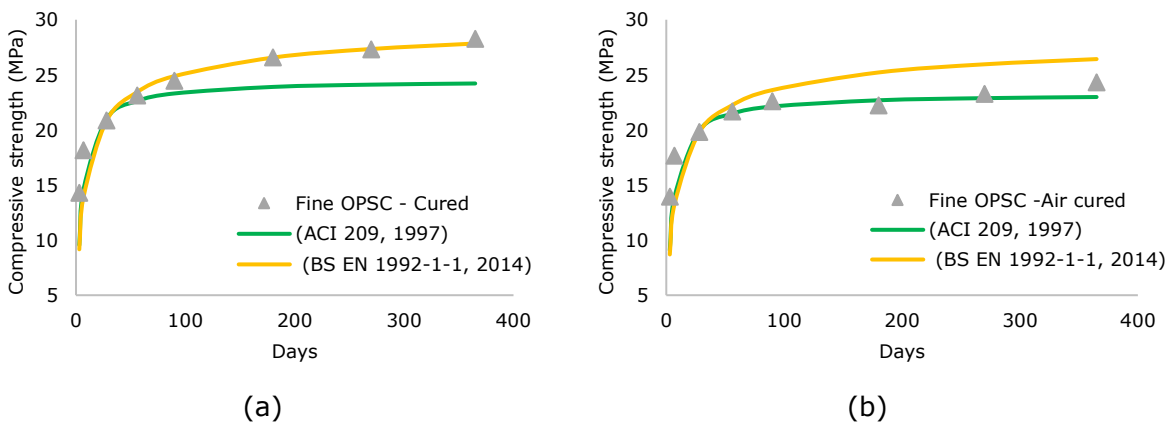
Figure 4.70 Compressive strength of (a) cured and (b) air cured fine OPSC with prediction models from ACI and BS

(a)   (b)
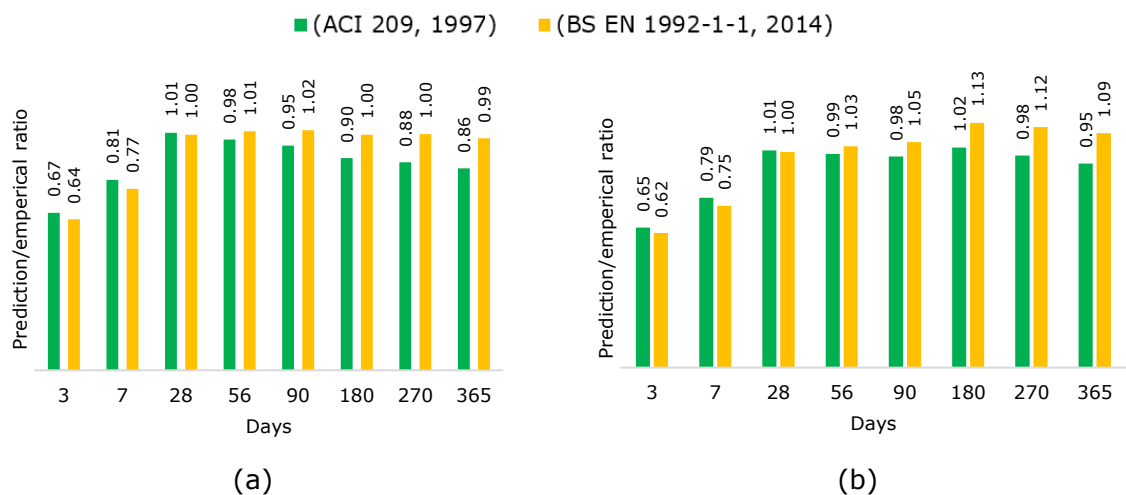
Figure 4.71 Predicted values to empirical results ratio for (a) cured and (b) air cured fine OPCS

158

4.3.3.4.   Concluding remarks

The compressive strength of the NWC, coarse, and fine OPSC exposed to cured and air cured environments from ages 3 to 365 days were tested and analysed in this investigation. Also, the compressive strength, the stress-strain graphs and the UPV of the concretes were also analysed.

For the cured specimens, it was found that the fine OPSC had the highest strength development from early up to later ages followed by the NWC and as last coarse OPSC. However, the coarse OPSC was also found to have a higher early strength development compared to the NWC. The higher early strength development of the OSPCs compared to the NWC was mainly attributed to the internal curing affect aiding with the cement hydration. The internal moisture was found within the high-absorbing OPS aggregate, especially for the coarse OPSC having a high-water absorption.

For the air cured specimens, both the NWC and fine OPSC showed a lower compressive strength than that of the cured specimens, though the fine OPSC developing slightly higher than the NWC. On the other hand, the air cured course OPSC performed better in early ages up to 28 days than the cured regime specimens. This was mainly reasoned with the following points:

- Since coarse OPSC has a high-water absorption of 15.5%, more than twice than that of the NWC and fine OPSC, the internal moisture aids with the hydration process.
- In addition, the absence of high moisture (i.e., curing tank) allows the C-OPS to be stiffer in a dry or not moist state.

The stress-strain curves indicated a more brittle behaviour for both OPSCs compared to the NWC in the early ages for the cured specimens, suggesting a rapid strength development. Also, the difference in average strain between the cured and air cured specimens suggested that the OPSCs are more brittle exposed to an air cured regime compared to the NWC. Thus, proving the internal curing effect of the OPSCs with the coarse OPSC being the highest. This reasoning is attributed to the understanding that higher strength concretes are more brittle. Noteworthy, in Section 4.2, it was found that the internal water in the OPS was absorbed by the surrounding cement matrix, which caused the OPS to shrink. From microscopic images it was found that this shrinking effect caused a void space between the OPS aggregate (both as fine and coarse) and the cement matrix. Due to this void space, a clear affect could be recognized in the stress-strain curves showing noises in the curve and an inward curve graph, opposed to an outward curve shown by the NWC. This inward curve showed a change in the stress-strain line resulting in a change from less steep to steeper slopes to less steep, and so on, until failure. These

sudden changes are believed to be caused by the abrupt closing-in of the cement matrix on the void spaces along with the noises on the curve. This behaviour was found for both the cured and air cured specimens.

The UPV analyses revealed that the cured NWC and fine OSPC improved from a 'Good' grading to 'Excellent' where the coarse OPSC only showed a 'Good' grading, in reference to (BS 1881-203, 1986). The lower UPV values for the coarse OPSC can be explained due to higher void spaces between coarse OPS and the matrix, as well as the use of C-OPS as coarse aggregate. On the other hand, the use of granite as coarse aggregate in fine OPSC may have contributed to higher UPV results. Conversely, the air cured specimens did not improve significantly for the concretes, mainly due to the absence of moisture for the continuation of the hydration process. It was also found that the coarse and fine OPSC showed a smaller difference between the cured and air cured UPV results as compared to the NWC. This was also reasoned to be caused by the internal curing effect of the OPSCs. In addition, good correlations were found between the compressive strength and UPV as seen in Table 4.22, though slightly lower for the air cured specimens.

Table 4.22 Relationship between compressive strength and UPV for cured and air cured specimens

Type	Cured		Air cured	
	Relationship	R^2	Relationship	R^2
NWC	$f_c = 0.04(UPV)^{4.01}$	0.88	$f_c = 0.15(UPV)^{3.27}$	0.70
Coarse OPSC	$f_c = 0.22(UPV)^{3.50}$	0.81	$f_c = 0.34(UPV)^{3.18}$	0.66
Fine OPSC	$f_c = 0.02(UPV)^{4.56}$	0.94	$f_c = 0.01(UPV)^{6.51}$	0.65

Where,
$f_c = compressive\ strength\ (MPa)$
$UPV = Ultrasonic\ pulse\ velocity\ (km/s)$

4.3.4. Flexural Tensile Strength

The NWC, coarse, and fine OPSC have been tested for their flexural tensile strength at ages 3, 7, 28, 56, 90, 180, and 365 under curing and air curing regimes. The results and discussions are divided into two subsections. The cured samples are discussed first, then the cured and air cured samples are compared followed by a concluding remark.

Typically, the cement bonding matrix is the limiting factor for tensile strength of most concretes. Consequently, a good comparison can therefore be demonstrated by comparing the three concrete types from this study with similar grade strengths.

4.3.4.1. Cured Regime

In the following subsections the flexural tensile strength exposed to a cured regime from ages 3 up to 365 days are discussed followed by a comparison between the flexural tensile strength and its respective compressive strength. In addition, the UPV analyses of the prisms are also discussed.

Flexural tensile strength

Cured prism specimens were tested for their flexural tensile strength at different ages for NWC, coarse, and fine OPSC and the results are plotted in Figure 4.72.
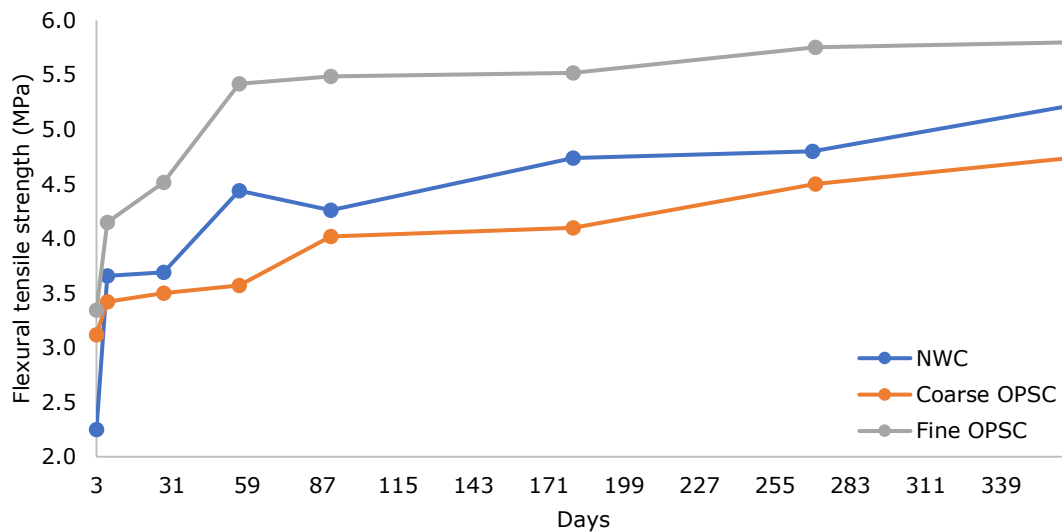
Figure 4.72 Flexural tensile strength of cured NWC, coarse, and fine OPSC

It is evident from the graph that the fine OPSC demonstrated the highest flexural tensile strength performance followed by NWC and coarse OPSC as last. Also, at 56 days, the fine OPSC already reached 98% of its peak strength as compared to 85% and 75% for NWC and coarse OPSC at 56 days, respectively. The reason for the higher flexural tensile strength and development for fine OSPC is most probable due to the high content of crushed coarse aggregate (granite) of 1236 kg/m^3 in the mix as compared to 1175 kg/m^3 for NWC and unlike coarse OPSC, using Tenera C-OPS, see Section 4.2.2. The conventional coarse aggregate is known to have a good bonding mechanism with hydrated cement (Neville, 1995). Thus, the coarse OPSC shows the least strength with the absence of the conventional coarse aggregate. Also, as was shown in earlier sections, the internal curing effect probably also plays an important role by increasing the strength development which consequently increases the bond mechanism for the fine OPSC.

As for the lower strength in the coarse OPSC, as was discussed in Section 4.2.2, no actual bonding was observed with the C-OPS aggregate and cement matrix due to the void space observed at the interfacial transition zone with microstructure analyses. Also, since it is believed that the OPS rots in a cured regime due to high moisture presence, it is possible that the C-OPS in coarse OPSC has rotted/decayed and therefore provided no aid in the flexural tensile strength. This effect is better observed when compared to the air cured specimens in Section 4.3.4.2. Nevertheless, the fine OPSC reached a strength of 5.8 MPa at 365 days being 11% and 27% higher than the NWC and coarse OPSC, respectively.

161

Flexural tensile strength and compressive strength relationship

The relationship between the flexural tensile strength and compressive strength has been plotted in Figure 4.73. Acceptable relationships were found for the NWC, coarse, and fine OSPC with an R^2 of 0.90, 0.79 and 0.96, hence the strongest correlation with fine OSPC.
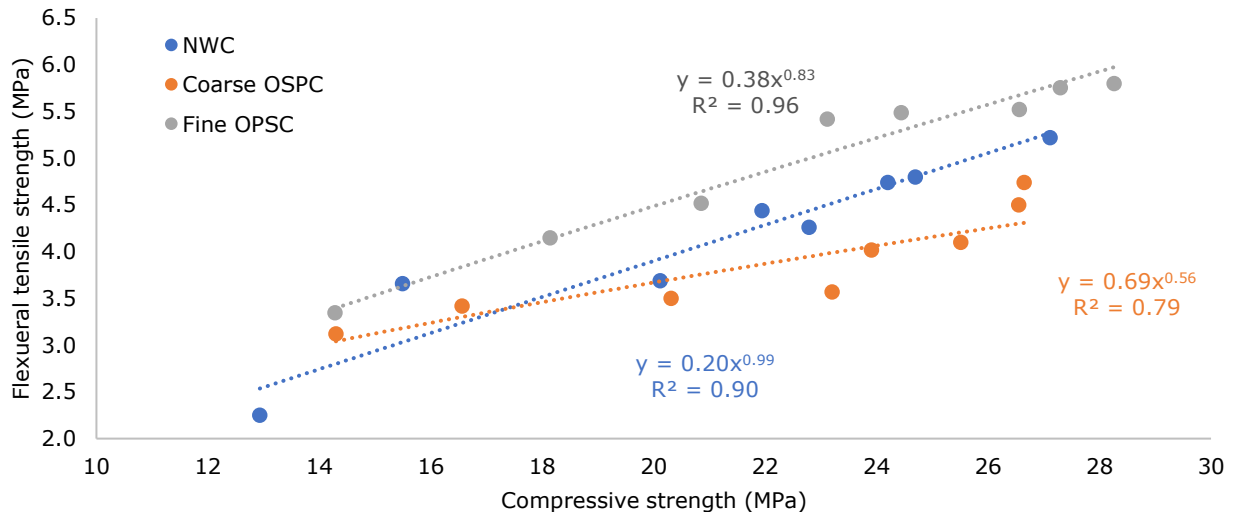
Figure 4.73 Flexural tensile strength and compressive strength relationship

UPV analysis

The UPV results over time of the prism specimens are shown in Figure 4.74. Also, the relationship between the flexural tensile strength with the UPV are plotted in the Figure 4.75. The highest UPV values were found for the NWC ranging from 3.7 – 4.9 km/s followed by fine OPSC ranging from 3.5 – 4.5 km/s, therefore performing quit similar. The slight lower value for fine OPSC is most probably due to the porous cellular structure of F-OPS aggregate, a similar conclusion given by (Serri, et al., 2015b). Similar difference in UPV values between NWC and fine OPSC were also seen for the cubes specimens used for compressive strength, though slightly higher for both, see Section 4.3.3. The minor variance between the cubes and prisms is probably due to compaction difference and different mould/specimen sizes. Similar to the cube specimens, coarse OPSC also demonstrated the lowest UPV values ranging from 3.0 – 3.9 km/s. Nonetheless, the fine OSPC demonstrated a maximum UPV value greater than coarse OPSC by 15%. The difference between the concretes with UPV values is greatly related to the different aggregate types and sizes used. As for coarse OPSC being the lowest, this is most probably due to the void spaces found in the interfacial transition zone between the cement matrix and OPS (Neville, 1995). Also, for the relationship between flexural tensile strength and UPV, the strongest coefficient of correlation factor (R^2) of 0.98 was obtained with fine OSPC, where NWC and coarse OPSC showed an R^2 of 0.94 and 0.95, respectively.
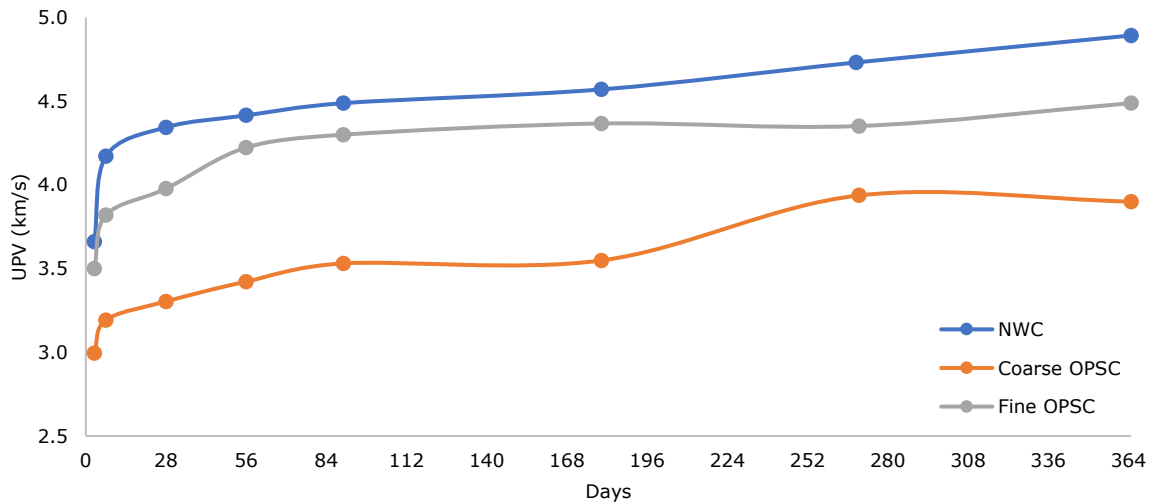
Figure 4.74 UPV results for the flexural tensile specimens
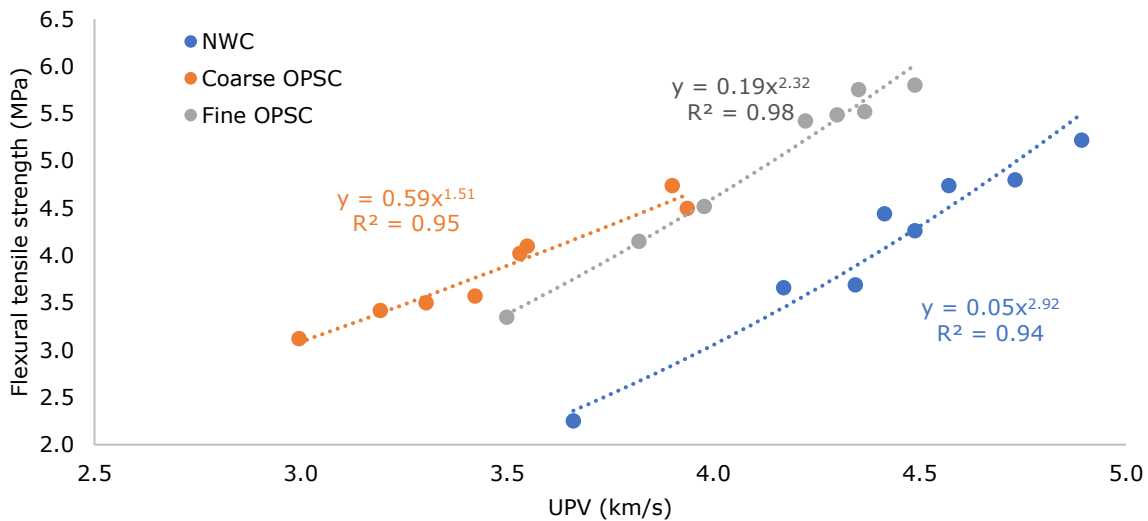
Figure 4.75 Flexural tensile strength and UPV relationship

4.3.4.2. Cured vs air cured regime

In this section, the air cured specimens are compared to the cured specimens from the previous section with respect to their flexural tensile strength, relationship between flexural tensile strength and compressive strength, and UPV analysis.

Flexural tensile strength

A comparison for the cured and air cured flexural tensile strength specimens for the NWC, coarse, and fine OSPC have been plotted separately in Figure 4.76 (a), (b), and (c), respectively, and the three cured and air cured concretes are compared in Figure 4.79 (a) & (b), respectively.

163
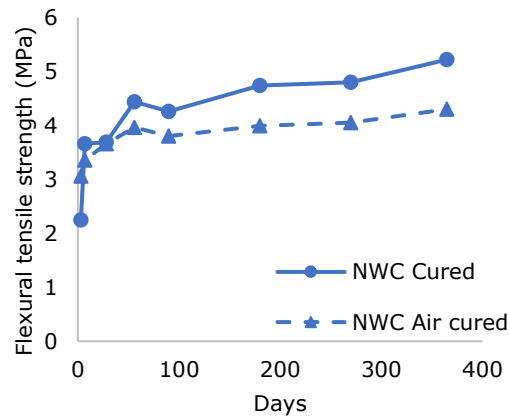
(a)
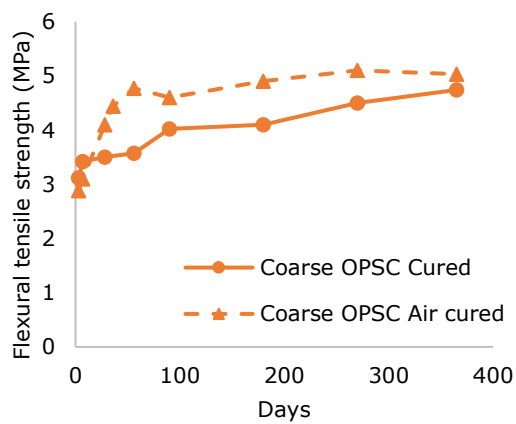
(b)
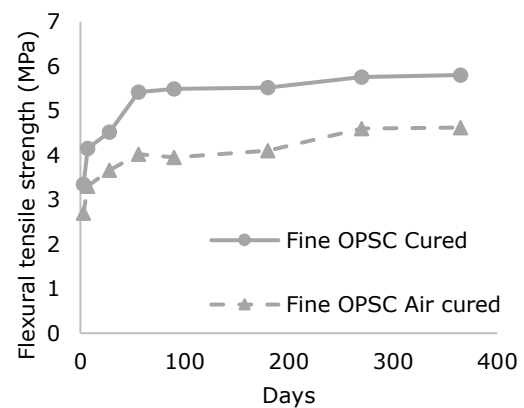
(c)

Figure 4.76 Cured vs air cured flexural tensile strength for (a) NWC, (b) coarse OPSC, and (c) fine OSPC

The air cured NWC showed flexural tensile strengths from 3.06 – 4.30 MPa compared to the cured specimens resulting in 2.25 – 5.22 MPa from 3 – 365 days. However, the NWC showed trivial differences between the cured and air cured results up to 28 days. Though, from 28 days onwards, an average of 12% difference was observed up to 365 days, therefore showing that cured specimens performed better as expected. The average difference from 3 – 365 days was only 5%.

The air cured fine OSPC resulted in strengths from 2.70 – 4.62 MPa compared to 3.35 – 5.80 MPa for the cured specimens. Therefore, showing that the fine OPSC is more sensitive to air cured regimes compared to the NWC, by showing an average difference of 22% from 3 – 365 days and 23% from 28 – 365 days. The lack of moisture, as show in Section 4.3.1, and lack of bonding mechanism between the cement and F-OPS due to presence of void space as shown in Section 4.2, is probably the main contribution to the lower strength in the air cured regime.

Nevertheless, the coarse OSPC exhibited a higher flexural tensile strength exposed to an air cured regime compared to a cured regime. The air cured specimens were 11% higher compared to cured specimens from 3 – 365 days and 17% higher from 28 -365 days. Considering the results from the NWC and fine OPSC, this seems unexpected. However, by bearing in mind that OPS has a similar composition to wood, it is known to be weaker in strength and more ductile when it is in a moisture state (Pestka, et al., 2018). This could therefore explain the lower strength of the specimens exposed to cured regime with the presence of high moisture. Consequently, this therefore could explain the OPS being stiffer in an air cured regime and subsequently result in higher flexural tensile strength. In other words, picture the C-OPS as a hook reinforcement in the concrete. Where the dry C-OPS is expected to be strong and stiff (i.e., not easily bendable), will obviously allow for a stronger hooking mechanism, consequently showing higher flexural tensile strength. Whereas a wet or damp C-OPS in the concrete would be a bendable and slippery material not aiding in the flexural tensile strength. This behaviour can also be seen from images taken of the prism samples of the coarse OPSC in Figure 4.77. The images depict the failure mechanism of the coarse OPSC under flexural loading. This failure mechanism perception is better illustrated in Figure 4.78.

In addition, the weaker wet/damp C-OPS, due to moisture presence, is could also be related to the white-rot fungi, explained earlier in Section 4.3.1. By the decaying effect, the C-OPS loses its integral strength.
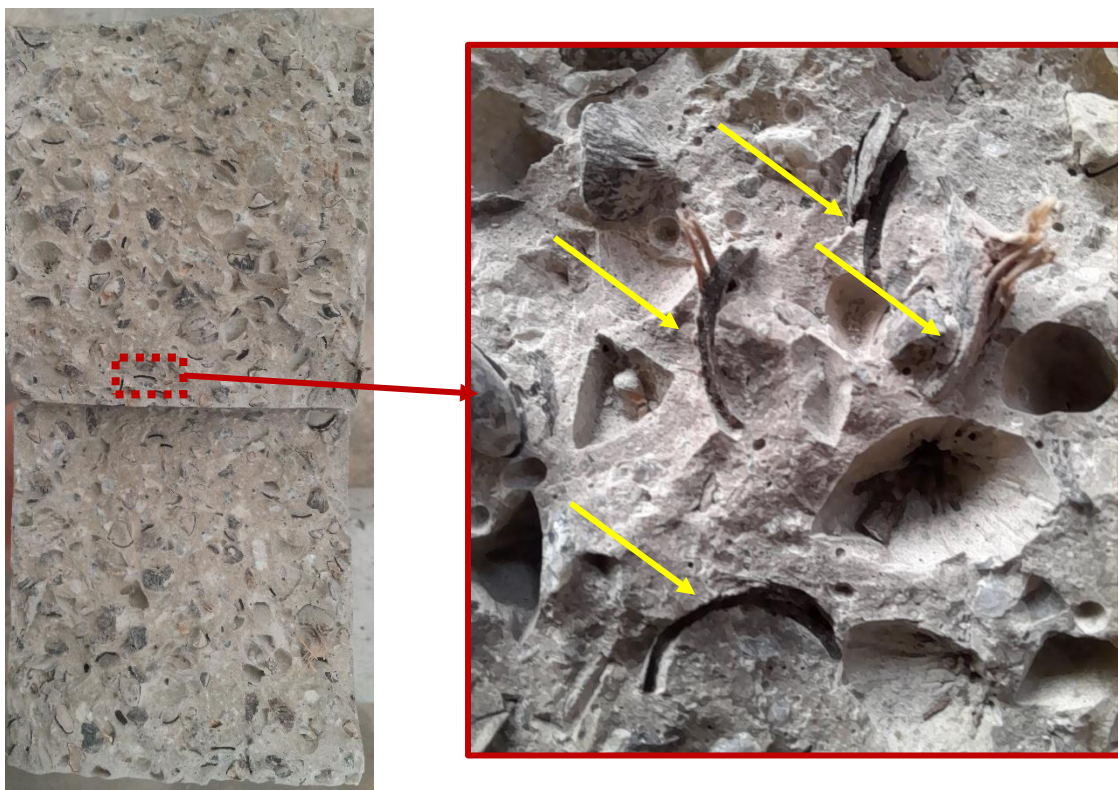
Figure 4.77 Flexural tensile strength failure mechanism of air cured coarse OPSC
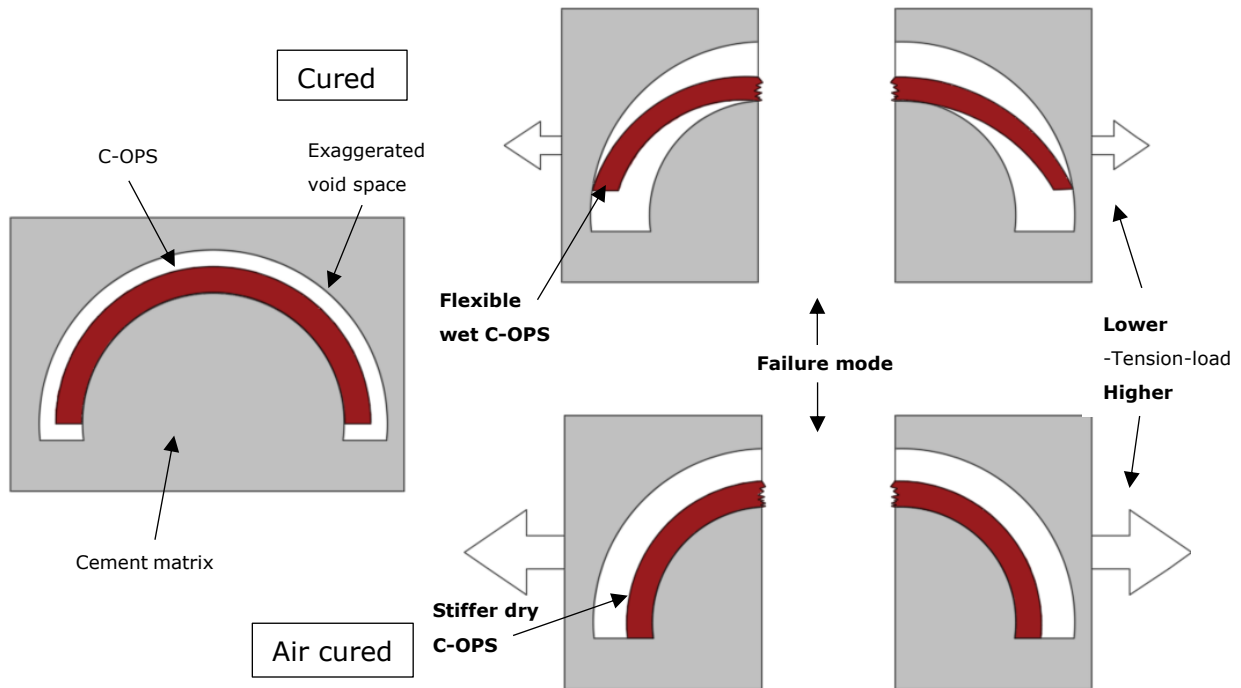
Figure 4.78 Schematic illustration of hooking mechanism of C-OPS in coarse OSPC under tensile load and failure mode for cured vs air cured specimens

As for the comparison between the three concretes, opposed to the cured specimens, the coarse OPSC outperformed both the NWC and fine OSPC by 17% and 9% between their strengths at 365 days, see Figure 4.79 a & b.

Although both the NWC and fine OPSC developed a higher early strength than the coarse OPSC up to 7 days, both reduced in their development at 56 days. However, the coarse OPSC continued to grow in strength up to 56 days being 12% and 11% higher than the NWC and fine OPSC, respectively, and significantly declining in strength development afterwards. The lower strength development for the coarse OPSC in the early ages could be that the C-OPS was still damp/wet, and as it got drier, it gained strength. The higher strength for the coarse OPSC may be due to:

- the advantage of its internal curing.

- no rotting due to absence of high moisture.

- the C-OPS acting as a hooking mechanism functioning as a reinforcement.

Nevertheless, it can therefore be concluded that fine OPSC performs similar to NWC in an air cured environment compared to a cured regime, where coarse OPSC exhibits higher flexural tensile strength in an air cured regime compared to cured.

166

(a)   (b)
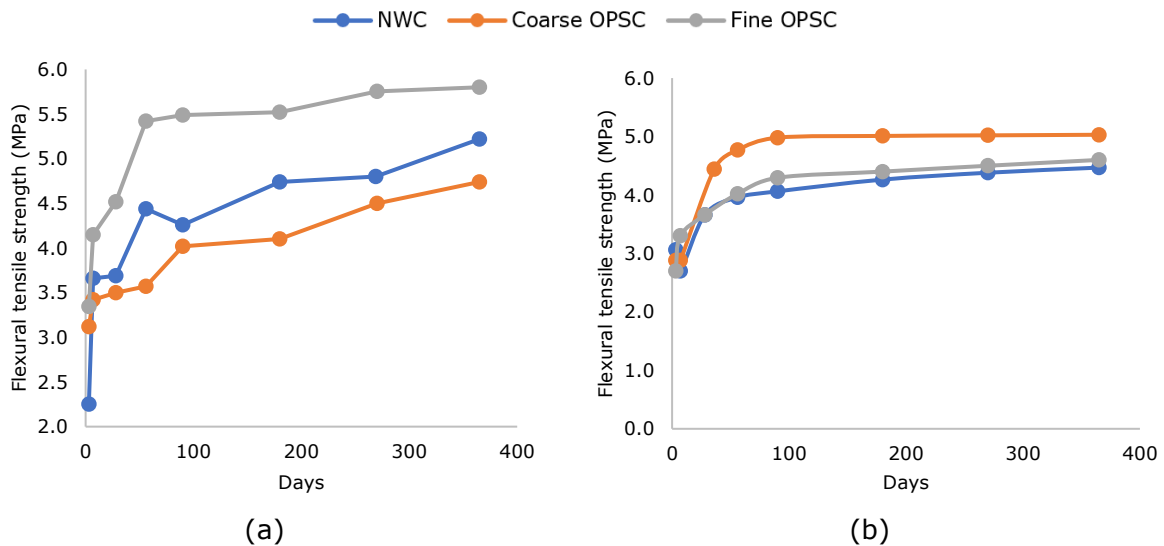
Figure 4.79 Flexural tensile strength of (a) cured and (b) air cured NWC, coarse, and fine OPSC

Flexural tensile strength and compressive strength relationship

In the case of the air cured specimens compared to the cured specimens, the coarse OPSC demonstrated a steeper line with a higher accuracy in the relationship as seen Figure 4.80. This was mainly due to the higher flexural tensile strength exhibited in the air cured regime for the coarse OPSC. Nevertheless, a more accurate relationship was shown for the air cured specimens with a coefficient of correlation factor (R^2) of 0.89, 0.93, and 0.95, hence, again, the strongest correlation with fine OSPC.

(a)   (b)
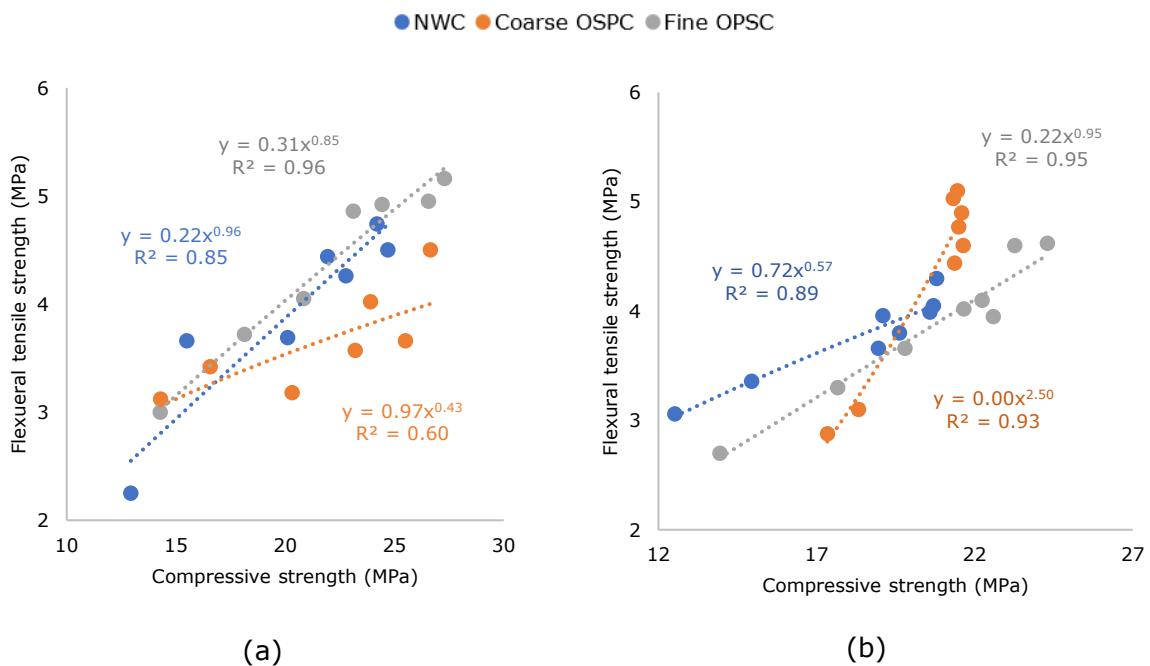
Figure 4.80 Flexural tensile strength and compressive strength relationship for the (a) cured and (b) air cured concretes

167

UPV analysis

The UPV results for the cured and air cured specimens are shown in Figure 4.81 (a) & (b), respectively, and plotted against the flexural tensile strength in Figure 4.82 (a) & (b), respectively.

(a)   (b)
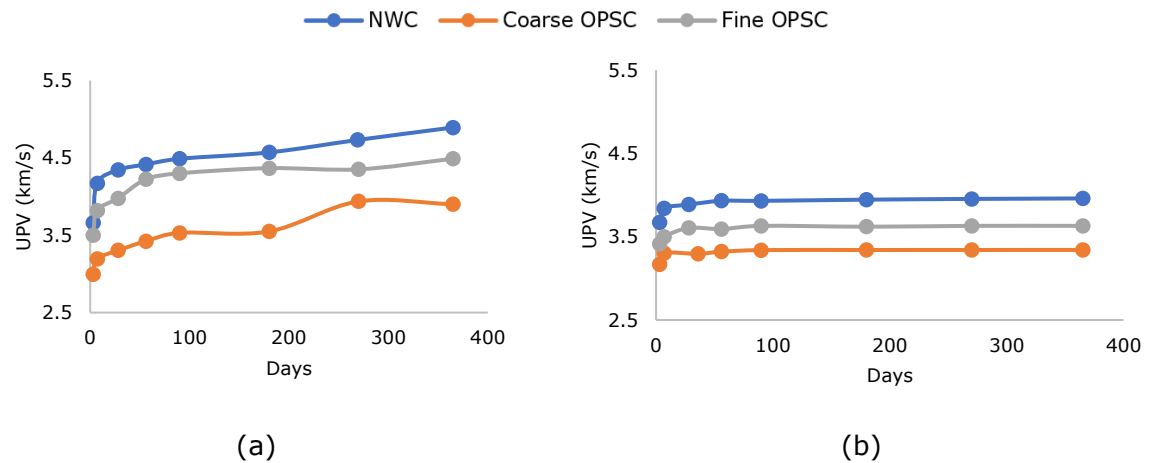
Figure 4.81 UPV results for the flexural tensile specimens, (a) cured and (b) air cured

A significant difference is observed between the cured and air cured graphs. The UPV values of the air cured specimens were found to be between 3.67 – 3.96 km/s, 3.17 – 3.34 km/s, and 3.42 – 3.63 km/s for the NWC, coarse, and fine OPSC between 3 – 365 days, respectively, indicating an increase of only 6 – 8%. While the cured NWC, coarse, and fine OPSC increased by 34%, 30%, and 28% from 3 – 365 days. This behaviour in the difference between the cured and air cured specimens was also observed for the compressive strength specimens in Section 4.3.3.2, therefore a similar conclusion can be derived for this investigation. To recall, this was mainly attributed to the absence of moisture for hydration. The lack of hydration process discontinues the closing-in on the pores, thus showing slower/lower UPV values. To note, the difference between the UPV results of concretes in the air cured specimens is similar to the cured specimens, where the NWC shows the highest followed by fine OPSC and coarse OPSC as last.

Nevertheless, the accuracy of the relationship between the flexural tensile strength and the UPV values for the air cured specimens show a coefficient of correlation factor (R^2) of 0.63, 0.61, and 0.89 for the NWC, fine, and coarse OPSC, respectively, indication a lower accuracy than that of the cured specimens.

168
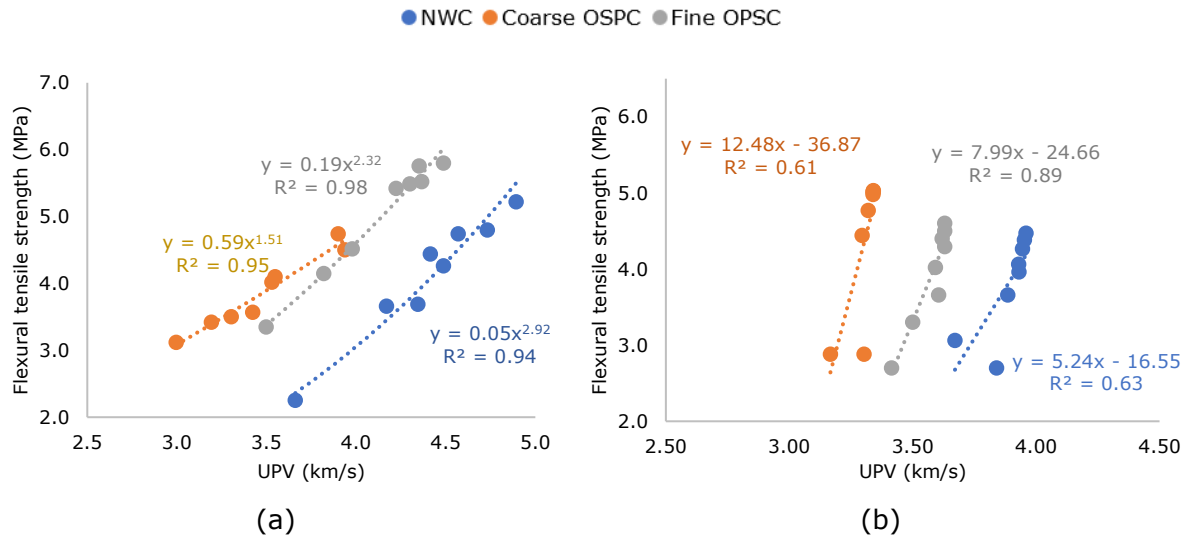
Figure 4.82 Relationship between the flexural tensile strength and UPV for (a) cured and (b) air cured concretes

4.3.4.3.   Concluding remarks

The flexural tensile strength of NWC, coarse, and fine OSPC was tested under both curing and air curing regimes up to 365 days. Overall, the results show that the fine OPSC exhibits the highest flexural strength when exposed to a cured regime, while the coarse OPSC shows the highest flexural tensile strength exposed to an air cured regime.

For the cured specimens, it was mainly concluded that the fine OPSC achieved the highest strength mainly due to the fact it contained he highest crushed coarse aggregate, which is known to have a good bonding mechanism with the binding material. The fine OPSC reached a strength of 5.8 MPa at 365 days being 11% and 22% higher than the NWC and coarse OPSC, respectively.

As for the coarse OPSC, an opposing comparison in flexural tensile strength to the other concretes between the cured and air cured specimens was observed. The probable reasons for such behaviour were that the drier or not moist C-OPS serves as a stronger anchoring material in the concrete under air curing conditions, owing to its non-susceptibility to rotting and stiffness in the absence of high moisture. The absence of high moisture (i.e., placed in a curing tank), allows the C-OPS to work as a reinforcement due to its shape. Conversely, no such difference was observed with F-OPS in fine OPSC, attributable to its distinct shape.

In addition, this study established good correlations between flexural tensile strength, compressive strength, and UPV, see Table 4.23. Nonetheless, the NWC, coarse, and fine OSPC revealed flexural tensile strength ranges as shown in Table 4.24. From Table 2.7, it was shown that previous studies obtained flexural tensile strengths in the range of 2.13 - 4.90 MPa for cured specimens, therefore similar to the results of this study.

169

Table 4.23 Flexural tensile strength and compressive strength relationship

Flexural tensile strength vs Compressive strength				
	Cured		Air cured	
Type		R^2		R^2
NWC	$\sigma_f = 0.2\, f_c^{0.99}$	0.90	$\sigma_f = 0.72\, f_c^{0.57}$	0.89
Coarse OPSC	$\sigma_f = 0.69\, f_c^{0.56}$	0.79	$\sigma_f = 0.01\, f_c^{2.50}$	0.93
Fine OSPC	$\sigma_f = 0.38\, f_c^{0.83}$	0.96	$\sigma_f = 0.22\, f_c^{0.95}$	0.95
Flexural tensile strength vs UPV				
NWC	$\sigma_f = 0.05(UPV)^{2.92}$	0.94	$\sigma_f = 5.24(UPV) - 16.55$	0.63
Coarse OPSC	$\sigma_f = 0.59(UPV)^{1.51}$	0.95	$\sigma_f = 12.48(UPV) - 36.87$	0.61
Fine OSPC	$\sigma_f = 0.19\,(UPV)^{2.32}$	0.98	$\sigma_f = 7.99(UPV) - 24.66$	0.89

$\sigma_f = Flexural\ tensile\ strength\ (MPa)$
$f_c = Compressive\ strength\ (MPa)$
$UPV = Ultrasonic\ pulce\ velocity\ (km/s)$

Table 4.24 Flexural tensile strengths from 3 – 365 days

Type	Flexural tensile strength (MPa)	
	Cured	Air cured
NWC	2.25 – 5.22	3.06 – 4.30
Coarse OPSC	3.12 – 4.74	2.88 – 5.03
Fine OSPC	3.35 – 5.80	2.70 – 4.62

4.3.5. Modulus of Elasticity

In this investigation, two types of MOE's are discussed for the three types of concretes in this study from ages up to 365 days. The first method comprises the dynamic MOE and the second method includes static MOE in Section 4.3.5.1 and 4.3.5.2, respectively.

In engineering design phases, the static MOE is of great importance, though the dynamic MOE through an NDT shows higher values. A relationship between the two methods can be used for field inspections. Therefore, the relationship between dynamic and static MOE is discussed in Section 4.3.5.3. Also, certain prediction models, presented in Section 2.2.7, are compared with the empirical values for the three types of concretes in this study in Section 4.3.5.4.

4.3.5.1. Dynamic modulus of elasticity

The Dynamic MOE was tested with cured and air cured specimens with the results shown in Figure 4.83. The results are discussed in the coming sub-sections for the cured, air cured, and the relationship between the Dynamic MOE and compressive strength.
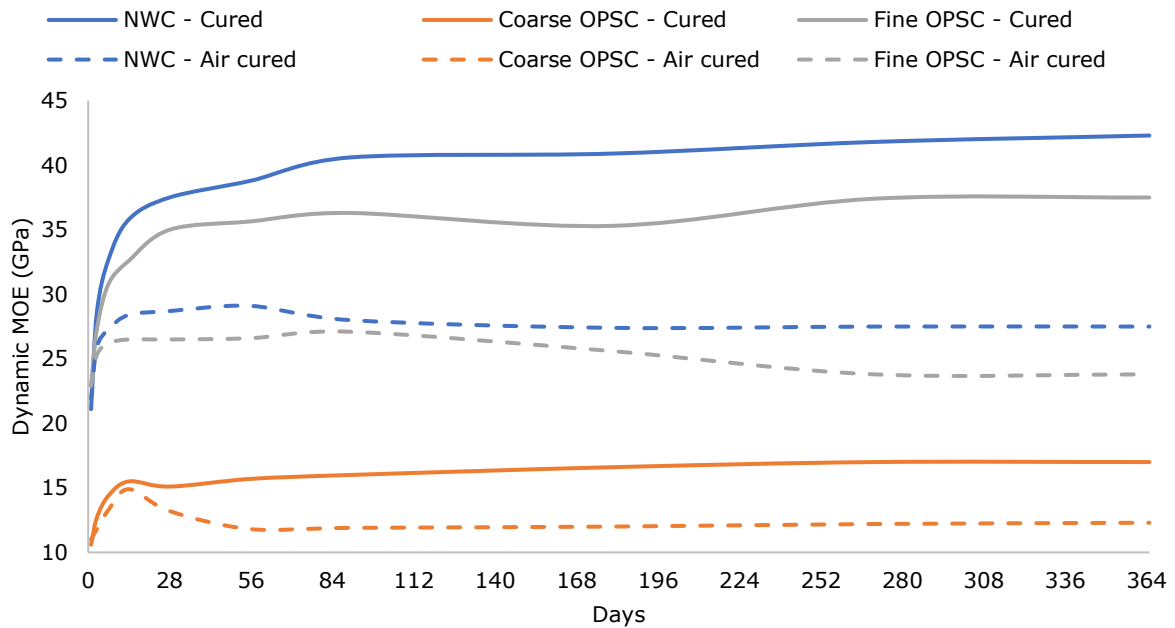
Figure 4.83 Dynamic MOE of the (a) cured and (b) air cured specimens

Cured regime

The NWC resulted in the highest values followed by the fine OPSC and the coarse OSPC with the lowest values. The fine OPSC showed slight lower values to the NWC with an average difference of 10%, where coarse OSPC showed a significant higher difference of 59% in average from 1 – 365 days. However, the Dynamic MOE of the coarse and fine OPSC seemed to cease at 14 and 28 days, respectively, whereas the NWC ceased at 90 days. Therefore, by considering the difference between the maximum values, the fine and coarse OPSC showed a difference of 11% and 60% to the NWC, respectively. The average Dynamic MOE over a period from 1 – 365 days were found to be 37.9, 15.6, and 34.2 GPa with peak values at 365 days of 42.3, 17.0, and 37.5 GPa for the NWC, coarse, and fine OSPC, respectively. In general, these comparisons are expected. this is mainly attributed to the type of aggregate used in the different concretes. Where the NWC uses both the conventional fine and coarse aggregate, higher results are expected. Where the difference between the fine OPSC and coarse OPSC is mainly attributed to the use of the conventional coarse aggregate in the fine OPSC making the concrete stiffer.

Cured vs air cured regime

As expected, the NWC, coarse, and fine OSPC exposed to an air cured regime showed a lower Dynamic MOE compared to the cured by 22.5%, 16.1%, and 21.6% in average from 1 – 365 days, respectively. Notable, the fine OPSC shows a similar reduction as the NWC. The difference between the coarse and fine OSPC to the NWC was quite similar to the cured specimens being 56% and 7% lower in value, respectively. Nevertheless, the fine OSPC was 120% and 108% higher than the coarse OPSC in the cured and air cured regimes,

respectively. Also noteworthy is that the three concretes seemed to decline in values after 56, 14, and 90 days by 5%, 17%, and 12% for NWC, coarse, and fine OPSC, respectively.

The sudden decline is most probably due to their weight loss caused by the evaporation of their internal moist, see Figure 4.84. Where the NWC, coarse, and fine OSPC ceased in weight change after 56, 90, and 56 days, respectively. The decline in the Dynamic MOE of the air cured concretes could be attributed to insufficient water availability for complete cement hydration. The rapid evaporation of water from the concrete surface contributes to its shrinkage, which results in tensile stresses in the internal structure and consequently induces the formation of microcracks. These microcracks exert a detrimental effect on the physical and mechanical properties of the concrete, thus reducing its durability, quality, and modulus of elasticity (Kocab, et al., 2017). The effect of the shrinkage of the concretes is further discussed in Section 4.3.6, with the coarse OPSC showing the highest shrinkage, thus reflected by the lowest value in Dynamic MOE.
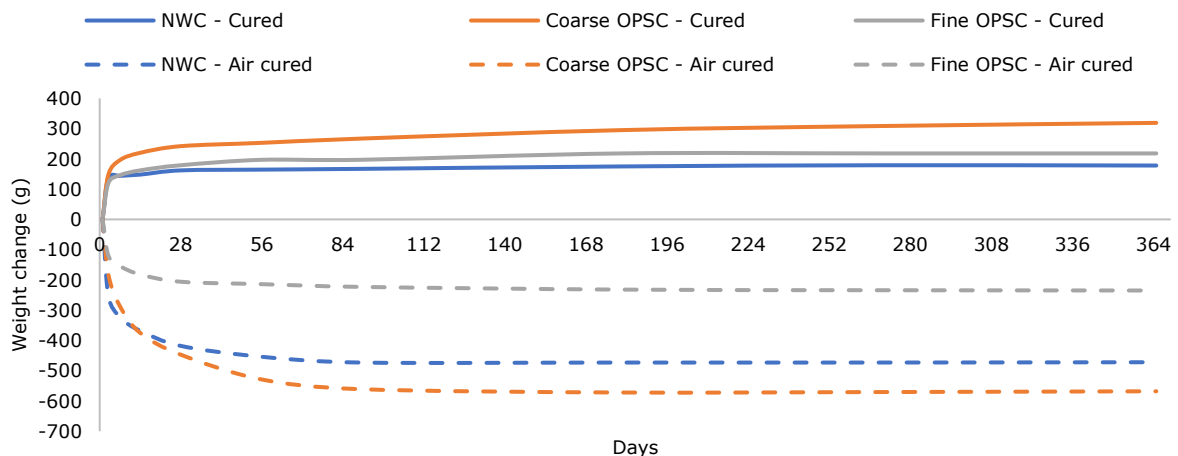
Figure 4.84 Weight change of cured and air cured D-MOE specimens

Relationship Between dynamic MOE and compressive strength

Strong correlations between the cured dynamic MOE and compressive strength were found with a coefficient of correlation factor (R^2) of 0.98, 0.97, and 0.90 for NWC, coarse, and fine OSPC, respectively, see Figure 4.85 (a) and Table 4.25. The steepest line observed for the cured coarse OSPC simply shows that its compressive strength development is higher than its dynamic MOE. This could indicate that little improvement over time is shown in the bonding mechanism between the cement matrix and the C-OPS aggregate.

Low coefficient of correlation factors with non-linear correlations were found for the NWC, coarse, and fine OSPC for the air cured specimens with R^2 values of 0.66, 0.31 and 0.53, respectively, see Figure 4.85 (b). However, the low regression for the coarse OPSC is most likely attributed to the high shrinking affect, as explained earlier.

172
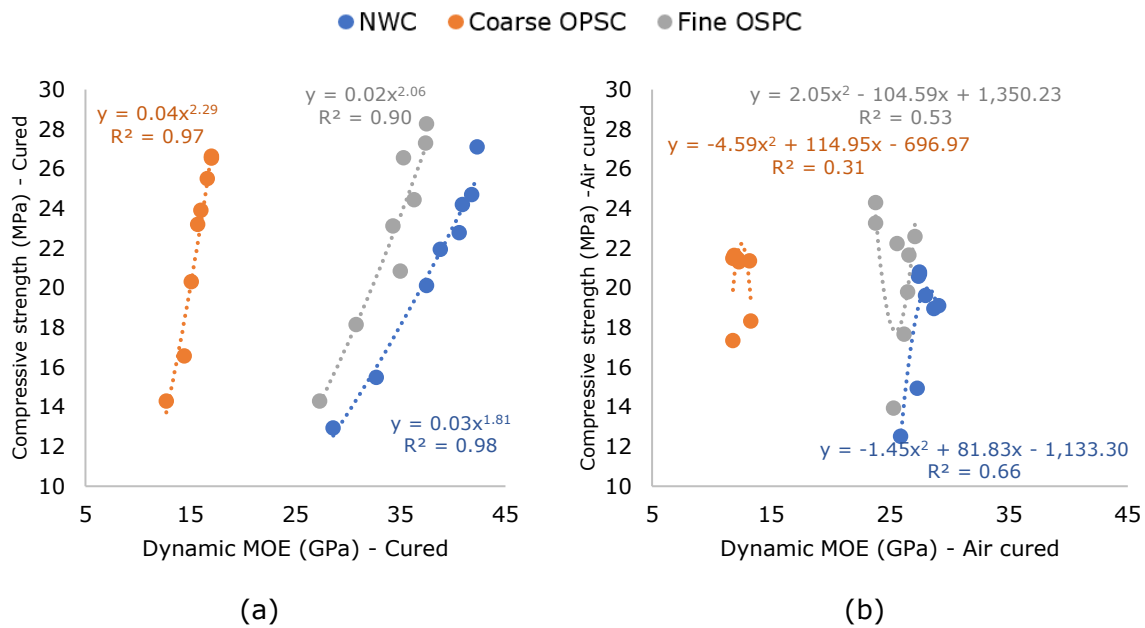
Figure 4.85 Relationship between compressive strength and Dynamic MOE with (a) cured and (b) air cured specimens

Table 4.25 Relationship between compressive strength and dynamic MOE

	Cured		Air cured	
Type		R^2		R^2
NWC	$f_c = 0.03E_d^{1.81}$	0.98	$f_c = -1.45x^2 + 81.83x - 1133.3$	0.66
Coarse OPSC	$f_c = 0.04E_d^{2.29}$	0.97	$f_c = -4.56x^2 + 114.95x - 696.97$	0.31
Fine OSPC	$f_c = 0.02E_d^{2.06}$	0.90	$f_c = 2.05x^2 - 104.59x + 1350.23$	0.53

Where,
$E_d = Dynamic\ modulus\ of\ elasticity\ (GPa)$
$f_c = Compressive\ strength\ (MPa)$

4.3.5.2.   Static modulus of elasticity

The Static MOE was found for the cured and air cured specimens with the results plotted in Figure 4.86 (a) & (b), respectively. The following sub-sections will discuss the static MOE of the cured, air cured, and the relationship between the static MOE and compressive strength.

173
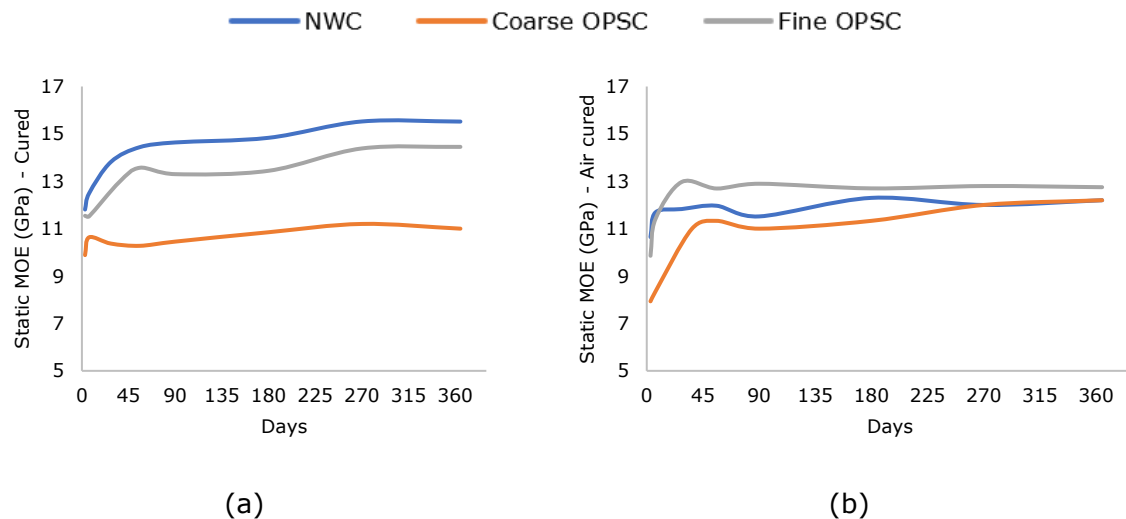
Figure 4.86 Static MOE of (a) cured and (b) air cured specimens

Cured regime

In general, the highest values were observed for the NWC followed by the fine OPSC and as last the coarse OSPC. Thus, showing a similar difference between the concretes as with their dynamic MOE. Though both the NWC and fine OPSC increased their static MOE value from 11 - 15 GPa from 3 – 365 days, the coarse OPSC performed similar in all ages with values between 10 - 11 GPa. One of the main factors influencing the MOE is the aggregate type and the void space between the cement matrix and aggregate (Neville, 1995). Since both the NWC and fine OPSC used the conventional crushed coarse aggregate, the similarity in results was therefore anticipated. Consequently, indicating that the use of tenera OPS as fine sized aggregate had little impact on the static MOE by only being 7% lower in average from 3 – 365 days than that of the NWC.

As for the coarse OPSC, the average static MOE from 3 – 365 days was measured to be 25% and 20% lower than that of the NWC and fine OSPC, respectively. The higher difference of the coarse OPSC, compared to the fine OSPC, than that of the NWC is most probably due to the similar explanation given in Section 4.3.3. To recall, a similar illustration as Figure 4.58 is redrawn in Figure 4.87 (a) & (b) for before loading and during loading only, respectively. The illustration shows that initial cracks start to propagate around the C-OPS due to the void space and continue when reaching the C-OPS. This internal cracking of the cement matrix surrounding the C-OPS cause high deflections and therefore reduce the slope of the stress-strain, thus consequently lowering the static MOE value. From the stress-strain graphs in Section 4.3.3.1 it was also found that a sudden decline in the line was found after 20 – 30% of the ultimate load. Therefore, by following the methodology from the (BS EN 12390-13, 2021), the upper applied load is a third that of the maximum load or 33%. This therefore explains that the coarse OPSC already

174

endured microcracks before reaching a third of the maximum applied load in the static MOE experiment, thus explaining the lower values in static MOE.
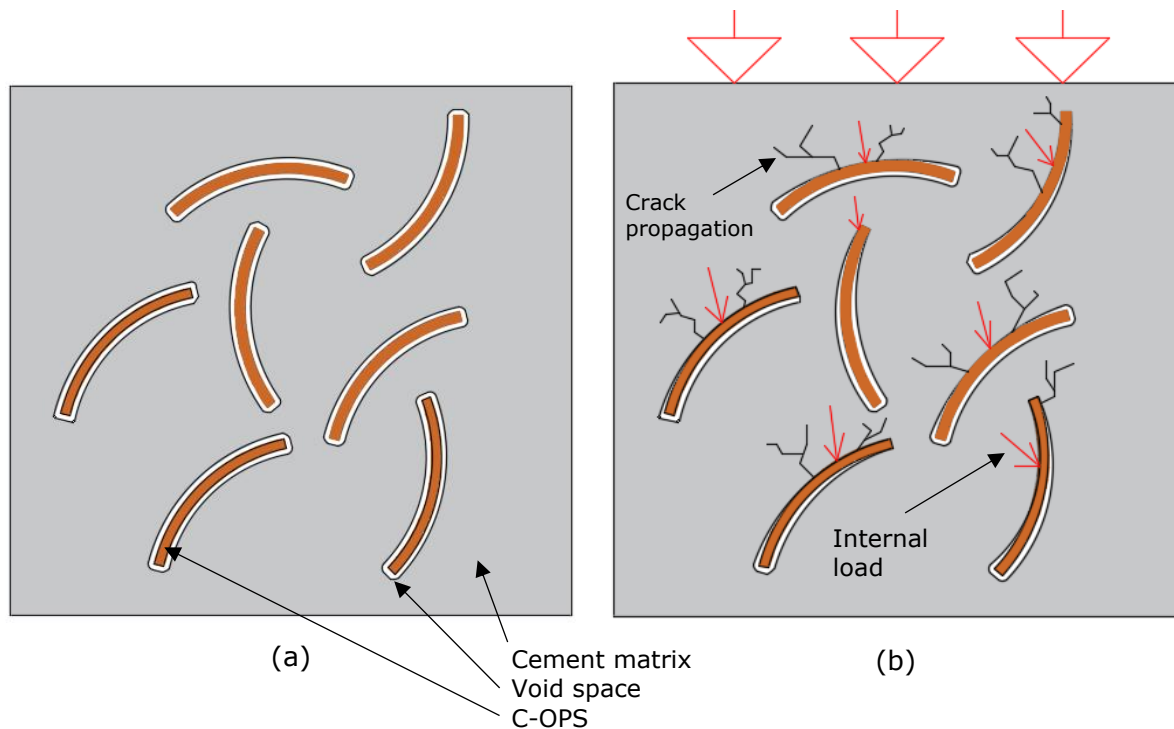
Figure 4.87 Illustration of coarse OPSC (a) before and (b) during loading similar to Figure 4.58

Cured vs air cured regime

For the air cured specimens, the NWC and fine OSPC showed lower static MOE results than that of the cured specimens by 17% and 7%, respectively, in average from 3 – 365 days, see Figure 4.86 (b). However, no difference was observed in average between the cured and air cured static MOE results for the coarse OPSC.

The highest static MOE at 365 days recorded for the air cured NWC, coarse, and fine OPSC was 12.30, 12.20, and 12.97 GPa. Although the coarse OSPC showed the lowest value of around 8 GPa at 3 days, it rapidly increased to almost 13 GPa at 365 days.

It can therefore be concluded that both the OSPCs are less sensitive to air cured conditions compared to the NWC. A similar explanation from the previous sections can be given for this case, mainly attributed to the internal curing effect of the OSPCs, allowing the concretes to develop higher strengths in air cured regimes compared to NWC.

Relationship between static MOE and compressive strength

The relationship between static MOE and compressive strength has been plotted in Figure 4.88 (a) & (b) for the cured and air cured regime, respectively, with the correlation formulas shown in Table 4.26. Acceptable coefficient of correlation factors was found with the cured NWC and fine OPSC by having an R^2 of 0.98 and 0.87, respectively. However,

though the coarse OPSC showed a lower accuracy with an R^2 of 0.55 in the cured regime, a higher accuracy was shown in the air cured regime with and R^2 of 0.91 with the fine OPSC showing a quite similar correlation. However, the NWC had a lower correlation with an R^2 of 0.75.

(a)   (b)
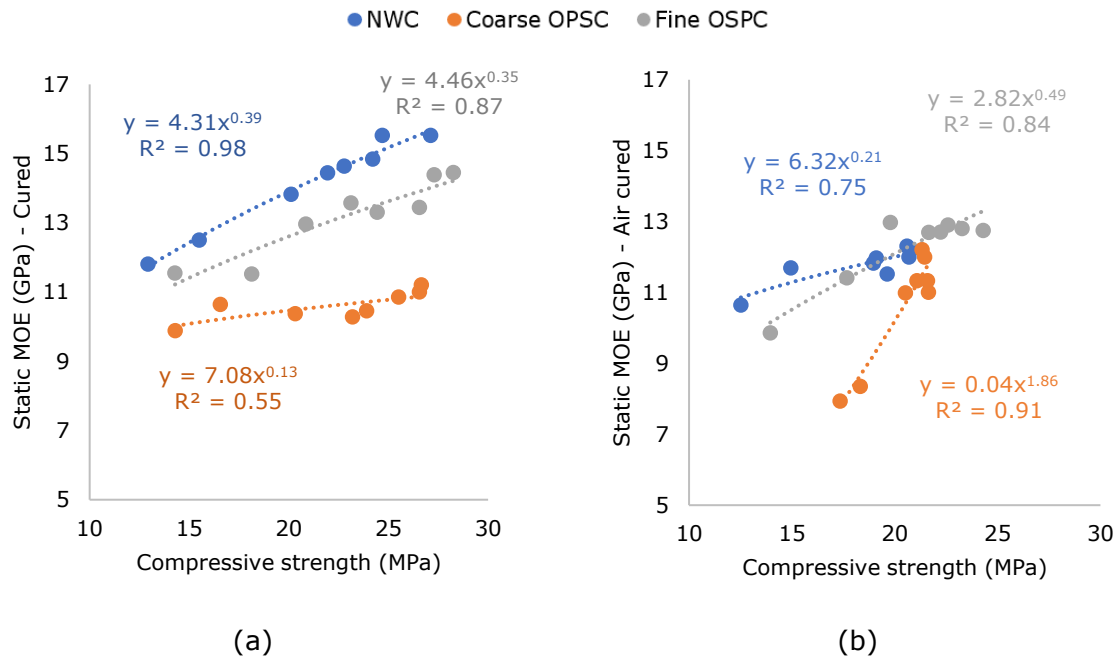
Figure 4.88 Relationship between Static MOE and compressive strength with (a) cured and (b) air cured specimens

Table 4.26 Relationship between Static MOE and compressive strength

Type	Cured		Air cured	
		R^2		R^2
NWC	$E_s = 4.31f_c^{0.39}$	0.98	$E_s = 6.32f_c^{0.21}$	0.75
Coarse OPSC	$E_s = 7.08f_c^{0.13}$	0.55	$E_s = 0.04f_c^{1.86}$	0.91
Fine OSPC	$E_s = 4.46f_c^{0.35}$	0.87	$E_s = 2.82f_c^{0.49}$	0.84

$Where,$
$E_s = Statis\ modulus\ of\ elasticity\ (GPa)$
$f_c = Compressive\ strength\ (MPa)$

4.3.5.3.   Relationship between dynamic and static modulus of elasticity

From the results in this study, it was shown that the dynamic MOE values did match that of the static MOE, as expected. Therefore, an attempt was made to establish a relationship between the dynamic and static MOE of the concretes in cured and air cured regimes seen in Figure 4.89 (a) & (b), respectively. This was done with regression techniques to correlate the coefficients.

In the case of the cured specimens, acceptable coefficient of correlation factors was found with R^2 of 0.98, 0.86, and 0.71 for the NWC, coarse, and fine OSPC, respectively. Thus,

showing that the lowest correlation is with the coarse OPSC. However, the air cured NWC, coarse, and fine OSPC showed lower correlations with R^2 of 0.69, 0.57, and 0.41, respectively.

(a)   (b)
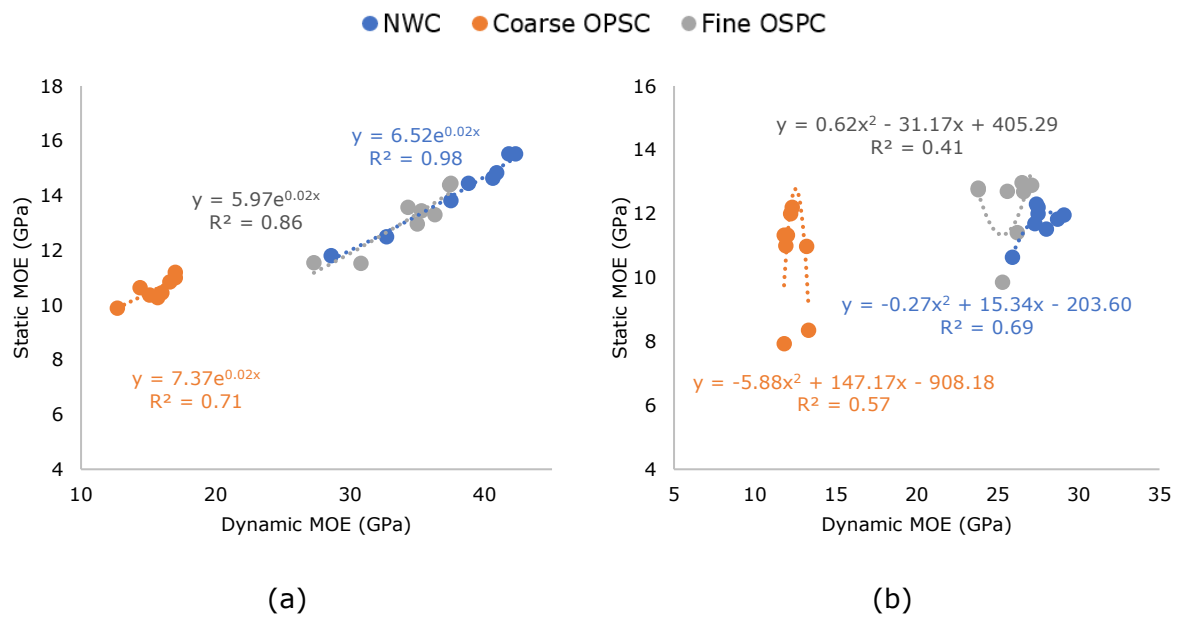
Figure 4.89 Static vs. dynamic MOE of (a) cured and (b) air cured specimens

While all three concretes showed a linear increment with roughly 45 degrees for the cured specimens, no such linearity were shown for the air cured specimens, especially for the OPSCs. This goes in agreement with the results of the previous sections, while an increase was shown in the static MOE, no change to an even decrease as observed in the dynamic MOE of the concretes, especially in the case of the coarse OPSC.

The difference between the static to dynamic MOE for the concretes is shown in Figure 4.90. While the NWC and fine OSPC show relatively the same difference for the cured and air cured regimes, the coarse OPSC shows roughly double that of the NWC.
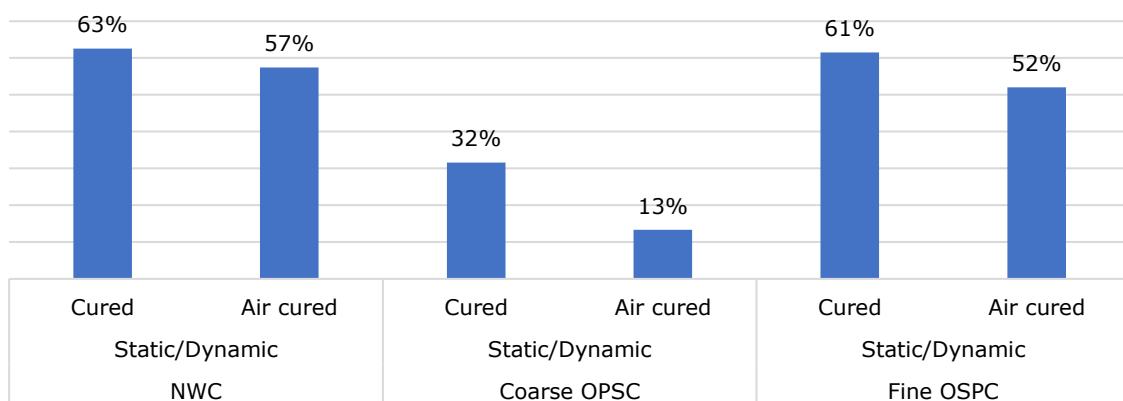
Figure 4.90 Difference between the static to dynamic MOE of the concretes

177

4.3.5.4. Prediction models - Static modulus of elasticity

In this investigation, the MOE prediction models mentioned in Section 2.2.7, proposed by (ACI Committee 213R-14, 2014), (BS EN 1992-1-1, 2014), and (Alengaram, et al., 2011a) were used and compared to the empirical values obtained from this study. Given that both the ACI and BS codes use different formulas for NWC and that Alengaram's model is only intended for OPSC, the NWC form this study was therefore excluded.

The Static MOE of the OPSCs along the predicted results from the three models are plotted in Figure 4.91 and Figure 4.92 for coarse and fine OSPC, respectively, along with the ratio of the predicted results, from the three models to the empirical values.

Days	ACI	BS	Alengaram et al.
3	92%	94%	84%
7	90%	92%	80%
28	91%	100%	90%
56	94%	101%	91%
90	95%	104%	94%
180	92%	100%	92%
270	90%	100%	92%
365	85%	99%	92%
Average	91%	99%	89%
Difference	-9%	-1%	-11%
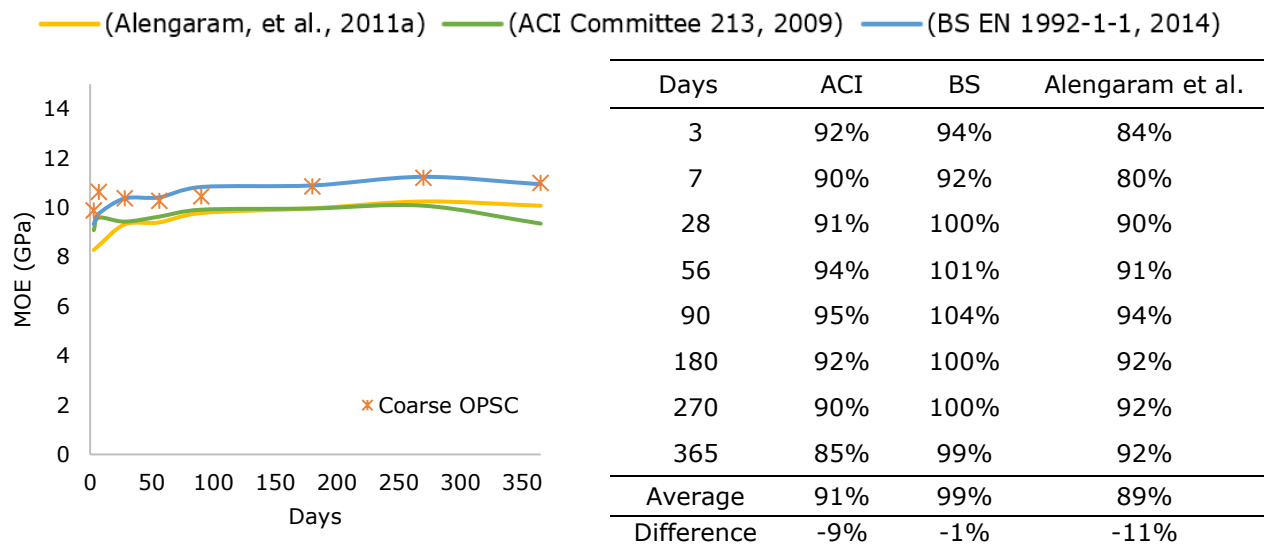
Figure 4.91 Static MOE of coarse OPSC with prediction models

In the case of the coarse OPSC, the ACI model under-predicted the static MOE by an average difference of 9% from 3 – 365 days, while only an average difference of 1% was shown with the BS model. The model proposed by Alengaram et al. under-predicted the values by an average of 11%. Therefore, the lowest average difference was 0.11 GPa with the model from the BS code compared to 0.95 GPa and 1.14 GPa from the ACI and Alengaram et al. models, respectively. The difference found for Alengaram's model is confirmative with the error value of ±1.5 GPa given by (Alengaram, et al., 2011a) and confirmed by (Foong, et al., 2015).

As for the fine OSPC, the ACI model under-predicting the empirical values by a high average of 22% from 3 – 365 days. Thus, showing a lower prediction accuracy with the ACI model compared with the coarse OPSC. Nonetheless, the models proposed by the BS code and Alengaram et al. showed much better prediction accuracies by having an average difference of 1% and 2%, respectively. Therefore, showing the lowest average difference

of 0.17 GPa by the BS model compared to 3.05 GPa and 0.24 GPa for the ACI and Alengaram's model, respectively.

To summarize, the BS model, compared to the ACI model, showed better predicted results, and had the highest accuracy for both the OPSCs. Though only for the fine OPSC, the model proposed by Alengaram et al. showed a higher accuracy then with the results of the coarse OPSC. The justification could be since the authors used mixed designs that had a similar w/c ratio as the fine OPSC of 0.35 and similar cement contents of between 465 – 596 kg/m^3, which is much lower than that of the coarse OPSC. In addition, it could also be due to the fact that Alengaram et al. used Dura OPS, which is known to be much stiffer than Tenera OSP.

Days	ACI	BS	Alengaram et al.
3	125%	100%	96%
7	133%	108%	101%
28	126%	100%	96%
56	115%	99%	96%
90	125%	102%	101%
180	123%	104%	102%
270	119%	98%	97%
365	113%	98%	96%
Average	122%	101%	98%
Difference	22%	1%	-2%
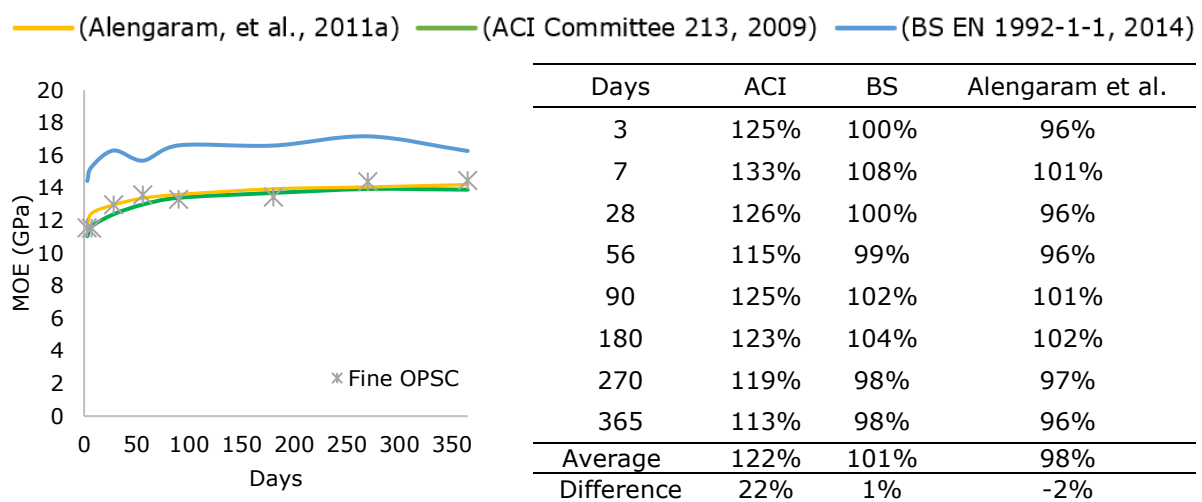
Figure 4.92 Prediction to empirical ratio for fine OSPC

4.3.5.5.   Concluding remarks

In this investigation the dynamic and static MOE were investigated on the concretes up to an age of 365 days. The concretes tested were exposed to cured and air cured regimes for comparison. Also, the static MOE was compared to the dynamic MOE in an attempt to establish a relationship. Furthermore, this was also done with both types of MOE's and their respective compressive strength in both curing regimes. In addition, prediction models proposed by the BS and ACI code as well as by Alengaram et al., were used to predict the concretes static MOE and were compared to the empirical values.

The average dynamic MOE of the concretes are shown in Table 4.27. The NWC and fine OSPC showed similar dynamic MOE while the coarse OPSC showed a value more than twice as low for the cured specimens in average over a span of one year. The air cured results were found to be lower than that of the cured results for the NWC and fine OPSC in average, except for the coarse OPSC no significant difference was observed. The dynamic MOE was found to decrease over time in the air cured regime for all three concretes. This was most

179

apparent for the coarse OSPC, mainly reasoned to be caused by the loss of internal water causing high shrinkage, creating microcracks and consequently reducing the dynamic MOE.

The results of the static MOE of the concretes displayed similar behaviours for the cured specimens. The average static MOE of the concretes are shown in Table 4.27. The results indicate that both the OPSCs are withing the recommended MOE values as per (FIP, 1983). However, when exposed to an air cured regime, the fine OPSC reached a slightly higher static MOE values at 365 days compared to the NWC. The coarse OPSC reached similar static MOE values at and after 270 days. This was mainly assumed to be caused by the internal curing effect in the OPSCs. An additional reason to the internal curing was that the C-OPS in the coarse OPSC was believed to be stiffer due to absence of moist, as was also deduced for its air cured compressive strength results in Section 4.3.3.2.

Among the ACI and BS codes for the prediction models, the BS model presented the highest accuracy for the OPSCs with average differences of 1% for both OPSCs. The ACI model under-predicted the coarse OPSC by an average 9% and over-predicted the fine OPSC by an average of 22%. As for the model proposed by Alengaram et al., it underpredicted the coarse and fine OPSC by 11% and 2% in average, respectively.

In brief, the different results in dynamic and static MOE of the concretes in study were mainly affected by various factors, including the difference in cement paste content, characteristics of aggregates, the interfacial transition zone, and concrete compaction (Neville, 1995). Both MOE's were also found to be influenced by the concrete age which is attributed to the stiffness of cement paste increasing over time (Silva, et al., 2016).

Table 4.27 Average MOE values of the concretes from 1 – 365 days

Type	Dynamic MOE (GPa)		Static MOE (GPa)	
	Cured	Air cured	Cured	Air cured
NWC	36.01	27.17	14.14	11.77
Coarse OPSC	15.06	12.44	10.58	10.64
Fine OPSC	32.94	25.43	13.15	12.26

4.3.6.   Drying Shrinkage

In this investigation, the drying shrinkage of the concretes were measured for up to one year. First, the drying shrinkage results of the concretes are compared and discussed followed by comparing the empirical results with prediction models and a concluding remark as last.

4.3.6.1.   Drying shrinkage concretes

Though, as discussed in Section 2.2.8, different curing ages were investigated for the drying shrinkage of OPSC by different authors, the three concrete types in this investigation were not cured so to simulate the worst-case scenario. However, the specimens were kept in a room environment which was withing the requirements specified in (BS ISO 1920-8,

2009). The resulting drying shrinkages up to 1 year for all the three concretes are plotted in Figure 4.93. Also, a semi-logarithmic plot of the same curves is shown in Figure 4.94.
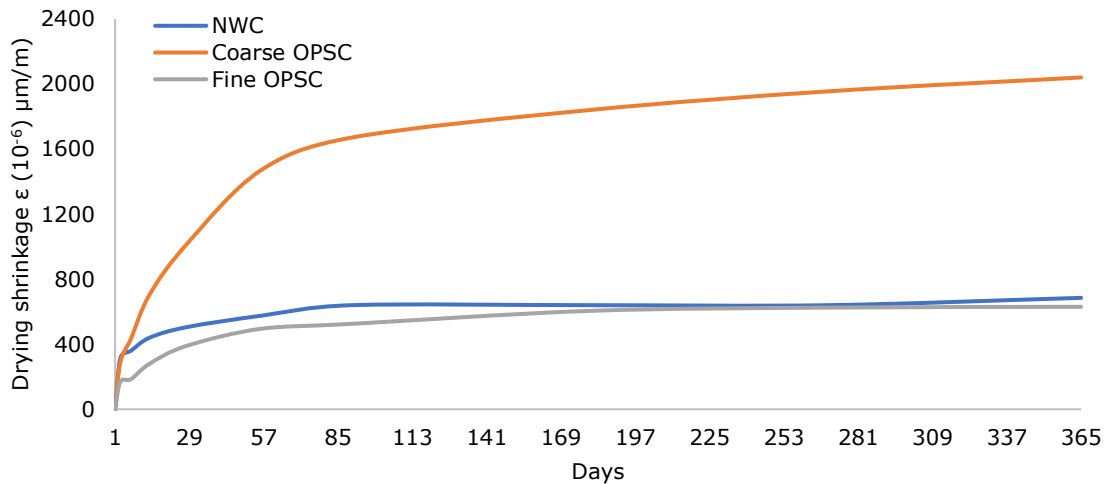
Figure 4.93 Drying shrinkage of concretes
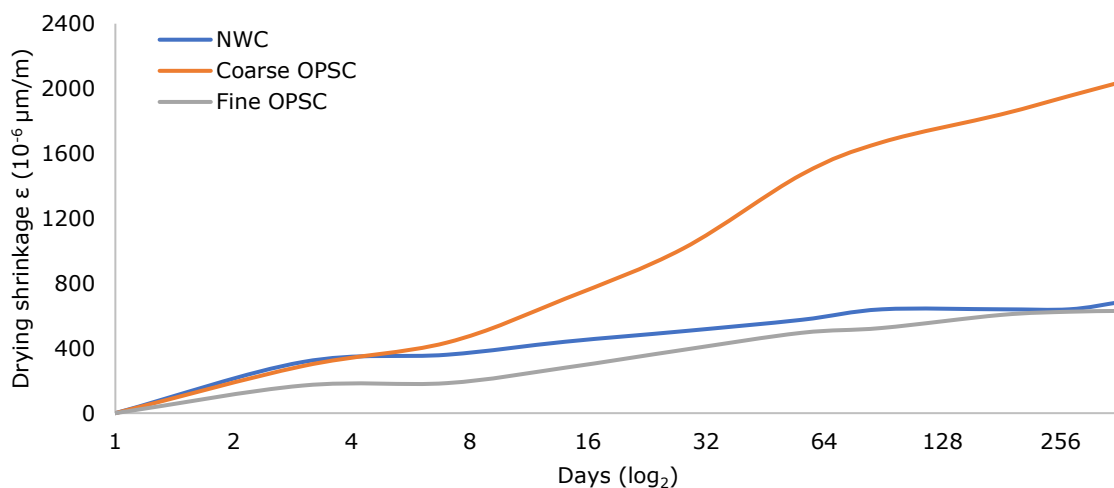
Figure 4.94 Semi-logarithmic plot of drying shrinkage of the concretes

Bearing in mind that all three concretes had similar 28 days grade strengths, similar drying shrinkage results were observed between the NWC and fine OPSC while, undoubtedly, the coarse OPSC displayed much higher results. Initially, the NWC and coarse OSPC reached similar drying shrinkage values around 400 x 10^{-6} µm/m up to 7 days, then the coarse OPSC continued shrinking, while the NWC gradually decreased reaching a shrinkage of 685 x 10^{-6} µm/m at 365 days. Thus, reaching typical NWC results by being between 400 – 700 x 10^{-6} µm/m (Li, 2011). Only the NWC and fine OSPC gradually ceased shrinkage after 7 days. On the other hand, the coarse OPSC continued shrinking rapidly up until 56 days having reached 72% of its 365 days shrinkage and gradually reduced at 90 days and onwards reaching a drying shrinkage of 2040 x 10^{-6} µm/m at 365 days. From Figure 4.94, it can be deduced that the coarse OPSC does not seem to cease shrinking even at 365

181

days. Due to time constraints of this research, further measurements were not possible, and therefore the author of this study highly recommends a studying the coarse OPSC for longer time range. Nevertheless, the fine OPSC resulted in a lower drying shrinkage by roughly 50% compared to both the NWC and coarse OPSC at 7 days and reached a drying shrinkage of 630 x 10^{-6} μm/m at 365 days. Although the fine OPSC was found to be 22% and 62% less in average from 1 – 365 days than the NWC and coarse OSPC, respectively, it reached 98% that of the NWC at 270 days, see Figure 4.95. From the figure below, it can also be seen that the coarse OPSC reached drying shrinkage values almost 3 times that of the NWC and fine OSPC at 365 days.
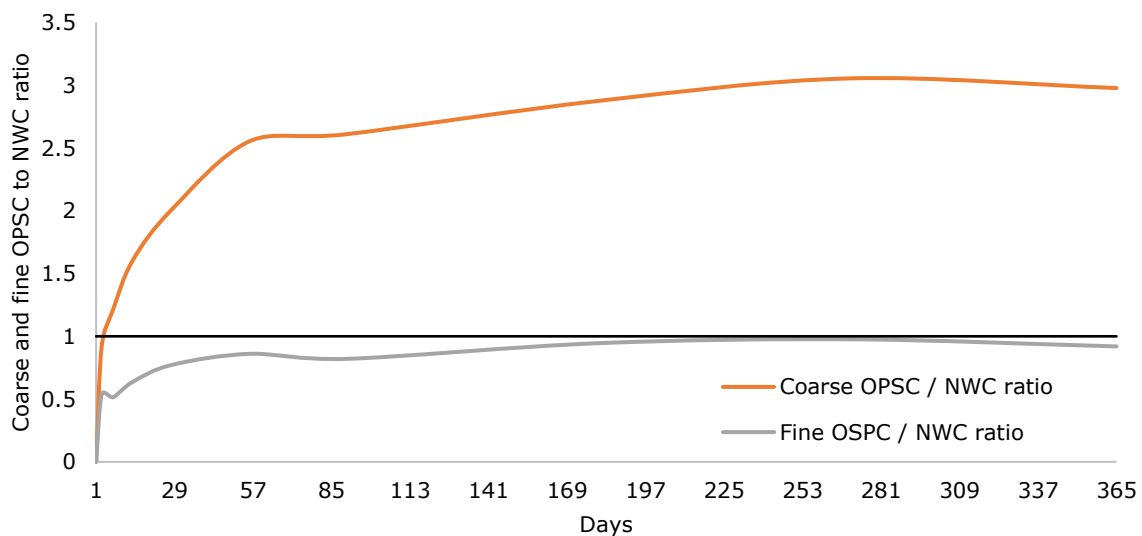
Figure 4.95 Coarse and fine OPSC to NWC drying shrinkage ratio over time

The rates of drying shrinkage of the concretes are plotted in Figure 4.96. It can be seen that the highest rate of drying shrinkage is for the NWC followed by fine OSPC and coarse OSPC as last. The rate of the drying shrinkage is influence by the amount of cement used, w/c ratio, aggregate size and type, and the exposed environmental conditions. Typically, concrete undergoes the highest amount of shrinking during the initial stages or early ages. In early ages, where the concrete is still quite weak, it contains high amounts of moisture. Subsequently, as the concrete loses it moisture over time and becomes stronger, the rate of shrinkage also slows down (Bentz, 2002). This explanation is apparent to the results of the concretes in this study. The lower rate for the coarse OPSC can be attributable to the higher amount of moisture presence as was shown in Section 4.3.1. As for the type and size aggregate, the low strength and shape of the C-OPS would allow for more volume change as there would be a less efficient packing of the particles as compared to the NWC and fine OPSC (Newman, 1993).
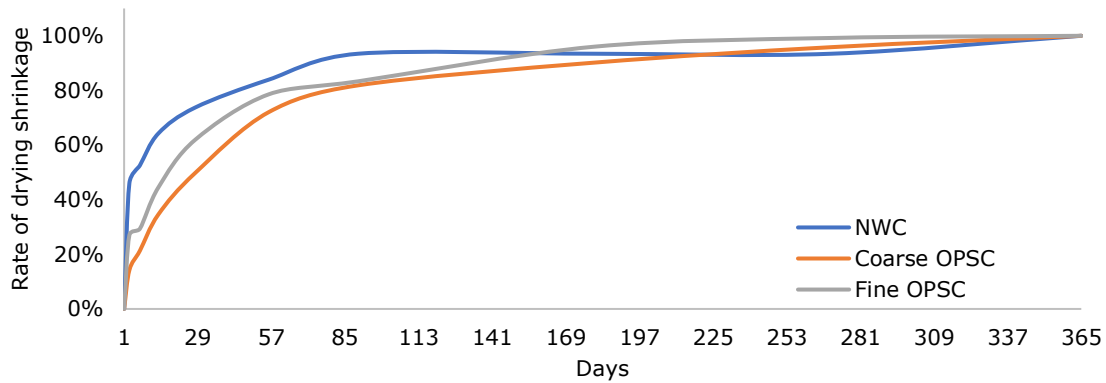
Figure 4.96 Rate of drying shrinkage of the concretes over time

According to (FIP, 1983), the shrinkage of LWC is in general approximately 50% greater than that of NWC. However, this is probably only with the conventional lightweight aggregates such as expanded clay, shale, vermiculite, etc. The low shrinkage of the fine OPSC can be explained due to the presence of high coarse aggregate content. Concretes with high coarse aggregates are known as lean concrete, as is the case with the fine OPSC, see Section 4.2.3. One of the advantages of high coarse aggregate content is that it reduces the shrinkage of the concrete as the contact points of the aggregates are very close and coarse aggregates are known not to shrink (Li, 2011). Therefore, when the coarse aggregates reach in contact with each other, the shrinkage would therefore stop or significantly reduce due to a restraining effect, see Figure 4.97.
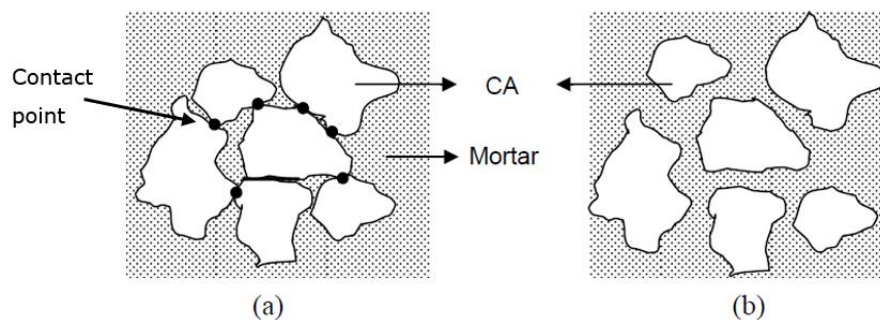
Figure 4.97 Effect of coarse aggregate content on the shrinkage of concrete, (a) lean concrete and (b) rich concrete (Li, 2011)

The high shrinkage of the coarse OPSC is undoubtedly concerning and most probably due to several reasons. Firstly, the coarse OPSC amounts to a high cement content of 1050 kg/m^3. In Section 4.2, it was shown that the coarse OPSC had 18% of water of its total volume compared to 9% and 7% for the NWC and fine OPSC, respectively. The high cement and water volume is very well known to cause high shrinkage (Li, 2011). The high volume of water is also known to cause a high volume of voids, which was confirmed in Section 4.3.2. The high permeable voids allow for higher moisture movement resulting in high ultimate drying shrinkage (Mehta & Monteiro, 2006). It was also found that the course

183

OPSC had the highest loss of water of 572 grams or almost 6% of its weight after 365 days, while the NWC and fine OSPC had a loss of 473 grams or 4% and 235 grams or 2%, respectively, see Figure 4.98.
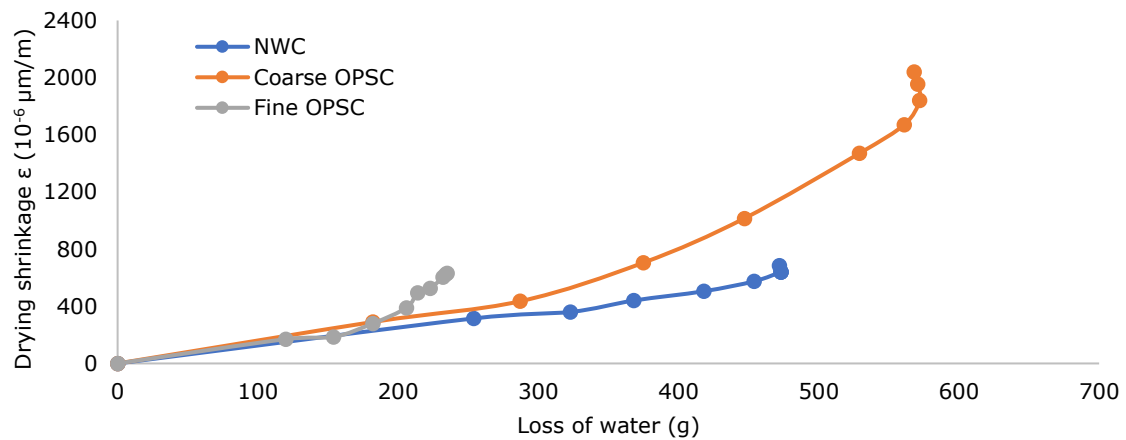
Figure 4.98 Shrinkage vs loss of water of concretes

Also, it can be seen that the higher the loss of water, the higher the drying shrinkage. However, though the fine OPSC had a lower loss of water than the NWC, it did reach a similar drying shrinkage. The high aggregate fraction of the fine OPSC probably makes the diffusion or migration of the water more difficult (Mehta & Monteiro, 2006). Also, the fine OPSC used 2% less water than the NWC in its mix, thus probably explaining the difference of 2% in their water loss. Nevertheless, Tenera C-OPS is definitely less stiff than the conventional coarse aggregates and consequently accommodate more movement caused by volume change, as explained earlier. This can be seen in the difference between the coarse and fine OSPC, despite the fact that a similar volume of OPS was used in their respective mix design. The influence of aggregate type has shown that the drying shrinkage of concrete can increase by 2.5 times when changing from high elastic modulus aggregate to low elastic modulus aggregate, see Figure 4.99. This is therefore also evident from this study, where the C-OPS is the lowest.
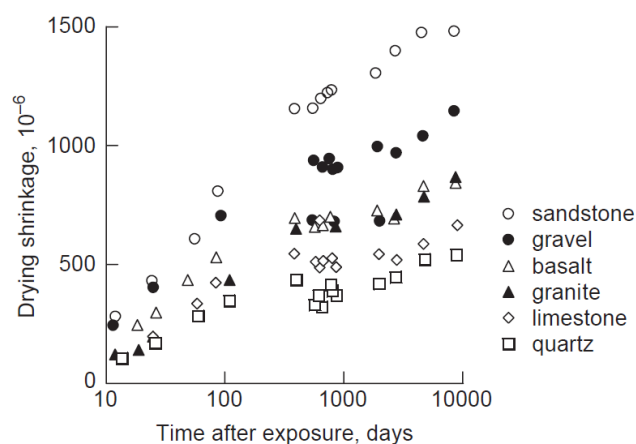
Figure 4.99 Influence of aggregate type on drying shrinkage (Mehta & Monteiro, 2006)

Overall, the fine OSPC has shown acceptable drying shrinkage values which were relatively similar to the NWC. However, the coarse OSPC has shown concerning high drying shrinkage results. The most promising solution and recommendation for further studies for the coarse OPSC would be by using shrinkage reducing admixtures (SRAs). SRA is proven to reduce the long-term drying shrinkage of concrete by 50% (Zhang, et al., 2022).

4.3.6.2.   Drying shrinkage prediction models

The drying shrinkage prediction models proposed by (ACI 209.2R-92, 2008) and (BS EN 1992-1-1, 2014), mentioned in Section 2.2.8, have been used and plotted along the empirical results of the NWC, coarse, and fine OSPC in Figure 4.100, Figure 4.101, and Figure 4.102, respectively.

NWC

Compared to the NWC, both ACI and BS models showed appreciable prediction results with the BS model showing the lowest average difference with the empirical results, see Figure 4.100. This might be because the key difference between both models is that the ACI mainly depends on a final drying shrinkage value as an input while the BS model depends on the 28-day compressive strength, environmental conditions, and notional dimensions as inputs. In general, it can be derived that both codes seem to be reasonably acceptable, though the BS model with the more accurate prediction compared to the ACI model.

Days	ACI/ Empirical	BS/ Empirical
1	0%	0%
3	-81%	-51%
7	-57%	-28%
14	-38%	-16%
28	-17%	-4%
56	-3%	1%
90	-1%	-1%
180	12%	7%
270	17%	9%
365	12%	4%
Average difference	-15.6%	-7.8%
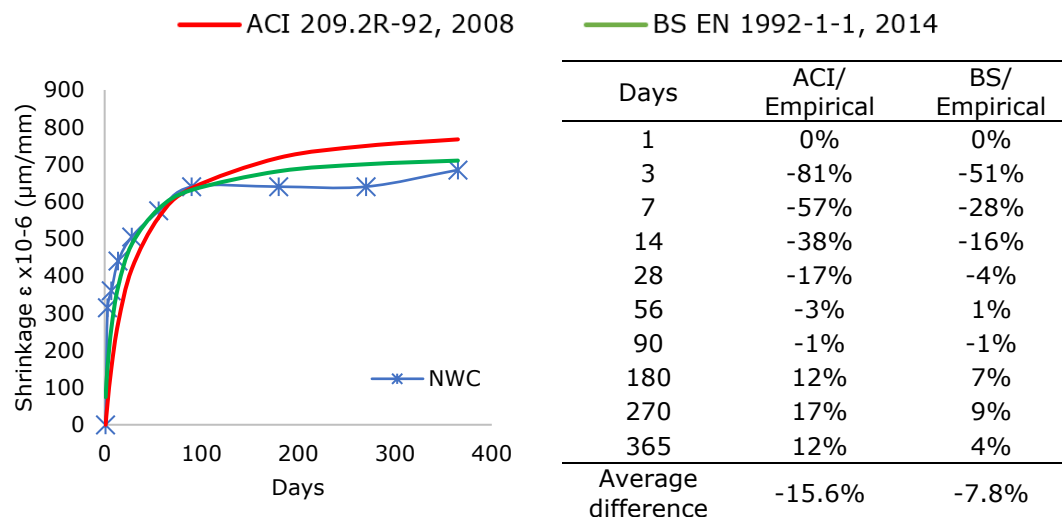
Figure 4.100 Drying shrinkage prediction models with the NWC

Coarse OPSC

As for the coarse OPSC, see Figure 4.101, while the ACI model slightly overestimated the empirical values by only 7.3%, the BS model underestimated it far off with an average difference of 48.3%. It can therefore be concluded that the ACI model is a better option due to a lower average difference. As mentioned earlier, this is most probably since the ACI depends on the final drying shrinkage as an input. The ACI code allows the final drying

shrinkage to be assumed or taken from previous known data. Consequently, the 365 days drying shrinkage values was used and therefore resulted in having higher accurate values than that of the BS model.

Days	ACI/Empirical	BS/Empirical
1	0%	0%
3	-40%	-43%
7	6%	-37%
14	16%	-45%
28	23%	-50%
56	13%	-59%
90	13%	-61%
180	16%	-61%
270	14%	-63%
365	12%	-64%
Average difference	7.3%	-48.3%
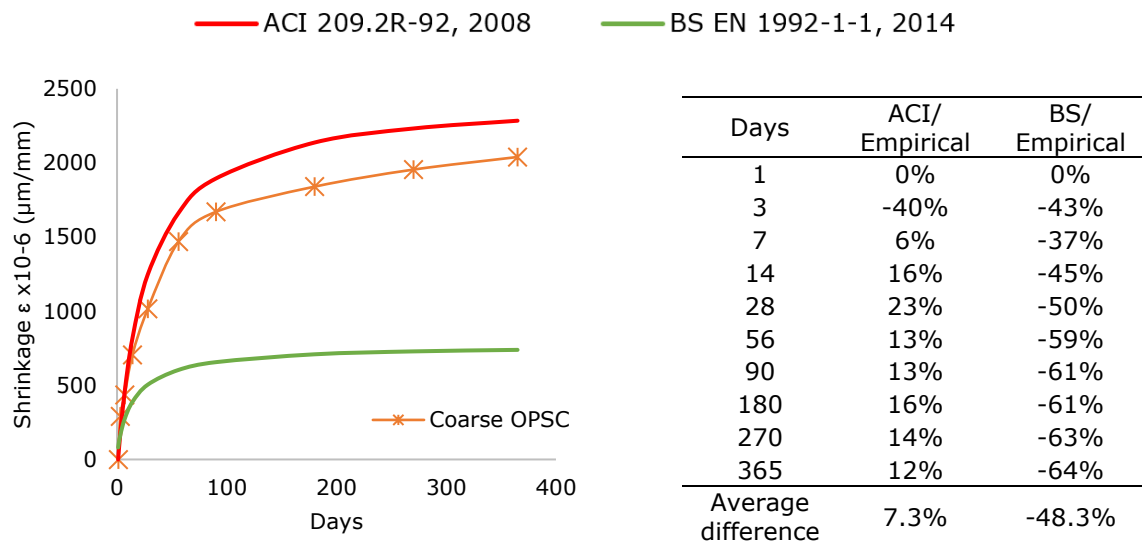
Figure 4.101 Drying shrinkage prediction models with the Coarse OPSC

Fine OPSC

As for the fine OPSC, see Figure 4.102, it can be seen that the BS model over predicted the values by an average difference of 18.9% while the ACI model underestimated the values with an average difference of 6.3%.

Days	ACI/Empirical	BS/Empirical
1	0%	0%
3	-68%	-6%
7	-24%	45%
14	-11%	36%
28	-2%	27%
56	3%	20%
90	11%	23%
180	8%	15%
270	9%	14%
365	11%	15%
Average difference	-6.3%	18.9%
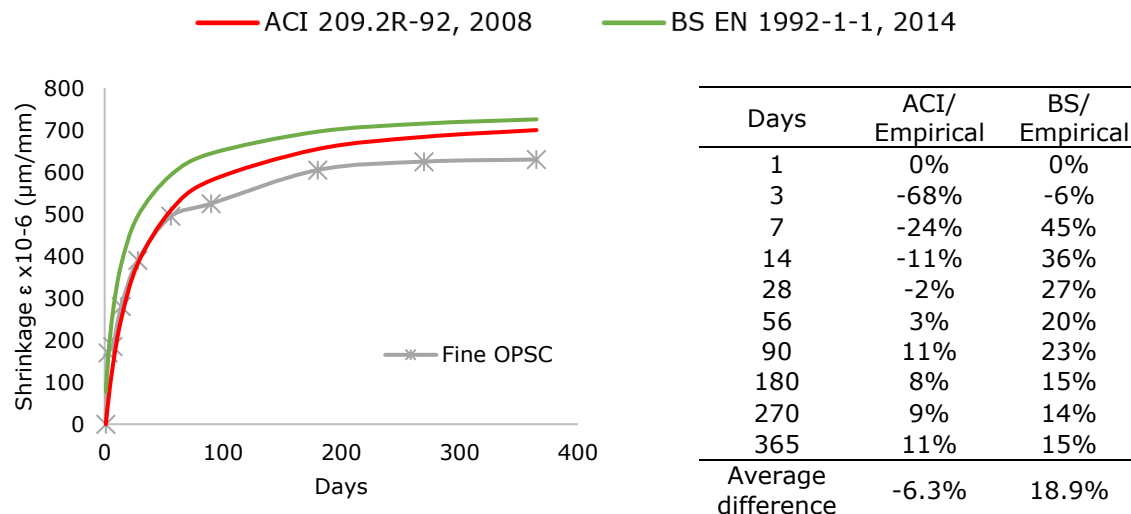
Figure 4.102 Drying shrinkage prediction models with the fine OPSC

4.3.6.3. Concluding remarks

In this section, the drying shrinkage of the concretes were investigated for a period of one year. All three concretes were exposed to the same environment following the BS standards (BS ISO 1920-8, 2009). In addition, prediction models proposed by the ACI and

186

BS codes were also used to compare their results to the empirical values of the three concretes.

The results have revealed that the fine OSPC exhibited similar and even slight lower drying shrinkage values than that of the NWC. This was mainly attributed to the advantage of using high coarse aggregate content allowing for less volume change due to close point contact. However, the coarse OPSC demonstrated drying shrinkage values more almost triple that of the NWC and fine OPSC. This was reasoned to be caused by its high cement content, high volume of water content, and low stiffness of the tenera C-OPS allowing for volume change. In point of fact, the high drying shrinkage value for the coarse OSPC was considered to be concerning as it did not cease to shrink and seemed to be able to continue in concerning rates at 365 days. On the contrary, the NWC and fine OPSC were found to slow down significantly in drying shrinkage values after 90 and 270 days, respectively.

Therefore, based on the values obtained from this study, the fine OSPC is deemed to have acceptable drying shrinkage values while for the coarse OSPC, further analyses on lowering the shrinkage are recommended. Perhaps, the use of SRAs could be used for investigation as a recommendation for further studies.

As for the prediction models, varying results were shown with both the ACI and BS model with the three concretes. Where more accurate prediction values were seen with the BS model for the NWC, the ACI model showed higher accurate values with both OSPCS. It was mainly rationalized that the ACI model predicted higher accurate values since it mainly depends on a final drying shrinkage value as an input, whether assumed or obtained from empirical results. Since the empirical results were used, it had therefore predicted acceptable prediction values up to one year and more accurate values than that of the BS model.

Studying the concretes for longer time periods (> 1 year) might not be necessary for the NWC and fine OPSC, though highly advised for the coarse OSPC as it continued to shrink in a high shrinkage rate even at 365 days.

Chapter 5. Conclusions and Recommendations

5.1. Conclusions

OPSC, particularly that made with Dura OPS, has been thoroughly experimented within various mechanical and structural investigations with promising results. However, almost no research has been found on the hybrid Tenera OPS, a thinner variety of the OPS family. It was found that Dura OPS is expected to no longer be available in the future since Tenera OPS produces more palm oil, one of the main reasons for its production. This study, therefore, highlighted the necessity to reinvestigate the use of Tenera OPS as both coarse and fine-sized aggregates in concrete separately to assess its viability.

First and foremost, it was found that Tenera OPS, when used as coarse-sized aggregates, did not perform as well as OPSC made with Dura OPS with the same mix design, the latter showing much lower strengths, substantiating the core thesis. Much higher cement contents were required to produce similar grade strengths, making it unviable for concrete practices. This disparity was attributed primarily to the thinner and weaker shell of Tenera OPS, along with its distinct shape. Another factor determined was the swelling and shrinking effect found within the OPS by means of microstructural analysis, causing large interfacial voids. Conversely, the proposed novel method of this study, by using Tenera OPS as a fine-sized aggregate in concrete, showed improvements compared to its coarse counterpart, mainly by reducing the cement content, making it more viable than its coarse counterpart while maintaining a similar volume content. Also noteworthy is that a straightforward washing process involving detergent cleaning and debris removal emerged as the optimal treatment method for fine OPSC, as was practiced most commonly by previous researchers and the coarse OPSC in this study.

By testing different hardened properties in the NWC, coarse OPSC, and fine OPSC, the results unveiled valuable insights for comparative analysis. While the NWC, functioning as a control with similar grade strength and used as a control, the different results between the two OPSCs showed that the fine OPSC exhibited improved mechanical performances compared to the coarse OPSC. The following highlight the key finding for each test:

- **Density**: The study on hardened density uncovered intriguing trends, particularly in air-cured regimes. The decline in dry density for coarse OPSC in cured conditions was linked to OPS rotting and palm oil extraction. This necessitates further examination and consideration of moisture prevention methods, emphasizing the importance of fine OPSC.

- **Permeable Voids and Water Absorption**: Analysis of permeable voids and water absorption reaffirmed declining trends over time, with fine OPSC exhibiting promising results. While acknowledging challenges in comparing lightweight and NWC, the study results provided a basis for acceptable trends.

- **Compressive Strength:** The investigation into compressive strength illuminated the distinct strengths of OPSCs, particularly the internal curing effect observed in early ages. Fine OPSC showcased superior performance, emphasizing its potential as a lightweight alternative with reduced environmental impact.

- **Flexural Tensile Strength**: Flexural tensile strength assessments underscored the influence of aggregate characteristics on performance. Fine OPSC exhibited superior flexural strength in cured conditions, outperforming both NWC and coarse OPSC, while the stiffness of C-OPS in coarse OPSC contributed to enhanced performance in air-cured regimes. This underscores the potential advantages of using fine OPSC in structural applications.

- **Modulus of Elasticity**: Dynamic and static modulus of elasticity analyses revealed intricate behaviours influenced by a range of factors. Fine OPSC exhibited characteristics comparable to NWC, emphasizing its viability in structural applications. The disparities between prediction models highlighted the need for ongoing refinement.

- **Drying Shrinkage**: Drying shrinkage investigations exposed differential behaviors in OPS-containing concretes. Fine OPSC exhibited favorable shrinkage values, presenting it as a promising solution with lower susceptibility to volume change over time. Meanwhile, concerns arose regarding the persistent shrinkage observed in coarse OPSC, necessitating further analyses and exploration of shrinkage-reducing agents.

This thorough investigation has delved into the promising domain of using Tenera OPS as an aggregate in concrete, scrutinizing its fundamental mechanical properties and revealing profound insights that have the potential to revolutionize the field of construction materials and sustainable practices.

The findings of this study offer numerous benefits and create new opportunities for creative applications in the field of concrete construction:

Eco-Friendly: Tenera OPS, especially in its fine form, promotes eco-friendly concrete production by significantly reducing cement usage, aligning with global sustainability efforts.

Lightweight: Its lightweight properties introduce an additional layer of environmental and structural advantages, rendering it an appealing selection for sustainable construction practices. Specifically, it contributes to reducing the structural dead load, thereby diminishing the required foundation size.

Enhanced Sustainability: Tenera Fine OPSC offers sustainability benefits, reducing resource consumption while maintaining concrete strength and durability, marking a pivotal step towards a more sustainable construction industry.

In conclusion, this research provided insights into the properties of using Tenera OPS in concrete, highlighting the effects of using Tenera OPS as coarse and fine aggregate with respect to their fundamental mechanical properties. Based on the findings of this study, the viability of using Tenera OPS as coarse and fine-sized aggregate in concrete was investigated. Based on the afore mentioned findings, it can be cautiously concluded that the use of Tenera OPS as a fine sized aggregate in concrete is more viable compared to using it as a coarse sized aggregate. However, it is important to consider additional factors such as mix design, curing methods, and long-term performance when making a final decision on the suitability of Tenera OPS as an aggregate, fine or course sized, in concrete. It is recommended to conduct further studies and experiments to explore optimization strategies and potential additives that can enhance the bonding between Tenera OPS and the cement matrix. This will contribute to a more comprehensive understanding of the viability and potential applications of Tenera OPS in concrete construction. Moreover, a detailed recommendation is discussed in the next section.

5.2. Recommendations

Based on the findings and conclusions drawn from this research, the following recommendations are suggested for further study and practical applications:

1. Understanding the behavior of OPS in different moisture states and investigating techniques to enhance bonding and reduce cement requirements are recommended for future studies in order to further optimize the use of Tenera OPS in concrete production. The focus should mainly be on reducing or eliminating the swelling and shrinking effect of the OPS in concrete to counteract void spaces.

2. Optimize mix design: Further optimization of the mix design for OPSC is recommended. Fine-tuning the proportions of fine and coarse OPS aggregates and exploring alternative additives can enhance the properties and performance of OPSC. The goal should be to achieve a desirable balance between strength, density, and other relevant characteristics.

3. Evaluation of SP Influence: The influence of SP on Tenera OPSC should be further assessed. SP are commonly used in concrete production to enhance workability and improve strength. Conducting experiments to evaluate the effects of SP on Tenera OPSC can provide insights into the optimal dosage and its impact on the mechanical properties of the concrete. Based on the findings, it is mainly recommended that chemical analysis is done between the SP and OPS.

4. Further study on white-rot fungi: It is recommended to conduct further analysis into the white-rot fungi observed in the OPS aggregates. The impact of these fungi on the density and properties of OPSC should be thoroughly studied. Preventive measures should be explored, such as the application of water-based liquid formulations like Nano waterproofing, to mitigate moisture penetration in the OPS aggregates.

5. Investigate palm oil extraction: A comprehensive analysis should be conducted to determine the effect of palm oil extraction from OPS aggregates on the hydration process of concrete. Chemical analysis and tests can help assess any potential implications of palm oil seeping out of the specimens during curing and drying processes.

6. Explore environmental conditions: Additional studies should explore the influence of different environmental conditions on the permeable voids and water absorption properties of NWC and OPSC. Factors such as temperature, humidity, and exposure to various elements can affect the performance and durability of concrete.

7. Investigate OPS shape and reinforcing effect: The effect of OPS shape on the flexural tensile strength of OPSC should be further studied. The reinforcing potential of OPS aggregates, particularly the C-OPS, should be explored under different curing regimes. Also recommend is to use different sizes by small, medium, and large sizes for comparison. This will help understand the possible use of C-OPS as a reinforcement and optimize its use in various applications.

8. Study on the potential of Tenera OPS as fine Aggregate in other concrete applications: Fine OPSC can be used to make other building components such as masonry blocks, pavement tiles, roads used for light traffic, ground slabs, underground utilities, etc.

9. Correlation with other mechanical properties: The relationship between different mechanical properties, such as compressive strength, flexural tensile strength, modulus of elasticity, and UPV should be further explored. Understanding these correlations can help predict and assess the performance of OPSC based on easily measurable properties.

10. Further analysis on drying shrinkage reduction: Considering the higher drying shrinkage values observed in the coarse OPSC, it is recommended to conduct additional analyses to mitigate this issue. Investigating the use of Shrinkage-Reducing Admixtures (SRAs) as a potential solution for reducing shrinkage in the coarse OPSC can help optimize its performance and enhance its durability.

11. Long-term durability and strength assessment: To determine the feasibility of incorporating Tenera OPS in concrete production, it is crucial to evaluate its long-term durability and strength characteristics compared to traditional NWC. Conducting extended tests and monitoring the performance of Tenera OPS-based concrete over an extended period, such as beyond 365 days, can provide valuable data on its long-term behaviour and assess its suitability for various structural applications.

12. Practical application considerations: Practical considerations should be considered when using OPSC in real-world applications. The potential impact of OPS rotting, palm oil extraction, and the presence of void spaces should be evaluated in terms of long-term durability, structural integrity, and performance. The use of OPSC should adhere to relevant codes and standards, ensuring compliance and safety.

13. Continuation of comparative Studies: The comparative analysis of prediction models for properties like compressive strength, MOE, and drying shrinkage should be extended to other relevant models and standards. Conducting further studies to compare and validate prediction models can provide more accurate and reliable estimations of the properties of interest, aiding in the design and construction of concrete structures. The prediction models proposed by codes (such as ACI and BS) should be further validated and refined using empirical data. This will enhance the accuracy and reliability of these models for practical applications.

It is important to note that the recommendations provided here are based on the specific context of the investigation and the conclusions drawn from the data presented. Further research and analysis are required to validate these recommendations and adapt them to specific project requirements and environmental conditions.

Chapter 6. References

Abbas, S. et al., 2006. Effect of thermal softening on the textural properties of palm oil fruitlets. *Journal of Food Engineering,* Volume 76, pp. 626-631.

Abdul kreem, O. M., 2012. Influence of Concrete Mix Proportions and Curing Regimes on Density, Absorption, and Voids in Hardened Concrete. *Al-Rafidain Engineering,* 20(4), pp. 103-117.

Abdullah, A., 1997. Palm oil shell aggregate for lightweight concrete. In: S. Chandra, ed. *Waste Materials Used in Concrete Manufacturing.* New York, USA: William Andrew Publishing, pp. 624-636.

Abdullah, A. A. A., Salam, S. & Rahim, A., 1984. *Basic Strength Properties of Lightweight Concrete Using Agricultural Wastes as Aggregates.* Roorkee, India, International Conference on Low Cost Housing for Developing Countries, pp. 143-146.

Abdullah, N. & Sulaiman, F., 2013. The Oil Palm Wastes in Malaysia Biomass Now - Sustainable Growth and Use. In: M. D. Matovic, ed. *Biomass Now - Sustainable Growth and Use.* Penang, Malaysia: IntechOpen, pp. 75-100.

ACI 209.2R-92, 2008. *Guide for modeling and calculating shrinkage and creep in hardened concrete,* Farmington Hills, USA: ACI commitee.

ACI 209, 1997. *Prediction of Creep, Shrinkage, and Temperature Effects in Concrete Structures,* Michigan, USA: American Concrete Institute.

ACI 211.1-91, 2009. *Standard Practice for Selecting Proportions for Normal, Heavyweight, and Mass Concrete,* Michigan, USA: American Concrete Institute.

ACI 211.2-98, 2004. *Standard Practice for Selecting Proportions for Structural Lightweight Concrete,* Michigan, US: The American Concrete Institute.

ACI 318M-08, 2008. *Building code requirements for structural concrete,* Farmington Hills, USA: American Concrete Institute.

ACI Committee 213R-14, 2014. *Guide for structural lightweight aggregate concrete,* Michigan, USA: American Concrete Institute.

ACI Committee 308, 2008. *Guide to Curing Concrete (ACI 308R-01),* Farmington Hills, USA: American Concrete Institute.

Ahmed, E. & Sobuz, H., 2010. Flexural and Time-Dependent Performance of Palm Shell Aggregate Concrete Beam. *KSCE Journal of Civil Engineering,* 15(5), pp. 859-865.

Ahmmad, R. et al., 2016. Performance evaluation of palm oil clinker as coarse aggregate in high strength lightweight concrete. *Journal of Cleaner Production,* Volume 112, pp. 566-574.

Ahmmad, R., Jumaat, M. Z., Bahri, S. & Islam, A. S., 2014. Ductility performance of lightweight concrete element containing massive palm shell clinker. *Construction and Building Materials,* Volume 63, pp. 234-241.

Akmal, A. et al., 2017. Utilization of fly ash as partial sand replacement in oil palm shell lightweight aggregate concrete. *Materials Science and Engineering,* Volume 271, pp. 1-7.

Alengaram, U. J., Al Muhit, B. A. & Bin Jumaat, M. Z., 2013a. Utilization of oil palm kernel shell as lightweight aggregate in concrete – A review. *Construction and Building Materials,* Volume 38, pp. 161-172.

Alengaram, U. J., Al Muhit, B., Jumaat, M. Z. b. & Jing, M., 2013b. A comparison of the thermal conductivity of oil palm shell foamed concrete with conventional materials. *Materials and Design,* Volume 51, pp. 522-529.

Alengaram, U. J., Jumaar, M. Z. & Mahmud, H., 2008a. Influence of cementitious materials and aggregates content on compressive strength of palm kernel shell concrete. *Journal of Applied Science,* 8(18), pp. 3207-3213.

Alengaram, U. J., Mahmud, H. & Jumaat, M., 2010b. Development of lightweight concrete using industrial waste material, palm kernel shell as lightweight aggregate and its properties. *In: 2nd International conference on chemical, biological and environmental engineering (ICBEE 2010),* pp. 277-281.

Alengaram, U. J., Mahmud, H., Jumaat, M. Z. & Shirazi, S. M., 2010a. Effect of aggregate size and proportion on strength properties of palm kernel shell concrete. *International Journal of the Physical Sciences,* 5(12), pp. 1848-1856.

Alengaram, U., Jumaat, M., Mahmud, H. & Fayyadh, M., 2011b. Shear behaviour of reinforced palm kernel shell concrete beams. *Construction and Building Materials,* Volume 25, pp. 2918-2927.

Alengaram, U., Mahmud, H. & Jumaat, M., 2010c. Comparison of mechanical and bond properties of oil palm kernel shell concrete with normal weight concrete. *International Journal of the Physical Sciences,* 5(8), pp. 1231-1239.

Alengaram, U., Mahmud, H. & Jumaat, M., 2011a. Enhancement and prediction of modulus of elasticity of palm kernel shell concrete. *Materials and Design,* 32(4), pp. 2143-2148.

Anuar, M. et al., 2017. Preliminary evaluation of physical and chemical characterization of waste palm oil shell as cool material replaced in asphaltic concrete as fine aggregate. *Materials Science and Engineering,* Volume 271, pp. 1-7.

Aria, M. & Cuccurullo, C., 2017. bibliometrix: An R-tool for comprehensive science mapping analysis. *Journal of Informetrics,* Volume 11, pp. 959-975.

Aslam, M., Shafigh, P. & Jumaat, M., 2015. Structural lightweight aggregate concrete by incorporating solid wastes as coarse lightweight aggregate. *Applied Mechanics and Materials ,* Volume 749, pp. 337-342.

Aslam, M., Shafigh, P. & Jumaat, M., 2016. Drying shrinkage behaviour of structural lightweight aggregate concrete containing blended oil palm bio-products. *Journal of Cleaner Production,* Volume 127, pp. 183-194.

Aslam, M., Shafigh, P., Nomeli, M. A. & Jumaat, M., 2017. Manufacturing of high-strength lightweight aggregate concrete using blended coarse lightweight aggregates. *Journal of Building Engineering,* Volume 13, pp. 53-62.

ASTM C330M-17a, 2017. *Standard Specification for Lightweight Aggregates for Structural Concrete,* West Conshohocken, PA, USA: ASTM International.

ASTM C642 - 13, 2013. *Standard Test Method for Density, Absorption, and Voids in Hardened Concrete,* West Conshohocken, USA: ASTM.

Awalludin, M. F. et al., 2015. An overview of the oil palm industry in Malaysia and its waste utilization through thermochemical conversion, specifically via liquefaction. *Renewable and Sustainable Energy Reviews,* Volume 50, pp. 1469-1484.

Azunna, S. U., 2019. Compressive strength of concrete with palm kernel shell as a partial replacement for coarse aggregate. *SN Applied Sciences,* 1(342), pp. 1-10.

Basri, H. B., Mannan, M. A. & Zain, M., 1999. Concrete using waste oil palm shells as aggregate. *Cement and Concrete Research,* Volume 29, pp. 619-622.

Baudouin, L. et al., 1997. Recurrent selection of tropical tree crops. *Euphytica,* Volume 96, pp. 101-114.

Bentz, D., 2002. Drying Shrinkage of Cement-Based Materials. *Concrete International,* 24(9), pp. 55-60.

Bjornstrom, J. & Chandra, S., 2003. Effect of superplasticizers on the rheological properties of cements. *Materials and Structures,* 36(1), pp. 685-692.

Brahami, Y., Saedi, A., Fiset, M. & Ba, K., 2022. The Effects of the Type and Quantity of Recycled Materials on Physical and Mechanical Properties of Concrete and Mortar: A Review. *Sustainability,* 14(1), pp. 1-22.

Brischke, C. & Alfredsen, G., 2020. Wood-water relationships and their role for wood susceptibility to fungal decay. *Applied Microbiology and Biotechnology,* 1(1), pp. 3781-3795.

BS 1881-125, 2013. *Testing concrete - Methods for mixing and sampling fresh concrete in the laboratory,* London, UK: BSI.

BS 1881-203, 1986. *Testing concrete - Part 203: Recommendations for measurement of velocity of ultrasonic pulses in concrete,* London, UK: BSI.

BS 1881-209, 1990. *Testing concrete - Recommendations for the measurement of dynamic modulus of elasticity,* London: BSI.

BS EN 1097-6, 2022. *Tests for mechanical and physical properties of aggregates,* London, UK: BSI.

BS EN 12350-2, 2019. *Testing fresh concrete,* London, UK: BSI.

BS EN 12390-1, 2021. *Testing hardened concrete Part 1: Shape, dimensions and other requirements for specimens and moulds,* London, UK: BSI.

BS EN 12390-13, 2021. *Determination of secant modulus of elasticity in compression,* London, UK: BSI.

BS EN 12390-2, 2019. *Testing hardened concrete - Making and curing specimens for strength tests,* London, UK: BSI.

BS EN 12390-3, 2019. *Testing hardened concrete Part 3: Compressive strength of test specimens,* London, UK: BSI.

BS EN 12390-5, 2019. *Testing hardened concrete Part 5: Flexural strength of test specimens,* London, UK: BSI.

BS EN 12390-7, 2019. *Testing hardened concrete - Part 7: Density of hardened concrete,* London, UK: BSI.

BS EN 12504-4, 2021. *Testing concrete in structures. Determination of ultrasonic pulse velocity,* London, UK: BSI.

BS EN 12620, 2008. *Aggregates for concrete,* London, UK: BSI.

BS EN 13055, 2016. *Lightweight aggregates,* London, UK: BSI.

BS EN 1992-1-1, 2014. *Design of Concrete Structures,* London, UK: BSI.

BS EN 206, 2021. *Concrete - Specification, performance, production and conformity,* London, UK: BSI.

BS EN 480-1, 2014. *Admixtures for concrete, mortar and grout. Test methods. Reference concrete and reference mortar for testing,* London, UK: BSI.

BS EN 933, 2021. *Tests for geometrical properties of aggregates,* London, UK: BSI.

BS EN 934-2, 2012. *Admixtures for concrete, mortar and grout. Concrete admixtures. Definitions, requirements, conformity, marking and labelling,* London, UK: BSI.

BS ISO 1920-8, 2009. *Testing of concrete Part 8: Determination of drying shrinkage of concrete for samples prepared in the field or in the laboratory,* London, UK: BSI.

Cartuxo, F. et al., 2015. Rheological behaviour of concrete made with fine recycled concrete aggregates – Influence of the superplasticizer. *Construction and Building Materials,* 89(1), pp. 36-47.

Cerro, C., Erickson, E. & Dong, T., 2021. Intracellular pathways for lignin catabolism in white-rot fungi. *PNAS,* 118(9), pp. 1-10.

Chaabene, W. B., Flah, M. & Nehdi, M. L., 2020. Machine learning prediction of mechanical properties of concrete: Critical review. *Construction and Building Materials,* Volume 260, pp. 1-18.

Chai, W., Teo, D. & NG, C., 2014. Improving the Properties of Oil Palm Shell (OPS) Concrete Using Polyvinyl Alcohol (PVA) Coated Aggregates. *Advanced Materials Research,* Volume 970, pp. 147-152.

Chandra, S. & Berntsson, L., 2002. *Lightweight Aggregate Concrete.* 1st ed. New York, USA: Noyes Publications.

Chang, P., 2004. An approach to optimizing mix design for properties of high performance concrete. *Cement and Concrete Research,* 34(1), pp. 623-629.

Chia, K. & Zhang, M., 2002. Water permeability and chloride penetrability of high-strength lightweight aggregate concrete. *Cement and Concrete Research,* 32(4), pp. 639-645.

Corinaldesi, V., 2011. Structural Concrete Prepared with Coarse Recycled Concrete Aggregate: From Investigation to Design. *Advances in Civil Engineering,* Volume 2011, pp. 1-7.

Cottrell, R. C., 1991. Introduction: nutritional aspects of palm oil. *The American journal of clinical nutrition,* 53(4), p. 989–1009.

CPOPC, 2023. *CPOPC Palm Oil Database.* [Online]
Available at: https://cpopc.org
[Accessed 6 April 2023].

Dalton, L., LaManna, J., Jones, S. & Pour-Ghaz, M., 2023. Does the Interfacial Transition Zone Influence Moisture Transport in Concrete?. In: E. Médici & A. Otero, eds. *Album of Porous Media.* s.l.:Springer, p. 107.

Désiré, T. J. & Léopold, M., 2013. Impact of clay particles on concrete compressive strength. *International Research Journal on Engineering,* 1(2), pp. 49-56.

Domagala, L., 2015. The effect of lightweight aggregate water absorption on the reduction of water-cement ratio in fresh concrete. *Procedia Engineering,* Volume 108, pp. 206-213.

Ellis, L. D. et al., 2020. Toward electrochemical synthesis of cement—An electrolyzer-based process for decarbonating CaCO3 while producing useful gas streams. *Proceedings of the national academy if sciences of the USA,* 23(117), pp. 12584-12591.

Evangelista, A. & Tam, V., 2020. Properties of high-strength lightweight concrete using manufactured aggregate. *Construction Materials,* 173(4), pp. 157-169.

Farahani, J. N., Shafigh, P., ALsubari, B. & Shahnazar, S., 2017. Engineering properties of lightweight aggregate concrete containing binary and ternary blended cement. *Journal of Cleaner Production,* Volume 149, pp. 976-988.

FIP, 1983. *FIP Manual of Lightweight Aggregate Concrete,* London, UK: Surry University Press.

Fitriyah, F. et al., 2022. Nutritional improvement of oil palm and sugarcane plantation waste by solid-state fermentation of Marasmiellus palmivorus. *Earth and Environmental Science ,* 974(1), pp. 12-21.

Foong, K. Y., ALengaram, U., Jumaat, M. & Mo, K., 2015. Enhancement of the mechanical properties of lightweight oil palm shell concrete using rice husk ash and manufactured sand. *Journal of Zhejiang University: Science A,* 16(1), pp. 59-69.

Gar, 2019. *Golden Agri-Resources.* [Online]
Available at: https://www.goldenagri.com.sg
[Accessed 8 12 2020].

Geiker, M., Bentz, D. & Jensen, O., 2004. *Mitigating Autogeneous Shrinkage by Internal Curing ,* Farmington Hills, USA: American Concrete Institute.

Ghanbari, S., Shahmansouri, A., Bengar, H. & Jafari, A., 2023. Compressive strength prediction of high-strength oil palm shell lightweight aggregate concrete using machine learning methods. *Environmental Science and Pollution Research,* 30(1), pp. 1069-1115.

Gibigaye , M., Godonou, G. F., Katte, R. & Degan, G., 2017. Structured mixture proportioning for oil palm kernel shell concrete. *Case Studies in Constructtion Materials,* Volume 6, pp. 219-224.

Golewski, G. L., 2019. A novel specific requirements for materials used in reinforced concrete composites subjected to dynamic loads. *Composite Structures,* Volume 223, pp. 1-8.

Gungat, L., Putri, E. E. & Makinda, J., 2013. Effects of Oil Palm Shell and Curing Time to the Load-Bearing Capacity of Clay Subgrade. *Procedia Engineering,* Volume 54, pp. 690-697.

Guo, S. et al., 2017. Ultrasonic Techniques for Air Void Size Distribution and Property Evaluation in Both Early-Age and Hardened Concrete Samples. *Applied Science,* 7(290), pp. 1-18.

Haach, V., Vasconcelos, G. & Lourenco, P., 2011. Influence of aggregates grading and water/cement ratio in workability and hardened properties of mortars. *Construction and Building Materials,* 25(1), pp. 2980-2987.

Hamada, H. M., Thomas, B. S., Tayeh, B. & Yahaya, F. M., 2020. Use of oil palm shell as an aggregate in cement concrete: A review. *Construction and Building Materials,* Volume 265, pp. 1-16.

Hirschi, T. & Wombacher, F., 2008. *Influence of different superplasticizers on UHPC.* Kassel, s.n.

Holm, T. & Bremmer, T., 2000. *State of the art report on high strength, high durability structural low-density concrete for applications in severe marine environments,* Vicksburg, USA: U.S. Army Engineer Research and Development Center.

Huda, M., Jumar, M. & Islam, A., 2016. Flexural performance of reinforced oil palm shell & palm oil clinker concrete (PSCC) beam. *Construction and Building Materials,* Volume 127, pp. 18-25.

Islam, M. M., Mo, K. H. & Alengaram, U. J., 2016. Durability properties of sustainable concrete containing high volume palm oil waste materials. *Journal of Cleaner Production,* Volume 137, pp. 167-177.

Islam, M. M. U., Mo, K. & Alengaram, U., 2015. Mechanical and fresh properties of sustainable oil palm shell lightweight concrete incorporating palm oil fuel ash. *Journal of Cleaner Production,* Volume 115, pp. 307-314.

Jagarapu, D. & Eluru, A., 2019. Experimental analysis of light weight fiber reinforced concrete by incorporating palm oil shells. *Materials Today: Proceedings,* Volume 19, pp. 850-858.

JPM, 2022. *Geotanih.* [Online]
Available at: https://geotanih.doa.gov.my
[Accessed 20 November 2022].

Jumaat, M. Z. et al., 2015. Characteristics of palm oil clinker as replacement for oil palm shell in lightweight concrete subjected to elevated temperature. *Construction and Building Materials,* Volume 101, pp. 942-951.

Jumaat, M. Z., Alengaram, U. J. & Mahmud, H., 2009. Shear strength of oil palm shell foamed concrete beams. *Materials and Design,* 30(6), pp. 2227-2236.

Kabeer, K. & Vyas, A., 2018. Utilization of marble powder as fine aggregate in mortar mixes. *Construction and Building Materials,* 165(1), pp. 321-332.

Kareem, M., Raheem, A., Oriola, K. & AbdulWahab, R., 2022. A review on application of oil palm shell as aggregate in concrete - Towards realising a pollution-free environment and sustainable concrete. *Environmental Challenges,* 8(1), p. 100531.

Katte, A., Mwero, J., Gibigaye, M. & Koteng, D., 2022. Effect of saponification-based treatment of palm kernel shell aggregates on the mechanical properties of palm kernel shell aggregates concrete. *Construction and Building Materials,* 357(1), p. 129343.

Kearsley, E. & Wainwright, P., 2001. Porosity and permeability of foamed concrete. *Cdement and concrete research,* 31(5), pp. 805-812.

Kemmelmeler, M., 2015. The closed-mindedness tha twasn't: need for structure and expectancy-inconsisten tinformation. *Frontiers in Psychology,* Volume 6, pp. 1-15.

Keshvadi, A. et al., 2011. The Relationship Between Palm Oil Index Development and Mechanical Properties in the Ripening Process of Tenera Variety Fresh Fruit Bunches. *Research Journal of Applied Sciences, Engineering and Technology,* 3(3), pp. 1-9.

Khankhaje, E. et al., 2016. Properties of sustainable lightweight pervious concrete containing oil palm kernel shell as coarse aggregate. *Construction and Building Materials,* Volume 126, pp. 1054-1065.

Khatib, J. & Mangat, P., 1995. Absorption characteristics of concrete as a function of location relative to casting position. *Cement and Concrete Research,* 25(5), pp. 999-1010.

Khayat, K., 1998. Viscosity-enhancing admixtures for cement-based materials—an overview. *Cement and Concrete Composites,* Volume 20, pp. 171-188.

Kim, Y. & Singh, A., 2000. Micromorphological characteristics of wood biodegradation in wet environments: a review. *IAWA,* 21(1), pp. 135-155.

Kocab, D. et al., 2017. Development of the Elastic Modulus of Concrete under Different Curing Conditions. *Procedia Engineering,* 195(1), pp. 96-101.

Kosmatka, S., 2006. Bleed Water. In: J. Lamond & J. Pielert, eds. *Significance of Tests and Properties of Concrete and Concrete-Making Materials.* West Conshohocken, PA, USA: ASTM International, pp. 99-122.

Kosmatka, S., Kerkhoff, B. & Panaresa, W., 2002. *Design and control of concrete mixtures.* 14nd ed. Illinois, USA: Portland Cement Association.

Kovler, K. & Roussel, N., 2011. Properties of fresh and hardened concrete. *Cement and Concrete Research,* Volume 41, pp. 775-792.

Krishnamurthy, M. & Vandanapu, S., 2019. Micro-structural and interfacial transition zone investigation on oil palm shell lightweight concrete. *International Journal of Microstructure and Materials Properties,* 14(5), pp. 448-461.

Kwan, A. & Fung, W., 2012. Roles of water film thickness and SP dosage in rheology and cohesiveness of mortar. *Cement Concrete Composites,* 34(1), pp. 121-130.

Lai, O., Tan, C. & Akoh, C., 2012. *Palm Oil: Production, Processing, Characterization, and Uses.* s.l.:Elsevier Inc..

Lin, W., 2020. Effects of sand/aggregate ratio on strength, durability, and microstructure of self-compacting concrete. *Construction and Building Materials,* 242(1), pp. 1-14.

Li, Y., 2022. Study on the Properties of Water Molecule at Different Temperatures. *Journal of Physics,* 2206(1), pp. 1-9.

Li, Z., 2011. *Advanced Concrete Technology.* 1st ed. New Jersey, USA: John Wiley & Sons.

Loh, L. et al., 2021. Mechanical and Thermal Properties of Synthetic Polypropylene Fiber-Reinforced Renewable Oil Palm Shell Lightweigth Concrete. *Materials,* 14(2337), pp. 1-16.

Loh, S. K. et al., 2013. Zero discharge treatment technology of palm oil mill effluent. *Journal of Oil Palm Research,* Volume 25, pp. 273-281.

Maghfouri, M. et al., 2021. Impact of Fly Ash on Time-Dependent Properties of Agro-Waste Lightweight Aggregate Concrete. *Journal of Composite Science,* 5(156), pp. 1-23.

Maghfouri, M., Shafigh, P. & Aslam, M., 2018. Optimum Oil Palm Shell Content as Coarse Aggregate in Concrete Based on Mechanical and Durability Properties. *Advances in Materials Science and Engineering,* 2018(1), pp. 1-14.

Maghfouri, M., Shafight, P. & Alimohammadi, V., 2019. Drying Shrinkage Strain Development of Agro-Waste Oil Palm Shell Lightweight Aggregate Concrete by Using the Experimental Result, ACI and Eurocode Prediction Models. *International Journal of Intergrated Engineering,* 11(9), pp. 225-263.

Mahmud, H., Jumaat, M. Z. & Alengaram, U. J., 2009. Influence of sand/cement ratio on mechanical properties of palm kernel shell concrete. *Journal of Applied Science,* 9(9), pp. 1764-1769.

Mailvaganam, N., Rixom, M., Manson, D. & Gonzales, C., 1999. *Chemical Admixtures for Concrete.* London, UK: CRC Press.

Maltais, Y. et al., 2006. Prediction of the long-term durability of lightweight aggregate concrete mixtures under severe marine environment. *Materials and structures,* 39(1), pp. 911-918.

Mamlouk, M. S. & Zaniewski, J. P., 2014. *Materials for Civil and Construction Engineers.* 3rd ed. Essex: Pearson.

Mannan, M. A. & Ganapathy, C., 2004. Concrete from an agricultural waste-oil palm shell (OPS). *Building and Environment,* Volume 39, pp. 441-448.

Mannan, M., Alexander, J., Ganapathy, C. & Teo, D., 2006. Quality improvement of oil palm shell (OPS) as coarse aggregate in lightweight concrete. *Building and Environment,* Volume 41, pp. 1239-1242.

Mannan, M., Basri, H., Zain, M. & Islam, M., 2002a. Effect of curing conditions on the properties of OPS-concrete. *Building and Environment,* Volume 37, pp. 1167-1171.

Mannan, M. & Ganapathy, C., 2001a. Mix Design for Oil Palm Shell Concrete. *Cement and Concrete Research,* Volume 31, pp. 1323-1325.

Mannan, M. & Ganapathy, C., 2001b. Long-term strengths of concrete with oil palm shell as coarse aggregate. *Cement and Concrete Research,* 31(1), pp. 1319-1321.

Mannan, M. & Ganapathy, C., 2002b. Engineering Properties of Concrete with Oil Palm Shell as Coarse Aggregate. *Construction and Building Materials,* Volume 16, pp. 29-34.

Mannan, T., Kurian, V. & Ganapathy, C., 2007. Lightweight concrete made from oil palm shell (OPS): Structural bond and durability properties. *Building en Environment,* 42(7), pp. 2614-2621.

Ma, X., Liu, J. & Shi, C., 2019. A review on the use of LWA as an internal curing agent of high performance cement-based materials. *Construction and Building Materials,* 218(1), pp. 385-393.

McCormac, J. & Brown, R., 2014. *Design of Reinforced Concrete.* 9th ed. Hoboken, USA: John Wiley & Sons, Inc..

Mehta, P. K. & Monteiro, P. J. M., 2006. *Concrete: microstructure, properties, and materials.* 3rd ed. New York: McGraw-Hill.

Meininger, R., 1966. *Drying Shrinkage of Concrete,* Silver Spring, USA: National Ready-Mixed Concrete Association.

MET Malaysia, 2022. *Malaysian Meteorological Department.* [Online]
Available at: https://www.met.gov.my
[Accessed 28 12 2022].

Meyer, C., 2009. The greening of the concrete industry. *Cement and Concrete,* Volume 31, pp. 601-605.

Mielke, I., 2000. *Oil World Annual,* Hamburg, Germany: GmbH.

Mindess, S., Young, J. & Darwin, D., 2003. *Concrete.* 2nd ed. New Jersey, USA: Prentice Hall.

Mo, K., Alengaram, U. & Jumaat, M., 2014c. Utilization of ground granulated blast furnace slag as partial cement replacement in lightweight oil palm shell concrete. *Materials and Structures,* Volume 1, pp. 1-12.

Mo, K., Alengaram, U., Jumaat, M. & Liu, M., 2015b. Contribution of acrylic fibre addition and ground granulated blast furnace slag on the properties of lightweight concrete. *Construction of Buildings and Materials,* Volume 95, pp. 686-695.

Mo, K. et al., 2016c. Assessing some durability properties of sustainable lightweight oil palm shell concrete incorporating slag and manufactured sand. *Journal of Cleaner Production,* Volume 112, pp. 763-770.

Mo, K., Alengaram, U., Jumaat, M. & Yap, S., 2015a. Feasibility study of high volume slag as cement replacement for sustainable structural lightweight oil palm shell concrete. *Journal of Cleaner Production,* Volume 91, pp. 297-304.

Mo, K. et al., 2018. Properties of metakaolin-blended oil palm shell lightweight concrete. *European Journal of Environmental and Civil Engineering,* 22(7), pp. 852-868.

Mo, K. et al., 2017a. Mechanical, toughness, bond and durability-related properties of lightweight concrete reinforced with steel fibres. *Materials and Structures,* Volume 50, pp. 1-14.

Mo, K. H. et al., 2015c. Influence of lightweight aggregate on the bond properties of concrete with various strength grades. *Construction and Building Materials,* Volume 84, pp. 377-386.

Mo, K. H. et al., 2014a. Impact resistance of hybrid fibre-reinforced oil palm shell concrete. *Construction and Building Materials,* Volume 50, pp. 499-507.

Mo, K., Visintin, P., Alengaram, U. & Jumaat, M., 2016a. Prediction of the structural behaviour of oil palm shell lightweight concrete beams. *Construction and Building Materials,* Volume 102, pp. 722-732.

Mo, K., Visintin, P., Alengaram, U. & Jumaat, M., 2016b. Bond stress-slip relationship of oil palm shell lightweight concrete. *Engineering Structures,* Volume 127, pp. 319-330.

Mo, K., Yap, K., Alengaram, U. & Jumaat, M., 2014b. The effect of steel fibres on the enhancement of flexural and compressive toughness and fracture characteristics of oil palm shell concrete. *Construction and Building Materials,* Volume 55, pp. 20-28.

Mo, K. et al., 2017b. Shear behaviour and mechanical properties of steel fibre-reinforced cement-based and geopolymer oil palm shell lightweight aggregate concrete. *Construction and Building Materials,* Volume 148, pp. 369-375.

Mollah, M., Adams, W., Schennach, R. & Cocke, D., 2000. A review of cement - superplasticizer interactions and their models. *Advances in Cement Research,* 12(4), pp. 153-161.

Money, N., 2016. Spore Production, Discharge, and Dispersal. In: S. Watkinson & L. Boddy, eds. *The Fungi.* Oxford, USA: Academic press, pp. 67-97.

MsCormac, J. & Nelson, J., 2006. *Design of Reinforced Concrete.* 7th ed. Hoboken, USA: Wiley & Sons.

Muthusamy, K. et al., 2021. Durability properties of oil palm shell lightweight aggregate concrete containing fly ash as partial cement replacement. *Materials Today: Proceedings,* Volume 41, pp. 56-60.

Muthusamy, K. et al., 2015. Effect of mixing ingredient on compressive strength of oil palm shell lightweight aggregate concrete containing palm oil fuel ash. *Procedia Engineering,* Volume 125, pp. 804-810.

Myers, R., 1999. Response Surface Methodology—Current Status and Future Directions. *Journal of Quality Technology,* 31(1), pp. 1-16.

Nabinejad, O. et al., 2014. The Effect of Alkali Treatment of OPKS Filler on Mechanical Property of Polyester-Composite. *Advanced Materials Research,* Volume 980, pp. 86-90.

Nadh, V. et al., 2021. Structural Behavior of Nanocoated Oil Palm Shell as Coarse Aggregate in Lightweight Concrete. *Journal of Nanomaterials,* Volume 1, pp. 1-7.

Neville, A. M., 1995. *Properties of Concrete.* 5th ed. Harlow: Pearson Education.

Newman, J. B., 1993. Properties of structural lightweight aggregate concrete. In: J. L. Clarke, ed. *Structural Lightweight Aggregate Concrete.* Abingdon: Taylor & Francis, pp. 19-22.

Noor, N. M. et al., 2017. Compressive strength, flexural strength and water absorption of concrete containing palm oil kernel shell. *Materials Science and Engineering,* Volume 271, pp. 1-6.

Nunez, I., Marani, A., Flah, M. & Nehdi, M. L., 2021. Estimating compressive strength of modern concrete mixtures using computational intelligence: A systematic review. *Construction and Building Materials,* Volume 310, pp. 1-17.

Okafor, F., 1988. Palm Kernel Shell as a Lightweight Aggregate for Concrete. *Cement and Concrete Research,* Volume 18, pp. 901-910.

Okafor, F., 1991. An Investigation on the Use of Superplasticizer in Palm Kernel Shell Aggregate Concrete. *Cement and Concrete Research,* 21(1), pp. 551-557.

Okpala, D., 1990. Palm Kernel Shell as a Lightweight Aggregate in Concrete. *Building and Environment,* Volume 25, pp. 291-296.

Paktiawal, A. & Alam, M., 2021. Effect of polycarboxylate ether-based superplasticizer dosage on fresh and hardened properties of cement concrete. *Materials Science and Engineering,* 1166(1), pp. 1-8.

Pantzaris, T. P. & Ahmed, M. J., 2002. *Properties and Utilization of Palm Kernel Oil,* Urbana, USA: Palm Oil Developments.

Pestka, A., Klosowski, P., Lubowiecka, I. & Krajewski, M., 2018. Influence of Wood Moisture on Strength and Elastic Modulus for Pine and Fir Wood Subjected to 4-point Bending Tests. *Materials Science and Engineering,* 471(1), pp. 23-32.

Pillai, U. & Menon, D., 2006. *Reinforced Concrete Design.* 1st ed. New Delhi, India: Tata McGraw Hill Publishers Company Ltd.

Prusty, J. K. & Patro, S. K., 2015. Properties of fresh and hardened concrete using agro-waste as partial replacement of coarse aggregate – A review. *Construction and Building Materials,* Volume 82, pp. 101-113.

Rahman, F. et al., 2020. Load-Displacement Response of Oil Palm Shell Concrete Compressive Test Using Digital Image Correlation. *IOP Conference Series: Earth and Environmental Science,* Volume 498, pp. 1-8.

Ray, S., 1995. *Reinforced Concrete: Analysis and Design.* 1st ed. London, UK: Blackwell Science Ltd..

ReportLinker, 2023. *Global Construction Aggregates Industry.* [Online]
Available at: www.reportlinker.com
[Accessed 6 April 2023].

Rosković, R. & Bjegović, D., 2005. Role of mineral additions in reducing CO 2 emission. *Cement and Concrete Research,* Volume 35, pp. 974-978.

Santos, R., Redrigues, F., Segre, N. & Joekes, I., 1999. Macro-defect Free Cements Influence of Poly (vinyl alcohol), Cement Type, and Silica Fume. *Cement and Concrete Research,* Volume 29, pp. 747-751.

Serri, E., Mydin, M. O. & Suleiman, M., 2015b. The Influence of Mix Design on Mechanical Properties of Oil Palm Shell Lightweight Concrete. *Journal of Materials and Environmental Science,* 6(3), pp. 607-612.

Serri, E., Suleiman, M. & Mydin, M. O., 2015a. The Effect of Curing Environment on Oil Palm Shell Lightweight Concrete Mechanical Properties and Thermal Conductivity. *Advances in Environmental Biology,* 9(4), pp. 222-225.

Setherton, G., 2022. *How to Identify and Treat Dry Rot & Wet Rot.* [Online]
Available at: https://www.permagard.co.uk
[Accessed 27 December 2022].

Shafigh, P., Alengaram, U., Mahmud, H. B. & Jumaat, M., 2013a. Engineering properties of oil palm shell lightweight concrete containing fly ash. *Materials and Design,* Volume 49, pp. 613-621.

Shafigh, P., Jumaat, M., Mahmud, H. B. & Alengaram, U. J., 2013b. Oil palm shell lightweight concrete containing high volume ground granulated blast furnace slag. *Construction and Building Materials,* Volume 40, pp. 231-238.

Shafigh, P., Jumaat, M. Z. & Mahmud, H., 2010. Mix design and mechanical properties of oil palm shell lightweight aggregate concrete: A review. *International Journal of the Physical Sciences,* 5(14), pp. 2127-2134.

Shafigh, P., Jumaat, M. Z. & Mahmud, H., 2011d. Oil palm shell as a lightweight aggregate for production high strength lightweight concrete. *Construction and Building Materials,* 25(4), pp. 1848-1853.

Shafigh, P., Jumaat, M. Z., Mahmud, H. B. & Alengaram, U. J., 2011b. A new method of producing high strength oil palm shell lightweight concrete. *Materials and Design,* Volume 32, pp. 4839-4843.

Shafigh, P., Jumaat, M. Z., Mahmud, H. B. & Hamid, N. A. A., 2012. Lightweight concrete made from crushed oil palm shell: Tensile strength and effect of initial curing on compressive strength. *Construction and Building Materials,* 27(1), pp. 252-258.

Shafigh, P., Mahmud, H., Jumaat, M. & Ahmmad, R., 2014a. Structural lightweight aggregate concrete using two types of waste from the palm oil industry as aggregate. *Journal of Cleaner Production,* Volume 80, pp. 187-196.

Shafigh, P., Mahmud, H. & Jumaat, M. Z., 2011a. Effect of steel fiber on the mechanical properties of oil palm shell lightweight concrete. *Materials & Design,* 32(7), pp. 3926-3932.

Shafigh, P., Salleh, S., Ghafari, H. & Mahmud, H. B., 2016. Oil palm shell as an agricultural solid waste in artificial lightweight aggregate concrete. *European Journal of Environmental and Civil Engineering,* Volume 22, pp. 165-180.

Shahbandeh, M., 2022. *Palm oil: global production volume 2012/13-2021/22,* Hamburg, Germany: Statista.

Shah, S., Sarigaphuti, M. & Karaguler, M., 1994. *Comparison of Shrinkage Cracking Performance of Different Types of Fibers and Wiremesh,* Detroit, USA: American Concrete Institute.

Shetty, M., 2005. *Concrete Technology: Theory and Practice.* 1st ed. New Delhi, India: Multicolour Illustrative Edition.

Sika, 2019. *Sika.* [Online]
Available at: https://mys.sika.com
[Accessed 29 May 2022].

Silva, R., Brito, J. & Dhir, R., 2016. Establishing a relationship between modulus of elasticity and compressive strength of recycled aggregate concrete. *Journal of Cleaner Production,* 112(1), pp. 2171-2186.

Singh, R. et al., 2021. An overview of the development of the oil palm industry and impact of the shell gene innovation as a quality control tool to improve productivity. *Journal of Oil Palm Research,* Volume 1, pp. 1-15.

Stamm, A. J. & Hansen, L. A., 1937. Minimizing Wood Shrinkage and Swelling. *Industrial and Engineering Chemistry,* 20(7), pp. 1-3.

Subramanian, N., 2021. *Elastic modulus of concrete,* New Delhi, India: CE&CR.

Sundalian, M., Larissa, D. & Suprijana, O., 2021. Contents and Utilization of Palm Oil Fruit Waste. *Biointerface Research in Applied Chemistry,* 11(3), pp. 10148-10160.

Sun, X. et al., 2016. Process optimisation of microwave-assisted extraction of peony (Paeonia suffruticosa Andr.) seed oil using hexane–ethanol mixture and its characterisation. *International Journal of Food Science and Technology,* Volume 51, pp. 2663-2673.

Swamy, R., 2007. Design for sustainable development of concrete construction. *Proceedings of the Fourth International Structural Engineering and Construction Conference (ISEC 4), Taylor & Francis Ltd England,* pp. 47-54.

Tan, C. & Nehdi, I., 2012. The Physicochemical Properties of Palm Oil and Its Components. In: O. Lai, C. Tan & C. Akoh, eds. *Palm Oil.* Urbana: AOCS Press, pp. 377-391.

Tavakolu, D. & Hashempour, M., 2018. Use of waste materials in concrete: A review. *Pertanika Journal of Science and Technology,* 26(2), pp. 499-522.

Teo, D. C., Mannan, M. A. & Kurian, V. J., 2010. Durability of lightweight OPS concrete under different curing conditions. *Materials and Structures,* Volume 43, pp. 1-13.

Teo, D. C., Mannan, M. A., Kurian, V. J. & Ganapathy, C., 2007. Lightweight concrete made from oil palm shell (OPS): Structural bond and durability properties. *Building and Environment,* Volume 42, pp. 2614-2621.

Teo, D., Mannan, M. & Kurian, V., 2006b. Structural Concrete Using Oil Palm Shell (OPS) as Lightweight Aggregate. *Turkish Journal of Engineering and Environmental Science,* Volume 30, pp. 251-257.

Teychenné, D. C., Franklin, R. E. & Erntroy, H. C., 1988. *Design of normal concrete mixes.* 2nd ed. Watford, UK: Building Research Establishment.

Ting, T. Z. H., Rahman, M. E. & Lau, H. H., 2020. Sustainable lightweight self-compacting concrete using oil palm shell and fly ash. *Construction and Building Materials,* Volume 264, pp. 1-17.

Tjahjono, E. et al., 2017. The Study of Oil Palm Shell (OPS) Lightweight Concrete Using Superplasticizer, Silica Fume, and Fly Ash. *Materials Science Forum,* Volume 902, pp. 65-73.

Traore, Y. et al., 2018. Effect of oil palm shell treatment on the physical and mechanical properties of lightweight concrete. *Construction and Building Materials,* Volume 161, pp. 452-460.

Tyler, I. L., 1956. *Uniformity, Segregation, and Bleeding: Significance of Tests and Properties of Concrete and Concrete Aggregates,* West Conshohocken, PA, USA: ASTM International.

Vincent, 2011. *Antara Hardware Home Centre.* [Online]
Available at: http://www.atr.com.my
[Accessed 8 12 2020].

Wang, Y. et al., 2023. Effect of curing conditions on the strength and durability of air entrained concrete with and without fly ash. *Cleaner Materials,* 7(1), p. 100170.

Washa, G., 1956. *Volume Changes and Creep,* West Conshohocken, USA: ASTM International.

Woittiez, L. S., 2019. *On yield gaps and better management practices in Indonesian smallholder oil palm plantations,* Wageningen. Netherlands: Wageningen University & Research.

Yahaghi, J., Muda, Z. C. & Beddu, S. B., 2016. Impact resistance of oil palm shells concrete reinforced with polypropylene fibre. *Construction and Building Materials,* Volume 123, pp. 394-403.

Yang, C. & Huang, R., 1998. Approximate Strength of Lightweight Aggregate Using Micromechanics Method. *Advanced Cement Based Materials,* Volume 7, pp. 133-138.

Yap, S., Alengaram, U. & Jumaat, M., 2015a. Torsional and cracking characteristics of steel fiber-reinforced oil palm shell lightweight concrete. *Journal of Composite Materials,* 50(1), pp. 115-128.

Yap, S., Alengaram, U., Jumaat, M. & Khaw, K., 2015c. Torsional behaviour of steel fibre-reinforced oil palm shell concrete beams. *Materials and Design,* Volume 87, pp. 854-862.

Yap, S., Alengaram, U., Mo, K. & Jumaat, M., 2019. Ductility behaviours of oil palm shell steel fibre-reinforced concrete beams under flexural loading. *European Journal of Environmental and Civil Engineering,* 23(7), pp. 866-878.

Yap, S., Khaw, K., Alengaram, U. & Jumaat, M., 2015b. Effect of fibre aspect ratio on the torsional behaviour of steel fibre-reinforced normal weight concrete and lightweight concrete. *Engineering Structures,* Volume 101, pp. 24-33.

Yap, S. P., Alengaram, U. J. & & Jumaat, M. Z., 2013. Enhancement of mechanical properties in polypropylene– and nylon–fibre reinforced oil palm shell concrete. *Materials and Design,* Volume 49, pp. 1034-1041.

Yap, S. P., Alengaram, U. J., Mo, K. H. & Jumaat, M. Z., 2017. High strength oil palm shell concrete beams reinforced with steel fibres. *Materials of Construction,* 67(328), pp. 1-11.

Yap, S. P. et al., 2014. Flexural toughness characteristics of steel–polypropylene hybrid fibre-reinforced oil palm shell concrete. *Materials and Design,* Volume 57, pp. 652-659.

Yew, M. et al., 2022. Performance of surface modification on bio-based aggregate for high strength lightweight concrete. *Case Studies in Construction Materials,* 16(1), pp. 1-15.

Yew, M. K., Mahmud, H. B., Ang, B. C. & Yew, M. C., 2014b. Effects of Oil Palm Shell Coarse Aggregate Species on High Strength Lightweight Concrete. *The Scientific World Journal,* Volume 2014, pp. 1-12.

Yew, M., Mahmud, H., Ang, B. & Yew, M., 2014a. Effects of heat treatment on oil palm shell coarse aggregates for high strength lightweight concrete. *Materials and Design,* Volume 54, pp. 702-707.

Yew, M., Mahmud, H., Ang, B. & Yew, M., 2015c. Influence of different types of polypropylene fibre on the mechanical properties of high-strength oil palm shell lightweight concrete. *Construction and Building Materials,* Volume 90, pp. 36-43.

Yew, M., Mahmud, H. B., Ang, B. & Yew, M., 2015a. Effects of Low Volume Fraction of Polyvinyl Alcohol Fibers on the Mechanical Properties of Oil Palm Shell Lightweight Concrete. *Advances in Materials Science and Engineering,* Volume 2015, pp. 1-11.

Yew, M. et al., 2015b. Effects of polypropylene twisted bundle fibers on the mechanical properties of high-strength oil palm shell lightweight concrete. *Materials and Structures,* Volume 49, pp. 1221-1233.

Yew, M. et al., 2021. Effects of pre-treated on dura shell and tenera shell for high strength lightweight concrete. *Journal of Building Engineering,* Volume 42, pp. 1-10.

YTL, 2016. *YTL Cement.* [Online]
Available at: https://www.ytlcement.com/product-brochure/castle.pdf
[Accessed 10 April 2021].

Zeyad, A. et al., 2022. Review on effect of steam curing on behavior of concrete. *Cleaner Materials,* 3(1), p. 100042.

Zhang, J., Li, D. & Wang, Y., 2020. Predicting uniaxial compressive strength of oil palm shell concrete using a hybrid artificial intelligence model. *Journal of Building Engineering,* Volume 30, pp. 1-9.

Zhang, W. et al., 2022. Influence of shrinkage reducing admixtures on the performance of cementitious composites: A review. *Construction and Building Materials,* 325(1), p. 126579.

Zhu, W., Huang, L., Mao, L. & Esmaeili-Falak, M., 2022. Predicting the uniaxial compressive strength of oil palm shell lightweight aggregate concrete using artificial intelligence-based algorithms. *Structural Concrete,* 23(1), pp. 3631-3650.

Zulkifli, H. et al., 2010. Life cylcle assessment for oil palm fresh fruit bunch production from continued land use for oil palm planted mineral soil (part2). *Journal for Oil Palm Research,* Volume 22, pp. 887-894.

Appendices

Appendix A - Formulas for Methodology

For Section 3.1.2.3

Apparent particle density	$\rho_a = \rho_w \dfrac{M_4}{M_4 - \left(M_2 - M_3\right)}$
Oven-dried particle density	$\rho_{rd} = \rho_w \dfrac{M_4}{M_1 - \left(M_2 - M_3\right)}$
SSD particle density	$\rho_{ssd} = \rho_w \dfrac{M_1}{M_1 - \left(M_2 - M_3\right)}$
Water absorption	$\mathrm{WA}_{24} = \dfrac{M_1 - M_4}{M_4} \times 100$

M_1 = the mass of the saturated and surface-dried aggregate in the air
M_2 (Coarse size) = the apparent mass in water of the basket containing the sample of saturated aggregate.
M_2 (Fine size) = the mass of the pycnometer containing the sample of saturated aggregate and water.
M_3 (Coarse size) = the apparent mass in water of the empty basket.
M_3 (Fine size) = the mass of the pycnometer filled with water only.
M_4 = the mass of the oven-dried test portion in air.
ρ_w = density of water.

For Section 3.3

Flexural strength	$f_{ct,fl} = \dfrac{F \times l}{d_1 \times d_2^2}$

F = maximum load
l = distance between lower rollers
d_1 & d_2 = lateral dimensions of the prism

Drying shrinkage	$\varepsilon_{cs}(t, t_0) = \dfrac{(l(t_0) - l_{cs}(t))}{L_0}$

L_0 = Gauge length
$l(t_0)$ = the initial length at time t_0
$l_{cs}(t)$ = length at time t
$\varepsilon_{cs}(t,t_0)$ = the total shrinkage strain of the specimen at time t

Absorption after immersion	$\dfrac{B - A}{A} \times 100\ (\%)$
Absorption after immersion and boiling	$\dfrac{C - A}{A} \times 100\ (\%)$
Dry Bulk density	$\dfrac{A}{C - D} \times \rho\ (\dfrac{g}{m^3})$
Bulk density after immersion	$\dfrac{B}{C - D} \times \rho\ (\dfrac{g}{m^3})$
Bulk density after immersion and boiling	$\dfrac{C}{C - D} \times \rho\ (\dfrac{g}{m^3})$
Apparent density	$\dfrac{A}{A - D} \times \rho\ (\dfrac{g}{m^3})$
Volume of permeable pore space (voids)	$\dfrac{C - A}{C - D} \times 100\ (\%)$

A = mass of oven-dried sample in air
B = mass of surface-dry sample in air after immersion
C = mass of surface-dry sample in air after immersion and boiling
D = apparent mass of sample in water after immersion and boiling
ρ = density of water (1 Mg/m^3 or g/cm^3)

Appendix B - Concrete BRE mix design

Concrete mix design form

Job title ...... NWC 1 ....

Stage	Item		Reference or calculation	Values

1   1.1 Characteristic strength   Specified ——
- 20 _____ N/mm² at __28__ _____ days
- Proportion defective __5__ _____ %

1.2 Standard deviation   Fig 3   ___8___ N/mm² or no data ____ N/mm²

1.3 Margin   C1 or Specified   (k = __1.64__) __1.64__ × __8__ = __13.12__ N/mm²
_____ N/mm²

1.4 Target mean strength   C2   __20__ + __13.12__ = __33.12__ N/mm²

1.5 Cement type   Specified   OPC/<u>SRPC</u>/RHPC

1.6 Aggregate type: coarse   <u>Crushed</u>/uncrushed
Aggregate type: fine   Crushed/<u>uncrushed</u>

1.7 Free-water/cement ratio   Table 2, Fig 4   0.62
1.8 *Maximum free-water/cement ratio*   *Specified*   ⎤ Use the lower value | 0.62 |

2   2.1 Slump or Vebe time   Specified   Slump __40__ mm or Vebe time _____ s

2.2 Maximum aggregate size   Specified   _____ mm

2.3 Free-water content   Table 3 | 210 kg/m³ |

3   3.1 Cement content   C3   210 ÷ 0.6 = 350 kg/m³

3.2 *Maximum cement content*   *Specified*   _____ kg/m³

3.3 *Minimum cement content*   *Specified*   _____ kg/m³

use 3.1 if ≤ 3.2
use 3.3 if > 3.1 | 350 kg/m³ |

3.4 Modified free-water/cement ratio   _____ | ____ |

4   4.1 Relative density of aggregate (SSD)   2.65 known/assumed

4.2 Concrete density   Fig 5   2340 kg/m³

4.3 Total aggregate content   C4   2340 − 210 − 350 = 1780 kg/m³

5   5.1 Grading of fine aggregate   Percentage passing 600 μm sieve   61 %

5.2 Proportion of fine aggregate   Fig 6   34 %

5.3 Fine aggregate content   ⎤ C5   0.34 × 1780 = | 605 kg/m³ |
5.4 Coarse aggregate content   ⎦   1780 − 605 = | 1175 kg/m³ |

Quantities	Cement (kg)	Water (kg or L)	Fine aggregate (kg)	Coarse aggregate (kg)		
				10 mm	20 mm	40 mm
per m³ (to nearest 5 kg)	350	210	605		1175	
per trial mix of _____ m³						

Items in italics are optional limiting values that may be specified (see Section 7)

1 N/mm² = 1 MN/m² = 1 MPa (see footnote to Section 3).
OPC = ordinary Portland cement; SRPC = sulphate-resisting Portland cement; RHPC = rapid-hardening Portland cement.
Relative density = specific gravity (see footnote to Para 5.4).   SSD = based on a saturated surface-dry basis.

Please refer to (Teychenné, et al., 1988) *for graphs and tables.*

208

Appendix C - Mix Design Dura OPSC 20 Grade

For Section 3.2.3.2

Reference	Cement	Fine Aggregate	OPS	Water	28 Day Strength	OPS/total aggregates
		Kg/m³			MPa	
(Mannan & Ganapathy, 2001a)	520	645	450	198	20.00	0.41
	600	492	438	246	20.25	0.47
(Mannan & Ganapathy, 2002b)	400	756	408	180	21.30	0.35
	400	764	412	172	21.80	0.35
	420	722	395	202	20.70	0.35
	420	739	399	189	21.20	0.35
	420	748	403	181	20.90	0.35
(Teo, et al., 2007)	500	850	290	195	20.00	0.25
	520	785	291	213	20.50	0.27
	530	769	339	217	21.00	0.31
(Alengaram, et al., 2011a)	560	446	560	196	22.50	0.56
(Serri, et al., 2015a)	400	721	525	160	20.28	0.42
(Serri, et al., 2015b)	400	760	508	160	21.50	0.40
	450	854	423	180	22.50	0.33
(Gibigaye , et al., 2017)	450	689	446	203	22.42	0.39
	500	740	370	225	21.74	0.33
	550	693	347	248	21.24	0.33
(Rahman, et al., 2020)	500	860	273	175	22.09	0.24

Appendix D - Cracking Strength OPS

Size	Tenera (Newtons)				Dura (Newtons)			
	>14mm		10 - 14 mm		>14mm		10 - 14 mm	
Samples	**Top**	**Side**	**Top**	**Side**	**Top**	**Side**	**Top**	**Side**
1	167.20	69.27	67.52	16.40	1780.00	574.30	107.98	646.90
2	120.00	36.10	78.36	37.27	430.00	1296.90	627.10	245.94
3	200.00	26.63	51.51	21.11	761.90	515.90	793.50	1932.96
4	195.81	86.00	136.83	88.78	620.30	1816.00	125.52	1010.00
5	152.66	56.81	80.59	46.14	418.80	483.05	405.10	532.32
6	153.09	42.99	47.82	73.85	642.40	426.45	645.11	251.20
7	228.20	106.75	58.70	79.78	2185.00	858.90	422.00	509.71
8	179.43	8.43	225.75	87.98	567.60	760.50	364.52	668.80
9	195.22	25.48	106.42	54.36	728.80	1725.80	371.10	399.58
10	222.41	14.92	88.84	70.08	1739.00	450.60	816.10	641.37
11	233.92	27.68	260.50	37.24	445.70	2241.71	380.01	602.67
Standard Deviation (sample)	35.67	30.92	71.28	26.01	638.42	648.96	237.46	467.88
Mean (Newtons)	186.18	45.55	109.35	55.73	938.14	1013.65	459.82	676.50
Coefficient of variation CV:	0.19	0.68	0.65	0.47	0.68	0.64	0.52	0.69

210

Appendix E - Measurement-index OPS

For Section 4.1.2.2

Tenera OPS

Retained at	No.	Length	Width	Thickness		Min. Average thickness	Max. Average thickness	Average Thickness	Average length	Average width
				mm						
14mm	1	19.31	15.52	0.91	1.13	0.66	1.62	1.14	20.17	13.70
	2	28.66	12.46	0.91	2.03					
	3	16.29	9.39	0.60	1.79					
	4	11.83	15.98	0.47	1.68					
	5	28.96	14.07	0.71	1.64					
	6	15.97	14.78	0.34	1.46					
10mm	1	30.62	13.17	0.82	2.13	0.72	1.68	1.20	22.39	13.53
	2	22.40	16.68	0.80	1.54					
	3	24.43	13.35	0.68	1.41					
	4	19.13	11.32	0.77	1.37					
	5	23.32	11.46	0.68	2.49					
	6	14.42	15.21	0.54	1.12					
5mm	1	16.00	8.89	0.96	2.74	0.63	1.44	1.03	13.85	9.64
	2	11.03	10.86	0.84	1.69					
	3	13.55	10.78	0.54	1.18					
	4	16.61	8.70	0.60	0.97					
	5	10.80	8.69	0.11	0.54					
	6	15.13	9.94	0.70	1.54					

Dura OPS

Retained at	No.	Length	Width	Thickness		Min. Average thickness	Max. Average thickness	Average Thickness	Average length	Average width
				mm						
14mm	1	28.03	18.47	2.05	4.41	2.31	5.95	4.13	23.51	17.73
	2	24.11	14.28	2.27	8.04					
	3	24.59	19.48	4.37	7.10					
	4	22.55	19.14	1.57	4.39					
	5	18.05	17.10	1.73	3.90					
	6	23.70	17.93	1.86	7.83					
10mm	1	22.28	13.55	3.33	6.33	2.05	3.38	2.72	22.03	13.04
	2	23.72	14.00	2.54	3.88					
	3	21.65	14.00	3.12	4.32					
	4	17.94	11.78	0.96	1.67					
	5	23.56	11.44	0.85	1.90					
	6	23.02	13.48	1.52	2.19					
5mm	1	16.52	4.08	1.05	1.68	1.44	2.26	1.85	16.32	7.45
	2	15.61	10.00	1.14	0.43					
	3	15.29	6.44	0.65	4.01					
	4	19.53	8.14	1.88	2.01					
	5	17.71	4.97	2.31	3.72					
	6	13.23	11.05	1.58	1.72					

Appendix F – Stress-strain curves of concretes

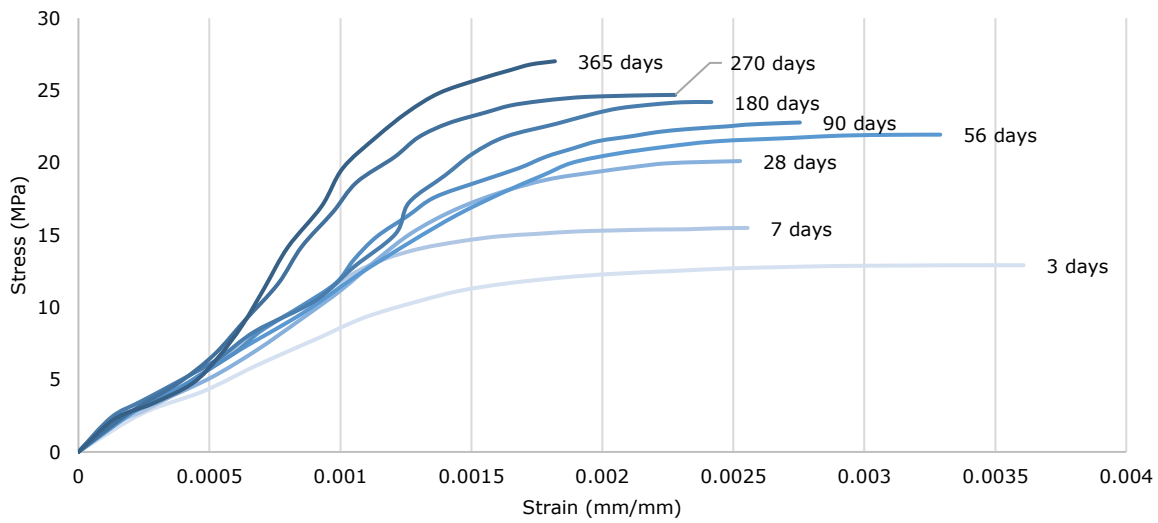**For cured regime for Section 4.3.3.1**.

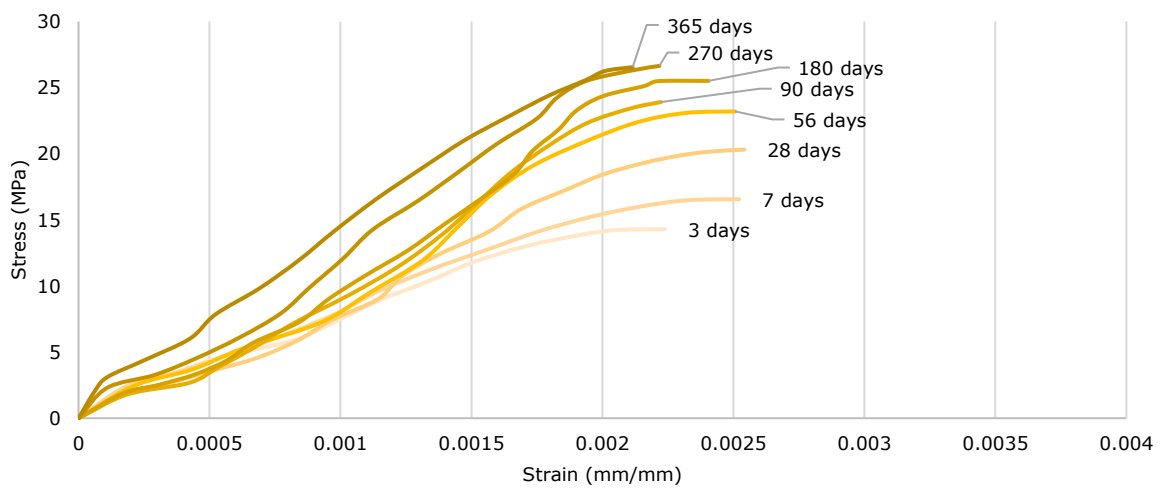Figure F.1 Stress-strain curves for NWC with different ages

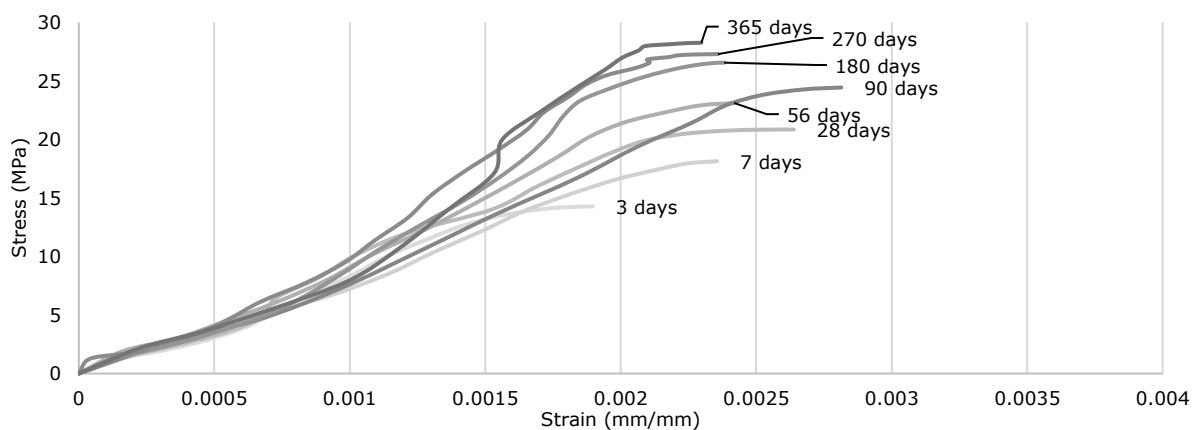Figure F.2 Stress-strain curves for coarse OPSC with different ages

212

Figure F.3 Stress-strain curves for fine OPSC with different ages

(a) 3 Days

(b) 7 Days
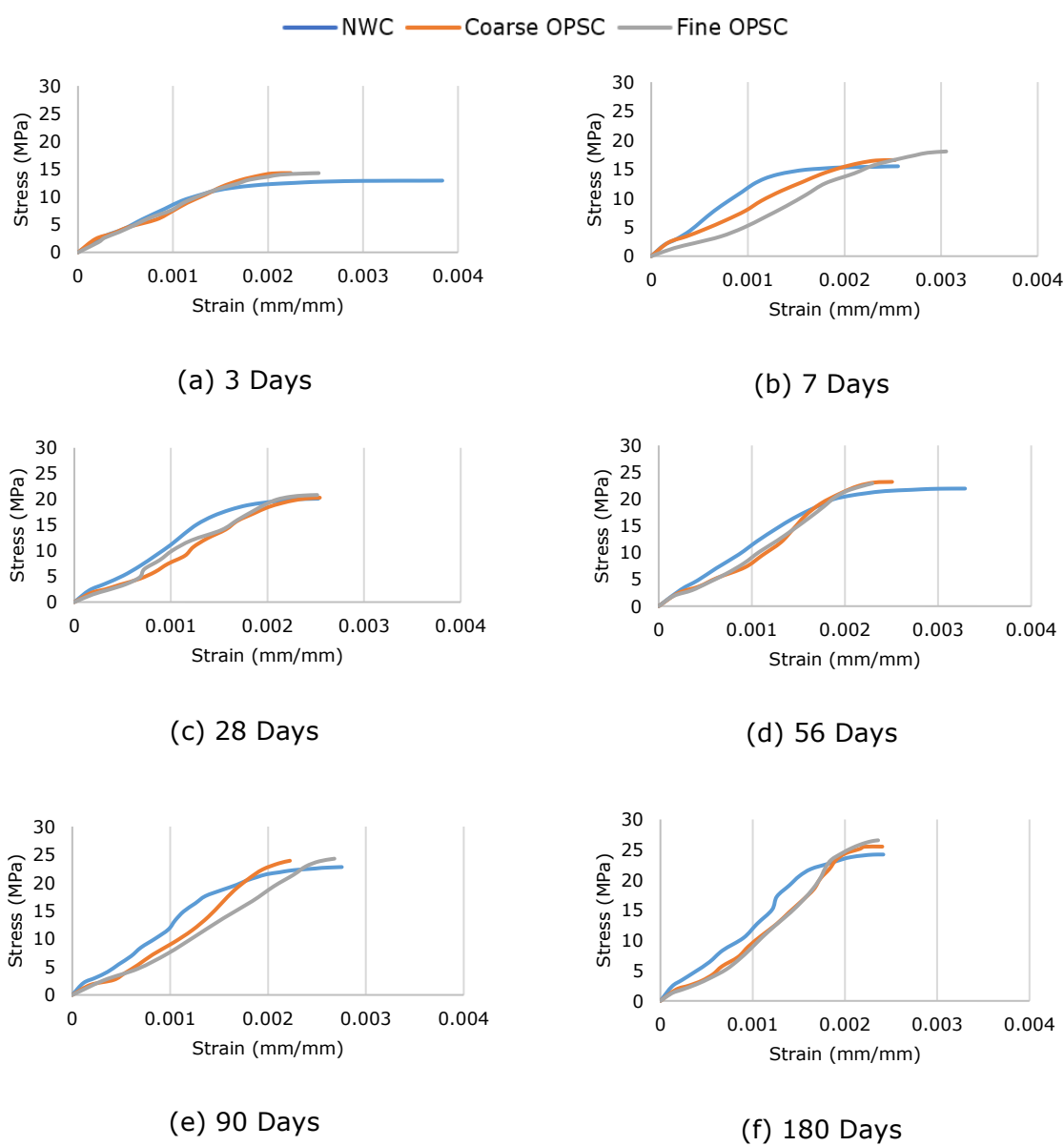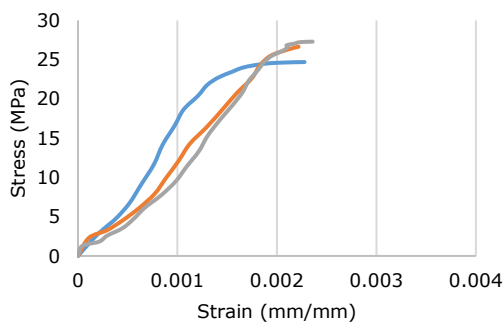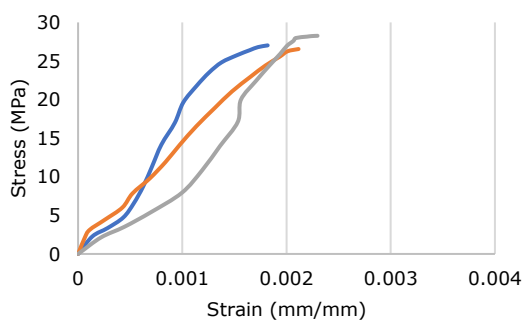
(c) 28 Days

(d) 56 Days

(e) 90 Days

(f) 180 Days

Figure F.4 Stress – strain curves of cured specimens at ages 3 – 365 days (a – h)
(continue to next page)

213

(g) 270 Days   (h) 365 Days

Figure F.4 Stress – strain curves of cured specimens at ages 3 – 365 days (a – h)

For cured vs air cured specimens in Section 4.3.3.2.
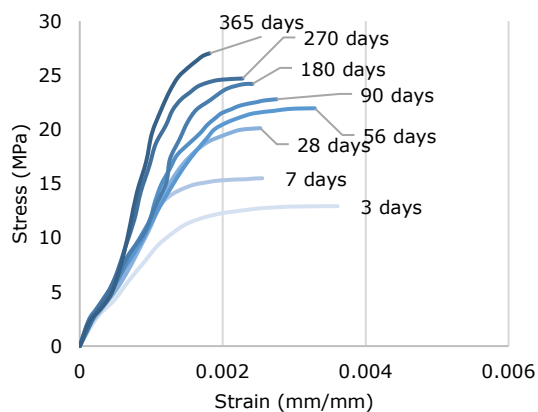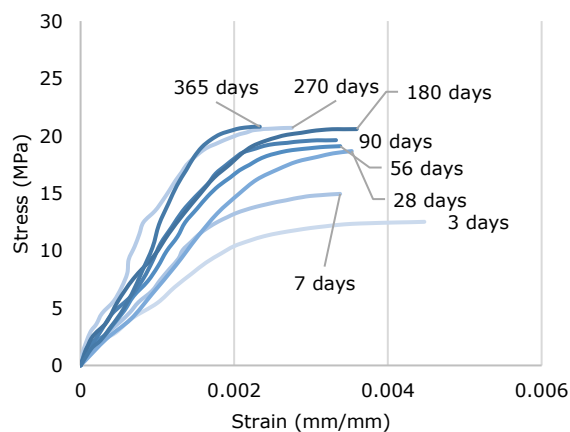
(a)   (b)

Figure F.5 Stress-strain curves for (a) cured and (b) air cured NWC
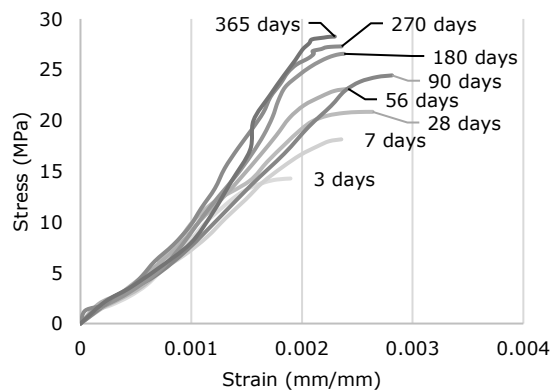
(a)   (b)
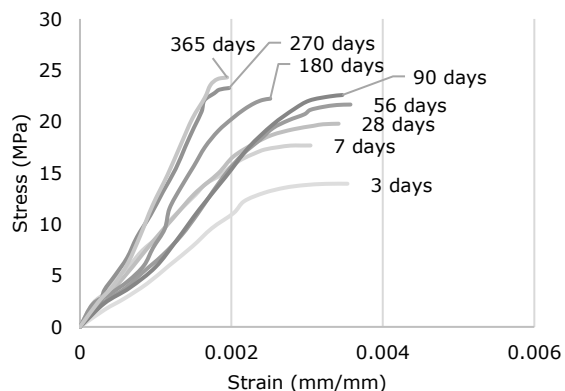
Figure F.6 Stress-strain curves for (a) cured and (b) air cured fine OPSC
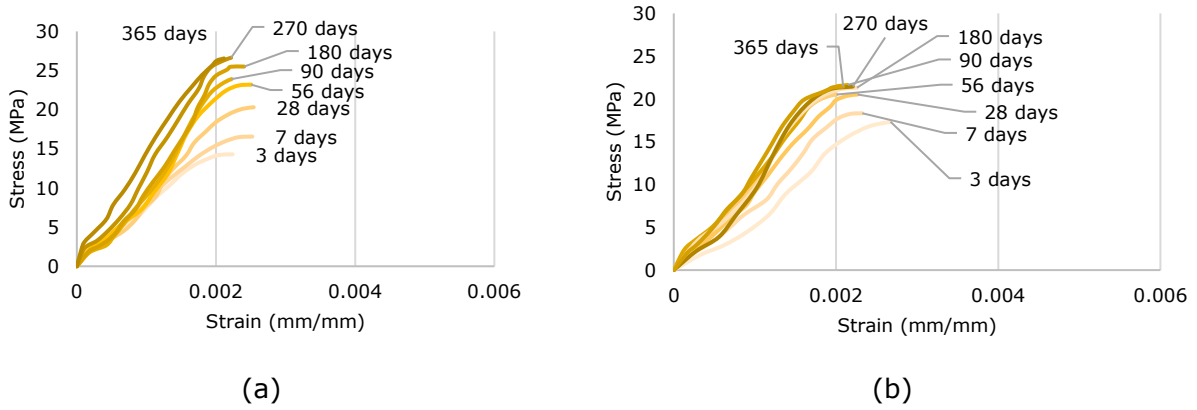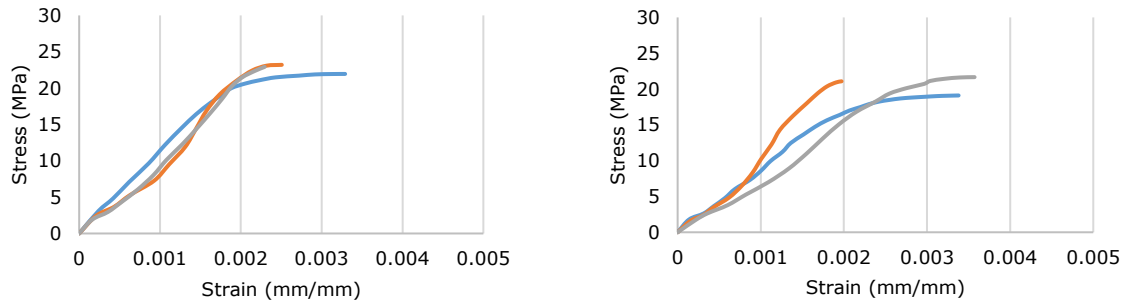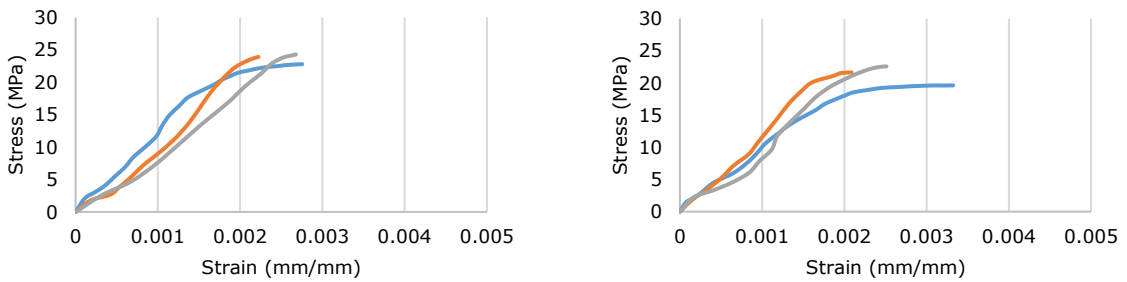
214

(a)   (b)

Figure F.6 Stress-strain curves for (a) cured and (b) air cured Coarse

Cured   **Air cured**

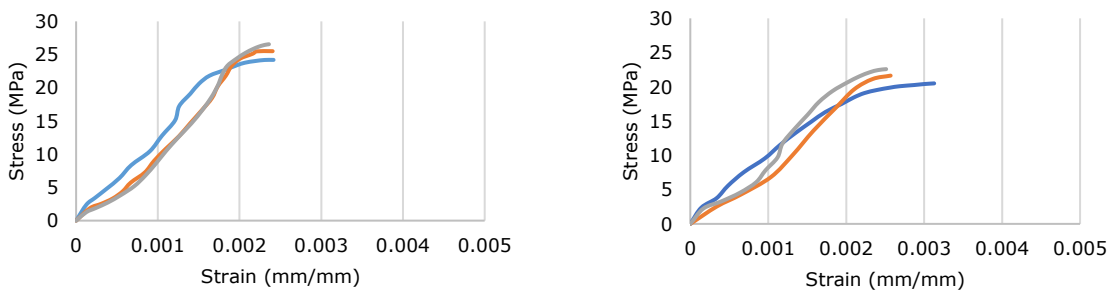(a) 3 days

(b) 7 days

(c) 28 days

Figure F.7 Stress-strain curves for cured and air cured NWC, coarse, and fine OPSC at different ages (continued)
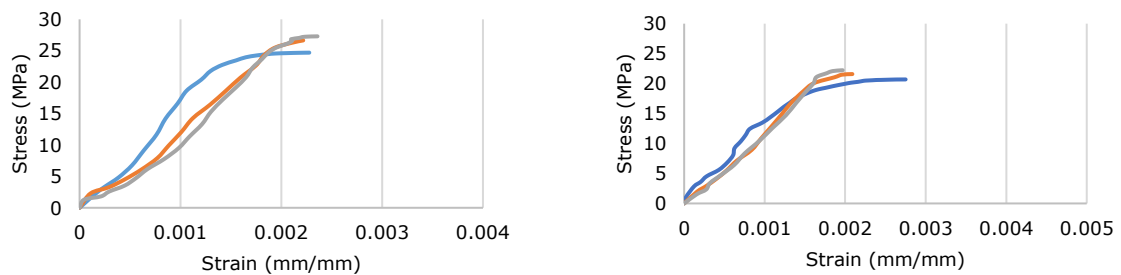
215
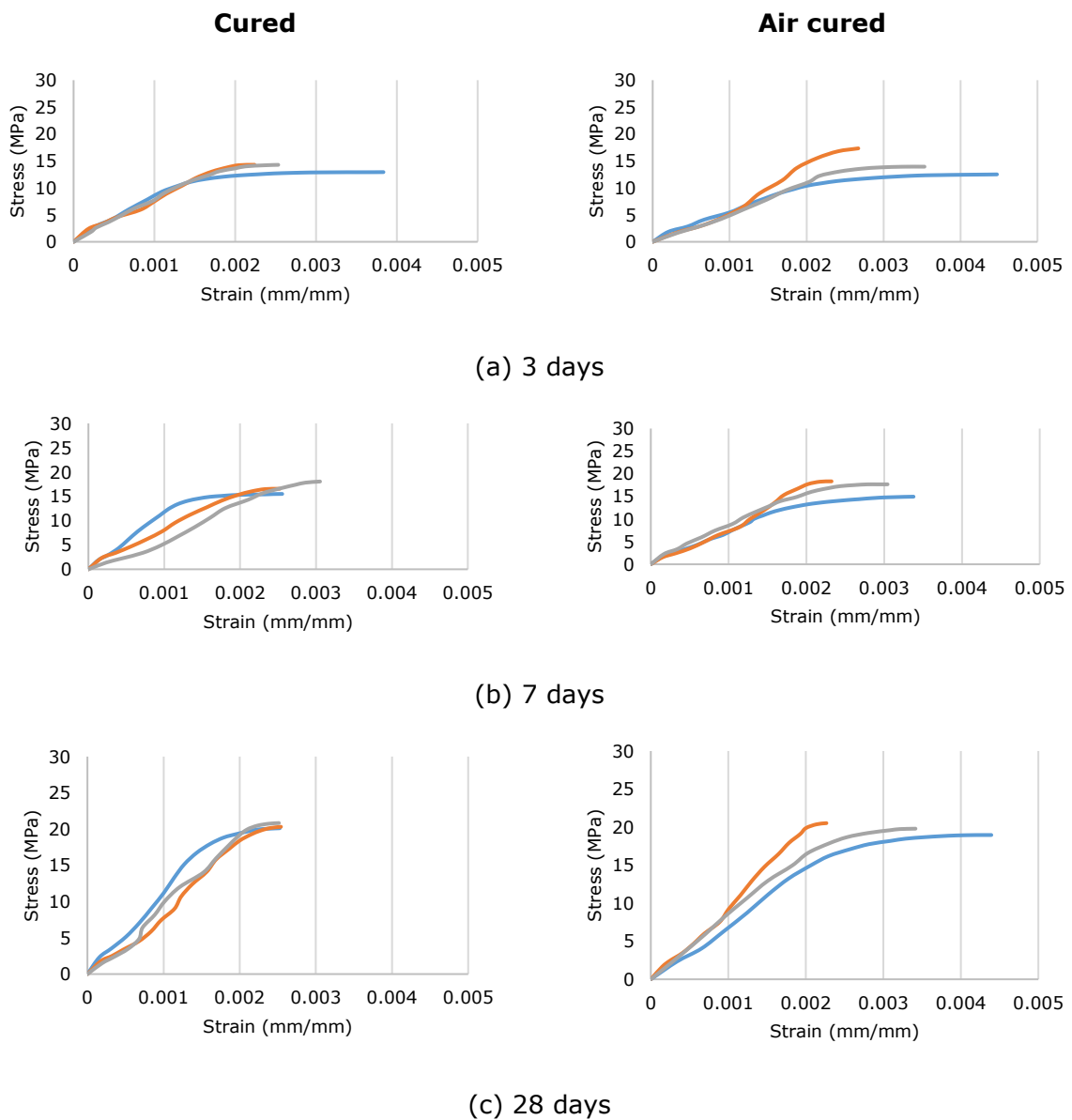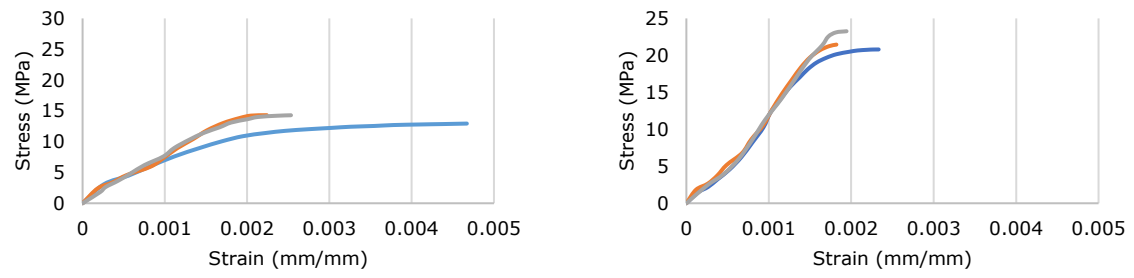
(d) 56 days

(e) 90 days

(f) 180 days

(g) 270 days

Figure F.7 Stress-strain curves for cured and air cured NWC, coarse, and fine OPSC at different ages (continued)

216

(h) 365 days

Figure F.7 Stress-strain curves for cured and air cured NWC, coarse, and fine OPSC at different ages